



University
of Glasgow

Tyler, Andrew Nicholas (1994) *Environmental influences on gamma ray spectrometry*. PhD thesis.

<http://theses.gla.ac.uk/4893/>

Copyright and moral rights for this thesis are retained by the author

A copy can be downloaded for personal non-commercial research or study, without prior permission or charge

This thesis cannot be reproduced or quoted extensively from without first obtaining permission in writing from the Author

The content must not be changed in any way or sold commercially in any format or medium without the formal permission of the Author

When referring to this work, full bibliographic details including the author, title, awarding institution and date of the thesis must be given

**ENVIRONMENTAL INFLUENCES ON
GAMMA RAY SPECTROMETRY**

by

© Andrew Nicholas Tyler, 1994

Submitted to

The Science Faculty, University of Glasgow, August 1994

for the degree of

Doctor of Philosophy

*This Research Work was Undertaken at the
Scottish Universities Research and Reactor Centre,
East Kilbride.*

ABSTRACT

Spatially representative sampling of both natural and anthropogenic deposits in the environment is limited by their inherent heterogenic distribution. This problem is compounded when trying to relate ground measurements which are spatially restricted to remote sensing observations which are not. This work examined these widely experienced problems in the context of the measurement of natural (K, U and Th) and anthropogenic (^{137}Cs and ^{134}Cs) radioactivity through the three techniques of soil sampling with laboratory based gamma ray spectrometry, in-situ gamma ray spectrometry, and airborne gamma ray spectrometry.

These three methods were applied systematically to estimate the radioactivity across a tight geometry valley in Renfrewshire. Activity estimates from field based and airborne gamma spectrometry were compared with each other and with the results of high resolution gamma spectrometry of soil samples to examine the relationship between each method under variable topographic conditions. These results demonstrated that the distribution, and post depositional migration, of activity had important influences on all measurement techniques, and affected the ability to make comparisons between them.

Further detailed studies were then conducted to examine these influences. The effects of variations in soil composition and characteristics on environmental gamma ray spectrometry were evaluated by calculation and experimental determination. Corrections to standard laboratory gamma spectrometric procedures were developed to improve systematic precision. These investigations also reviewed soil sampling depth for direct effective comparison with in-situ gamma spectrometry.

The effects of small scale sampling errors on activity estimates were demonstrated to have a quantifiable influence on the precision of activity estimation. Lateral variability of activity distribution of natural radioactivity and anthropogenic radioactivity deposited both from the atmosphere and from marine sources has been studied in detail at a number of sites. The extent of variability depends on the nature of activity,

its deposition mode and local environmental characteristics. Spatial variability represents an important constraint on the interpretation of activity estimates derived from all methods examined, and on comparisons between them. Statistically representative sampling plans were developed and applied to enable spatial comparisons to be made between soil sample derived activity estimates and in-situ and remotely sensed observations.

The influence of the vertical activity distribution on in-situ and airborne measurements has been recognised as an important variable affecting calibration. The use of the information from the scattered gamma ray spectrum to quantify and correct for source burial effects was examined in a series of modelling experiments. A relationship between ^{137}Cs source burial and forward scattering was determined and subsequently applied to a salt marsh environment which showed pronounced subsurface maxima. A spectrally derived calibration correction coefficient was shown to account for variations in source burial across a single site. This provides a potential means for surmounting one of the principal limitations of in-situ gamma spectrometry.

As a result of this work it has been possible to account for important environmental factors which affect gamma ray spectrometry in the laboratory, in the field and from aircraft. This has led to the development of sound methodology for comparison between sampling, field based and remote sensing techniques.

ACKNOWLEDGMENTS

I would like to gratefully acknowledge my supervisors, in particular Dr David Sanderson for his help and guidance and Dr Marian Scott for her friendly advice and continual encouragement. I would also like to thank Prof. Roger Scott for his helpful comments of my thesis draft and to Prof. Murdoch Baxter who helped initiate this research project and providing me with this opportunity for undertaking it. Thanks also to the Natural Environmental Research Council for funding this research.

In particular I would also like to thank my good friend and colleague David Allyson for his help, cooperation, companionship, for the philosophical discussions on this research area and for being so easy to work with particularly during times of intensive contract work. In addition, I would like to thank Dr Gordon Cook for extensive use of his Ge(Li) detector during the course of this research and Dr Paul McDonald for "*showing me the ropes*" and for his helpful advice particularly in the early stages of this work. I would also like to acknowledge the kind loan of surveying equipment from the Department of Geography and the *unburied* Land Rover from the Department of Geology at Glasgow University.

I also gratefully acknowledge all my friends, colleagues and staff at the Reactor Centre who have all helped me in some way, particularly with field work support. Also many thanks for the encouragement and support of Christine Slater and Lorna Carmichael.

I would also like to warmly thank my family, particularly my Mother, for their continual support. In particular, deep gratitude to my fiancée Catherine Skinner for her support, encouragement, patience and finally for proof reading my thesis!

Many thanks also to Prof. Donald Davidson and Prof. Mike Thomas for their patience and support during the final stages of my thesis write up at Stirling. Finally, many thanks to the numerous interested and uninterested farmers, land owners, wardens and the Forestry Commission for allowing both earthly and heavenly invasions.

SUBJECT INDEX

Title Page	i
Abstract	ii
Acknowledgements	iv
Subject Index	v
Appendices Index	xii
Figure Index	xiii
Table Index	xix
1. INTRODUCTION	
1.1 Research in Context	1
1.2 Historical Approach to the Measurement of Environmental Radioactivity	2
1.3 Thesis Aims and Contributions	5
1.4 Summary	8
2. THE ORIGIN AND DISTRIBUTION OF GAMMA EMITTING RADIONUCLIDES	
2.1 Introduction	9
2.2 The Sources of Radionuclides and Radiation	9
2.2.1 Primordial Radioactivity and Natural Sources of Radionuclides	9
2.2.2 Fission and the Production of Anthropogenic Radionuclides	12
Nuclear Fuel Cycle	12
Nuclear Weapons	15
Anthropogenic Radionuclides of Interest	16

2.3 The Distribution of Radionuclides in the Environment	17
2.3.1 Primordial Radionuclides	17
Igneous Rocks	18
Sedimentary Rocks	19
Metamorphic Rocks	21
U and Th enrichment to economic grade	21
2.3.2 Anthropogenic Radionuclides	22
Weapons Testing Fallout	23
Nuclear Industrial Accidents	24
Nuclear Discharges into the Environment	26
2.4 The Chemical Behaviour of Radionuclides in Soils	27
2.4.1 Primordial Radionuclide Assimilation and Concentration in Soils	28
2.4.2 Anthropogenic Radionuclide Behaviour in Soils and the Environment	31
Caesium in Soils	31
Americium and Plutonium in Soils and the Environment	34
2.5 Summary	36
3. METHODS AND TECHNIQUES	
3.1 Introduction	37
3.2 Soil Sample Collection and Preparation	37
3.2.1 Soil Sampling	38
3.2.2 Laboratory Sample Processing	39
3.3 Gamma Ray Spectrometry	41
3.3.1 Semiconductor (Solid State) Detectors	42
3.3.2 Scintillation Detectors	43
3.3.3 Detector Instrumentation	44
Instrumentation for Semiconductor Detectors	44
Instrumentation for Scintillation Detectors	46
Signal Processing and Output	46
3.4 Spectral Characteristics	48
3.5 Gamma Ray Spectroscopy - Laboratory Set Up	51
3.5.1 Detector Configuration	51
3.5.2 Background Reduction and Subtraction	52

3.5.3 Spectral Analysis	53
3.5.4 Energy Calibration	54
3.5.5 Efficiency Calibration	55
3.5.6 Quantitative Analysis	58
3.6 Gamma Ray Spectroscopy - In-Situ Use in the Field	59
3.6.1 Detector and MCA set up	60
3.6.2 Regions of Interest or Windows	61
3.6.3 Background Radiation and Background Subtraction	62
3.6.4 Stripping Spectral Interferences	63
3.6.5 Full Spectral Stripping	67
3.6.6 Sensitivity Calibration	67
3.6.7 Software	67
3.6.8 Field Work Procedure	68
3.7 Gamma Ray Spectroscopy - Aerial Survey	68
3.7.1 Aerial Survey Equipment Developed by SURRC	69
3.7.2 Regions of Interest or Windows	71
3.7.3 Background Subtraction	72
3.7.4 Stripping Spectral Interferences	72
3.7.5 Height Correction Coefficients	73
3.7.6 Calibration	74
3.7.7 System Operation	74
3.8 Detector Response Characteristics	75
3.8.1 Photon Fluence Equations and the Calculation of Fields of View of In-Situ and Aerial Gamma Detectors	75
3.8.2 Analytical Solutions to Photon Transport Equations	77
3.9 Minimum Detection Limits	84
3.9 Conclusions	87
4. COMPARISONS BETWEEN SOIL SAMPLE ANALYSIS, IN-SITU AND AERIAL GAMMA RAY SPECTROMETRIC DETERMINATIONS OF RADIONUCLIDE INVENTORIES	
4.1 Introduction	88
4.1.1 Objective	88
4.1.2 Experimental Design	89
4.1.3 Valley Selection and Criteria	89

4.2 Method	90
4.2.1 Field Work Design and Method	91
4.2.2 The Principals of Semivariogram Analysis	95
4.3 Results	98
4.3.1 Data Statistics	98
4.3.2 Three Dimensional Comparison Between Data Sets.	100
4.3.3 Comparisons between transect data	104
4.3.4 Semivariogram Analysis	109
4.4 Discussion	114
4.4.1 Discussion of the Main Distributional Characteristics	114
4.4.2 Identification of the Environmental Factors Controlling the Relationships Between Soil Sample, In-Situ and Aerial Survey Inventory Data	116
4.5 Summary and Conclusions	121
5. SELF ABSORPTION CHARACTERISTICS OF SOILS AND THEIR INFLUENCE ON GAMMA SPECTROMETRY	
5.1 Introduction	123
5.2 Changes in Soil Density as an Environmental Variable	125
5.3 The Measurement of the Mass Attenuation Coefficient of a Range of British Soils	127
5.3.1 Objective	127
5.3.2 Method	127
5.3.3 Results	129
5.3.4 Summary	132
5.4 Calculation of the Mass Attenuation Coefficients of a Range of Soils	133
5.4.1 Objectives	133
5.4.2 Method	134
5.4.3 Results and Discussion	136
5.5 Discussion and Implications of Soil Self Absorption	142
5.5.1 Summary	142
5.5.2 Implications for Laboratory Based Gamma	

Ray Spectrometry	142
5.5.3 Implications for In-Situ and Airborne Gamma Ray Spectrometry	143
5.6 Sample Self Absorption Correction for Absolute Efficiency Calibration of Laboratory Based Detectors	145
5.6.1 Objectives	145
5.6.2 Method	145
5.6.3 Results and Discussion	146
5.6.4 The Variation of μ and μ_m for environmental samples from that associated with the calibration of soils for 59.6 keV Photons	153
5.6.5 Verification and Quality Assurance	155
5.7 Summary and Conclusions	157
6. ACCOUNTING FOR SOIL SAMPLING ERRORS, SPATIAL VARIABILITY AND FIELDS OF VIEW IN ENVIRONMENTAL GAMMA RAY SPECTROSCOPY	
6.1 Introduction	159
6.1.1 Spatial Variability	160
6.1.2 Sampling and Sub-sampling Errors in Radionuclide Inventory Estimation	164
6.2 Sub-sampling Errors and Sample Reproducibility - Experimental Precision	166
6.2.1 Objective	166
6.2.2 Method	167
6.2.3 Results and Discussion	167
6.2.4 Conclusions	172
6.3 Field Sampling Error	173
6.3.1 Objective	173
6.3.2 Method	173
6.3.3 Results and Discussion	173
6.4 Improvement in Sampling Error	175
6.4.1 Objective	175
6.4.2 Method	175
6.4.3 Results and Discussion	176

6.5 Matching Samples to Fields of View of In-Situ and Airborne Gamma Spectrometry	178
6.5.1 Objective	178
6.5.2 Principles and Method - A Simple Centre Weighted Sampling Plan	179
6.5.3 Results	180
6.6 Accounting for Within Site Variability and Variable Detector Height for In-situ and Aerial Survey Calibration	187
6.6.1 Objective	187
6.6.2 Solution - The Expanding Hexagonal Sampling Plan	187
6.6.3 Method	189
6.6.4 Spatially Weighted Results	191
6.6.5 Results, the Study of Spatial Variability	191
6.6.6 Determination of Height Correction Coefficient	197
6.7 Discussion	202
7. RADIONUCLIDE DEPTH DISTRIBUTION PROFILES AND IN-SITU GAMMA SPECTROSCOPY	
7.1 Introduction	206
7.2 Soil Sampling and the Depth Distribution Profile	211
7.2.1 Objectives	211
7.2.2 Method	211
7.2.3 Results	212
7.2.4 Discussion	217
7.3 Calculation of Mass Per Unit Area or Mass Depth and the Mean Mass Depth	219
7.3.1 Objective and Theory	219
7.3.2 Results and Discussion	221
7.3.3 Summary	225
7.4 Mean Mass Depth and Photon Fluence	225
7.4.1 Objective and Theory	225
7.4.2 Results and Discussion	227

7.5 Experimental Modelling of In-Situ Spectral Observation with Buried Sources	232
7.5.1 Objective	232
7.5.2 Principles	233
7.5.3 Method	234
7.5.4 Results and Discussion of the Determination of Source Burial from Spectral Characteristics	236
7.6 Experimental Modelling of the Change in Stripping Coefficients with Source Burial	240
7.6.1 Objective	240
7.6.1 Method	240
7.6.3 Results and Discussion of the change in stripping coefficients with absorber perspex sheets to simulate low activity organic rich geological overburden	241
7.6.4 Results and discussion of the change in stripping coefficients with absorber perspex sheets to simulate increase in air path length	246
7.7 The Determination of Mean Mass Depth (β) from In-Situ Spectral Information	246
7.7.1 Objective	246
7.7.2 Method	247
7.7.3 Results and Discussion	248
7.7.4 ^{137}Cs Calibration Correction for Changes in Mean Mass Depth (β)	252
7.8 Summary and Discussion	256
8. DISCUSSION AND CONCLUSIONS	
8.1 Some of the Environmental Influences on the Measurement of Radionuclide Inventories	259
8.2 The main Implications and Contributions of this Thesis	260
8.2.1 Radionuclide Distribution and Measurement	260
8.2.2 Identification of Environmental Influences on Radioactivity Estimation	261
8.2.3 Quantification of Self Attenuation Characteristics of Soils	262
8.2.4 Effective Soil Sampling Depth	264
8.2.5 Laboratory Based Gamma Spectrometry	265
8.2.6 Sampling and Sub-sampling Errors	266

8.2.7 Spatial Variability and Statistically Representative Sampling Plans	267
8.2.8 Source Burial	269
8.3 Summary	271
8.4 Areas for Future Research	272
8.5 Final Conclusions	276
REFERENCES	278

APPENDICES

APPENDIX A The Calibration of an In-Situ 3"x3" NaI(Tl) Detector	295
APPENDIX B Aerial Survey Detector Calibration	304
APPENDIX C Raw Data for the Determination of μ and μ_m for a Range of British Soils	307
APPENDIX D The Absolute Efficiencies Determined from Peat and Elginhaugh Soil for the Coaxial Ge(Li) and HPGe Detector ..	309
APPENDIX E Absolute Efficiency Calibration for Specific Radionuclides with Sample Density	310
APPENDIX F Observations on the Temporal Change in Detector Response with Soil Water Content	311
APPENDIX G Installation of the Concrete Calibration Pads	313
APPENDIX H The Construction of an Extended layer ^{137}Cs Calibration Sheet	316
APPENDIX I Choice of Absorber Materials	318
APPENDIX J Modelling Changes in Stripping Coefficients with Increase in Air Path Length	321

FIGURE INDEX

Figure 3.1 Soil Corers: a) 38mm x 150 mm corer, and b) 105 mm x 450 mm corer	39
Figure 3.2 The Main Components of a HPGe or Ge(Li) Detector System	44
Figure 3.3 Schematic representation of gamma ray spectrum observed from a pure source such as ^{137}Cs or ^{40}K	49
Figure 3.4 Sketch Cross-section of HPGe Detector and Cryogenic Dewar	52
Figure 3.5 The Absolute Efficiency Curves for a Ge(Li) and HPGe Detector	58
Figure 3.6 The Bicron 3"x3" NaI(Tl) Detector-PMT-Preamplifier Configuration	60
Figure 3.7 Showing the Net Spectra from the Concrete Calibration pads and the Working Regions of Interest	65
Figure 3.8 The SURRC Aerial Survey Equipment	69
Figure 3.9 The Spherical Coordinate System for In-situ Gamma Ray Detector with Integration Limits $R_2 \leq R \leq \infty$, $\Theta_1 \leq \Theta \leq \pi/2$ and $0 \leq \phi \leq \pi/2$ for Field of View Calculations	77
Figure 3.10 The Volume of Source Material given from Equation 3.12	78
Figure 3.11 Circles of Investigation for ^{40}K , after Duval <i>et al</i> 1971	78
Figure 3.12 The Increase in the Circle of Investigation with Platform Height for ^{137}Cs	80
Figure 3.13 The Change in the Field of View of a Detector at 1m Height with Energy	81
Figure 3.14 The Change in the Field of View of Detectors at Aerial Survey Height with Gamma Ray Energy	81
Figure 3.15 The Influence of the Mass Relaxation per Unit Area (g/cm^2) for a Detector at 1 m Height	82
Figure 3.16 The Mass Relaxation per Unit Area (g/cm^2) on the Field for View of Detectors at Aerial Survey Height	82
Figure 4.1 3 Dimensional Map Representing the Topography of the Raithburn Valley	91

Figure 4.2 Sampling Plan within the Raithburn Valley, Lochwinnoch	93
Figure 4.3 The Spherical Semivariogram Model	96
Figure 4.4 Semivariogram Models	97
Figure 4.5 3 Dimensional Maps of ^{137}Cs activity (kBq m^{-2}) across the Raithburn Valley from Soil Samples (400 x 200 m grid), 3" x 3" NaI(Tl) In-situ Measurements (200 m grid) and Aerial Survey Measurements	101
Figure 4.6 3 Dimensional Maps of ^{134}Cs activity (kBq m^{-2}) across the Raithburn Valley from Soil Samples (200 m x 400 m grid)	102
Figure 4.7 3 Dimensional Maps of ^{40}K (Bq kg^{-1}) across the Raithburn Valley from Soil Samples (200m x 400m grid), 3" x 3" NaI(Tl) In-situ Measurements (400 m grid) and Aerial Survey Measurements	103
Figure 4.8 ^{137}Cs Distribution across Transect 30400	105
Figure 4.9 ^{137}Cs Distribution across Transect 30000	106
Figure 4.10 ^{137}Cs Distribution across Transect 29200	106
Figure 4.11 ^{40}K Activity Concentration across Transect 30400	107
Figure 4.12 ^{40}K Activity Concentration across Transect 30000	108
Figure 4.13 ^{40}K Activity Concentration across Transect 29200	108
Figure 4.14 ^{137}Cs Semivariograms (kBq m^{-2}) ² showing Spatial Variability at Raithburn	111
Figure 4.15 ^{134}Cs Semivariograms (kBq m^{-2}) ² showing Spatial Variability at Raithburn	114
Figure 4.16 ^{40}K Semivariograms (Bq kg^{-1}) ² showing Spatial Variability at Raithburn	115
Figure 5.1 Diagram showing the detector-sample geometry	124
Figure 5.2 Density Ranges Observed across and within Soil Sample Site Investigations	126
Figure 5.3 Apparatus Used to Determine μ and μ_m of Soils	128
Figure 5.4 The Dependence of a) μ and b) μ_m on the Photon Energies Associated with ^{241}Am , ^{137}Cs and ^{60}Co	130

Figure 5.5 The Scatter of μ_m with Density and thus the Dependence of μ_m on the Chemical Composition of the Sample as well as Gamma Ray Energy, a) 59.54 keV, b) 661.7 keV and c) 1333 keV	131
Figure 5.6 The Contribution of Scattering and Absorption to the Total μ_m for a) Beck's Soil and Two Extreme Soil Compositions; b) Organic; and c) Mineral Rich	137
Figure 5.7 Comparison of μ_m Relative to Beck's Soil Composition, with Energy	138
Figure 5.8 Variation of μ_m with Atomic Number (Z) and Selected Photon Energies	139
Figure 5.9 The Relationship Between μ_m and Z_{mean} , for soils and also for pure elements of Z	146
Figure 5.10 The Change in Absolute Efficiency with Energy and Sample Density	149
Figure 5.11 The Change in Absolute Efficiency with Sample Density for Anthropogenic Radionuclides with 150cc Geometry Containers	150
Figure 5.12 The Change in Detector Absolute Efficiency for Primordial Radionuclides in 150cc Geometry Containers	151
Figure 5.13 The Change in Detection Efficiency with Sample Weight Reduction i.e. Sample Under-filling	154
Figure 5.14 The Change in the Linear Attenuation Coefficient with Sample Density for the Calibration Samples, Caerlaverock Samples and IAEA 306 Standard	154
Figure 5.15 The Variation of μ_m with Sample Density for the Calibration Samples, Caerlaverock Samples and IAEA Soil 6	155
Figure 5.16 ^{241}Am Detector Calibration Correction Based on Changes in Sample μ at 59.6 keV	157
Figure 6.1 Ingamells' Sampling Model adapted from Ingamells (1974a)	166
Figure 6.2 The Reproducibility of the Broughton Mains Bulk Sample with Time	171
Figure 6.3 2m x 2m Sampling Grid	173
Figure 6.4 Ayrshire Ground Sampling Plan	179

Figure 6.5 Comparison between ^{137}Cs Activity Determinations from Soil Samples and In-Situ Gamma Spectroscopy at Lochwinnoch	185
Figure 6.6 Comparison between ^{134}Cs Activity Determination from Soil Samples and In-situ Gamma Spectroscopy at Lochwinnoch	185
Figure 6.7 Spatial 2 Dimensional Comparison of ^{40}K (kBq m^{-2}) Activity Estimation at Lakin Farm, Arran	186
Figure 6.8 Spatial 2 Dimensional Comparison of ^{40}K (kBq kg^{-1}) Activity Estimation at Lakin Farm, Arran	186
Figure 6.9 The Expanding Hexagonal Sampling Plan and Typical Sampling Sets	188
Figure 6.10 The Relationship Between the Circles of Investigation for ^{137}Cs and the Hexagonal Sampling Strategies	190
Figure 6.11 Variation of Sampling Error with Radionuclide within each Hexagonal Shell Sampled at Caerlaverock	194
Figure 6.12 Coefficient of Variation (<i>CV</i>) of Anthropogenic Radionuclides across the Caerlaverock Salt Marsh with Sample Spacing	195
Figure 6.13 Coefficient of Variation (<i>CV</i>) of Primordial Radionuclides across the Caerlaverock Salt Marsh with Sample Spacing	195
Figure 6.14 Coefficient of Variation with Sample Spacing at the Long-bridgemuir Calibration Site	196
Figure 6.15 ^{137}Cs Detector Response with Altitude at Myres Hill	197
Figure 6.16 ^{134}Cs Detector Response with Altitude at Myres Hill	197
Figure 6.17 Variation of Detector Response for ^{137}Cs at Caerlaverock	198
Figure 6.18 The Spatially Corrected Variation of Detector Response with Height for ^{137}Cs at Caerlaverock	201
Figure 6.19 Change in Detector Response with Altitude at Lakin Farm and Caerlaverock	201
Figure 7.1 Depth Distributions of ^{137}Cs , ^{134}Cs , ^{40}K , ^{214}Bi , ^{208}Tl for Grassland Site, SURRC (23/2/90)	212
Figure 7.2 Depth Distribution Profiles of ^{137}Cs in peat determined from: a) 38mm corer - 15cm intervals; b) 105 mm corer - 15cm intervals; c) 105mm corer - 5cm intervals; and d) 105mm corer - 2 and 5 cm intervals	213

Figure 7.3 Depth Distribution Profiles of ^{134}Cs in Peat determined from: a) 38mm corer - 15cm intervals; b) 105mm corer -15cm intervals; c) 105mm corer - 5cm intervals; and d) 105mm corer - 2 and 5cm intervals	214
Figure 7.4 The Depth Distribution Profiles of ^{137}Cs , ^{241}Am , ^{134}Cs , ^{40}K , ^{214}Bi , ^{208}Tl at the Centre of the Caerlaverock Hexagonal Sampling Site. Position 01. (2/92)	215
Figure 7.5 The Depth Distribution Profiles at Caerlaverock (position 44) for ^{137}Cs , ^{241}Am , ^{40}K , ^{214}Bi and ^{208}Tl	216
Figure 7.6 Demonstrates a Range of ^{137}Cs Soil Core Profiles across the Caerlaverock Calibration Area	216
Figure 7.7 The Depth Distribution Profiles of ^{137}Cs across Warton Bank (Ribble Estuary). 128 m Spacing between Sampling Points	217
Figure 7.8 SURRC Mass Depth Distribution Profiles for ^{137}Cs (5.9 g cm^{-2}) and ^{134}Cs (4.0 g cm^{-2})	222
Figure 7.9 Longbridgemuir Mass Depth Distribution Profiles for ^{137}Cs on 17/5/92 (2.3 g cm^{-2}) and 11/7/92 (2.6 g cm^{-2})	222
Figure 7.10 Caerlaverock Mass Depth ^{137}Cs profiles: 14 (7.20 g cm^{-2}), 12 (10.78 g cm^{-2}), 01 (11.24 g cm^{-2}), 53 (13.23 g cm^{-2}), 34 (20.7 g cm^{-2}) and 44 (26.50 g cm^{-2})	224
Figure 7.11 Warton Bank Mass Depth ^{137}Cs Profiles: Sample 15 (7.69 g cm^{-2}), 14 (12.97 g cm^{-2}), 01 (12.66 g cm^{-2}), 44 (13.17 g cm^{-2}), 45 (19.74 g cm^{-2}) . . .	224
Figure 7.12 The detected flux rate with the log of <i>mean mass depth</i> (β) for ^{137}Cs at Caerlaverock Salt Marsh	227
Figure 7.13 ^{137}Cs Mass Depth Profile at Kirkconnel	228
Figure 7.14 The Correlation between Caerlaverock, Kirkconnel and Warton Bank Salt Marsh Characteristics	229
Figure 7.15 The Change in Mean Mass Depth with 0-15 cm Water Content at the Centre of the Longbridgemuir Calibration Area	230
Figure 7.16 The Relationship between Soil Profiles with "Exponential" Mass Depth Distributions with those of Subsurface Maxima	231
Figure 7.17 Schematic Representation of Gamma Ray Spectrum Observed from a Pure Source such as ^{137}Cs or ^{40}K	234

Figure 7.18 The Method for Measuring the Change in Detector Response with Source Burial	235
Figure 7.19 The True Net Spectral Response from the ¹³⁷ Cs Sheet with Burial	236
Figure 7.20 The Change in Spectral Characteristics with Increasing Source Burial Relative to the Photopeak	237
Figure 7.21 The Change in the Photopeak/Valley-Step Ratio with Number of Perspex Absorber Sheets	238
Figure 7.22 Two Different Depth Distributions, both totalling 400 kBq and with Mean Depths of 4.215 cm	239
Figure 7.23 Both profiles have a mean depth = 4.215 cm. Total activity distribution 406.5 kBq.	239
Figure 7.24 The Experimental Set up Used to Determine the Change in Stripping Coefficient with Increasing Peat/Water Overburden	241
Figure 7.25 The Change in Relative Peak Intensities for ²³⁸ U Calibration Pad with Source Burial	242
Figure 7.26 The Change in Peak Intensities for the ²³² Th Calibration Pad with Absorbing Media	243
Figure 7.27 The Change in Photopeak Intensities and Scattering associated with the ⁴⁰ K Calibration Pad with Attenuating Media	243
Figure 7.28 The Change in Stripping Coefficients with Number of Absorber Sheets	244
Figure 7.29 The Change in Stripping Coefficients for ²³² Th with Attenuating Media	245
Figure 7.30 The Change in Stripping Coefficients for ⁴⁰ K with Attenuating Media	245
Figure 7.31 The Whole and Stripped Spectrum Collected at the Centre of the Caerlaverock Calibration Site	249
Figure 7.32 The Unstripped and Stripped ¹³⁷ Cs Photopeaks with the Regions of Interest used to Determine the Valley-step Values	250
Figure 7.33 The Valley-step Ratio vs Mean Mass Depth (β) Determined with Pure ¹³⁴ Cs Deconvolution	251
Figure 7.34 The Valley-step Ratio vs Mean Mass Depth (β) Determined with the	

Modified ^{134}Cs Deconvolution	251
Figure 7.35 Demonstrating the Change in Detector Response across the Caerlaverock Salt Marsh Calibration Site	253
Figure 7.36 The Change in the Calibration Coefficient with β (g cm^{-2}) for the Caerlaverock Salt Marsh	253
Figure 7.37 The Comparison Between In-Situ Detector Uncorrected Calibrations and Soil Core Derived ^{137}Cs Activity Estimations (Bq m^{-2}) across the Caerlaverock Calibration Site	254
Figure 7.38 The Comparison between In-situ Detector β Corrected Calibrations and Soil Core Derived ^{137}Cs Activity Estimations (Bq m^{-2}) across the Caerlaverock Calibration Site	254
Figure 7.39 The GMX HPGe Detector Spectrum of ^{137}Cs Calibration Sheet Representing a Surface Source	257
Figure 7.40 The GMX Spectrum Collected on the Kirkconnel Salt Marsh	257

TABLE INDEX

Table 2.1 Primordial Radionuclides and gamma rays of interest	11
Table 2.2 Fission Products of Potential Biological Importance	13
Table 2.3 Some Neutron Activation Products of Biological Significance	14
Table 2.4 Typical Ranges of U, Th and K in Geological Media	20
Table 2.5 Activities Released from the Windscale Reactor Accident, 1957	24
Table 2.6 Chernobyl Releases	25
Table 3.1 Showing Details of the Mixed Radionuclide Spike for Efficiency Calibration for 1 February, 1991	56
Table 3.2 Showing the 8 Regions of Interest for Series 10" MCA and 3"x3" NaI(Tl) Detector, compared with the IAEA (1990) Recommended Windows	62
Table 3.3 Net Counts per Second within the Working Windows	64
Table 3.4 Stripping Ratios for each Channel	66
Table 3.5 Showing the 8 Regions of Interest for Series Aerial Survey NaI(Tl) Detector Array, compared with the IAEA (1990) Recommended Windows	86

Table 3.6 Detection Limits of the 3"x3" NaI(Tl) Detector with 1000 second live times for ¹³⁷ Cs, ¹³⁴ Cs, ⁴⁰ K, ²¹⁴ Bi, ²⁰⁸ Tl.	86
Table 3.7 Detection Limits of the 16 Litre NaI(Tl) Detector with 10 second live times for ¹³⁷ Cs, ¹³⁴ Cs, ⁴⁰ K, ²¹⁴ Bi and ²⁰⁸ Tl.	86
Table 4.1 Mean Detection Limits for the 3"x3" NaI(Tl) and 16 litre NaI(Tl) over the Raithburn Valley, Renfrewshire.	94
Table 4.2 Statistical Results of the Soil Sample, In-situ and Aerial Survey Data Sets	99
Table 5.1 Typical Density Ranges observed through Soil Sampling	125
Table 5.2 The Variation of μ and μ_m with Photon Energy and expressed in terms of the <i>CV</i>	132
Table 5.3 The variation of $D_{1/2}$ depth with energy	133
Table 5.4 List of Soil Samples and References for Chemical Composition used in the Calculation of μ_m	135
Table 5.5 The variation in μ_m with selected energies with soil chemical composition	140
Table 5.6 The Photo-peaks used in Density Correction Efficiency Calibration	147
Table 5.7 Absolute Efficiency Calibration Equations for Sample Self Absorption	148
Table 5.8 Quality Assurance and Calibration Verification	156
Table 6.1 The Sub-Sampling Errors of a Homogenised Gley Sediment	168
Table 6.2 Statistics for Broughton Mains Bulk Sample over a 3 Year Period	170
Table 6.3 Radionuclide Inventory Analysis from SURRC 2m x 2m Sampling Grid	174
Table 6.4 Number of Samples Required for Mean Result to be within 5 and 10% of the True Mean	175
Table 6.5 Longbridgemuir Basin and Valley Peat Inventory Results from a 2m Hexagonal Sampling Plan	177
Table 6.6 Caerlaverock Salt Marsh Inventory Results (1992), 2m Hexagonal Sampling Plan	177

Table 6.7 Calculation of Radial Sampling Pattern for Prismatic Detector at 100m Altitude for ^{137}Cs	180
Table 6.8 Calibration Area Site Selection	180
Table 6.9 Myres Hill Calibration Area Data, Eaglesham Moor Comparison between Soil Core Inventories and 3" x 3" NAI In-Situ Measurements	181
Table 6.10 Lochwinnoch Calibration Pad Data. Comparison between Soil Core Inventories and 3" x 3" NaI In-Situ Measurements	182
Table 6.11 Leana Hill Calibration Pad Data. Comparison between Soil Core Inventories and 3" x 3" NaI In-Situ Measurements	183
Table 6.12 Lakin Farm Calibration Pad Data, Isle of Arran Comparison between Soil Core Inventories and 3" x 3" NaI In-Situ Measurements	184
Table 6.13 The Natural Spatial Sample Weighting of a $\times 2$ Expanding Hexagon	189
Table 6.14 The Natural Spatial Sampling Weighting Sampling Weighting for the Caerlaverock	190
Table 6.15 The Spatially Weighted Mean Activities or ^{137}Cs at Caerlaverock Sampling Site	192
Table 6.16 The Spatially Weighted Mean Activities or ^{137}Cs at Longbridgemuir Sampling Site	193
Table 6.17 Height Correction Coefficients (I_o and a) for Radiocaesium (^{137}Cs and ^{134}Cs)	199
Table 6.18 Height Correction Coefficients (I_o and a) for ^{40}K , ^{214}Bi and ^{208}Tl .	200
Table 7.1 The Change in Mean Mass Depth (g cm^{-2}) across the Caerlaverock Calibration Site	230
Table 7.2 Spectral Components used to Determine a Relationship with Mean Mass Depth of Source Burial	251
Table 7.3 The Change in Mean Mass Depth (g cm^{-2}) Derived from Spectral Data, across the Caerlaverock Calibration Site	252

1. INTRODUCTION

"It is only the half-truths that are dangerous!"

George Bernard Shaw

1.1 RESEARCH IN CONTEXT

Reliable estimates and representative surveys of environmental quantities which have inherently heterogenic distributions have remained a well established problem for earth and environmental scientists. To obtain spatial representations of environmental quantities requires a costly and time consuming collection and examination of a large number of samples. Remote sensing techniques have, to a large extent, overcome these problems with their ability to map spatial distributions of environmental entities. However, interpretation of remote sensing data requires comparison with ground based information. A related problem then arises in comparing environmental measurements derived from spatially restricted samples, with direct field observations with extended spatial characteristics such as those derived from remote sensing techniques. This work examines these widely experienced problems in the context of the measurement of both anthropogenic (^{137}Cs and ^{134}Cs) and natural (K, U and Th) radionuclides.

It is important that measurements made of environmental radioactivity are representative not only in terms of absolute quantity, but also have meaning in terms of their relation to the underlying lateral and vertical spatial distributions of the activity. Traditional techniques for measuring environmental radioactivity have relied upon either passive methods of measurement or more interactive techniques of measuring activity through sampling. This work investigates the measurement of environmental radioactivity through the following three techniques:

- i) Soil sampling with accurate laboratory based gamma ray spectrometry.
- ii) In-situ gamma ray spectrometry.
- iii) Airborne gamma ray spectrometry.

Providing each of these techniques has been appropriately applied, reliable estimates of environmental radioactivity can be made. However, the results may be open to misinterpretation if environmental controls, which can influence each determination, are not considered.

Each of these three different techniques of environmental radioactivity monitoring and measurement has attractions and limitations. Soil sample analysis is required to determine chemical speciation, behaviour and distribution of radionuclides within the soil profile determined. However, the representability of the sample may be in doubt and multiple soil core analysis is often not economically viable for spatial mapping. In-situ and aerial measurements of environmental radioactivity have the advantage of spatially averaging activity within the detectors' field of view and providing estimates of environmental radioactivity very rapidly. Remote sensing through aerial gamma ray spectrometry also has the additional advantage of providing surveys in inaccessible locations and in near real time. However, these passive techniques have the disadvantage of losing source depth profile information within the soil column which can in turn make their interpretation more difficult.

1.2 HISTORICAL APPROACH TO THE MEASUREMENT OF ENVIRONMENTAL RADIOACTIVITY

Pedological investigations have demonstrated that spatial variability is a major factor in explaining the observed variability in field or laboratory based estimates of soil constituents. The study of variability has received considerable attention by soil scientists (e.g. Wilding and Drees 1983, Burgess and Webster 1980, Webster and Burgess 1980, McBratney and Webster 1986).

Radioactive pollution as a result of fallout and marine dissipation and deposition, coupled with the soil's own natural variability in pH, clay and organic content observed by pedologists, can lead to highly heterogenic depositional patterns. As a result, "ad-hoc" or randomly sampled measurements made in response to environmental accidents (e.g. Cambray *et al* 1987) can lead to misrepresentations of the spatial distribution of

activity. It is, therefore, not surprising that discrepancies are observed between different data sets derived from regional soil sampling such as in Scotland (e.g. Miller *et al* 1989, Baxter *et al* 1989) particularly when coupled with contoured surfaces. These problems have been observed in regional random and stratified sampling studies (Horrill *et al* 1988, Horrill and Lindley 1989). Other statistical studies of spatial variability have been undertaken in the USSR (Drichko *et al* 1977, Drichko and Lisachenko 1984), Canada (Sutherland and De Jong 1990) and USA (Sully *et al* 1987), with more detailed small scale and regional studies undertaken by the Nevada Applied Ecology Group (e.g. Fowler *et al* 1974, Gilbert *et al* 1974, Barnes 1978, Barnes *et al* 1980). Few examples exist where spatial variability and sample representability have been studied on a small scale in the UK (e.g. Parkinson and Horrill 1984).

One approach to overcoming sampling error and the problems introduced by spatial variability is to make many rapid in-situ measurements which spatially average the activity distribution. The calibration of in-situ methods for measuring environmental radioactivity introduces a new set of problems. Historically, in-situ gamma spectroscopy systems used for geological exploration relied upon calibrations or sensitivity estimates determined from fixed concrete calibration facilities, typically enriched with ^{40}K , equilibrated U and Th. For aerial survey calibration, these calibrated in-situ detectors are used to quantify calibration areas typically 1 km by 3 km (IAEA 1976, 1979, 1991, Alexander and Kosanke 1978, Løvborg *et al* 1978a). The calibrations were quantified in terms of activity per unit dry weight or as concentration as determined directly from the concrete calibration pads. Comparisons of aerial survey and in-situ gamma spectroscopic measurements with associated soil or sediment samples analysed in the laboratory were often found to be less favourable than comparisons between ground based in-situ measurements and aerial gamma spectroscopy measurements (Darnley 1984, Løvborg *et al* 1978a, IAEA 1976). This was attributed to changes in the environmental conditions between soil overburden and soil type, water concentrations and density, and problems associated with uranium series disequilibrium in the field and within the sample collected and analysed in the laboratory (Alexander and Kosanke 1978). Even in the mapping of a region of exposed rock outcrop with a collimated in-situ NaI(Tl) detector, Løvborg *et al* (1971) observed difficulties in relying

on a calibration derived from rock samples collected with each in-situ measurement. This was due to the heterogeneity of U and Th and their daughters in the rock, and as a result Løvborg relied upon calibrations derived from concrete calibration pads.

Thus, because of these perceived difficulties, geological applications using field and aerial based gamma ray spectroscopy rely on calibrations determined from concrete calibration pads. Comparisons made by Løvborg (1982) between five international calibration facilities provided good traceability between similarly calibrated detection systems for K and Th with a 2 % accuracy, whilst U calibrations were consistent between 4 and 6 %. However, the comparison between laboratory determined soil concentrations and in-situ determinations remains problematic.

With the growth of the nuclear industry and the subsequent dispersal into the environment of anthropogenic radionuclides through weapons testing, licensed discharges and nuclear accidents, these former geophysical techniques were used to monitor gamma emitting anthropogenic radionuclides in the environment. These techniques have been applied to the detection of point sources (Grasty *et al* 1978, Grasty 1980 and Bristow 1978) as well as to the mapping of environmental radioactivity (Williams *et al* 1957 and Chamberlain *et al* 1961, Mellander 1989). Given this new environmental application, the problem of relating in-situ and aerial based gamma spectrometric measurements of environmental radioactivity with soil sample derived estimates reappeared. Calibrations of these instruments based on soil samples proved difficult due to lateral and vertical spatial variability of radionuclide distributions.

The typical solution adopted to determine detector calibrations for anthropogenic radionuclides, principally ^{137}Cs , was to analytically derive solutions through photon fluence equations. Such equations, initially used for uniform geological sources (e.g. Duval *et al* 1971), were modified to account for assumed negative exponential depth distributions of radionuclides in soil (Beck *et al* 1972, 1978, Grasty *et al* 1979, ICRU 1993, Allyson 1994). The photon fluence equation derived by Beck *et al* (1972) has since been extensively applied (e.g. Dickson *et al* 1976, Jacob and Paretzke 1986, Helfer and Miller 1988, Sowa *et al* 1989, Jacob *et al* 1993). However, the assumption

of a constant negative exponential profile can lead to under or overestimation of radionuclide concentrations, and with time the exponential profile assumption will fail.

Thus the problem remains of relating in-situ and aerial gamma spectroscopic measurements of both natural and anthropogenic radionuclides with soil sample derived estimates. Although some of the environmental influences on in-situ and detector response characteristics have been discussed by Kogan *et al* 1971 and IAEA 1976, and quantified through modelling (e.g. Beck *et al* 1972, Beck 1978, Saito and Moriuchi 1985 and Allyson 1994), little until now has been done through experimental work.

Ultimate use of in-situ and aerial based gamma spectroscopy systems relies on the interpretability of the results and this may be best achieved when measurements of environmental radioactivity through different techniques are in agreement. Thus empirical methods of calibration through experimental comparisons with soil sampling techniques provide an effective approach. Similarly, use and interpretation of soil sampling techniques can be best achieved when represented in a spatial context.

1.3 THESIS AIMS AND CONTRIBUTIONS

This thesis examines some environmental factors which must be considered and accounted for to improve the reliability of activity estimates derived from soil sample analysis, in-situ and aerial gamma spectrometry and investigates the relationship between the techniques. Experimental comparisons are therefore made between these three techniques throughout this work under conditions which attempt to isolate the environmental factors of interest.

Chapter 2 discusses the natural (K, U and Th) and anthropogenic (^{137}Cs and ^{134}Cs) radionuclides which due to their abundance, environmental characteristics, environmental implications and their gamma photon yield are of particular interest to this study. It also reviews the environmental controls and their effect on the distribution of these radionuclides in the environment. Chapter 3 discusses the principal methods and techniques of measuring environmental radioactivity through soil sampling followed

by laboratory based gamma spectroscopy. A discussion on in-situ and airborne based detector and system formats along with their characteristic fields of view and spectral behaviour is also given.

The thesis objective is realised through the remaining chapters. Chapter 4 undertakes a case-study to compare the conventional techniques of monitoring environmental radioactivity (including aerial and in-situ gamma spectroscopy and soil sampling followed by laboratory based gamma spectroscopy) with a view to identifying the major factors which influence the relationships between these three techniques across a valley. These techniques were applied systematically to a detailed examination of a narrow "V" shaped valley in Renfrewshire. Soil samples and in-situ gamma ray spectra were collected on a 200 m sampling grid across the valley. Airborne gamma ray spectra were collected using a large NaI(Tl) detector operated from a helicopter. This investigation highlighted several factors requiring further detailed study. In particular, spatial variability of anthropogenic radionuclides was controlled by depositional and redistributive mechanisms providing a significant influence on the estimations of radioactivity across the valley on all three measurement techniques. Examination of the results led to further detailed experimental investigations isolating, quantifying and accounting for these environmental influences. These are discussed in the following chapters.

The observed changes in density and soil type characteristics required an investigation into their potential influence on environmental gamma ray spectrometry. Chapter 5 calculates and measures the effect of changes in soil chemical composition and thus Z_{eff} on the linear and mass attenuation coefficients of soils and their energy dependency. The results are reviewed in the context of laboratory based gamma spectroscopy and soil sampling depth required for effective comparison with in-situ based gamma spectroscopy. These factors are quantified and methods are demonstrated for laboratory based gamma spectrometry which enable systematic corrections to be made for sample self absorption making significant improvements to experimental precision. The calibration of laboratory based detectors is important as these provide the fundamental internationally traceable results (International Atomic Energy Agency, *IAEA*, and

National Bureau of Standards, *NBS*) which form the basis for in-situ and aerial survey detector sensitivity estimates.

The influence of soil sampling error in contrasting sites is then investigated in chapter 6, and its influence on the precision of conventional laboratory based estimates of natural and anthropogenic radionuclide concentrations discussed. Chapter 6 goes on to investigate in detail lateral variability of both natural radioactivity and anthropogenic radioactivity from both atmospheric (weapons testing and Chernobyl fallout) and marine derived sources. Spatially representative sampling plans are developed to enable effective comparisons between soil samples and the fields of view of in-situ and airborne remote sensing techniques to quantify and characterise spatial variability. The sampling plan developed also provides the ability to spatially correct the height correction coefficients.

Having investigated and provided a solution to the problems of matching soil sampling strategies with in-situ and aerial based gamma spectrometric measurements in chapter 6, chapter 7 investigates source burial through different soil types, densities and modes of radionuclide deposition. Source-soil profile shapes are measured and characterised for the different depositional environments and quantified in terms of mass depth (g cm^{-2}). In addition, air path length and its influences on photon fluence are measured from detector response characteristics with laboratory based modelling experiments. Following Zombori *et als'* (1992) observations of forward scattering with point source burial under water, the spectral response characteristics are modelled experimentally. The scattered gamma spectral characteristics are measured in response to burial of an extended layered ^{137}Cs source under perspex sheets. This enabled source burial to be determined and quantified from spectral information and thus provided a spectrally derived calibration correction coefficient. Following further experimental observations to verify full spectral stripping on concrete calibration pads, a spectrally derived calibration correction coefficient is used to account for source burial in salt marsh environments and provide corrected activity estimates (Bq m^{-2}). This is the first practical example of a spectrally derived calibration correction coefficient, providing a technique for the correction of systematic changes in source burial. This potentially

provides a technique for surmounting the traditional handicap of in-situ gamma ray spectrometry.

The main conclusions from this thesis and the contributions it makes to the field of measuring environmental radioactivity are discussed in chapter 8.

1.4 SUMMARY

The environmental factors which control the spatial lateral and vertical distribution of radioactivity in soils have considerable influence on the estimation of environmental radioactivity through soil sampling and laboratory analysis, in-situ and aerial based gamma spectroscopy. These factors are rarely accounted for in environmental radioactivity studies and are crucial when direct comparisons are to be made between soil sampling, in-situ and aerial survey techniques.

Having made experimental comparisons between soil sample derived estimates of environmental radioactivity and in-situ and aerial determinations and the discrepancies in doing so, this thesis presents feasible solutions to reducing these difficulties and determines calibrations and calibration corrections which are readily interpretable in terms of source burial characteristics. In this way corrected comparisons may be made between in-situ, aerial and laboratory based gamma spectrometric estimates of environmental radioactivity with increased reliability. Objective radioactive environmental impact assessment is reliant upon reliable and representative estimates of activity, requiring the spatial vertical and lateral extent to be measured. This is best achieved by the combined use of soil sampling techniques with laboratory based gamma spectrometric analysis, in-situ gamma spectrometry and airborne gamma spectrometry. However, in doing so, these techniques must be used in a mutually compatible manner.

2. THE ORIGIN AND DISTRIBUTION OF GAMMA EMITTING RADIONUCLIDES

2.1 INTRODUCTION

This chapter discusses the main radionuclides of interest, their origin and the environmental controls which affect their distribution in the environment, such as depositional mechanisms and assimilation into soils. These environmental controls lead to factors which can influence radioactivity estimation through soil sampling with laboratory based gamma analysis, in-situ and aerial gamma ray spectrometry.

2.2 THE SOURCES OF RADIONUCLIDES AND RADIATION

2.2.1 Primordial Radioactivity and Natural Sources of Radionuclides

Of the primordial radionuclides, ^{40}K , ^{238}U and ^{232}Th are of importance due to their abundance and relative ease of detection and measurement through their daughter products and their characteristic gamma photon emission (table 2.1). The different geochemical and geophysical behaviour of these three radionuclides and their decay series makes them useful for characterising geological formations.

Primordial radionuclides are those which appeared at the time of the formation of the Earth. As the Earth is about 4.7×10^9 years old, radionuclides with a half life of 10^8 years or greater will still be present in measurable quantities. There are four transuranic decay series which are genetically independent, the thorium, uranium, neptunium and actinium series. The transuranium elements with $Z > 92$, for example neptunium (^{239}Np and ^{239}Pu), are too unstable to be found in great quantities today. However, they are found in small quantities via natural nuclear reactors such as the Oklo natural fission reactor through fission bombardment of ^{235}U (Myres and Lindner 1973, Durrance 1986).

The neptunium decay series no longer exists in nature and the actinium series having

its longest lived member ^{235}U (7.13×10^8 years) is in very low abundance relative to ^{238}U . The neptunium and actinium series are not considered further here.

In the thorium series, the longest lived member is ^{232}Th with a half life of 1.39×10^{10} years permitting it to occur naturally. Geophysical evidence suggests that ^{236}U and even ^{240}Pu were present when the Universe was young of which ^{232}Th is now a decay product. ^{236}U is no longer present due to its short half life of 2.4×10^7 years (Ivanovich and Harmon, 1982). ^{232}Th has a very long half life and decays via α particle emission to ^{228}Ra . The decay of ^{228}Ra is via β emission and is rather weak and difficult to detect, being obscured by its daughter ^{228}Ac . ^{228}Ac decays rapidly ($T_{1/2} = 6.13$ hrs) via a number of electrons and associated γ rays to ^{228}Th . ^{228}Th is also a decay product through α decay of ^{232}U and electron capture of ^{228}Pa (Ivanovich and Harmon, 1982, Lederer and Shirley, 1979). The remaining members of the decay series are all short lived decaying via α particle decay to ^{212}Pb which is the longest lived member of the remaining decay series with a half life of 10.64 hours. ^{212}Pb decays via β emission to ^{212}Bi of which 33.7 % decays to ^{208}Tl via α particle emission and 66.3 % decays to ^{212}Po via β emission. Both ^{208}Tl and ^{212}Po decay to the stable end product of the $4n$ decay series of ^{208}Pb . Further details of this series can be found in Lederer and Shirley (1979), whilst the principle gamma photon energies are shown in table 2.1.

The Uranium series is the longest known series, starting with ^{238}U , and passing twice through $Z=92$ via an α and β decay sequence. ^{238}U has a long half life of 4.47×10^9 years which permits it to exist naturally today and its abundance is 99.27 %. ^{238}U emits α particles only. β emission is introduced by the immediate daughters of ^{234}Th and ^{234}Pa . 98% of the ^{234}Pa decays directly to the ground state of ^{234}U , whilst the isomer of ^{234}Pa exhibits a complex β , γ and conversion electron spectrum. A series of four α emissions follows through ^{230}Th , ^{226}Ra , ^{222}Rn and ^{218}Po . The next series of decays occurs via a mixture of α and β decays and predominates through ^{214}Pb , ^{214}Bi , ^{214}Po , ^{210}Po and ^{210}Tl and rapidly reach equilibrium with ^{222}Rn . The series decays through 2 β 's and α particle emission to ^{206}Pb . The principal gamma photon energies for the U decay series are shown in table 2.1.

Table 2.1 Primordial radionuclides and gamma rays of interest.

Radionuclide/ daughter product	Half Life	Gamma Ray Energy KeV	Gamma Yield > 2%		
⁴⁰ K	1.26 x10 ⁹ yr	1460.83	10.67		
²³⁸ U	²³⁴ Th	63.28	3.8		
		²²⁶ Ra	1620 yr	188	4
		²¹⁴ Pb	26.8 min	241.9	7.46
	²¹⁴ Bi	19.9 min	295.1	19.2	
			351.9	37.1	
			609.31	46.1	
			768.35	4.9	
			934.04	3.16	
			1120.3	15	
			1238.1	5.92	
			1377.7	4.02	
			1408.0	2.48	
			1509.2	2.19	
			1764.5	15.9	
	²¹⁰ Pb	22.3 yr	1847.4	2.12	
			46.52	4.05	
	²³² Th	²²⁸ Ac	6.13 hr	105.36	2
			129.03	2.9	
			209.39	4.1	
			270.26	3.8	
			328.07	3.5	
			338.42	12.4	
			463.1	4.6	
			581.52	< 3	
			794.79	4.6	
			911.6	29	
			968.97	17.4	
			1588.23	3.6	
²¹² Pb			10.64 hr	238.57	43.6
				300.03	3.34
²¹² Bi			1.009 hr	727.25	6.65
²⁰⁸ Tl 33.6%	3.053 m	277.28	6.8		
		510.606	21.6		
		583.022	86		
		860.3	12		
		2614.35	99.79		
²¹⁰ Po	22.3 yr	46.52	4.05		

Of all the other long lived primordial radionuclides occurring in nature, ^{40}K is the only one which exists in abundance and is readily detectable through its gamma emissions. 11% of ^{40}K decays to ^{40}Ar via β^+ and a 1.46 MeV γ ray emission and 89% decays to ^{40}Ca via β^- decay (Lederer and Shirley 1979).

Other contributions to the natural radioactive background are from cosmic rays. Cosmic rays are of importance to this study as they form part of the natural background to both laboratory based, in-situ and aerial gamma spectroscopy. They are high energy charged particles of which 87% are protons, 12% are α particles and 1% are heavier nuclei typically Li, Be, B, C, O and F (Durrance 1986) which rain down upon the earth and originate from the stars. Their energies typically vary from a few MeV to 10^{14} MeV. The lower energy or softer components typically ionise the atmosphere and are stopped, whilst the others (primaries) undergo collisions with the nuclei of atmospheric gases and produce new subatomic particles (secondaries) via spallation.

2.2.2 Fission and the Production of Anthropogenic Radionuclides

This section addresses the use of uranium and plutonium in the nuclear fuel and nuclear weapons cycle and the additional sources of radionuclides they create.

Nuclear Fuel Cycle

The nuclear fuel cycle involves mining of uranium ore, milling to economically transportable sizes, chemical conversion and purification, enrichment of ^{235}U to 3% for fuel fabrication for reactor operation and over 90% for weapons manufacturing. Following use in the reactor, the fuel elements must be stored to allow decay of short lived fission fragments and then either disposed of or reprocessed to separate unused fissile material from waste products. Due to the lack of abundance of ^{235}U , it is thought to be economically advantageous to reclaim unused ^{235}U and ^{239}Pu which is fissile and is formed in the reactor from neutron capture of ^{238}U , where $^{238}\text{U} + n \rightarrow ^{239}\text{U} \rightarrow \beta \rightarrow ^{239}\text{Np} \rightarrow \beta \rightarrow ^{239}\text{Pu}$. An alternative addition to the cycle is through natural thorium to produce fissile ^{233}U , through the reaction sequence $^{232}\text{Th} + n \rightarrow ^{233}\text{Th} \rightarrow \beta \rightarrow ^{233}\text{Pa} \rightarrow \beta \rightarrow$

^{233}U . The production of ^{239}Pu and ^{233}U is termed "breeding".

^{235}U and ^{239}Pu are principally used in nuclear reactors due to their high *fission* probability. The addition of a neutron to ^{235}U produces ^{236}U , which is unstable and tends to split the nucleus into two fragments of roughly equal mass, as well as releasing a large amount of energy (approximately 200 MeV per fission) and two or three neutrons. The decay energy is absorbed within the reactor vessel as heat which is used to turn turbines for electricity generation through steam. This nuclear chain reaction is controlled in a nuclear reactor, as the speed with which this chain reaction takes place is dependent upon the density and geometry of the fissile material and the presence of materials which will slow or moderate the neutrons or capture them. This is typically carried out by neutron absorbing rods which can be lowered into the reactor core. At concentrations of 3 % ^{235}U , many of the neutrons are captured by ^{238}U which subsequently forms ^{239}Pu .

Table 2.2 Fission Products of Potential Biological Importance

Radio-nuclide	Fission yield (%)	Radiation	Half-Life	Important element analogues
^3H	0.01	β	12 year	H
^{85}Kr	0.29	β, γ	10 year	
^{89}Sr	4.79	β	51 year	Ca
^{90}Sr	5.77	β	28 year	Ca
^{91}Y	5.4	β, γ	58 day	
^{95}Zr	6.2	β, γ	65 day	
^{103}Ru	3.0	β, γ	40 day	
^{106}Ru	0.38	β, γ	1.0 year	
^{129}I	0.9	β, γ	1.7×10^7 year	I
^{131}I	3.1	β, γ	8.1 day	I
^{137}Cs	6.15	β, γ	30.2 year	K
^{144}Ce	6.0	β, γ	285 day	
^{140}Ba	6.32	β, γ	12.8 day	Ca
^{143}Ce	5.7	β, γ	33 hr	

The vast majority of the fission fragments range in mass number from 72 to 158 and include some two hundred radionuclides of 34 different elements. The most probable

fission fragments will have mass ranges between 90 to 106 and 134 to 144. A small fraction of fissions are ternary and produce light nuclei, including ^3H . Table 2.2 shows some of the more biologically important fission products.

Table 2.3 Some Neutron Activation Products of Biological Significance in Nuclear Reactors.

Radionuclide	Radiation	Half-Life	Important Elemental Analogues
^3H	β	12.3 year	H
^{14}C	β	5568 year	C
^{24}N	β, γ	15 hr	Na
^{32}P	β	14 day	P
^{35}S	β	87 day	S
^{41}Ar	β, γ	110 min	
^{45}Ca	β	164 day	Ca
^{54}Mn	γ	291 day	Mn
^{55}Fe	X (EC)	2.6 year	Fe
^{59}Fe	β, γ	45 day	Fe
^{57}Co	γ	270 day	Co
^{58}Co	β^+, γ	71 day	Co
^{60}Co	β, γ	5.2 year	Co
^{65}Zn	β^+, γ	245 day	Zn
^{134}Cs	β, γ	2.1 year	K
^{239}Pu	α, γ	24,360 year	
^{239}Np	β, γ	2.3 day	
^{241}Am	α, γ	470 year	
^{242}Cm	α, γ	163 day	

EC: *electron capture*

Radionuclides produced in the reactor are termed *anthropogenic* or man made. These not only include fission products but also neutron activation products which include elements as light as tritium to as heavy as plutonium, americium and curium. Neutron activation occurs with non fissile nuclei. The quantity and type of activation products produced are governed by the neutron flux, the range of elements within the fuel, the coolant and the structural parts of the reactor within range of the neutrons. Table 2.3 illustrates some of the biologically significant activation products.

The gradual build up of fission products in the reactor core limits the extent of burn-up that is practical and damages the fuel structure (Billington 1959). Many of the fission products have fairly high neutron capture cross sections and poison the core by absorbing the neutrons' productivity. Thus the fuel rods are removed after about 75 % of the ^{235}U has been consumed. After 3 to 6 months storage the fuel is then sent to reprocessing plants to recover ^{235}U and ^{239}Pu (Eichholz 1977).

In addition to the disposal of waste, some of the reactor core inventory does escape due to the inevitable impossibility of maintaining perfect integrity with fuel elements, pipes, fuel cladding and many other solid barriers during the nuclear fuel cycle. The significant fission products, activation products and transuranium products are listed in tables 2.2 and 2.3.

Nuclear Weapons

Nuclear explosions differ according to the type of reaction; nuclear fission, nuclear fusion or a combination of the two. In a nuclear fission weapon (atom or nuclear bomb), much higher concentrations of ^{235}U or ^{239}Pu are required to create a critical mass. Thus when two subcritical masses are forced together with the appropriate geometry and length of time with a lack of neutron absorbing material, the chain reaction can be explosive. A nuclear explosion equivalent to 1000 ton of TNT would require 56 g of fissile U or Pu. These devices produce a large quantity of fission products and are termed the dirty bomb. Nuclear fusion and the thermonuclear bombs (H bomb) produce less radioactivity. Fusion reactions involve the coalescence of light nuclei forming heavier nuclei. They are termed thermonuclear because they operate at temperatures of several million degrees. Thus to achieve these temperatures, a fission explosion or detonation is required. A large number of neutrons are released upon detonation from the fission and fusion reactions, resulting in activation of the surrounding materials, as well as the generation of fission products. The effects of thermonuclear bombs are, therefore, "cleaner" than nuclear bombs (Hunt 1980, Whicker and Schultz 1982, Kogan et al 1971).

In a nuclear explosion, tremendous quantities of heat are produced within a small fraction of a second. The fission fragments, structural fragments of the bomb and the immediate surroundings are raised to several million degrees and vaporized to form a *fireball*. If formed on or above the earth's surface, the *fireball* expands and begins to rise into the atmosphere reaching 20 or 30 km in altitude. As it rises it cools allowing the vaporized materials to condense into droplets which fall back to earth.

Anthropogenic Radionuclides of Interest

The anthropogenic radionuclides of particular interest to this work are those which emit gamma radiation of sufficient energy and gamma yield and are present in sufficient quantities to be readily detected in the field as well as within samples analyzed in the laboratory. Fission of uranium creates two unequal halves, fission products, which tend to concentrate across certain mass numbers. ^{137}Cs and ^{131}I are of particular interest because of their biological and chemical importance as well as initial abundance (Kaye and Labey 1991, Whicker and Schultz 1982). Activation products which are readily measured in the environment are ^{241}Am , ^{134}Cs and ^{60}Co . This discussion has been made with reference to Lederer and Shirley (1979) and Browne and Firestone (1986).

^{137}Cs is formed as a consequence of fission within nuclear reactors and forms from the decay of ^{137}Xe which decays with a half life of 3.82 min to ^{137}Cs via β particle emission and a complex series of low yield gamma-rays. ^{137}Cs itself decays via β particle decay of which 85.21 % of the decays result in a gamma ray of energy 661.165 keV and is also associated with a 32.9 keV ^{137m}Ba X-ray which forms the stable ground state.

^{134}Cs has a more complicated decay scheme. It is an activation product and forms the first nuclide in the decay scheme. ^{134}Cs has a half life of 2.062 yrs of which 99+ % decays to ^{134}Ba via β^- decay and a complex of gamma emissions. However, about 3×10^{-4} % of the decays are via electron capture (E.C.) to ^{134}Xe . From each of four β decays series, the nucleus is left in an excited state, from which energy is lost to reach its ground state via γ -ray emission, resulting in two principle gamma rays at 604.66 keV (97.56%) and 795.76 keV (85.44%).

^{241}Am forms as a result of β^- decay from ^{241}Pu which is a neutron activation product and also forms by electron capture of ^{241}Cm . ^{241}Am has a half life of 432.7 yr and decays via α -particle decay and γ -ray emission to ^{237}Np . The principle gamma ray of interest is at 59.54 keV with a 35.7 % yield.

In the event of a nuclear accident, the distributions of ^{131}I and ^{60}Co are of particular importance, although the latter occurs usually in small concentrations. ^{131}I is of particular biological significance due to its potential thyroid dose (Fry and Milton 1986). It decays to ^{131}Xe via β and gamma (364 keV, 84 % yield) with a half life of 8 days. ^{60}Co has a half life of 5.272 years and decays into ^{60}Ni via β decay with an end energy of 0.315 MeV for 99.88% of the decays. This is followed by a gamma at 1.173 MeV and another gamma ray at 1.332 MeV, both with almost 100 % yield.

2.3 THE DISTRIBUTION OF RADIONUCLIDES IN THE ENVIRONMENT

This section discusses the distribution of the primordial and anthropogenic radionuclides in the environment. The distribution of radionuclides is dependent upon their pathway or emplacement into the environment and soil and the subsequent weathering, erosion and remobilisation processes acting on the soil. Their distribution is also governed by the chemical characteristics of the radionuclide elements.

2.3.1 Primordial Radionuclides

The distribution of primordial radionuclides is principally dictated by the underlying geology. The concentration of K, U and Th is controlled by their physical and chemical behaviour and upon rock forming processes, ie, crystal fractionation in igneous rocks, metamorphic and hydrothermal processes, and erosion and depositional mechanism forming sedimentary rocks.

^{40}K is an isotope of natural potassium and is the most common naturally occurring radioactive element. It is homogeneously mixed with potassium with an isotopic abundance of about 0.0118 % by mass. K is an alkali metal and is thus easily oxidised.

Its chemical behaviour is very similar to that of Na and thus both form essential constituents of the alkali feldspars and feldspathoids. However, K and Na have different ionic radii ($\text{Na}^+ = 1.10 \text{ \AA}$, $\text{K}^+ = 1.46 \text{ \AA}$) and thus compete with each other under different temperatures and pressures in rock forming minerals (Cox *et al* 1984). Plagioclase feldspars concentrate more Na than K whilst the reverse is true of biotite micas. Hence, the distribution of K follows very closely the distribution of silica and the alkali rich minerals and the $\text{K}_2\text{O}/\text{Na}_2\text{O}$ ratio increases with alkali content. The absolute K content in sedimentary rocks depends mainly upon the relative proportions of feldspars, mica and clay mineral aggregate content, and is thus dependent upon the composition of the source rock and the proximity to it. Typical ^{40}K concentrations are demonstrated in table 2.4.

Uranium and Thorium have strong electronegativity and display strong lithophile characteristics. U most commonly occurs as oxides, hydroxides, phosphates, carbonates, sulphates arsenates, vanadates, molybdonates and silicates and tends to have affinities with hydrocarbon complexes. Th has a strong tendency to form ions with chloride, fluoride, nitrate, sulphate, carbonate and hydroxide, whilst silicate, phosphate and organic complexes are also possible, although they render Th mobile under certain pH and Eh conditions. They both form strong ionic bonds, though covalent and semi-metallic structures also occur. U can exist in four valency or oxidation states, U^{3+} , U^{4+} (uranous), U^{5+} and U^{6+} (uranyl), whilst Th only exists in one oxidation state Th^{4+} and is generally insoluble in water. Geochemically, at high temperatures, U and Th are similar and undergo mutual substitution particularly where there is a lack of water. Under low temperature processes where water prevails, UO_2 ore contains much lower concentrations of Th (Durrance 1986, Ivanovich and Harmon 1982).

Igneous Rocks

In comagmatic suites of igneous rocks, U and Th appear to follow the usual differentiation sequence, with concentration increasing with silica and potassic content. This occurs because their large ionic radii preclude them from early crystallising silicates. Thus granites are enriched with U and Th by several orders of magnitude

over oceanic rocks. U/Th ratios are between 3 and 4 for crustal rocks and between 1 and 2 for primitive basalts (undifferentiated mantle material) suggesting some crustal enrichment of U over Th during crustal evolution. The Th/K ratio tends to remain constant at about 3×10^{-3} for a large variety of igneous rocks.

U and Th are distributed in igneous rocks in three ways: i) by cation substitution in the silicic lattice of major rock forming minerals; ii) as a minor or major component of accessory minerals also intimately associated with biotite mica; iii) by absorption onto lattice defects or on crystal grain boundaries.

Table 2.4 illustrates typical U and Th concentrations in igneous rocks. Generally, U and Th tend to be evenly distributed within fine grained intrusive igneous rocks whilst they tend to be concentrated towards the periphery of coarse grained batholiths and stocks. Volcanic rocks tend to have higher concentrations of U and Th than their plutonic equivalents.

Sedimentary Rocks

The distribution of U and Th in sedimentary rocks is dependent upon the chemical and physical conditions under which the sediments are transported and deposited. Weathering of rock releases U easily due to its solubility in water. Other minerals such as monazite and uraninite are not readily weathered in-situ, but are reduced by attrition during transportation. During water transportation, U can be removed from solution by precipitation, absorption or extraction by organisms. Uraniferous compounds are precipitated in reducing environments.

U in sediments may be deposited: i) indigenously to clastic sediments, ii) simultaneously with clastic sediments and/or iii) epigenetically after sedimentation has ended in fractures or porous formations, usually in a reducing environment (Osburn 1965). Most clastic sediments contain low concentrations of U (0.5 to 4 ppm) whilst, because of low Th solubility in water, Th concentrations are dictated by the source rock concentrations and both exist as resistates. The primary U and Th tends to decrease

Table 2.4. Geological U, Th and K concentrations. *After Ivanovich and Harmon (1982), Durrance (1986), Harmson and De Haan (1980), Wollenberg et al (1994, 1969), Wollenberg and Smith (1990) and Osburn (1965).*

Rock Type Class	U ppm	Th ppm	Th/U	% K
Igneous				
Granites	15-120	40	3-4	2-3.5
Rhyolites	2.2-20	8-33	3-6	3.7
Andesites	2.1	6.7	3	2
Gabbros	0.8	3.8	4	0.2-0.9
Basalts	0.1-1	0.2-5	1-5	0.7
Ultramafics	<0.015	<0.05	variable	0.8
Metamorphic				
Eclogites	0.3-3	0.2-0.5	2-4	
Granulites	4.9	21	4	2-4
Gneiss	2	5-27	1-30	
Schist	2.5	7.5-19	>3	
Phyllite	1.9	5.5	2.8	3
Slate	2.7	7.5	2.8	
Sedimentary				
Quartzite	0.45-3.2	1.5-9	1.6-3.8	
Arkoses	<1-3	5	2-6	4-5
Greywackes	0.5-2	1-7	~2	4.8
Shales	2-4	10-13	2.7-7	4-6
Bauxite	11.4	4	~5	
Limestones	~2	<2	<1	2
Dolomites	0.03-2			
Evaporites	<0.01	<1		3.6
Lithosphere Mean	3-4	8-12	3	4.5
Soil Mean	1-2	6	3	2
Soil Range	1-4	2-12	3	1.4-2.2

with distance travelled before deposition. However, some sandstones contain high concentrations of Th because of sorting processes which concentrate minerals according to their density such as monazite, apatite and xenotime forming placer deposits. Carbon rich black shales and schists contain high concentrations of U (400 ppm) and tend to occur either as a coating around mineral or organic particles or as disseminated masses throughout the rock matrix (Durrance 1986 and Ivanovich and Harmon 1982).

Humic substances are particularly important in enriching U with respect to Th in recent sediments. Organic deposits formed from bituminous and sapropelic materials contain little U. Fixation of U by cation exchange is thought to be the concentrating process which occurs after the death of the plant (Ivanovich and Harmon 1982). The uranyl ion may subsequently be reduced to the uraneous state because of a decrease in oxidation potential (Eh) upon burial. H₂S may also bring about reducing conditions due to decomposition of the organics themselves.

Metamorphic Rocks

Metamorphic reworking of U rich rocks often results in the U concentrating into segregation associated with minerals such as uraninite, uranothorite and allinite. This has been observed in gneisses and graphitic schists where uraninite occurs in discrete layers. Uranium mobilisation in regional metamorphism takes place in hydrous phases, where U is precipitated from high temperature solutions. Th concentrations are highly variable and are generally dependent upon the original concentration in the rock prior to metamorphism. However, with increasing temperature, pressure and partial melting, Th is concentrated into the liquid phases more readily than U. There is a decrease in Th/U ratio with increasing grade of metamorphism although the overall U and Th content of metamorphic rocks decreases with increasing grade (table 2.4). U may thus also be concentrated in skarns and hornfels of contact aureols.

U and Th Enrichment to Economic Grade

The principle economic sources of U are the uranous oxides, uraninite (UO₂), and pitchblende (UO₂ to U₃O₈) and the silicate, coffinite (USiO₄), and are thought to have been formed by precipitation from hydrothermal solutions or ground waters in a reducing environment. The majority of U mineralization has occurred along veins. As U is extremely mobile, reworking and recrystallisation can occur at any time after emplacement. Thus either meteoric water or magmatic hydrothermal water and fluids can dissolve U and reprecipitate it at a redox front. Leaching of U from the Hercynian granites of southwest England and kaolinisation process was considered to be a product

of thermal draw-down of meteoric water carrying CO₂. The dissolved and transported U then appears to have been deposited in zones of upwelling. Also the oxidation processes of meteoric water remobilises U deposited in anoxic conditions within sandstones. Precipitation often occurs at the boundary of oxygenated ground waters carrying U meeting O₂ deficient waters or where the oxidation potential of the water is reduced. Similar processes led to U mineralization around the Criffel pluton in southwest Scotland (Scott *et al* 1991, Miller and Taylor 1966).

Economic deposits of Th are found with the silicates, thorite (ThSiO₄) and throgumite (Th(SiO₄)_{1-x}(OH)_{4x}), and the oxide, thorianite (ThO₂). However, the most important rare earth orthophosphate, monazite, is the most important economic source because of its frequent occurrence as placer deposits in detrital sands.

2.3.2 Anthropogenic Radionuclides

Anthropogenic radionuclide releases into the environment are distributed through natural atmospheric, erosional and tidal processes. Subsequent depositional patterns may be characteristic of whichever environmental processes and pathways predominate.

In terms of global pollution, the radionuclides introduced into the atmosphere from weapons testing during the late 1940's, 50's and 60's, when the majority of weapons testing took place above the ground, are likely to have been the most significant contribution to environmental radioactivity levels. However, incidents such as Chernobyl created pollution levels which are important on a continental scale, with some fractional contribution to world wide levels. Local incidents, such as the 1957 Windscale fire and licensed discharges of radioactivity into the environment such as the Irish Sea, are of major importance on a local scale whilst contributing very little to the global environmental radioactivity levels through dispersal. Thus the importance of these incidents is governed by the quantities of radioactivity involved as well as their pathway, distribution and dilution.

Weapons Testing Fallout

Atmospheric testing of nuclear weapons made a significant input to environmental radioactivity during the mid fifties and early sixties until the partial test ban treaty in 1963. Atmospheric testing produced 10^9 TBq of ^{131}I , 10^6 TBq of ^{137}Cs and about 5×10^5 TBq of ^{90}Sr (Fry, 1987 and UNSCEAR, 1982). The pollution from nuclear explosions may be termed *local* or *global*. The degree to which either the local or global environments are affected depends upon the relative amounts of material which can be termed local, tropospheric or stratospheric fallout. This in turn depends upon the magnitude and origin of weapons detonation.

Local fallout is produced by particles larger than 10 microns and these typically have track lengths of several hundred kilometers, depending upon the conditions of the explosion. The residence time of the particles in the atmosphere is of the order of hours to days (Gilbert *et al* 1974, Barnes 1978, Barnes *et al* 1980).

Tropospheric fallout (30 to 60000 feet) is composed of particles up to 10 microns in size. The half-residence time of the particles in the troposphere is typically 20-40 days and they can travel several times around the earth. Rain removes between 70 and 80 % of the radioactive products from the troposphere via precipitation scavenging, whilst 20-30 % is removed by dry fallout due to turbulent dispersion of aerosols and their interaction with topography and vegetation (Eichholz 1977). The interaction of weather patterns with topography and scavenging via precipitation can lead to "hot spots". The most important constituents of tropospheric fallout with respect to dose delivered would include some of the radionuclides with intermediate half lives, such as ^{131}I , ^{140}Ba , ^{147}Nd , ^{133}Xe , ^{103}Ru , ^{95}Zr , ^{141}Ce and ^{90}Sr (Kogan *et al* 1971, Whicker and Schultz 1982).

Stratospheric fallout (60000 to 160000 feet) consists of particles up to 1 micron in size which enter the stratosphere with high altitude explosions or high yield explosions at the earth's surface. The majority of worldwide fallout produced is stratospheric in origin and the products of explosions may remain in the stratosphere for up to 5 years. This enables many of the shorter and intermediate-lived radionuclides to decay allowing

the longer-lived materials such as ^{90}Sr , ^{137}Cs , ^{144}Ce and ^{14}C to become more important (Whicker and Schultz 1982 and Kogan et al 1971).

Nuclear Industrial Accidents

The first recorded nuclear incident was that of the Windscale fire in October 1957. Table 2.5 illustrates activities of isotopes released from the Windscale fire via a 400 ft high stack (Beattie 1981). At the time coastal areas were contaminated with ^{131}I and milk consumption was banned in the area for a few weeks. Today ^{137}Cs from the Windscale Fire is still measurable in the Lake District (Sanderson *et al* 1989).

Table 2.5 Activities Released from the Windscale Reactor Accident, 1957. *after Beattie (1981)*.

Iodine-131	740 TBq	Strontium-89	2.96 TBq
Tellurium-132	444 TBq	Strontium-90	74 GBq
Caesium-137	22.2 TBq	Cerium-144	2.96 TBq
Ruthenium-106	2.96 TBq		

Two other minor accidents have occurred since Windscale. In 1961 a water-steam explosion at the National Reactor Testing Station (Idaho Falls) caused the release of 2.96 TBq of ^{131}I , 18.5 GBq of ^{137}Cs and 3.7 GBq of ^{90}Sr . In 1979 the Three Mile Island accident received wide media coverage following the release of 0.592 TBq of ^{131}I and noble gases from a stack. However, these accidents produced small radiation doses to the public.

A single example of a severe nuclear accident was brought to the world's attention when the Nuclear Power Unit 4 of the Chernobyl plant in the western Ukraine was allowed to overheat resulting in two explosions and a fire. Most of the activity was released over a period of 10 days between the 26th April and 5th May, 1986, although much lower releases persisted until September 1986, when the power plant was effectively sealed. Almost all the noble gases escaped and between 10 and 20 % of the more volatile elements such as iodine and caesium and a few percent of other fission

and activation products were released. Table 2.6 illustrates the estimated quantities of the more volatile products released.

Table 2.6. Chernobyl Releases. *After Fry (1987).*

	Activity - TBq	
	1 st day	10 days
¹³¹ I	1.7x10 ⁵	4.4x10 ⁵
¹³⁴ Cs	5x10 ³	2.5x10 ⁴
¹³⁷ Cs	1x10 ⁴	5x10 ⁴
⁹⁰ Sr	500	9x10 ³
²³⁹⁺²⁴⁰ Pu	100	700

Beardsley (1986) suggested that as much as half of the initial release from Chernobyl was borne to a height of over 3 km or more through an inversion layer, and hence Chernobyl derived caesium was detected in Japan (NEA. 1987). However, although the heat of the fire caused considerable plume rise, the rest of the initial release was injected at lower

altitude and its movement determined by surface winds. During this time a complex and varying set of meteorological conditions developed over Europe dispersing the cloud over a very wide area. Consequently, it was Europe which received the majority of the contamination from Chernobyl, although two other segments of the cloud were detected at some distance, one in North America and the other in China and Japan (Clark and Smith 1988b, Clark 1986b, Królas *et al* 1987, Smith and Clark 1986, 1989, Papastefanou *et al* 1988, Roca *et al* 1989, Veen and Meijer 1989, Meijer *et al* 1990). Measurements by Michio *et al* (1991) suggested that Chernobyl derived fallout from the stratosphere continued until the end of 1988.

Deposition from the contaminated cloud resulting from Chernobyl was very uneven, both within and between European countries. This was primarily due to the interaction of the cloud with frequent and heavy localised precipitation, thus enhancing deposition (Clark, 1986b, Clark and Smith 1988a) as well as the interaction of the cloud with topography. The highest levels of deposition outside Chernobyl occurred during convective storms where heavy rainfall and associated strong air currents swept material from the surrounding air into the clouds and were effective in depositing material in localised areas (NEA 1987). Hence, initial distribution patterns within the UK were estimated with meteorological data in conjunction with some sporadically collected soil core data (Clark and Smith 1988a,b). As acknowledged, this technique has its

limitations as rainfall can vary considerably over small distances and rainfall stations tend to be based in accessible lowland locations which do not provide a representative spatial distribution. In addition, as suggested by Clark and Smith (1988a), deposition patterns between ^{131}I and ^{137}Cs are likely to be very different, because ^{137}Cs was present in particulate form with wet deposition mechanisms dominating, whilst ^{131}I was present in particulate and vapour phase and thus both wet and dry depositional mechanisms were important. Hence the geographical distributions were likely to be different, resulting in a $^{131}\text{I}/^{137}\text{Cs}$ ratio of 18 in areas of little rain and $^{131}\text{I}/^{137}\text{Cs}$ ratio of 3.5 in areas of high rainfall.

Nuclear Discharges into the Environment

In the UK there are four major organisations involved in the nuclear fuel cycle which discharge radioactive effluents into the environment. These include: i) British Nuclear Fuels plc (BNF), ii) Nuclear Electric, iii) Scottish Nuclear, and iv) the United Kingdom Atomic Energy Authority (AEA Technology).

Of these operators, the Sellafield site now operated by BNF plc has provided by far the most significant contribution to the total inventory budget discharged to the Irish Sea. Most of the liquid waste from Sellafield which is of a high level is routed to interim storage and is converted into vitrified glass waste. The medium active waste is routed to a salt evaporator and stored. The remaining low level waste is discharged to sea via the pipe line. This waste originates from storage ponds associated with the magnox reactor decanning plant, the storage of oxide fuel at the Thermal Oxide Reprocessing Plant (THORP) and minor waste originating from laundry effluent. There has been a significant decrease in marine pipeline discharges into the marine environment from 8500 TBq (1975 peak) to 62.3 TBq (1991) per annum for β and 180 TBq (1973 peak) to 2.1 TBq (1991) per annum for α .

However, the proposed start of THORP operations in 1994 following licensing, would see the total reprocessing throughput rise, particularly with increased releases to sea of tritium. Since the early 1980's, medium active waste has been accumulated on site,

allowing shorter lived radionuclides such as ruthenium-106 to decay. With the use of the Enhanced Actinide Removal Plant (EARP), commissioned in late 1992, most radiologically significant radionuclides (plutonium and americium) will be removed with a high efficiency from this waste. However, radionuclides such as technetium-99, with a long half life will remain after treatment. Hence β discharges into the environment will rise to about 300 TBq by the year 2000.

Radioactive discharges to the atmosphere also take place from Sellafield via stacks. Aerial discharges consist principally of ventilation air from the processing plants and Calder Hall. The radioactive content comprises noble gases (e.g. argon and krypton), and other gases and vapours (e.g. hydrogen, iodine and carbon dioxide) and suspended particulates. Particulate filters are used to reduce quantities of radioactivity discharged. Resuspension of material from storage ponds and other places contributes to atmospheric discharges and is detected at the site perimeter. There has been a similar reduction in atmospheric discharges since the 1970's. Numerically, discharges are dominated by tritium, argon-41 and krypton-85.

MacKenzie *et al* (1987) showed the sediments of the Irish Sea and coastline to be contaminated to globally significant levels. Much work has been undertaken to determine the behaviour and distribution of radionuclides (eg. Garland *et al* 1988, 1989, Baxter *et al* 1989, Cook *et al* 1984) and hot particles (e.g. Hamilton and Clifton 1987) within and around the Irish Sea along with potential uptake into the food chain. Sea to land transfer of Sellafield derived radionuclides via sediments and in particular sea spray has also been studied by, for example, Hursthouse *et al* (1991), McDonald *et al* (1990), McKay and Pattenden (1990) and Eakins *et al* (1981).

2.4 THE CHEMICAL BEHAVIOUR OF RADIONUCLIDES IN SOILS

Once deposited into the environment, the behaviour of the radionuclides is governed by their chemical interaction with soils and sediments. The behaviour and retention of radionuclides is predominantly dictated by ion-exchange mechanisms.

Soils principally consist of mineral, organic matter, soil air and soil water content (Brady 1984 and Faniran and Areola 1978). Mineral materials include all inorganic substances in soil. These include rock fragments and primary and secondary minerals resulting from the chemical decomposition of rock materials. These include: i) *Silicate elements*, such as Si, Fe and Al, ii) *Macro-nutrients*, consisting of metallic cations, Ca, Mg and K and non-metallic organic cations P, N and S, and iii) Micro nutrients or trace elements such as Mn, Mo, Ti, Cu, Pb, Zn and Vn.

Particles are classified as sand (0.02 to 2.0 mm), silt (0.02 to 0.002 mm) and clay (<0.002 mm). The clay particles are of the most fundamentally important soil mineral constituents, composed entirely of chemically active secondary minerals. Each clay particle is surrounded by a film of water saturated with negative charges which constitutes the soils cation exchange capacity.

Clay minerals are formed by silica and alumina sheets combining in two ways: i) *The montmorillonite group*, which includes the expanding (montmorillonite of high cation exchange capacity), and non-expanding (fine grained micas and illite of moderate cation exchange capacity), and ii) *The kaolinite group*, (low cation exchange capacity).

Soil organic matter is decomposed by living organisms to form humus. Humus has the ability to hold and exchange nutrient cations on negative exchange sites. About 50 % of the soil cation exchange capacity is made up of the negative charges associated with humus. Clay and humus are usually mixed up in the soil to form the *clay-humus complex* which has colloidal properties and is stable in soil with low acidity.

2.4.1 Primordial Radionuclide Assimilation and Concentration in Soils

The chemical and physical factors which determine the distribution of radionuclides in rocks also control the distribution within soil as well as their mobility and bioavailability. Principally, U and Th accumulate in soils as a result of rock weathering and soil formation. However, in an open system, a wide variety of geochemical and geophysical processes dictate the distribution of U, Th and K in the soil profile.

The solubility of U and Th in soils depends on pH, redox potential, texture and mineral composition of the solid phase, concentrations of inorganic compounds in the soil and soil solution, competitive interactions between heavy metals, soil temperature, moisture content and microbial activity. Alpha recoil mechanisms are likely to form an important role in the weakening of the more resistant minerals such as zircon and aid their weathering and disequilibrium in the decay series. Thus, as dissolved U atoms decay by α disintegration, recoiling daughter nuclides are adsorbed or driven into particulate matter (Ivanovich and Harmon, 1982).

Transport of U and Th in soil-water occurs mainly in dissolved or suspended form, by diffusion or mass flow. Under oxidizing conditions U occurs in solution at low pH as a uranyl ion or as hydrolysis products of this ion. At higher pH the uranyl ion may form complexes with carbonate ions. These complexes may be relatively mobile in soils and ground water, because of their negative charge. Thorium occurs in the soil solution at low pH as a thorium ion or its hydrolysis product. Above pH 4 the major species in solution will be $\text{Th}(\text{OH})^{2+}$ and at high pH, thorium is virtually absent in soil solutions. Additional organic acids, such as acetic and oxalic acid, may form soluble complexes with U and Th, thus increasing the solubility of these elements in soils.

Processes which lead to the removal of U and Th from solution include incorporation on biological systems, coagulation of suspended matter, precipitation or coprecipitation, adsorption and solid state diffusion. Positively charged U and Th compounds will be strongly adsorbed in soils. Adsorption of free metal ions, hydrolysis products or complexed species may be caused by electrostatic attraction, London-van der Waals interactions, hydrogen bonding or chemical bonding (Harmon and de Haan 1980). As with other heavy metal ions, adsorption is favoured when in low concentrations and in high pH conditions. The presence of U and Th in hydrolysed form together with the actinide affinity to oxi-anion groups and in particular U to the carboxylic-acid groups, make it very likely that U and Th will be strongly absorbed in soils, both by organic and mineral soil constituents.

Given the wide variety of physical and chemical processes acting upon soils and their

substrata which are governed by geologic, geographic, hydrologic and climatic controls, Osburn (1965) offers some generalizations on the distributions of radionuclide concentrations in soils. The amount and type of a radionuclide found in a particular soil depends initially on the parent rock, and secondly upon the type and intensity of weathering and erosion.

However, given the different chemical characteristics of the U and Th daughters, disequilibrium within the individual decay series is likely to occur (Talibudeen 1964, Hanson and Stout 1968, Megumi et al 1982). For example, radon gas emanation will lead to disequilibrium in the Uranium series. The soil radon generating power tends to be concentrated in the heavy clay layers of soils, typical of the lower levels of the soil profile in podzolic, red-brown earths and prairie soils. Limestone soils tend to concentrate the radon producing power in the upper levels of the soil, due to solubilization of the limestone, concentrating the Ra bearing minerals in the upper levels of the soil. Soils associated with arid and semi-arid climates are poorly weathered and thus their radon producing ability is uniformly distributed throughout their horizons. Similarly deeply weathered subtropical soils tend to have evenly distributed radon activity with depth.

Disequilibrium of Ra with respect to U may occur as a result of leaching of soils and the difference in the chemical reactivity between Ra and U. Although this is likely to be a minor contributor to U series disequilibrium, Talibudeen (1964) illustrates that Ra^{2+} tends to accumulate in colloidal fractions which are less easily leached out and hence heavier soils are found to be richer in Ra. Soils on carbonate rocks tend to accumulate Ra, whilst on igneous rocks Ra levels do not differ markedly from their parent rock concentration. The Ra/U ratio of surface soils generally increases with leaching, although increased organic content favours the retention of U relative to Ra, as do reducing conditions associated with water logged soils and the formation of H_2S . Because the Th/U ratio increases with depth, there must be a preferential downward movement of Th, especially in the presence of organic complexes.

Chemical weathering of the parent rock results in fewer mineral species in the

subsequent soil. This generally results in a reduction in the transfer of radionuclides from the bed rock to the soil profile and thus a reduction in the nuclide concentration, particularly for U. However, micaceous clay minerals are formed as a result, which have been demonstrated to be efficient absorbers of K, Ru and Ra. In general, micaceous minerals are resistant to physical weathering and consequently regions which have mica concentrations in bedrock will also have mica in the soil. In areas where physical forces dominate over chemical forces, the natural radioactivity of the soils may increase above that of the parent rock (Hanson and Stout, 1968). U and Th appear to have concentrated as a result of rock weathering. U is often preferentially retained in primary soils, whilst in alluvial soils Th was preferentially retained.

2.4.2 Anthropogenic Radionuclide Behaviour in Soils and the Environment

Caesium in Soils

The radiocaesium isotopes ^{134}Cs and ^{137}Cs form part of the alkali metals group along with K and Rb and thus have very similar physiological and ecological behaviour. Numerous investigations have revealed that soils, particularly those rich in clays, act as a sink for radiocaesium released into the environment.

In an attempt to find a correlation between the magnitude of the caesium distribution coefficient (K_d) and measured soil properties such as ion-exchange capacity, major cation concentrations, clay mineral composition, carbonate mineral content and pH, Gillham *et al* (1980) found that there were no discernable correlations except with natural exchangeable caesium. In contrast, Ritchie *et al* (1970) found the maximum retention of ^{137}Cs in the first inch of the soil column was due to its rich organic content. However, Cremers *et al* (1988), Cook *et al* (1984), Evans *et al* (1983), Coleman and Le Roux (1965), Sawney (1972) and Francis and Brinkley (1976) suggest that the retention behaviour of radiocaesium is essentially controlled by the clay content in the soils and in particular by illite and micas (non-expanding group), the dominant clay mineral in Western Europe. In addition, Schultz *et al* (1960), suggested that the absorption energy of caesium on clay minerals and soil colloids is greater than any

other alkali ion and is irreversibly fixed by many soil colloids and clay minerals especially by the non-expanding group of minerals. Cook *et al* (1984) and Fahad and Shihab (1989) showed by sequential leaching of soils with river water, NH_4OAc , KCl , CaCl_2 and EDRA that the major soil constituents responsible for the retention of caesium were clay silt and Fe oxides. Continual leaching showed an increasing fraction of the caesium to be bound to the clay minerals. Thus the displaced portion is thought to be associated with organic matter and caesium exposed on less selective sites.

Evans *et al* (1983) identified three types of site important in the binding of ^{137}Cs : i) sites on planar surfaces of clays (or exterior surfaces of other sediment minerals), ii) sites at the edges of clay interlayers of 10 Å spacing (in particular the frayed edges or wedge sites of partially weathered micas such as illite), and iii) sites along the interlattice layers of collapsed or non-expanding clay minerals where fixed ^{137}Cs is not readily exchanged with any cation.

The consequence of selective absorption of caesium to caesium fixing minerals strongly influences the availability of ^{137}Cs cycling to the biotic component of ecosystems. Release of ^{137}Cs is 8x greater from montmorillonite and kaolinite than from mica and illite (Francis and Brinkley 1976).

The interaction of caesium with organic material is predominantly ionic. The electro positive caesium can form phenoxide salts or form bonds with ligands via oxygen bonds. Displacement of caesium is possible either by an ion with a greater affinity for the site or its presence in much higher concentrations. Hydrogen ion content and thus pH plays an important role in metal complexing within organic substances. Hydrogen ions have a high affinity for many complexing sites (Livens and Baxter 1988 b). McKay and Baxter (1985) showed that the presence of oxides and organics in the soil, was important in coating particles and thus preventing the release of ^{137}Cs from the clay mineral fractions. As a result of diagenetic changes removing these mineral coatings a significant fraction of ^{137}Cs may be made available.

For a given atmospheric deposition of ^{137}Cs and ^{134}Cs , the vertical distribution of

caesium will be controlled ultimately by the clay minerals present and the diffusion mechanisms acting upon that profile and additional organic (eg. grass and forest litter) and sediment input (eg. salt marsh) on top of the profile. The maximum published depth of penetration for ^{137}Cs was 2.25 m in unsaturated sandy soils (Veen and Meijer 1989). However, typical values within clay and loam soils are between 20 and 30 cm (Torgessen and Longmore 1984, Miller *et al* 1990) with typically most of the activity concentrated within the top 15 cm (Livens and Baxter 1988 b). Ohnuki and Tanaka (1989) described two additional processes of caesium migration: i) absorption near the soil surface and ii) caesium migration downwards attached to soil particulates. The resulting profiles are often described as exponential.

Miller *et al* (1990), Silant'ev and Shkuratova (1988) and Bunzl and Kracke (1988) observed differences in radiocaesium absorption in the top layers of soil between forest soils and grass land soils. Explanations evolve around the ability of the forest litter layer to act as a buffer by absorbing water from precipitation, thus slowing the movement of trace constituents into and through the mineral soil layers. However, some authors have found no differences between open grass land and woodland soils (Cawse 1983) whilst others have observed greater depth penetration of ^{137}Cs under oak vegetation (up to 70 cm) than in bare soil (Veen and Meijer 1989). These variations in observations may be explained by the differences in organic matter and differences in canopy coverage between deciduous forests and evergreen forests (Ritchie *et al* 1970). Mathematical modelling of caesium migration in soils has been undertaken by Silant'ev and Shkuratova (1988).

Allen (1991) and Allen and Rae (1986) observed that the distribution of metals within salt marsh sites on the Severn estuary could be used for the timing of sedimentological events. Research by Allen 1994 and within this thesis demonstrate that the distribution and deposition of sediments contaminated by the discharge of anthropogenic radionuclides from Sellafield has led to a very different source depth distribution from that observed on terrestrial sites. Sediments from the Irish Sea are deposited in accretionary zones forming salt marsh sites often over 1 kilometer in width and several kilometers in length. Since the peak Sellafield discharges in the 1970's, subsequent

accretion of lower activity contaminated sediments have produced a subsurface maximum. The depth of the subsurface maximum is tidally controlled and typically deeper in the higher energy intertidal sediments than in the far shore environment.

Americium and Plutonium in Soils and the Environment

Since 1944, increasing amounts of the transuranic elements have been produced by nuclear reactors. Americium and plutonium form part of the actinide group and are associated with weapons testing fallout or Sellafield discharges leading to contaminated sediments of the Irish Sea.

Of the 14 Pu isotopes, most interest has been focused in the fissile ^{239}Pu , with rather less on ^{238}Pu and ^{241}Pu . Consequently, there has been much research into the behaviour of Pu in the environment. Also of particular interest is ^{241}Am , because of its ease of detection in the laboratory and field. Its origin in the environment is complicated by the fact that it is both discharged directly from Sellafield and also forms as a result of the β decay of ^{241}Pu .

Continual change is occurring in the relative amounts of americium and plutonium in the environment purely as a result of the decay of ^{241}Pu to ^{241}Am , observed as a change in the $^{241}\text{Am}/^{239+240}\text{Pu}$ ratio. The activity ratio in mixed fallout has been observed as 0.22 in 1970, 0.28 in 1974 and 0.35 in 1980 (Koide and Goldberg 1981).

Bondietti (1981) illustrates how the mobility of the actinides is dependent upon: redox potential (reduction in oxidation state increases mobility), inorganic and organic components, sorption specificity of environmental surfaces, residence time (for equilibrium) and pH. Of importance in the environment are plutonium in a tri- and tetravalent oxidation state (Pu^{3+} and Pu^{4+}) and americium in the trivalent oxidation state (Am^{3+}). Both the tri and tetravalent states form stable organic complexes, with the tetravalent state approximating Fe^{3+} in strength. Americium may be maintained in solution by the formation of soluble complexes in which organic ligands are thought to play an important role. However, the pronounced hydrolytic character of these

actinides, making them insoluble, enables them rapidly to form particulates or to be absorbed to existing suspended particulates and thus interact strongly with rocks, soils and sediments. Even actinides in complexes with organic or inorganic particles can be subject to sorption, the degree being a function of the solid-phase or solution-phase chemistry. As a result of their strong attachment to particulate surfaces, they tend to accumulate in soils and sediments which act as storage reservoirs (Whicker and Schultz 1982) and thus physical transport of contaminated sediments is a major factor in the relocation of many radionuclides (Bondietti 1981).

From examining the chemistry and binding of americium and plutonium in soils via batch equilibrium techniques, Rouston *et al* (1977) concluded that ion-exchange was not the only sorption reaction that occurred and that Am^{3+} organic complexes could occur and dominate solubility control. They also concluded that plutonium is an unsuitable analogue for the behaviour of other actinides in soil. For example, plutonium is better sorbed relative to americium and thus ^{241}Am is more mobile in the environment. The distribution coefficient (K_d) values for americium are greater than plutonium by 0.5 to 1.0 orders of magnitude. Am and Pu in both the tri- and tetravalent states are also strongly bound to humic compounds. Binding of americium to soil components may be very similar to plutonium, although the strength of binding is less due to organic complexing. Thus, decreasing sorption to soil and increased mobility, allows for greater plant uptake or vertical transport (Coughtrey *et al* 1984). Plutonium is predominantly associated with the organic fractions and to a lesser extent oxide phases of soils and sediments in Cumbria (Livens and Baxter 1988 a,b) and Dounreay (Cook *et al* 1984).

The adsorption of americium to sediments is dependent upon the physico-chemical speciation of americium and on the surface characteristics of the sediment. Both of these may change with pH and thus the K_d for sorption of americium may also vary (Sanchez *et al* 1981). Generally, K_d increased with pH.

As in sediments, americium does not behave in a similar manner to plutonium in the aquatic ecosystem. Americium is strongly associated with particulates and sediments,

and is thus more easily removed from the water column. The association of americium with particulate matter leads to its preferential entry into the sediments and thus its enrichment with respect to plutonium in areas of high influx of terrestrial derived material. Similar observations of preferential removal of americium relative to plutonium from the water column from nuclear discharge points have been made (McDonald *et al* 1990, Livingston and Bowen 1976).

2.5 SUMMARY

The natural radionuclides of interest are ^{40}K , ^{238}U and ^{232}Th . Their abundance, gamma yields of their daughter products and geochemical distribution have encouraged their use in geological applications of gamma spectrometry. Of the anthropogenic radionuclides, the abundance, gamma yields, origin, longevity and biological importance make the study of ^{137}Cs and ^{134}Cs particularly appealing for in-situ and airborne gamma spectrometry. In addition ^{241}Am is of particular interest in coastal environments and with certain detector formats is readily detected in the field. Of additional interest in the event of an accident is ^{131}I which is initially detectable and of biological importance.

Over and above the factors which determine the geological distribution of the natural radionuclides in soils, the climate, soil type, pH and geophysical processes acting on the soil are the major environmental factors. Deposition pathway is the major factor which dictates the distribution characteristics of anthropogenic radionuclides in soils. Scavenging via precipitation from radioactive plumes in the troposphere and plume interaction with topography are the major control on fallout from accidents such as Chernobyl and often lead to a highly heterogenous distribution. Diffusion and migration processes acting on the soil horizons and ion exchange capacity control the movement of activity through the soil profile. The depth of penetration is ultimately determined by the soil composition, and in particular by the type of clays present and organic matter. The deposition of contaminated Irish Sea sediments in coastal environments provides more homogenised and tidally controlled distribution of activity. However, subsequent deposition of lower activity sediments leads to a buried source profile.

3. METHODS AND TECHNIQUES

3.1 INTRODUCTION

Having reviewed the factors which control the distribution of radionuclides in the environment in chapter 2, this chapter discusses the traditional techniques used to measure environmental radioactivity. Failure to recognise the limitations of these techniques may render their results difficult to interpret. Thus a comparative study between these techniques is made throughout this research work to determine and quantify their limitations and determine effective methods for comparison.

A wide range of measurement techniques is available today for the scientist to determine levels and distributions of environmental radioactivity. This chapter discusses the broad theory and methods behind the three techniques used for the measurement of radioactivity through environmental gamma spectrometry. These techniques involve many aspects and hence this chapter includes: principles of scintillation and solid state gamma spectroscopy and their application to environmental monitoring via laboratory analysis of soil samples, in-situ and aerial based platforms. The discussion begins by describing the soil and sediment sampling technique and sample preparation methods used.

3.2 SOIL SAMPLE COLLECTION AND PREPARATION

Typical soil sampling techniques available today include auguring, coring and digging trenches. For this work a quick and efficient method is required for soil sample collection, and thus soil corers were used. However, the methods of sampling and sub-sampling have a direct bearing on the final inventory estimates, a fact which has gained only a tacit recognition in the literature. Equally, careful laboratory practice is required in order to minimize further potential errors on the final inventory estimate.

3.2.1 Soil Sampling

For the estimation of environmental radioactivity from soils, two soil corers were used. For inter-laboratory compatibility, a 38 mm diameter soil corer was initially used as recommended by AEA, Harwell (McKay *et al* 1991, Cawse and Horrill 1986, Pierson *et al* 1982). Other core sizes cited in the literature range from 4 cm (Brisbin *et al* 1974), 5cm (Arnolds *et al* 1989, Sutherland and de Jong 1990 and El-Fawaris and Knaus 1984), to 10 cm (Dickson *et al* 1976, ASTM 1983). Digging soil blocks is an alternative to coring as demonstrated by Horrill *et al* (1988) who dug 20 cm x 20 cm x 15 cm block turfs for analysis of Chernobyl derived inventories.

The 38 mm corer illustrated in figure 3.1.a. is supplied by Leonard and Farnell and was originally designed for coring in stony field conditions. A 38 mm diameter x 170 mm length stainless steel corer was attached to a hammering shaft via screws. The core was then hammered into the ground by vigorously pumping the hammer shaft. The corer was then pulled out of the ground and the corer detached. The soil core was retrieved by extruding the sample from the stainless steel corer. This process was then repeated to the depth required, usually 30 cm, though in peaty locations soil cores were taken to 45 cm. Up to 10 soil samples were collected per location. The cores were then double bagged to retain moisture content and labelled.

A 105 mm diameter corer was later used and was constructed from a B.M.S. Turfmaster golf hole cutter which was adapted so that 105 mm diameter intact soil cores could be sampled to depths up to 45 cm. Figure 3.1.b. illustrates the corer. It is simply two semicircular core cutting shafts which were hit into the ground separately with a rubber mallet. The shafts were guided by three rings attached to the steadying handle. Once the required depth was reached, the handles were given a half turn to break the sod, and the corer was lifted out of the ground. One shaft was pulled back to reveal an intact core with no soil compression and negligible stratigraphical smearing. The sample was then cut up on site to the required depth intervals, bagged and labelled.

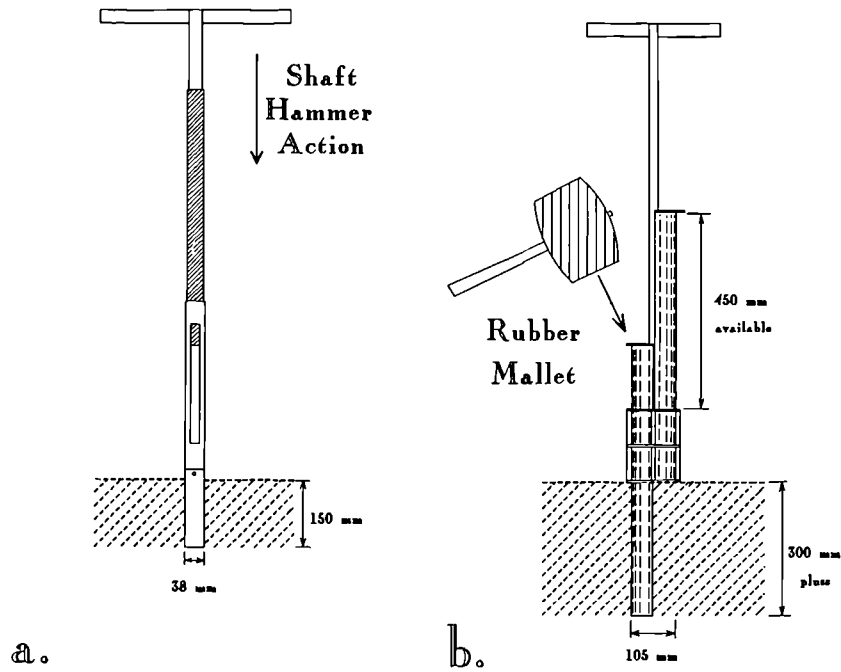


Figure 3.1 Soil Corers: a. 38 mm x 150 mm corer. b. 105 mm x 450 mm corer. (Drawn to scale).

The 105 mm corer collects 7.6 times more material than the 38 mm corer for the same depth of sample. In addition the larger core size allows less biasing of stone size and content within the sample, thus allowing a more representative sample to be collected.

3.2.2 Laboratory Sample Processing

On return to the laboratory, the samples were stored in a cool environment, if not processed immediately. If not already cut in the field, they were cut into 2 cm, 5 cm or 15 cm intervals. The 105 mm corer provided accurately cut soil samples, from which, by accurate subdivision, sample volumes were easily calculated.

The samples were placed on trays of known weight, weighed and placed in ovens at between 40° and 60°C to be dried. Drying times required depended upon sample water content, and ranged from a few days to about two weeks. Where necessary, water content was checked by reweighing the sample until the weight stabilized. From the dry weight the soil moisture content was calculated.

The wet bulk density was calculated by dividing sample wet weight by its volume as collected and subdivided in the field. However, dry bulk density was more difficult to measure. The bulk densities of sediments and sandy soils could be easily and quickly estimated by using measuring cylinders. Soils with moderate organic content dried into compacted shapes, making bulk density estimation difficult. Dry bulk density was therefore calculated with core volume and the dry sample weight after FitzPatrick (1983).

Stone content was determined by sieving through a 2 mm mesh. The stone fraction was weighed and returned to the whole sample. The pH was determined on dry soil separates using a 1:2.5 ratio of soil to 0.01 M CaCl_2 (Cawse and Horrill 1986, Baxter *et al* 1989) and a calibrated electrometric pH meter (Bolt and Bruggenwert 1976).

Chapter 6 discusses the need for a homogeneous sample for sub-sampling. In order to achieve this, a rock crusher was used to break the samples into <10 mm fragments. The samples were then ground and homogenised for several minutes in either a 125 g capacity Tema Mill or a 1 kg capacity Mixer Mill. The samples were ground to <0.5 mm (approx) fragments. Where the sample size exceeded the capacity of the mill, sub samples were taken and ground separately. These sub-samples were subsequently bulked and homogenised by tumbling in a large container for between 8 and 24 hours.

The homogenous sample was then placed into clear polystyrene containers of fixed geometry. The geometry (container) sizes used were 30 cc (petri dish), 75 cc or 150 cc and were chosen to optimise the amount of sample used. The container was weighed empty and the ground soil was poured into the container, which was frequently tapped to maximise compaction during filling. The container was reweighed and the sample weight and density calculated. The container was sealed to allow equilibration of ^{222}Rn with its parent ^{226}Ra . Two weeks storage was allowed prior to gamma spectrometric analysis.

3.3 GAMMA RAY SPECTROMETRY

The detection and quantification of radionuclides present in a source is dependent upon the detection of gamma photon energy and the relative abundance of these photons. The detection of gamma rays is critically dependent upon the gamma ray photon undergoing an interaction that transfers all or part of the photon energy to an electron in the absorbing material. Thus, to serve as a gamma ray spectrometer, a detector must act as a conversion medium in which incident gamma rays have a high probability of interacting to yield one or more fast electrons and at the same time act as a detector for these secondary electrons. There are principally two detectors of major importance in the detection of gamma rays: i) inorganic scintillators, such as sodium iodide thallium activated crystals (NaI(Tl)); and ii) solid state semiconductors such as the hyper pure germanium (HPGe) or lithium drifted germanium (Ge(Li)). NaI(Tl) detectors have a higher sensitivity but poorer energy resolution than HPGe and Ge(Li) detectors. Hence, the choice of gamma detector is based upon: i) the required resolving power; ii) the detector efficiency; and iii) the simplicity of the arrangement.

Relative efficiency comparisons between detector types are often made by comparison with the intrinsic efficiency of a 3" x 3" NaI(Tl) detector at 1333 keV (^{60}Co). NaI(Tl) detectors of this standard size have virtually identical properties and thus this relative comparison can be readily made, typically with a ^{60}Co point source. Ideally this should be a measure of intrinsic efficiency relative to the detector's active volume. However, to eliminate the difficulties this imposes, relative efficiencies between detectors are typically calculated with a ^{60}Co source at a distance of 25 cm from the detector crystals.

A convenient definition of energy resolution is the full width at half maximum (FWHM) of the amplitude of the photopeak and can be quoted in terms of energy or divided by the peak centroid position and quoted as a percentage. For comparison between different detectors, the FWHM is often quoted at 662 keV (^{137}Cs), or at ^{60}Co for high energies and ^{57}Co (122 keV) for low energies.

The two main types of gamma ray detector and their operation are described. Their application to laboratory and in-situ based spectroscopy will be illustrated along with SURRC developments for in-situ applications. Much of the following discussion is taken from Shafroth (1967), Adams and Dams (1975), Knoll (1979, 1989) and Ivanovich and Harmon (1982).

3.3.1 Semiconductor (Solid State) Detectors.

The principle of semiconductor detectors is based on the semiconductor energy band gap principle, where electrons in the valence band are excited by ionization and cross the forbidden band to the conduction band and are subsequently collected by the influence of an electric field (Adams and Dams 1975, Knoll 1979, Ivanovich and Harmon 1982).

Germanium (Ge) is the preferred material for this because of its high Z. In early semiconductors, Ge was not very pure causing an imbalance of electrons and holes in the crystal lattice (extrinsic), with sufficient electrons in the conduction band for the material to be a conductor at room temperatures. At liquid nitrogen temperatures (77 K), the thermal excitation produced noise is reduced. Highest purity Ge was typically p-type (excess of holes) which could be effectively neutralised by the ion drift method, where lithium (valency 5) was drifted through Ge (valency 4) to provide a neutral (intrinsic) layer. This process was carried out in different geometries to provide *coaxial open ended* or *single ended* detectors. To avoid the redistribution of Li, these detectors are maintained at 77 K.

Today germanium is available at very high purities, and reverse biasing at 1000 V or more provides a depletion zone (intrinsic) of 10 mm or more providing high purity germanium. The impurities which remain still cause excess leakage current and hence still require the detectors to be operated at liquid nitrogen temperatures.

3.3.2 Scintillation Detectors

Absorption of energy by ionisation can result in an electron being elevated from the valence band to the conduction band, thus leaving a hole in the valence band. In a pure crystal such as NaI, the return of the electron into the valence band is an inefficient process and results in the emission of a photon, a condition known as scintillation. However, typical forbidden band widths in pure crystals lead to resulting photon emissions with too high an energy to lie within the visible region. To enhance the probability of visible photon emission during the de-excitation process, small amounts of an impurity or "activator" such as thallium (Tl) are commonly added to the inorganic scintillator. The impurities create energy states within the forbidden band through which the electron can de-excite back to the valence band. Thus the transition is less than the full forbidden band gap, and the transition will give rise to a visible photon which forms the basis of the scintillation process.

NaI(Tl) has the highest light yield of all known scintillation materials. It has a linear response to electrons and gamma rays. Although NaI(Tl) can be easily machined into required sizes and shapes, it is fragile and easily damaged through mechanical and thermal shocks and is also hygroscopic.

The light collection from a scintillator must be as efficient as possible and be reflected towards the photomultiplier tube which converts the light signals into electrical signals. To achieve this, the scintillator must be as transparent as possible and surrounded by a reflector usually graded MgO powder. These light collection conditions affect the eventual energy resolution of the detector in two distinct ways:

- i) The statistical broadening of the response function will worsen as the number of scintillation photons which contribute to the measured pulse is reduced through self absorption and internal reflectance.
- ii) The uniformity of light collection will determine the variation in signal pulse

amplitude as the position of the photon interaction is varied throughout the scintillator.

The highest light transfer between crystal and photomultiplier tube is achieved through direct coupling. The photomultiplier consists of two electronic systems mounted within the same unit: i) a photosensitive cathode which converts the photons into photoelectrons; ii) a multiplier tube where the electrons are repeatedly multiplied by secondary emission from dynodes.

3.3.3 Detector Instrumentation

The pulses leaving the detectors require suitable amplification and signal processing for interpretable data to be produced. Thus equipment of the highest linearity and stability must be used so that the pulse height distribution reflects the resolution capabilities and linearity of the detector with the least possible degradation of data. Figure 3.2 shows the components required for efficient operation of solid state detectors, although this is generally the same for any gamma detector.

Instrumentation for Semiconductor Detectors.

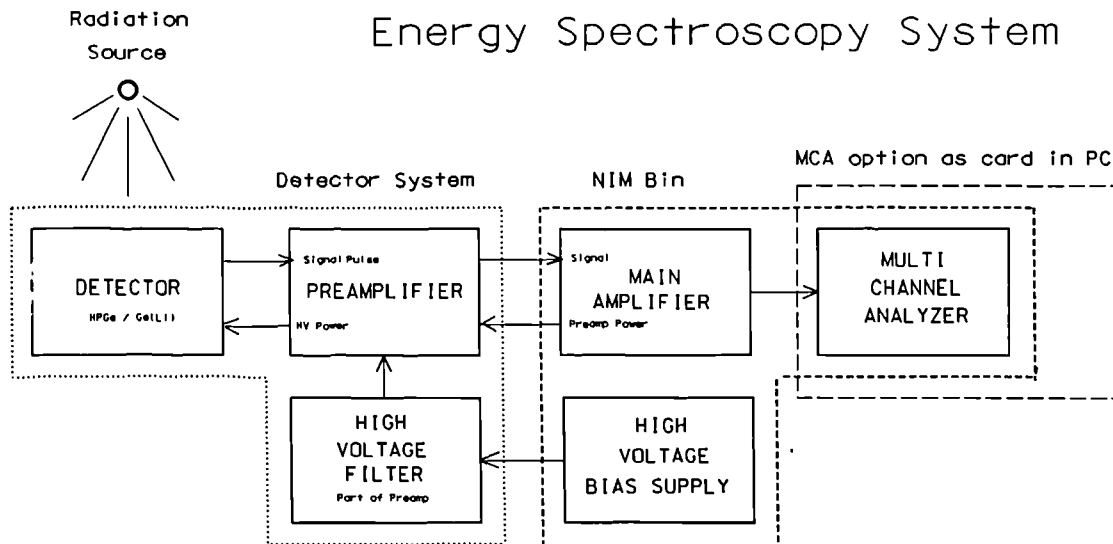


Figure 3.2 The Main Components of a HPGe or Ge(Li) Detector System

Amplifiers contain pulse shaping networks and amplify the signal from the detector.

Their location with respect to the detector can affect the signal to noise ratio. Thus the amplifier is divided into two. The first part or preamplifier is placed close to the detector which minimizes the capacitive load on the detector. In addition the preamplifier provides a high impedance to the detector whilst providing a low impedance output to drive successive components. The output signal is typically a pulse with an exponential tail. The rise time of the output is kept as short as possible, usually equal to that of the charge collection time on the detector itself. It is through this process that the preamplifier maximises the signal to noise ratio.

The main part of the amplifier, is positioned further away along with the rest of the nuclear electronics required. The amplifier must allow for the selection of the optimal pulse shaping network for an optimum resolving power consistent with the noise characteristics for a given detector preamplifier combination at one end, and the practical count rate requirements for experimental conditions at the other. This flexibility is taken into account with commercially available amplifiers with pulse shaping methods and RC time constant adjustable over a range of 0.1 to 10 μ s. This allows the ready selection of the best signal to noise ratio. For high counting rates a delay line differentiation circuit or second RC circuit should be provided. The amplifier accepts tail pulses as an input and produces a shaped linear pulse with standard polarity and span. The amplification factor or gain required varies greatly with application, but is typically a factor of between 100-5000. This gain can be adjusted and if the product of the input and gain exceeds the maximum designed output amplitude, the amplifier will saturate and produce a distorted output pulse. Linear amplification will only be realised for those pulses which are short of this saturation level. An additional requirement for high resolution gamma spectroscopy is base line restoration between pulses at high counting rates to reduce the signal to noise ratio and the deterioration in the photopeak resolution.

The nuclear electronics required to power semiconductor detectors and process their signal information are usually housed within a Nuclear Instrument Module (NIM) Bin which also acts as an ac to dc converter. The primary interconnections between modules and components are carried out using shielded coaxial cables. The shielded

construction is designed to minimize pick-up of noise from stray electric and electromagnetic fields, which is of paramount importance with signal cables. The high voltage or detector bias is commonly up to 5000 volts. Extreme stability is not required as fluctuations in the voltage supply do not lead to changes in photopeak position.

Instrumentation for Scintillation Detectors

Amplification of pulses from a NaI(Tl) detector is usually achieved through at least two stages. The first stage as discussed is performed by the photomultiplier tube. The signal from the photomultiplier is usually quite large due to the high voltage applied across it. Thus although pre-amplification is often used and usually placed at the back of the detector (figure 3.6), its primary role is for fine adjustment of the signal emanating from the photomultiplier tube. The preamplifier is then connected to the amplifier, as with semiconductor detectors, via a coaxial cable.

As the high voltage power supply is vital in the preamplification process, it is very important that the power supply is of the highest precision, unlike that for the semiconductor detector. The high voltage power is supplied via an extra high tension (EHT) high voltage cable.

The amplification of the preamplified NaI(Tl) detector output proceeds in much the same way as that of semiconductor detectors.

Signal Processing and Output

The output pulses from the amplifier are converted to a digital number by an Analogue to Digital Converter (ADC). The digital number is proportional to the amplitude of the pulse at the input to the ADC. The performance of the ADC is characterised by the speed of the conversion, the linearity of the conversion and the resolution or fineness of the conversion. The resolution depends upon the number of channels the ADC can subdivide into, typically up to 16284. The stability of the

ADC must be such as to ensure that a pulse of constant amplitude will be stored in a certain single channel.

The ADC forms a key part of the Multi-Channel Analyzer (MCA) and determines its performance. The MCA is a device used for recording and storing data which is then used for displaying pulse height distribution measurements or spectra. The number of channels available is usually a power of 2. By providing a large number of channels, the width of one channel can be made very small and the resulting discrete spectrum will be a close approximation to the continuous distribution. Therefore, if at least 4 channels are required to be over the Full Width Half Maxima (FWHM), one would require at least 100 channels for a detector with a 4% energy resolution. Similarly, for an energy resolution of 0.4%, 1000 channels are required.

Once a pulse has been processed by the ADC, the analyzer control circuits seek out the memory location corresponding to the digitised amplitude stored in the address scaler, and the location is incremented by one. A plot of the content of each channel (number of pulses) versus the channel number will be the same representation of the differential pulse height distribution of the input pulses.

An MCA also incorporates an input gate which blocks pulses from reaching the ADC during the time it is busy digitizing a previous pulse. Inevitably, during times of high count rate, some fraction of the input pulses will be lost to dead time. Hence, any attempt to quantitatively measure the number of pulses presented to the analyzer must take into consideration the dead time. This is remedied by an internal clock pulse which is routed through the input gate and stored in channel zero. The number of clock pulses being blocked by the input gate must be the same as those signal pulses being blocked. The number of pulses collected in channel zero is a measure of the live time.

To further ease the congestion through the ADC, the input pulses are presented to a Single Channel Analyzer (SCA) which has input limits allowing pulses through to the ADC of certain amplitude only. These limits are set by the Lower Level of

Discrimination (LLD) and Upper Level of Discrimination (ULD). Thus, the very small noise pulses at one end and the very large pulses at the other are excluded and never reach the ADC. Failure to cut out the larger input pulses when operating at high fractional dead time, due to high pulse rate, will lead to spectral distortions because there is a greater probability that input pulses will arrive at the gate just as it is opening or closing.

Graphical display of the channel number x versus channel content y is displayed on an oscilloscope to give the spectrum. As MCA's now form an integrated part of personal computer systems, the spectral characteristics are readily displayed on the monitor.

3.4 SPECTRAL CHARACTERISTICS

This discussion is a summary illustrating the spectral characteristics and consequences of scattering within the detector, detector can, surrounding air and the source itself. It is referenced from: Adams and Dams (1975), Knoll (1979, 1989) and Shafroth (1967).

Figure 3.3 shows a schematic representation of a gamma spectrum of a single photon energy emitting radionuclide such as ^{137}C or ^{40}K . Although figure 3.3 is perhaps typical of a NaI(Tl) detector, this discussion is relevant to semiconductor detectors.

The photo-peak or full energy peak is the result of primary (unscattered) photons interacting wholly with the detector crystal resulting in complete absorption. The width of the photopeak is usually described in terms of the *full width at half maximum* (FWHM) and determines the energy resolving characteristics of the detector. The size of the photopeak is a function of source geometry as well as upon the size of the detector. The smaller the detector, the fewer the number of photons interacting wholly with the crystal, resulting in a larger scattered Compton contribution to the spectrum.

The Compton continuum is made up of the Compton edge, the back-scatter peak and

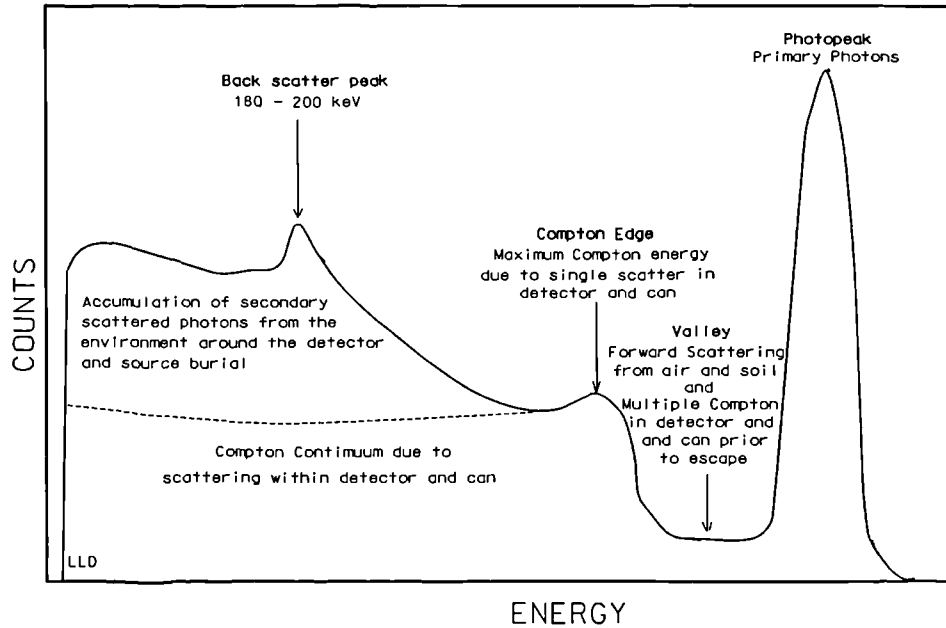


Figure 3.3 Schematic representation of gamma ray spectrum observed from a pure source such as ^{137}Cs or ^{40}K .

the accumulation of photons which have undergone many scattering events. The continuum is made up of scattering events from within the soil profile, air pathway, the detector can and crystal. The Compton edge is in a characteristic position away from the photopeak. It represents the maximum possible energy an electron can possess after a single Compton interaction within the detector crystal or can. The shape of the continuum is also characteristic of the detector material. If the mean free path of a photon is much greater than that of the dimensions of the crystal, then the photo fraction (photopeak area/total area) will be very small. If the detector crystal is large compared to the photon mean free path, then the photo fraction will be larger. Thus the size of the photo peak and Compton continuum is also a function of crystal size. When pair production is prevalent (ie. photon energy $> 2m_0c^2$), a double escape peak will develop at a point $(h\nu - 2m_0c^2)$ in the spectrum of small detectors because of the escape of both annihilation photons without further interaction. If one of these annihilation photons is totally absorbed, this will result in a single escape peak at $(h\nu - m_0c^2)$.

As the source is buried further into the soil, or the detector is raised to increase the

air path-length, or the soil atomic number Z and density change, the proportion of the scattering within the continuum associated with the soil and air pathway increases relative to that associated with the detector can and crystal itself.

The valley area between the Compton edge and the photopeak has two contributions:

i) At medium energies, the possibility of multiple Compton scattering in the detector followed by escape of the final scattered photon can lead to total energy deposition greater than that expected for a single photon interaction. This contribution is likely to be directly proportional to the size of the photopeak.

ii) Forward scattering in the soil profile, air path-length and detector can. This is due to Compton scattering within the lower Z media such as soil, water and air. Thus as the source is effectively buried, there is a higher probability of Compton scattering as the photon leaves the source leading to a lower energy secondary photon which gives rise to an event in the continuum, which may include the valley between the photopeak and the Compton edge.

Other factors can complicate the spectral response characteristics, and these are summation effects and effects of surrounding materials. Summation effects are additional peaks caused by the coincidental interaction and detection of two or more gamma ray photons. This can be caused by: i) isotopes which emit multiple cascade gamma rays in which the life time of the intermediate state is so short that they are emitted in coincidence and deposit their energy in the detector in a time that is short compared with the response time of the detector, ii) the accidental combination of two separate events in a time that is short compared to the resolving time of the detector. This chance coincidence increases with increasing counting rate.

The summed peak from these two possibilities will be observed in the spectrum at a point which coincides with the sum of the two individual gamma-ray energies. The size of the summed peak will have an intensity proportional to the square of the counting rate. A continuum will also develop due to partial interactions with the

detector.

The effects of surrounding materials on detector response have been discussed with reference to the detector can. However, to reduce background, most gamma ray detectors are shielded by high Z material such as lead. However, lead shielding provides a secondary effect as a consequence of the gamma photons from the source interacting with the shielding. Photoelectric absorption by the shield or other materials surrounding the detector can lead to the generation of a characteristic X-ray which may reach the detector. If the Z of the material is high, then a characteristic X-ray (e.g. lead X-ray) photon will be relatively energetic. A graded shield is therefore ultimately required to absorb these X-ray contributions to the spectrum. In addition, for high primary gamma photons, annihilation radiation may be significant resulting in a peak at 511 keV in the spectrum due to the detection of these secondary photons.

The backscatter peak is a consequence of scattering within the source, air path and can around the detector crystal. As the scattering angle increases there is a tendency for the resulting photon energy interacting with the detector to tend towards 180-200 keV, irrespective of the original primary photon energy.

3.5 GAMMA RAY SPECTROSCOPY - LABORATORY SET UP

3.5.1 Detector Configuration

Laboratory analysis of soil samples benefits from the ability to use: a) accurate calibrations for given container geometries; and b) long counting times to determine activities to high degrees of precision where required. Long counting times enable many low gamma yield photopeaks to be detected for which high resolution gamma spectroscopy is suited. Hence the discussion is concentrated around high resolution HPGe and Ge(Li) detectors.

The typical solid state detector configuration in the laboratory is illustrated in figure 3.4. HPGe and Ge(Li) detectors require cooling to 77 K (liquid nitrogen

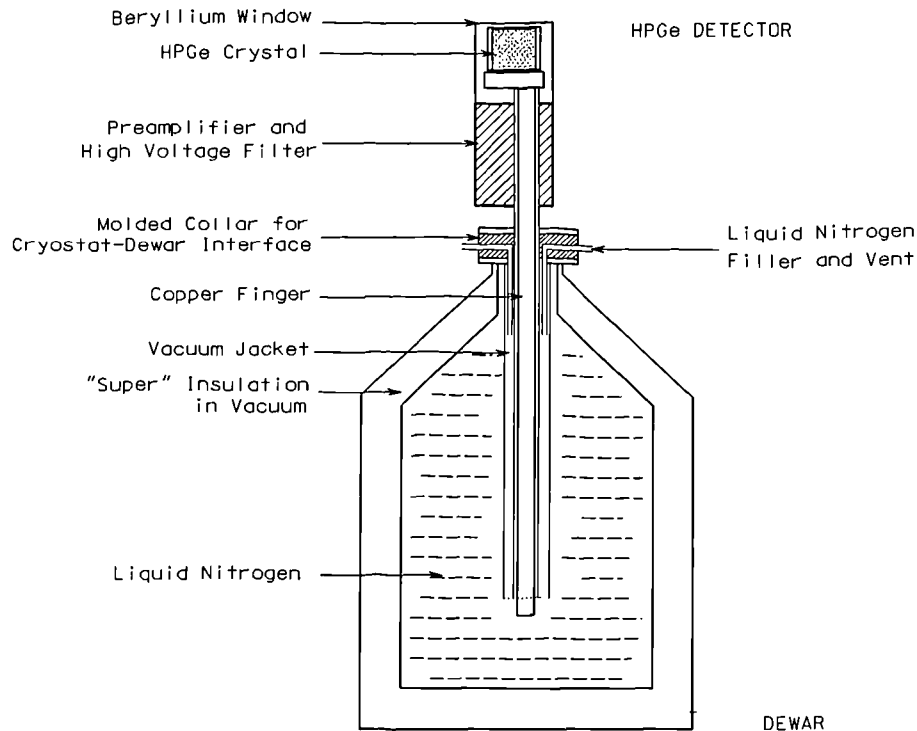


Figure 3.4 Sketch Cross-section of HPGe Detector and Cryogenic Dewar

temperatures). This reduces the detectors' portability and they are thus most suited for laboratory operation, although smaller dewars are now available to aid portability.

3.5.2 Background Reduction and Subtraction

The typical detector radiation background is made up of approximately 30% cosmic radiation, 60% from shielding materials, and 10% from radioactivity from within the detector and other contributions (Kaye *et al* 1973). Lead is conventionally used for the construction of low background shielding for laboratory based gamma spectroscopy. It has a high density and atomic number with photoelectric absorption predominating up to 500 keV. Lead also absorbs higher energy external background sources efficiently and thus only a few centimetres of lead will provide a significant reduction in the background of many gamma ray detectors. Lead is also reasonably useful in removing many cosmic components from the background, although as thicknesses increase beyond 10 cm there is an appreciable increase of secondary radiations and lead X-rays caused by the interactions from cosmic and primary photons with the lead itself. This is reduced by lining the inside of the lead castle

with copper and tin plate.

Prior to analysing spectra from samples counted within these shields, net photopeak areas from a previously recorded background spectrum are subtracted from the sample spectra before quantitative analysis is performed on the photopeaks of interest.

3.5.3 Spectral Analysis

Given that laboratory conditions are constant (ie. low and constant background radiation and constant detector to source geometry), interpretation and analysis of spectra is simplified. For the operation and data processing of the HPGe and Ge(Li) detectors and data the *Canberra Spectran AT CISE 525* and *Ortec Maestro 2* software were used. The software runs on IBM PCs (or clone) and reads information from the MCA card.

Both sets of software are able to search for and identify photopeaks in the spectrum. However, the program is limited in that in order to identify a peak clearly, the minimum separation required between peaks is about the FWHM. Peak identification also depends upon relative peak intensity, data statistics, and the smoothing applied.

The gamma ray intensities are determined from the full energy peak areas by summing the pulse height spectra after the underlying background continuum has been subtracted. The background is approximated by averaging the data either side of the peak and linearly interpolating between the averaged points. The standard deviation of the photopeak area is calculated with Poisson statistics and includes background contributions.

Following peak location and energy identification, a library is consulted where gamma ray energies are matched with nuclide names. Also, information on gamma ray yields and half lives, as well as additional gamma rays that must be found in the spectrum to confirm the presence of a radionuclide, are provided by the library file. A radionuclide analysis report is then provided in which peak activities and their

appropriate radionuclide associations are listed. After background subtraction, and with the appropriate efficiency calibration, the radionuclide activities can be calculated.

3.5.4 Energy Calibration

In order to identify the peaks within the spectra, the pulse height scale has to be calibrated in terms of gamma ray energy. The *Canberra Spectran-AT* software used to run the laboratory based HPGe and Ge(Li) detectors enables a quick and efficient energy calibration to be carried out either manually or automatically. This section illustrates the theory of energy calibration.

The energy calibration procedure for the laboratory based detectors enables three sets of calibration coefficients to be generated: a) energy as a function of channel number, b) FWHM as a function of energy, and c) photopeak low energy tailing as a function of energy.

These parameters are determined by making a weighted least-squares fit of the modified Gaussian function to the pulse height data for each peak. The calibration coefficients are determined using the following polynomial functions:

a) Energy versus channel:

$$E = A_1 \cdot C^2 + A_2 \cdot C + A_3 \quad (3.1)$$

where:

- E = energy in keV
- C = channel number
- A_1 = the non-linearity in keV/ch²
- A_2 = the gain (or slope) in keV/ch
- A_3 = the offset in keV

b) FWHM versus energy:

$$F \cdot A_2 = B_1 \cdot E^2 + B_2 \cdot E + B_3 \quad (3.2)$$

where in addition to the above:

- F = FWHM in channels

$B_1, B_2, B_3 =$ coefficients determined from fit

c) Peak tailing versus energy:

$$T \cdot A_2 = K_1 \cdot E + K_2 \quad (3.3)$$

where in addition to the above:

$T =$ tailing parameter in channels

$K_1, K_2 =$ coefficients determined from fit.

For the best results energy calibration sources that produce intense well defined peaks spaced uniformly over the entire range of interest should be chosen, e.g. ^{152}Eu .

Peaks are sought manually and appropriate energies allocated to their mean channel number. Because the energy - channel number relationship is not quite linear, more than two photopeaks are required for identification. A manual energy calibration is required if drift occurs such that the software is unable to identify the energy peaks.

3.5.5 Efficiency Calibration

The efficiency calibration is required to determine the detection efficiency of the HPGe or Ge(Li) detector as a function of energy. Any measurement of the absolute emission rates of gamma rays requires knowledge of detector efficiency. Variations in detector dimensions and the detector active volumes, along with long term changes in charge collection efficiency, can lead to drifts in detector efficiencies and require that efficiency calibrations be carried out periodically for an individual detector. Such drifts are periodically checked by counting a laboratory or international standard.

Absolute efficiency calibrations are carried out for particular container geometries and soil type so that the calibration is valid for the sample whose radionuclide activities are being measured. To maintain the integrity of a particular absolute efficiency calibration, the container geometry and soil type must be identical.

For a given source detector geometry, the absolute efficiency of the detector varies

with photon energy. This is due to the mean atomic number of the detector material and containment material and window thickness, the effective atomic number of the soil, and the effects these have on absorption and scattering of photons. Thus to determine this variation of absolute efficiency with energy, a range of photo peaks is required.

For the absolute efficiency calibration of detectors, an Amersham International, QCY44 with the addition of ^{241}Am liquid radionuclide spike was used to spike blank soils. This gave a range of energies and activities shown in Table 3.1.

Table 3.1 Showing Details of the QCY44 Mixed Radionuclide Spike + ^{241}Am for Efficiency Calibration, 1st February, 1991

Nuclide	Gamma keV	$t_{1/2}$ days	Gammas per second in solution		Error %
			per gram	per ml	
^{241}Am	59.6	1.5785×10^5	---	159.0	3.1
^{109}Cd	88.03	462.6	638	598.8	3.2
^{57}Co	122.06	271.79	586	550.0	1.9
^{139}Ce	165.8	137.64	705	661.7	1.9
^{203}Hg	279.2	46.595	1987	1865	2.2
^{113}Sn	391.69	115.09	1021	950	4.2
^{85}Sr	514.0	64.849	3956	3713	2.2
^{137}Cs	661.64	1.102×10^4	2433	2284	3.0
^{88}Y	898.0	106.63	6228	5845	3.8
^{60}Co	1173.21	1925.5	3355	3149	0.6
^{60}Co	1332.48	1925.5	3358	3152	0.6
^{88}Y	1836.01	106.63	6600	6195	2.7

For spiking soils the spike was diluted using the Amersham recommended technique. 1 ml aliquot of the QCY44 spike was taken and diluted with 1 ml of N441 diluent (carrier solution) and 8 ml of 4 ML HCL. This was carried out by calibrating a pipette carefully by weighing its delivery of distilled water. The dilution was determined to be within 2 % accuracy by pipette calibration.

Two approaches were used for spiking soils. The main approach will be referred to

as the *wet* method approach whilst the second, used ultimately to verify the first, is referred to as the *dry* method.

The *wet* technique. The container geometries to be calibrated were filled with the appropriate dry soil. The soils were free of anthropogenic radionuclides. The soil was weighed and then placed into 1 litre beakers. The soils were slurried by adding distilled water and acetone to aid drying and thoroughly mixed. The carrier solution was used to prevent "plate out" later and thus the loss of radionuclides on the sides of the beaker.

A pipette was calibrated and 2 ml of the diluted QCY44 and 0.5 ml of ^{241}Am was added to the slurried soil and well mixed. The soil was allowed to dry and periodically stirred to ensure a homogeneous distribution of activity within the soil. The weight of the soil was checked periodically until there was no further moisture loss. This procedure was repeated three times and the reproducibility of the calibration for a given soil type was measured to rule out the possibility of "plate out" of radionuclides on to the sides of the glass beaker and potential variations in pipette delivery. Knowing the activity in the soil sample, the activity per gram of soil could be calculated with appropriate error.

The *dry* technique. The dry technique involved pipetting a known quantity of spike into the centre of a known quantity of soil in its final geometry. The spike was allowed to dry and plate out into the surrounding soil. Once dry the soil was tumbled and homogenised for several hours and then replaced in its container.

Figure 3.5 shows the variation of absolute efficiency with energy for a HPGe detector and a Ge(Li) detector.

The contrast in the order of magnitude of ^{241}Am efficiency calibration between the two detector types is due to the predominance of the photoelectric absorption below 150 keV. The mass attenuation coefficient is directly related to the effective atomic number (Z_{eff}) of the material through which it is transmitted. Hence the reduction in the absolute efficiency of the Ge(Li) system, which has an Al window, with respect

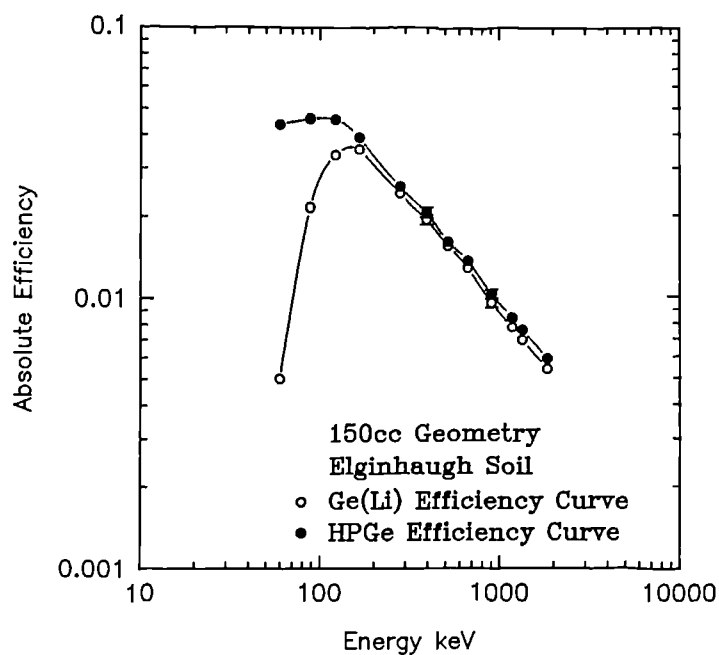


Figure 3.5 The Absolute Efficiency Curves for a Ge(Li) and HPGe Detector.

to the HPGe detector, which has a beryllium window. This is shown in figure 3.5. Also, the Ge(Li) detector crystal has a thin dead layer in the surface of the detector which will cause extra absorption of lower energy photons prior to detection.

Two polynomial equations are fitted to determine the efficiency between the calibration points. The polynomials are fitted about the cross over point which is close to 200 keV for the Ge(Li) detector. The common point chosen is 165.8 keV.

Quality assurance is provided by verifying the calibration with IAEA and NBS standard reference materials.

3.5.6 Quantitative Analysis

Having determined the net peak area for the radionuclide of interest, the activity per unit mass of sample (Bq kg^{-1}) is calculated from equation 3.4.

$$I_m = \frac{A \cdot \exp(0.693 \cdot T_d / T_{1/2})}{T_l \cdot Y \cdot \epsilon \cdot M} \quad (3.4)$$

where:

A	=	peak area
T_d	=	decay time
$T_{1/2}$	=	isotope half life
T_l	=	live collection time
Y	=	gamma ray yield
ϵ	=	absolute detection efficiency
M	=	sample mass

Given the activity per unit mass, conversion to activity per unit area in the field sampled I_a (Bq/m²) for each sample depth interval, is given by equation 3.5:

$$I_a = \frac{I_m M}{S} \quad (3.5)$$

where:

M	=	total dry mass of soil sample collected
S	=	field surface area of sample collected

3.6 GAMMA RAY SPECTROSCOPY - IN-SITU USE IN THE FIELD

This section concentrates on field based measurements using a Bicron 3" x 3" NaI(Tl) crystal and photomultiplier coupled with a Canberra Series 10^{plus} MCA. The benefit of using a NaI(Tl) crystal is the far higher detector efficiency. Thus relatively large amounts of information can be collected in a short space of time. However, the resolution of about 8% (662 keV) requires spectral deconvolution or stripping for analysis.

The use of detectors for in situ application involves exposing the detector to changing environmental parameters which may affect the detector response. For example, the source - detector geometry varies with detector height and orientation, which is discussed separately in section 3.8. Also, other environmental factors such as radionuclide spatial and horizontal distribution within the soil profile affect the detector response, as do topographical geometrical effects. These all have significant influences on calibration and are discussed in the following chapters. In addition, because the detector is exposed to constantly changing conditions, such as temperature which is interrelated with the high voltage power supply, the gain settings have to be

constantly monitored to maintain the energy calibration.

Recent developments have been made in the application of HPGe detectors to environmental gamma ray spectroscopy. The equipment used for this part of the aerial survey system is discussed in section 3.7. Here the discussion is focused on the detector instrumentation, operation and transfer of data from MCA to personal computer and the processing of the data to obtain in-situ based inventory estimates.

3.6.1 Detector and MCA set up.

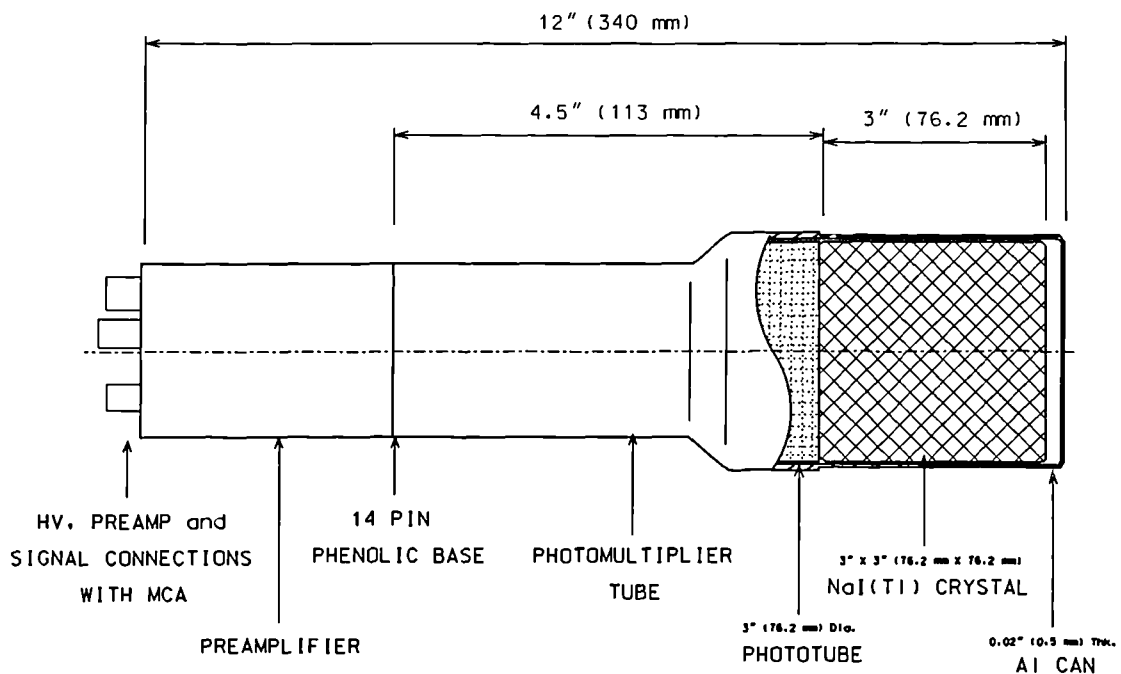


Figure 3.6 The Bicon 3" x 3" NaI(Tl) Detector - PMT - Preamplifier Configuration

A Bicon 3"x3" monoline NaI detector was used for all field based work. The photomultiplier tube (PMT) was coupled directly to the crystal and is part of a hermetically sealed unit. At the end of this configuration, as shown in figure 3.6, is a preamplifier. The crystal is partially surrounded by graded MgO and canned in an 0.5mm thick aluminium. The gain across the PMT is a sensitive function of the applied voltage across the PMT and interdynode voltage can be adjusted by gain or

potentiometer controls.

The preamplifier is primarily used for signal processing (pulse shaping) of the PMT signals prior to sending the pulses to the MCA, whilst little signal amplification is usually required. The detector preamplifier is connected to the MCA via a preamplifier earthed cable, a coaxial signal cable and an extra high tension (EHT) high voltage cable. The Series 10 MCA incorporates a rechargeable high precision power supply in the unit along with a computer for spectral analysis, manipulation and a programmable sequence in which the detector can be set up to make a series of recordings and data transmission sequences. High voltage power output up to 1250 V to the PMT, preamplifier gain, SCA lower limits and upper limits and the number of channels per spectrum are also controlled via the computer. The poorer resolution associated with a NaI detector requires fewer channels per spectral recording, typically 512 channels per spectrum. This is also common to other users of environmental NaI gamma spectrometers (Grasty *et al* 1985, IAEA 1976).

The Series 10 MCA has a maximum of 4096 channels available, and thus with 512 channels per spectrum, is able to store up to 8 spectra. Once the memory is full, the spectra can be transferred to cassette or to a personal computer.

3.6.2 Regions of Interest or Windows

In addition to the recording of full spectral information, regions of interest are also recorded. The regions of interest data are ultimately used for photopeak processing and quantification. The photopeaks (full energy peaks) are defined in a similar manner to those recommended by the IAEA (1990). The extension of this method to a wider selection of radionuclides probably provides the most rapid means for ultimate quantification.

The selection of the regions of interest or windows is based upon energy resolution and small potential changes in energy calibration (gain shift). The window is set up

Table 3.2 Showing the 8 Regions of Interest for Series 10⁺ MCA and 3"x3" NaI(Tl) Detector, compared with the IAEA (1990) recommended windows.

No.	Channel Numbers	Peak Position	Radionuclide and Energy Range keV	IAEA (1990) keV
1	97 - 131	114	¹³⁷ Cs (563.3-760.7)	
2	126 - 150	138	¹³⁴ Cs (646.4-769.6)	
3	218 - 267	243	⁴⁰ K (1332-1606)	(1370-1570)
4	267 - 313	290	²¹⁴ Bi (1620-1900)	(1660-1860)
5	383 - 470	427	²⁰⁸ Tl (2350-2884)	(2410-2810)
6	82 - 490	---	> 450 keV	
7	199 - 228	214	⁴¹ Ar (1193-1367)	
8	14 - 82	---	15 - 450 keV	

around each photopeak or energy range which is easily achieved with the MCA. Eight regions of interest are recorded with each spectrum as illustrated in table 3.2. The final widths of the windows chosen are slightly wider than those recommended by the IAEA. However, experiments in later chapters show their usefulness, and they are used throughout the duration of this research.

The total sum of the channels within each window is associated with each photo peak of interest, the background contribution and the interferences caused by scattering and interferences from overlapping photopeaks. Thus for quantification purposes, these interferences have to be subtracted from the regions of interest data.

3.6.3 Background Radiation and Background Subtraction

IAEA (1976) defines the term *background* as the radiation which does not originate from the lithosphere. Thus for a detector placed in the open, background should be defined as the sum effect of cosmic rays, atmospheric activity and the radioactivity of the measuring system itself.

The background of the 3"x 3" detector, PMT and preamplifier was measured with a lead castle usually used for laboratory based HPGe detectors. The spectrum consists principally of scattered cosmic rays, and activity from the NaI crystal (⁴⁰K, Ra and

Th), container (U and Th) and the photomultiplier tube (occasional K and Ra depending on glass) (Shafroth 1967). Scattered cosmic rays appear within the spectra although they form a very small continuum across the whole spectrum.

The presence of airborne radioactive gases has to be monitored whilst carrying out field surveys. ^{41}Ar is not normally a problem unless in the vicinity of a nuclear reactor, but is easily detected by its presence in the spectrum (table 3.2). ^{222}Rn and its daughter isotopes ^{214}Bi and ^{214}Pb are more difficult to account for. The daughters are present as positive ions attached to airborne dust particles (aerosols), for which the concentration and distribution are strongly influenced by atmospheric mixing conditions as well as the underlying geology. However, rapid variations in their concentrations rarely occur and even under the most favourable conditions, rarely account for more than 5% of the background contribution (IAEA 1979).

3.6.4 Stripping Spectral Interferences

NaI(Tl) detectors have a resolution (FWHM) of about 8% and thus the photopeaks contain contributions from scattered higher energy photons and peaks from natural decay series of ^{238}U and ^{232}Th . These influences are difficult to resolve without prior knowledge of potential spectral interferences. For example, ^{208}Tl is measured to represent 36% of the ^{232}Th present. The window for ^{208}Tl is centred around the 2.62 MeV photopeak (figure 3.7). However, ^{208}Tl has two further principal photopeak energies at 510 and 580 keV. In addition, the ^{232}Th decay series includes ^{212}Bi (730 keV), ^{212}Pb (240 keV) and ^{228}Ac (910 and 960 keV) as illustrated in table 2.1. These all contribute to the spectrum by a factor directly proportional to the amount of ^{208}Tl measured at 2.62 MeV. Similarly, ^{214}Bi forms part of the ^{238}U of the natural series and is measured at 1.76 MeV (figure 3.7). ^{214}Bi has photopeaks at energies 610 keV and 1.12 MeV. In addition, of the natural ^{238}U series, ^{214}Pb provides photopeaks at 290 and 350 keV also illustrated in table 2.1. ^{40}K is a simple example, where the influence on lower energy regions of interest occurs purely as a result of scattering of the primary photons at 1462 keV within the environment and within the detector. All these photopeaks and their scattered secondary photons contribute to the total counts

recorded in the windows illustrated in table 3.2.

Thus, to determine the net count rates within each window, the spectrum has to be stripped through a process known as deconvolution. To measure the stripping ratios ^{238}U , ^{232}Th and ^{40}K sources are required. For this purpose a set of concrete calibration pads is used as recommended by Grasty (1981), Løvborg *et al* (1981) and Løvborg (1983) and Løvborg *et al* (1978b) and IAEA (1976, 1979, 1990, 1991). A set of four concrete calibration pads was purchased from the Canadian Geological Survey. These simulate the scattering of natural radionuclides from rock exposures.

The set of four concrete 1 m² pads includes one blank concrete pad while the others are doped with ^{40}K and equilibrated U and Th (Appendix G). The background pad was used to subtract the activity associated with the pure concrete in the pad and surrounds from the doped pads. This leaves a spectrum associated with the doped activity and its scattering from within a concrete matrix only. Figure 3.7 shows the net spectra observed and the interferences each has within the working windows used.

Table 3.3 shows the net counts per second recorded within each window. For each pad, the influence on the other windows is ratioed with respect to the window used to measure that particular concentration. These ratios are given in table 3.4.

Table 3.3 Net Counts per Second within the Working Windows

	^{137}Cs	^{134}Cs	^{40}K	^{214}Bi	^{208}Tl
Calibration Pad	Ch.1	Ch.2	Ch.3	Ch.4	Ch.5
Potassium Pad	16.73	14.62	23.03	0	0
Uranium Pad	82.17	35.83	19.75	16.86	0.97
Thorium Pad	76.70	17.4	15.61	13.08	17.45

The stripping ratios for ^{137}Cs and ^{134}Cs are also given in table 3.4 and spectra shown in figure 3.7. These were measured with point sources, which may not reflect the scattering conditions observed in soils. The majority of the spectral interference would appear to be from ^{134}Cs upon ^{137}Cs . However, ^{134}Cs has a shorter half life than

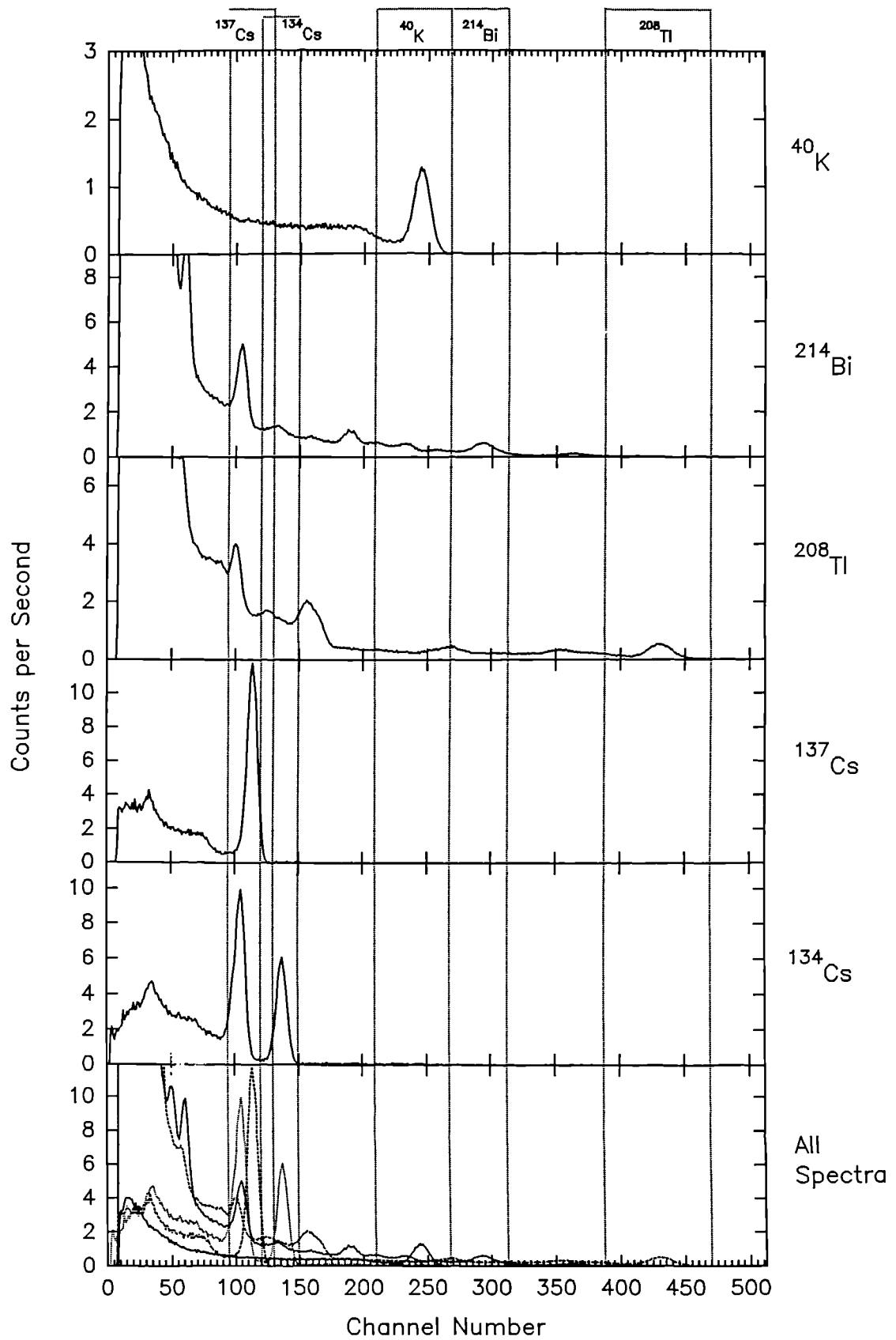


Figure 3.7 The Net Spectra from the Concrete Calibration pads and the Working Regions of interest.

^{137}Cs , and, when measured, tends to occur closer to the soil surface, thus scattering of ^{134}Cs in the soil profile would be less than that associated with ^{137}Cs .

The contributions to each spectral window are given in table 3.4. The net count rate in each window can be determined by gaussian elimination or matrix inversion. However, a simplified technique is used for the in-situ detector as given in equation 3.6 for primordial radionuclides and in equation 3.7 for anthropogenic radionuclides.

$$\begin{aligned} N_{Th} &= N'_{Th} \\ N_U &= N'_U - \alpha N'_{Th} \\ N_K &= N'_K - \beta N'_{Th} - \gamma N'_U \end{aligned} \quad (3.6)$$

$$\begin{aligned} N_{Cs137} &= N'_{Cs137} - aN'_{Th} - bN'_U - cN'_K - dN'_{Cs134} \\ N_{Cs134} &= N'_{Cs134} - eN'_{Th} - fN'_U - gN'_K - hN'_{Cs137} \end{aligned} \quad (3.7)$$

where: N_{Th} , N_U , N_K , N_{Cs137} = stripped or true counts
 N'_{Th} , N'_U , N'_K , N'_{Cs137} = measured counts
 α , β , γ , a , b , c , d , e , f , g , h = the stripping coefficients

Table 3.4 Stripping Ratios for each channel.

	^{137}Cs	^{134}Cs	^{40}K	^{214}Bi	^{208}Tl
Calibration Pad	Ch.1	Ch.2	Ch.3	Ch.4	Ch.5
Potassium	0.726	0.635	1	0	0
Uranium	4.874	2.125	1.171	1	0.058
Thorium	4.395	0.997	0.895	0.750	1
Caesium-137	1	0.0219	0	0	0
Caesium-134	1.871	1	0.026	0	0

However, as suggested by Potts (1978), the uncertainty of the final stripped count rate can be strongly influenced by the stripping ratios and the relative intensities of the signals within that window. For example, if the ^{137}Cs signal is weak whilst the natural series contribution is strong, then the uncertainties on the ^{137}Cs net count will be dominated by the natural series contribution. This is discussed further in section 3.9.

3.6.5 Full Spectral Stripping

Full spectral stripping is also undertaken with spectra collected with the 3"x3" NaI(Tl) detector. A simple procedure, similar to that demonstrated for window stripping, was adopted. However, here the pure spectra measured from concrete calibration pads are stripped out of composite spectra collected in the field in the proportions determined from the net full energy peak counts. The pure thorium spectrum is stripped out of the spectrum first, leaving the uranium window minus the thorium contribution. The Uranium contribution is then stripped out leaving the K window net U and Th. This is continued appropriately for K, and ^{134}Cs leaving the ^{137}Cs spectrum. Some residual contribution will remain from the other radionuclides, as clearly the scattering characteristics associated with the concrete sources do not represent exactly environmental conditions. However, this is likely to provide a systematic residual contribution.

3.6.6 Sensitivity Calibration

The calibration of an in-situ detector forms part of the theme of this thesis. There are three possible approaches to the calibration of in-situ gamma spectrometers: i) through analytical solutions to photon transport equations (section 3.8), ii) through measurement of the activity of a known spiked area (e.g. concrete calibration pad), and iii) through comparison with laboratory derived results of soil sample activities sampled from within the field of view of the detector. This ultimately forms a route for the verification of the first two approaches and the problems involved are discussed in the following chapters.

3.6.7 Software

The software used to process the spectra was developed in-house by Scottish Universities Research and Reactor Centre (SURRC). The spectra and regions of interest are transferred to PC and stored on disk via a data logging program. The regions of interest data are then collated to form summary files of regions of interest

data. The software then subtracts the recorded background associated with each window in the summary file data to produce a net data summary file. The program then strips the data with the appropriate stripping coefficients and then converts the data into activities using the appropriate calibration coefficients.

All data are recorded on disk at each stage of the calculation for backup and for quality assurance. Should the windows of interest require changing, then the old spectra can be reintegrated to create new summary files.

3.6.8 Field Work Procedure

The detector was supported from a tripod so that the crystal was at 1 m above the ground. The counting live time was typically between 500 and 1000 seconds depending upon the count rate to minimise counting errors. The operator stood at a distance from the detector so as not to interfere with its field of view. Once the spectrum was collected, it was stored along with the recording time and date into one of the eight memory segments in the series 10^{plus} MCA. It could then be reused to collect another 7 spectra. The regions of interest data and full spectra were then transferred to disks via a computer, such as a lap top computer operating in the field, using SURRC data logging software. The regions of interest data and spectra were then processed as discussed.

3.7 GAMMA RAY SPECTROSCOPY - AERIAL SURVEY

This section concentrates on the aerial survey equipment at SURRC and its operation. It also illustrates the current and future capabilities of HPGe detectors used in parallel with large volume NaI detectors. The basic system comprises a large volume NaI detector, custom built high precision power supply, data logging computer and navigational equipment. The operation of the equipment in aerial survey mode and the interpretation of the data has further complications over and above those experienced with in-situ gamma spectroscopy. Here the stripping ratios and calibration of the detectors are height dependent. This aspect is discussed in the

following chapters. The basic principles of detector design and instrumentation have already been discussed at length. This section therefore provides only a brief description of the detector hardware.

3.7.1 Aerial Survey Equipment Development by SURRC

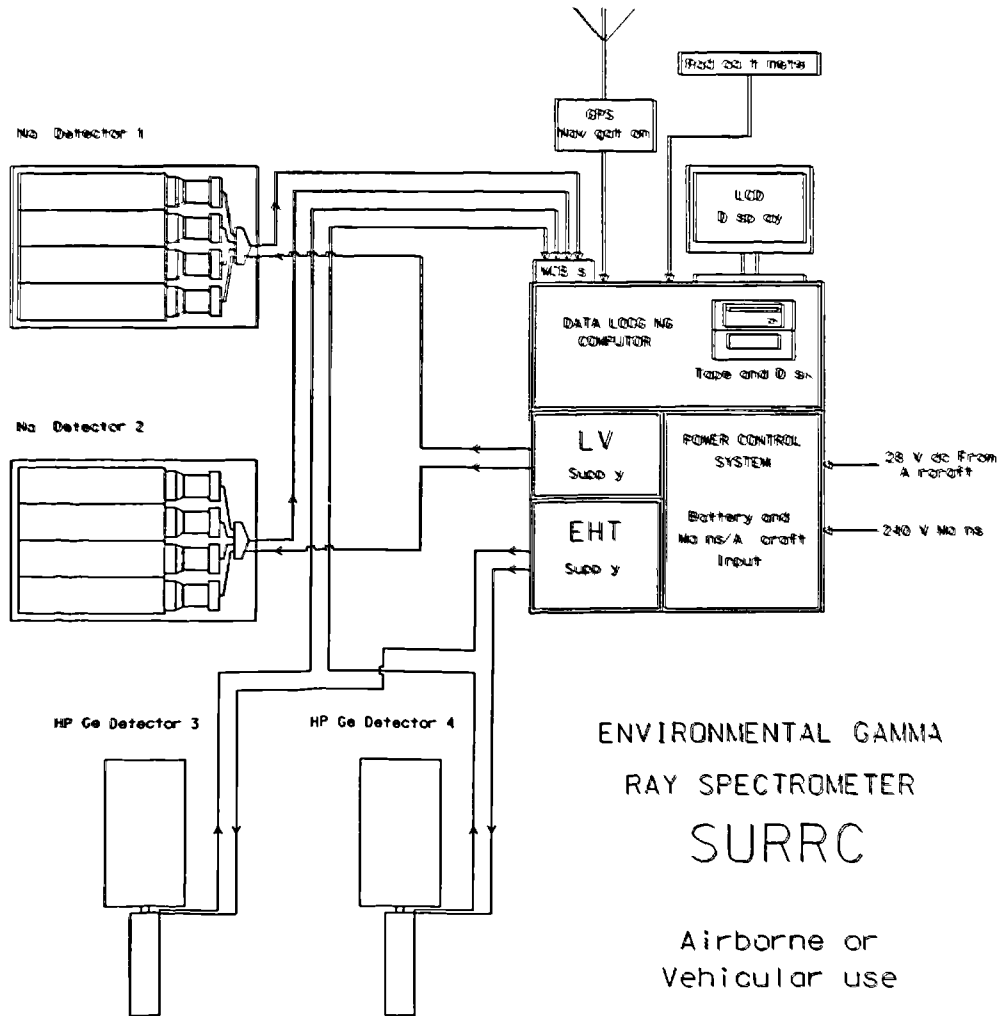


Figure 3.8 The SURRC Aerial Survey Equipment (not drawn to scale)

The current version of the system is shown in figure 3.8. It is able to operate up to two 16 litre detectors and two HPGe detectors simultaneously (or 4 HPGe detectors via two summing amplifiers). The whole system can be mounted on a custom built shock mounted base plate and installed into an Aerospatial Squirrel helicopter within one hour for emergency response purposes. Each 16 litre detector box (detector 1 and 2 in figure 3.8) is made up of an array of four prismatic 10x10x40 cm detectors

typical of those used by geological exploration companies since the 1980's. The detectors are housed in GRD 1500 gamma ray detector boxes which are designed to provide physical and thermal shock protection. Each detector is viewed directly by a 3" diameter photomultiplier tube, resulting in individual resolutions of about 8% at 662 keV. A pre-amplifier is also attached to each detector through which the gain and focus of the photomultiplier can be individually adjusted. The four detectors are connected by a crystal pack Printed Circuit Board (PCB). The PCB's primary purpose is to distribute cleanly the necessary interconnections of power and signals required for each detector which includes low voltage power to the preamplifiers and high voltage to the photomultipliers. A regulator in the PCB also filters the signal before sending the pulses back to the Multi Channel Buffers (MCB's) via a signal cable.

The detection system is also able to operate two HPGe detectors. There are two principle types of portable HPGe detector available for use with the detection system. The first type are EG&G Ortec *GMX* (gamma-X) photon detectors which are n-type crystals of high purity germanium which permit the entire outer surface to be ion implanted. The use of a thin ion implanted wrap-around window allows the detector to be used effectively at photon energies as low as 3 keV. It is also able to be used up to 10 MeV, similar to other coaxial germanium detectors. These detectors have 50 % relative efficiency and are thus useful for aerial survey applications. To obtain the full benefit at low energies the detector is supplied with a large beryllium window.

As an alternative, the system is being developed to operate up to four EG&G n-type *LO-AX* photon detectors for in-situ and aerial survey applications. These detectors have a shorter axis but a larger surface area and are particularly useful for low energy photon use with a superior energy resolution. These *LO-AX* HPGe detectors also have a thin ion-implanted front contact and a useful energy range of between 3 keV and 1 MeV. Both types of HPGe detector are cooled with portable dewars providing a useful operation time of between 48 and 72 hours. Apart from the size of the dewars, their configuration is very similar to that illustrated in figure 3.4. For the purposes of aerial survey, the HPGe detectors have to be mounted on vibration damping mounts.

The power for the NaI(Tl) detectors is supplied by a custom built high precision EHT high voltage power supply and low voltage power supply which is fed to the PCB via a single earthed EHT power cable. This system also supplies power to the NIM bin which powers the portable HPGe detectors. The NIM bin itself contains two 5 kV bias supply units and two linear amplifiers. These nucleonics can be powered from 240 V ac mains supply, 28 V dc aircraft supply or by their own in built 24 V battery supply. The custom built power supply control unit contains inverters and transformers which provide the output required to power the computer and display, navigation system, detector system and/or recharge of its own batteries. The signal pulses from the detectors are fed into EG&G multi channel buffers (MCB's). The MCB's are housed in the back of the PC, which along with MCA emulation software transforms the PC into a versatile multichannel analyser.

The height of the detector is fed into the computer from the aircraft's radar altimeter. The position is recorded automatically from a Global Position and Navigation System (GPS-Navstar). The system tracks up to 8 satellites from an antenna position on the aircraft's tail. By monitoring known time pulses sent out from satellite atomic clocks at known positions and times, it calculates its own position in latitude and longitude with a nominal accuracy of less than 100 m. By entering in way points, the GPS system can be used to help navigate the aircraft in straight lines.

The majority of this research is based upon the use of NaI(Tl) detectors as the incorporation of HPGe detectors into the system represents a recent development. Thus the discussion will continue by focusing on the use of the 16 litre NaI(Tl) detectors.

3.7.2 Regions of Interest or Windows

As with the in-situ detector, the use of regions of interest represents an extension of the IAEA (1990) method. In addition to the reasons discussed in section 3.6.2, the windows chosen must be tolerant of resolution degradation which can occur with multicrystal detector arrays through small gain shifts. In practice gain shifts of 1 %

Table 3.5 Showing the 8 Regions of Interest for Series Aerial Survey NaI(Tl) detector array, compared with the IAEA (1990) recommended windows.

No.	Channel Numbers	Peak Position	Radionuclide and Energy Range keV	IAEA (1990) keV
1	95 - 130	110	¹³⁷ Cs (544-761)	
2	125 - 150	138	¹³⁴ Cs (730-885)	
3	220 - 270	240	⁴⁰ K (1319-1629)	(1370-1570)
4	270 - 318	294	²¹⁴ Bi (1629-1927)	(1660-1860)
5	390 - 480	435	²⁰⁸ Tl (2374-2932)	(2410-2810)
6	82 - 490	---	> 450 keV	
7	14 - 82	---	15 - 450 keV	

stability or better are observed and the extra window width serves as a quality assurance aid. The windows used are given in table 3.5.

3.7.3 Background Subtraction

The background of the airborne detector also includes the radiation emanating from the aircraft and its contents. Background measurements are made by hovering over large expanses of deep water and/or by making measurements at above 1500 - 2000 feet where the terrestrial component to the background radiation is negligible. Summary files are formed and the mean background contribution to each region of interest is calculated and used in the data processing procedure. These background measurements are repeated on a daily basis to measure the variation in airborne ²²²Rn contributions.

3.7.4 Stripping Spectral Interferences

As with field based gamma spectrometry, the stripping of net spectral data is required to determine the true count rate associated with the window of interest. For aerial survey, true window count rate was determined by multiplying the net window count rates with the corresponding inverse stripping coefficient.

However, as the detector is raised above the ground, the increased pathlength changes the scattering conditions considerably from those associated with concrete calibration pads. Attempts to account for this changed behaviour have involved the simulation of the air-pathlength by addition of plywood absorbers between the source and detector (Grasty, 1981). This is explored further in chapter 7 and Appendix J.

3.7.5 Height Correction Coefficients

As the detector is raised above the ground, the source detector geometry changes and the scattering pathlength also increases. This results in changes in the photopeak response and has to be corrected for. Thus by raising the detector above a uniform homogenous plane, the change in detector response can be calculated. All aerial survey measurements are corrected to a nominal altitude (e.g. 100 m).

From Kogan (1971) and Grasty (1971) the physical form of the height correction coefficient can be approximated by a simple exponential. For each of the window stripped count rates, the coefficients (a) can be approximated by linear regression of the exponential relationship. These are used to determine the corrected detector (N) response for 100 m altitude (N_{100}) from equation 3.8:

$$\begin{aligned}
 N_x &= N_o \cdot e^{-ax} \\
 N_{100} &= N_o \cdot e^{-100a} \\
 \therefore \frac{N_{100}}{N_x} &= e^{a(x - 100)}
 \end{aligned}
 \tag{3.8}$$

The calibration factors are determined for a nominal 100m altitude.

In practice a uniform distribution of activity across a plane rarely exists in the environment and thus changes in the spatial distribution of activity ideally need be corrected for in the determination of the height correction coefficient.

3.7.6 Calibration

The means to achieve an optimal calibration is one of the issues addressed by this thesis. As discussed in chapter 1, historically, the solution to calibration of geological exploration equipment was to use concrete calibration facilities, with calibration areas constructed with similarly calibrated field based spectrometers (IAEA 1976, 1979, 1990, 1991, Alexander and Kosanke 1978, and Løvborg *et al* 1978a,b). However, no anthropogenic radionuclide concrete calibration facilities exist, which, in any case, would be inappropriate due to the inherently different scattering conditions and source distributions observed in the environment. Thus calibrations are based on comparisons with soil samples. This latter approach to calibration is discussed in chapter 6 and 7.

An alternative method for determining calibration is to obtain analytical solutions to photon transport equations. In addition full spectral response characteristics can be modelled using Monte Carlo simulations (Allyson 1994). Given the random and systematic errors imposed upon empirical calibration methods and the potential systematic errors upon calibration simulations, calibration validation benefits greatly from a mutual comparison between simulated and experimental data.

3.7.7 System Operation

The SURRC spectrometer, as illustrated in figure 3.8, has been developed for experienced single person operation. The following is a discussion concerning the operation of a single MCB. However, the system can operate up to four MCB's simultaneously. The start up procedure involves input from the keyboard during which the spectral response characteristics are checked through the MCB by the operator. Thereafter, the datalogging program is initiated with choice of a root filename which is common to data collected during the flight or flight line. This is entered and automatically starts the first data acquisition period of the MCB (using the appropriate integration time). The position (latitude and longitude) are read in, since 1992 directly from a GPS system along with the time of the positional reading. The computer defines and opens the first filename. It reads in the detector's altitude from

the aircraft's radar altimeter and averages it with previous readings whenever the computer is not busy with other functions. Once the MCB has finished counting, the computer captures the data, records the time, clears and restarts the MCB. The computer updates the positional estimate from the GPS and interpolates a mean position for that data set. The full spectrum is recorded and labelled with times, mean position and altitude in the open file on either hard disk or floppy drive. The computer then integrates the spectrum into 8 regions of interest (ROI) and stores it in a compressed form. The ROI data are displayed on screen. The detector gain is monitored by measuring the symmetry or otherwise of the ^{40}K peak with respect to its required position, which is also displayed to the operator. The first file is then closed and the computer selects the second filename and the recording procedure with position and altitude repeats itself until the required number of spectra have been collected or the operator interrupts the program.

Once this is complete, summary files of the ROI data are created or are generated by reintegrating from full spectra. The background is subtracted from the summary files to form identically structured net summary files. These net files are then stripped appropriately. The data are then normalised to 100 m altitude using the predetermined height correction coefficients. The data are then converted to activity per unit area (Bq m^{-2}), activity concentration (Bq kg^{-1}), and dose rate (mGy a^{-1}) based on a linear relationship between ground based estimates from calibration sites and the altitude corrected stripped count rates. Again the standard summary file format is maintained.

3.8 DETECTOR RESPONSE CHARACTERISTICS

3.8.1 Photon Fluence Equations and the Calculation of Fields of View of In-situ and Aerial Gamma Detectors

There are two principle techniques of quantifying the circle of investigation. The first is to use point sources (Cutshall and Larsen 1986) or spiked areas, with quantified amounts of activity of known photon energy, and measure the signal with distance from the detector to determine the detector response. The detector spatial response is

determined by integrating these responses over the area represented by each radial distance. However, it is difficult to adapt this technique experimentally to allow for the effect of source burial.

The alternative and more efficient technique is to solve photon transport equations analytically. Beck *et al* (1972), Anspaugh *et al* (1972), Helfer and Miller (1988), Sowa *et al* (1989) and ICRU (1993) discuss the fundamental quantities used for in-situ gamma spectroscopy. The parameters are: N the photopeak count rate (s^{-1}), A the activity per unit area ($Bq\ m^{-2}$), per unit volume ($Bq\ m^{-3}$) or per unit mass ($Bq\ kg^{-1}$) in the soil, and ψ the fluence rate ($cm^{-2}s^{-1}$). The calibration coefficient at some energy E is defined as N/A , which is given by:

$$\frac{N}{A} = \frac{N}{N_o} \cdot \frac{N_o}{\psi} \cdot \frac{\psi}{A} \quad (3.9)$$

where:

N/N_o is the angular correction factor of the detector at energy E for a given source distribution in the soil. This is measured relative to $\Theta = 0^\circ$ or 0 radians, and is dependent upon detector shape as well as the source distribution profile within the soil.

N_o/ψ is the full energy peak count rate per unit fluence rate for a plane parallel beam of photons at energy E , that is normal to the detector face. This is purely dependent upon detector characteristics.

ψ/A is the number of photons arriving at the detector unscattered due to a gamma transition for a particular nuclide, of energy E . This is purely dependent upon the source distribution characteristics within the soil.

Of importance from this photon fluence equation is the determination of the circle of investigation. The contribution of fluence rate to a point above the ground is given by plotting the fraction of the total fluence rate (ψ/A) with radius. By incorporating the detector angular correction factor, the circles of investigation can be calculated.

3.8.2 Analytical Solutions to Photon Transport Equations

One solution for calculating the circle of investigation was given by Duval *et al* (1971). Duval assumed that the signal originated from an infinite source depth, the detector was spherical with uniform angular characteristics and that the mass attenuation coefficient was dependent upon photon energy though, for the purposes of this discussion, independent of the chemical composition of air, soil and rock. Duval defined the observed photopeak intensity as dC in equation 3.10:

$$dC = \frac{A\epsilon\gamma}{4\pi} \cdot e^{-\frac{\mu\rho_a h}{\cos\theta}} \cdot e^{-\mu\rho_s \frac{R-h}{\cos\theta}} \sin\theta d\theta d\phi dR \quad (3.10)$$

where A = detector cross-sectional area
 ϵ = detector efficiency for a particular photopeak energy
 γ = is the number of gamma's emitted per cubic meter of source material
 μ = mass attenuation coefficient
 ρ_a = density of air
 ρ_s = density of soil or rock

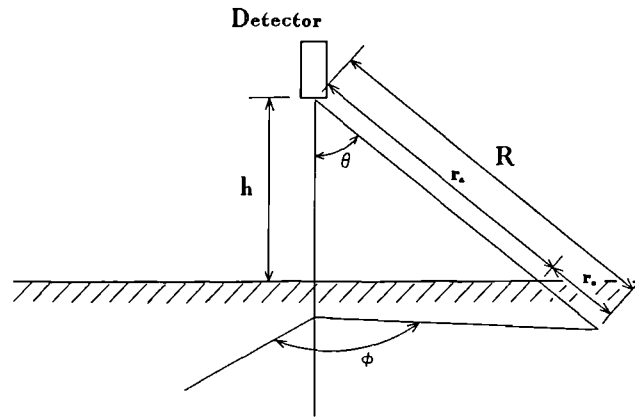


Figure 3.9. The Spherical Coordinate System for In-situ Gamma Ray Detector with Integration limits $R_1 \leq R \leq \infty$, $\Theta_1 \leq \Theta \leq \pi/2$ and $0 \leq \phi \leq 2\pi$ for Field of View Calculations.

Integrating this with limits illustrated in figure 3.9 gives equation 3.11:

$$C = \frac{A\epsilon\gamma}{4\pi} \int_{R_1}^{\infty} \int_0^{2\pi} \int_{\Theta_1}^{\pi/2} e^{-\mu\rho_s R} \cdot e^{-\frac{\mu(\rho_a - \rho_s)h}{\cos\theta}} \sin\theta d\theta d\phi dR \quad (3.11)$$

Duval *et al* solved this by integrating with respect to R , ϕ and Θ to give equation 3.12 where $\lambda = 0.5772157$. The equation gives the count rate outside a dish-shaped volume

$$C(h,z,\theta_1) = \frac{A\epsilon\gamma}{2\mu\rho_s} \cdot e^{-\mu\rho_s d} \cdot \cos\theta_1 \left[e^{\frac{-\mu\rho_a h}{\cos\theta}} + \frac{\mu\rho_a h}{\cos\theta_1} \right. \\ \left. \cdot \left[\lambda + \log\left(\frac{\mu\rho_a h}{\cos\theta_1}\right) + \sum_{n=1}^{\infty} \frac{\left(\frac{\mu\rho_s h}{\cos\theta_1}\right)^n (-1)^n}{n \cdot n!} \right] \right] \quad (3.12)$$

within the circle of investigation of radius $r = h \tan \theta_1$. The determination of the yield from within this volume is give in equation 3.13:

$$(3.13) \quad C(h,r) = C(h,0,0) - C(h,0,\theta_1) - C(h,z,0) + C(h,z,\theta_1)$$

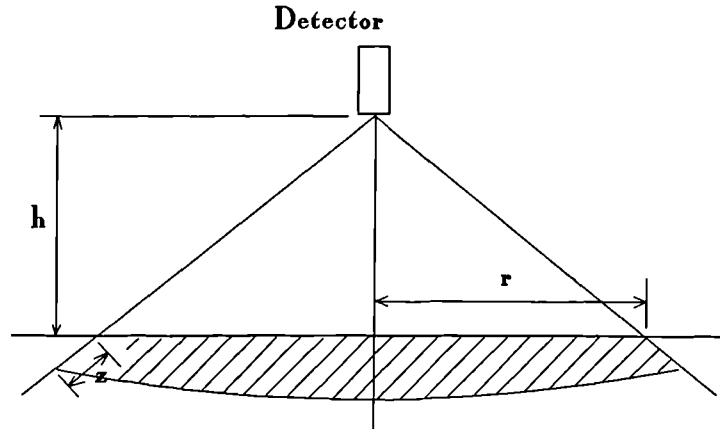


Figure 3.10 The Hatched Area Illustrates the Volume of Source Material which is given from Equation 3.12

This represents the volume shown in figure 3.10. As we are looking at the relative detector response with distance, the absolute detector characteristics of A , ϵ , γ can be cancelled out of the analysis. An example of the results is illustrated in figure 3.11. However, the use of this solution is limited to geological applications. It assumes a photon flux from an infinite source depth, which can only be realistically applied to exposed geological rock masses. In reality, rock has an overburden, and for anthropogenic studies the activity distribution forms either a planar sheet on the surface of the soil or, as in most cases, exhibits a depth distribution profile within the soil, be it exponential or otherwise. Also the detector geometry is assumed to be uniform and thus the angular response variation negligible. Even though Lønborg and Kirkegaard (1974) illustrate the angular response to be unimportant for energies above

500 keV for 3" x 3" NaI(Tl) activated crystals, larger volume crystals exhibit more marked dependence on the angular response.

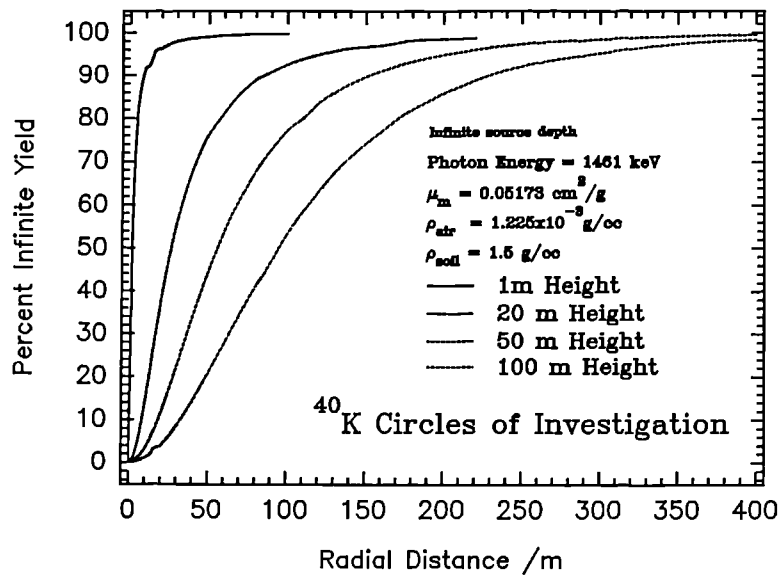


Figure 3.11 Circles of Investigation for ⁴⁰K after Duval *et al* 1971.

Since Duval *et al's* (1971) paper, the problem of the mass relaxation depth of radionuclides (Beck *et al* 1972; Dickson *et al* 1976; Helfer and Miller 1988) and the importance of the angular response of detectors (Beck *et al* 1972; Grasty *et al* 1979; Helfer and Miller 1988) have been recognised.

The application of the field of view calculations has traditionally been applied to ⁴⁰K, ²¹⁴Bi and ²⁰⁸Tl. The need to determine the field of view and detector response for the anthropogenic radionuclides ¹³⁷Cs, ¹³⁴Cs, ¹³¹I and even ²⁴¹Am, stimulated a development of the application of this approach.

Allyson (1994) describes in addition the influence of the angular response of detectors. Instead of integrating by parts, the circle of investigation of radius *R* is defined as *COI* in equation 3.14.

$$COI_R = \frac{C_R}{C_\infty} \quad (3.14)$$

where C is given by 3.15 (Beck *et al* 1972):

$$C = \int_0^{2\pi} \int_0^{\frac{\pi}{2}} \int_{\frac{h}{\cos\theta}}^{\infty} \frac{A e^{[-(\alpha/\rho_s)\rho_s z]} \gamma_{100} \sigma_{det,\theta,\phi}}{4\pi P_{tot}^2} P_{tot}^2 \sin\theta e^{-\mu_a \rho_a P_a} e^{-\mu_s \rho_s P_s} dR d\theta d\phi \quad (3.15)$$

- where $\sigma_{det,\phi}$ = effective detection cross-section and its angular dependence
 P_{tot} = Total gamma-ray path length = $P_a + P_s$
 α = the reciprocal of the relaxation length of the assumed exponential-distributed source activity with depth, cm^{-1}
 μ_a = mass attenuation coefficient in air
 μ_s = mass attenuation coefficient in soil
 ρ_a = density of air
 ρ_s = density of soil or rock
 z = vertical depth from surface
 R = radius of circular area
 A = Activity
 γ_{100} = no. of gamma-rays emitted per 100 decays

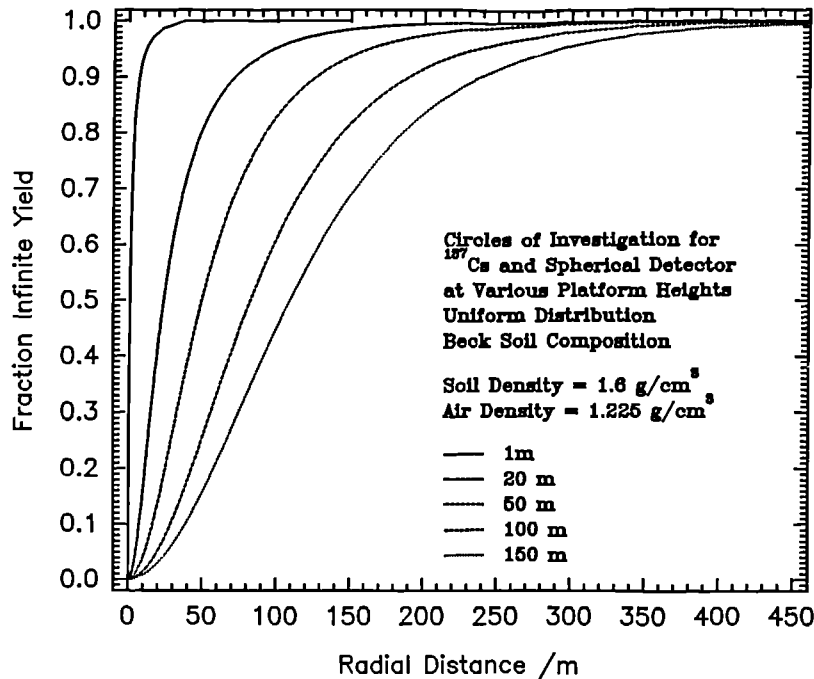


Figure 3.12 The Increase in the Circle of Investigation with Platform Height for ^{137}Cs , after Allyson (1994).

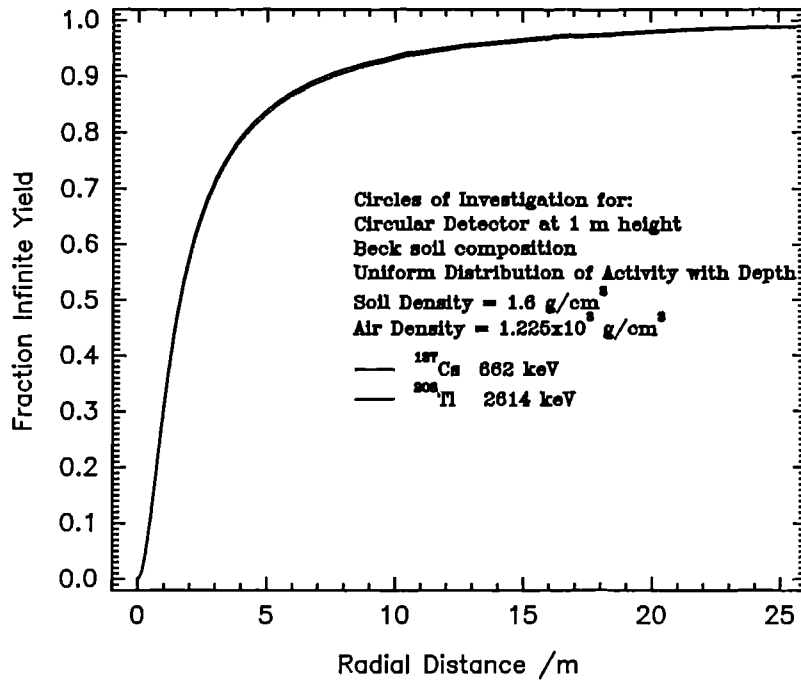


Figure 3.13. The change in the field of view of a detector at 1 m height with energy, after Allyson (1994).

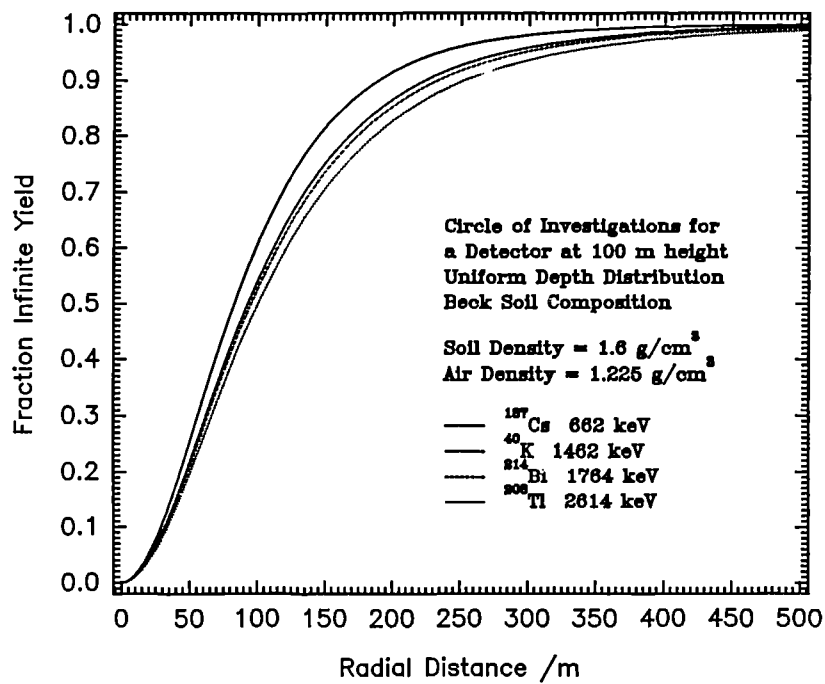


Figure 3.14 The change in the field of view of detectors at aerial survey height with gamma ray energy, after Allyson (1994).

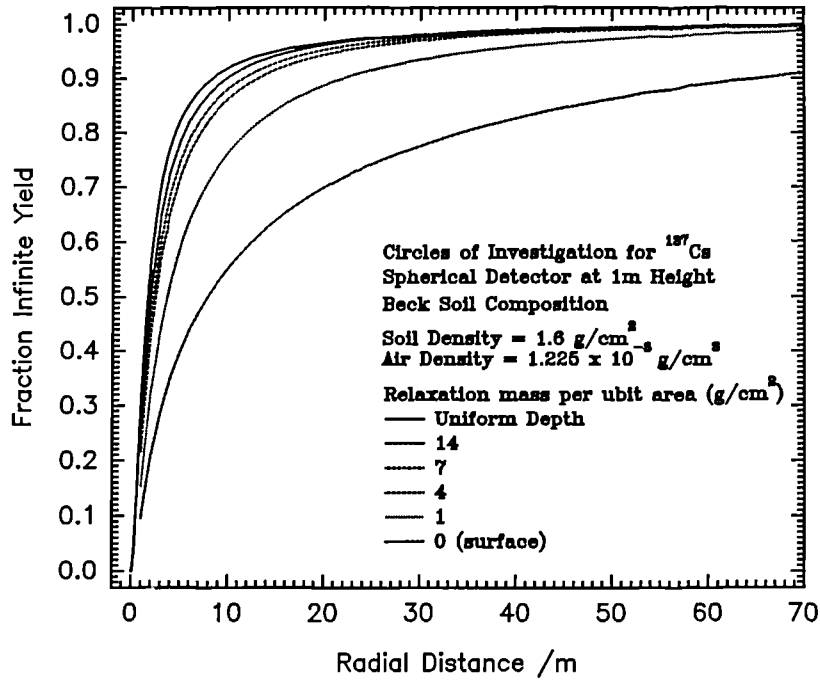


Figure 3.15 The Influence of the Mass Relaxation per unit Area (g/cm^2) for a Detector at 1 m Height, after Allyson (1994).

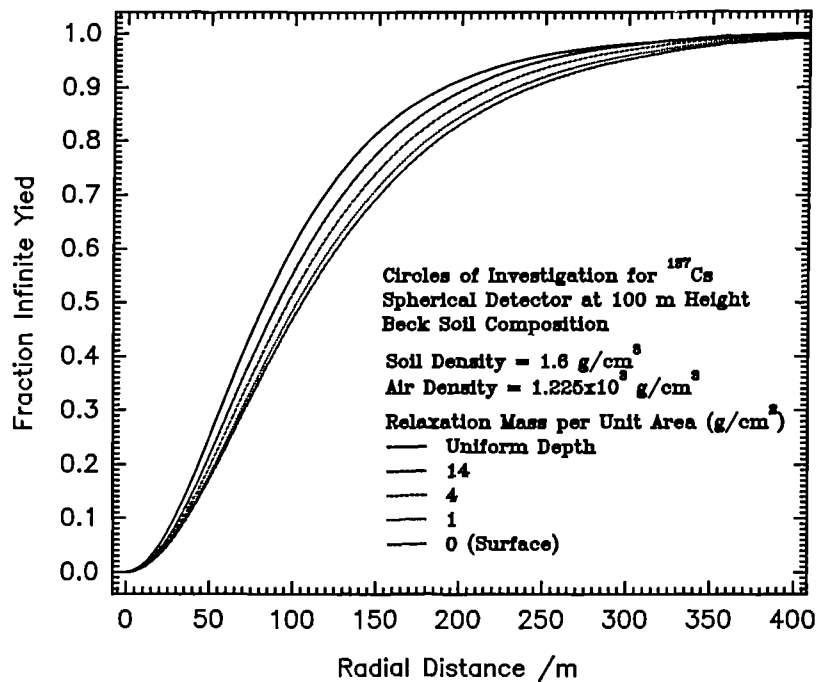


Figure 3.16 The Mass Relaxation per Unit Area (g/cm^2) on the Field of View for Detectors at aerial survey Height, after Allyson (1994).

The results from equations 14 and 15 are illustrated in figures 3.12 to 3.16. Figure 3.12 shows the increase in the field of view of the detector with increase in platform

height with 90 % of the infinite yield originating from a circle of investigation of 9 m radius for a detector at 1 m height increasing to about 180 m radius for a detector at 100 m altitude. The influence of photon energy on the field of view of a detector is important at aerial survey altitudes as illustrated in figure 3.14, though clearly an increase in photon energy has a negligible influence on the circle of investigation of a field based detector at 1 m height (figure 3.13).

The source distribution with depth will clearly have a significant influence on the circle of investigation. The distribution of anthropogenic radionuclides with depth is often modelled by a single exponential relationship. Whilst this may provide an approximation for fresh or nearly fresh deposition (ICRU 1993), this assumption will break down rapidly as diffusion and migration processes acting upon the radionuclides develop with time. Thus with time a more complex profile shape develops, such as a subsurface maximum. A similar feature develops in coastal salt marsh environments as a consequence of deposition of less active sediments over more active ones. Post depositional processes may also serve to complicate this shape. Thus with time the mathematical description of these profile shapes is complicated.

The exponential decrease in radioactivity with soil mass depth, equation 7.3, is described by α/ρ or β^{-1} , the reciprocal of the mass relaxation per unit area parameter ($\text{cm}^2 \text{g}^{-1}$) (Beck *et al* 1972). This is discussed further in section 7.3. Figures 3.15 and 3.16 show the influence of the mass relaxation per unit area parameter on the circles of investigation for a field based detector at 1 m height and an aerial survey detector at 100 m altitude. Figure 3.15 shows the importance of the mass relaxation per unit area with a field based detector. This is due to the increased photon path travelled through soil due to the wider field with respect to detector height, observed as a large solid angle Θ . For an aerial based detector, the distance travelled by photons in the soil is not so great given the smaller Θ , and thus the distribution of the source in the soil is not as important. This is illustrated by comparing figure 3.15 with 3.16.

The effect of detector shape on the circles of investigation can be efficiently calculated by Monte Carlo simulation. This is illustrated and discussed by Allyson (1994).

However, for the purposes of this discussion, the influence of detector shape on the field of view is not considered, particularly when other environmental factors involved in empirical comparisons, such as sampling errors, are quite considerable (chapter 6).

Clearly the field of view of a detector is an important factor to be considered when relating soil samples with in-situ detector measurements. The spatial averaging of each detector measurement is not uniform and is dictated by several environmental and physical parameters which also have to be taken into consideration when calculating the field of view of these detectors. Thus, although detector height largely determines the magnitude of the circle of investigation, the mass relaxation per unit area parameter is of significant importance for field based detectors, though as the detector is raised to aerial survey altitudes, photon energy becomes equally important in determining the circles of investigation.

3.9 MINIMUM DETECTION LIMITS

As discussed by Currie (1968), a minimum detection limit can be described as the critical level (L_c) below which a signal cannot be reliably detected. In the following discussion, the components of a photopeak are considered to be:

i) *Background*: Background under the photopeak due to the activity of the detector crystal, can, photomultiplier and the scattering contributions from these sources only.

B = background under peak

σ_B = standard deviation of B

ii) *Interference*, contributions to the photopeak area from the Compton scattering of higher energy photons and spectral interferences from other photopeaks. These interferences have been quantified in terms of stripping coefficients.

I = Measured interference, may be from several sources, eg. I_U , $I_{T\theta}$ and I_K .

σ_I = standard deviation of I

iii) *Gross Area*, total area under the photopeak

$G = (S+B+I)$ = total (integral) photopeak area

σ_G = standard deviation of G

iv) *Net Area*, the photopeak area due only to the activity of interest, or *signal*

$$S = (G-B-I) = \text{observed net signal}$$

$$\sigma_s = \text{standard deviation of } S$$

$$\text{where } \sigma_s = (\sigma_G^2 + \sigma_B^2 + \sigma_I^2)^{1/2}$$

In each case, σ is given by:

$$\sigma = \frac{\sqrt{\text{total counts}}}{\text{live time}} \quad (3.16)$$

The counts from a radiation detector are governed by Poisson distributions. For a signal to have been reliably detected, it must exceed a critical level L_c , given by:

$$L_c = k_\alpha \cdot \sigma_0 \quad (3.17)$$

where k_α is a constant chosen to give the appropriate error rate α (ie, the probability α , of deciding a signal is present when it is not) and σ_0 is the standard deviation of the net observed signal when it is assumed that the true 'net' signal is 0. Thus:

$$L_c = k_\alpha (B + I + \sigma_B^2 + \sigma_I^2)^{1/2} \quad (3.18)$$

Thus, for example, L_c for ^{40}K can be estimated from equation 3.19

$$L_{c_K} = k_\alpha \cdot (B + I_U + I_{Th} + \sigma_B^2 + \sigma_{I_U}^2 + \sigma_{I_{Th}}^2)^{1/2} \quad (3.19)$$

It can be seen that L_c is not a fixed value and will depend upon the relative contributions from other photopeaks and scattered compton contributions and will therefore also depend upon the environment of measurement. Thus, for example, the L_c for ^{137}Cs will be lower in an area covered with 1 or 2m of peat with a low geological signal than in an area with thin soil cover on granitic basement rock. Tables 3.6 and 3.7 show examples of L_c for ^{137}Cs , ^{134}Cs , ^{40}K , ^{214}Bi and ^{208}Tl for averaged regions of interest data collected at the Raithburn Valley (see chapter 4) for 3"x3" NaI(Tl) and 16 litre NaI(Tl) detector where k_α is 1.645 corresponding to an α of 0.05.

Table 3.6 Detection limits of the 3"x3" NaI(Tl) with 1000 second live times for ^{137}Cs , ^{134}Cs , ^{40}K , ^{214}Bi and ^{208}Tl .

	^{137}Cs	^{134}Cs	^{40}K	^{214}Bi	^{208}Tl
Background cps					
	0.537±0.023	0.296±0.017	0.262±0.016	0.079±0.009	0.063±0.008
Example from averaged Raithburn valley spectra					
Gross cps					
	18.67	3.51	2.84	0.51	0.40
At 95 % confidence, L_c cps:					
	4.23	2.56	1.48	0.92	0.504
L_c Calibrated Equivalents					
	kBq m ⁻²	kBq m ⁻²	Bq kg ⁻¹	Bq kg ⁻¹	Bq kg ⁻¹
	2.3	0.92	169.6	34	4.56

Table 3.7 Detection limits of the 16 Litre NaI(Tl) with 10 second live times for ^{137}Cs , ^{134}Cs , ^{40}K , ^{214}Bi and ^{208}Tl .

	^{137}Cs	^{134}Cs	^{40}K	^{214}Bi	^{208}Tl
Background cps					
	43.4±2.08	20.9±1.45	19.1±1.38	9.6±0.98	8.4±0.92
Example from averaged Raithburn valley spectra					
Gross cps					
	200.9	66.68	70.88	17.16	16.83
at 95 % confidence, L_c cps:					
	11.84	13.53	9.023	6.38	5.44
L_c Calibrated Equivalents					
	kBq m ⁻²	kBq m ⁻²	Bq kg ⁻¹	Bq kg ⁻¹	Bq kg ⁻¹
	1.32	1.1	83.9	10.66	3.8

3.10 CONCLUSIONS

This chapter has discussed the theory of the techniques available for measuring environmental radioactivity and the standard techniques used to calibrate the systems used. The factors which influence the application of these methods to environmental radioactivity estimation and the relationships between the techniques are investigated within the following chapters.

This work makes a comparative study of the three techniques of i) soil sampling with laboratory based high resolution gamma ray spectrometry using Ge(Li) and HPGe detectors, ii) in-situ gamma spectrometry with a 3"x3" NaI(Tl) detector, and iii) airborne gamma ray spectrometry using a 16 litre NaI(Tl) detector, to identify and quantify the environmental factors which influence the comparison between the measurements derived from these methods. To identify some of the environmental influences on the measurement of environmental radioactivity, chapter 4 investigates the relationships between measurements made with these three techniques.

4. COMPARISONS BETWEEN SOIL SAMPLE ANALYSIS, IN-SITU AND AERIAL GAMMA RAY SPECTROMETRIC DETERMINATIONS OF RADIONUCLIDE INVENTORIES

4.1 INTRODUCTION

4.1.1 Objective

The experimental objective was to estimate the distribution of ^{137}Cs across a valley using the three conventional techniques of soil sampling with laboratory based gamma spectrometric analysis, in-situ gamma ray spectrometry and aerial gamma ray spectrometry in the summer of 1990. The experiment was designed to enable the results from the different techniques to be compared and used to identify the factors which have traditionally made effective comparison between these techniques difficult. This includes the influence of valley geometry on the measurement results.

The theory of detector response through analytical solutions to photon transport equations assumes an infinite uniform plane, subtending a 2π geometry to a detector. However, as discussed by Kogan *et al* 1971, Schwarz *et al* 1992 and Allyson 1994, topographical unevenness influences the structure of the gamma ray field. Thus as the topography either curves towards or away from the detector, there is likely to be an increase or decrease, respectively, of the solid angle Θ (figure 3.10), and thus an appropriate increase or decrease in the detector response. Theoretical corrections for this effect have generally been based on extreme examples. However, reality is far from uniform and thus the potential influence would be usefully determined from a real example. In addition, real environments are expected to show that activity concentration variations within the field of view of the detector are averaged out and that there are variations in the vertical distribution of radioactivity concentrations.

The comparison between soil sample estimates, in-situ and aerial survey measurements would enable the influence of varying topography and vertical and spatial distributions of activity on the estimation of its distribution across the valley to be identified.

4.1.2 Experimental Design

The experiment was designed to characterise the distribution of ^{137}Cs , specifically, across a valley through soil sampling with laboratory based soil analysis, in-situ and aerial gamma ray spectrometry. The most rapid means of achieving this was thought to be by the construction of a series of transects across the valley with the aim of ultimately producing a grid of sampling locations. From such a regular grid, contouring of activity distribution and subsequent statistical interrogation with semivariogram analysis could be easily achieved allowing spatial variability across the site to be quantified. Russo (1984) considered between 30 and 50 data points to be a minimum for an effective semivariogram analysis. With sufficient data, directionality and anisotropy can be monitored by estimating the semivariogram for specific directions (Huijbregts 1975 and Zirschky 1985). In addition, a direct comparison between the data sets would then allow a point to point comparison as well as an overall structural comparison between data sets to be made.

To limit the number of possible variables, an area of simple geology with a low natural radioactive background is desirable. In addition, uniform organic rich and peaty soils were preferred to aid sampling and reduce the possible assimilation of natural radionuclides from the underlying rock into the soil profile.

4.1.3 Valley Selection and Criteria

To minimise the possible number of variables, the following valley selection criteria were determined:

- i) Low natural radioactive background, to minimise spectral interference complications,
- ii) To contain significant amounts of ^{137}Cs from weapons testing and Chernobyl fall out,
- iii) Variable "V" geometry valley with relatively small spatial extent, to maximise:
 - a) sampling density, and b) the detection of topographic contributions,
- iv) Peaty soil with minimal spatial variation in soil type,
- v) Logistical limitations, ie. good access and within easy reach of SURRC.

This task was attempted in 1990, in association with the Ayrshire aerial survey (Sanderson *et al* 1990c). Several valleys were selected in the Ayrshire region of SW Scotland before the survey. Two valleys were explicitly examined by aerial survey.

i) *Arran* - large topographic structures were surveyed by helicopter. This was undertaken by flying along ridges, valley sides and valley bottom. No marked change in the detector response was observed principally due to the large nature of these structures in comparison with the field of view of the detector.

ii) *Raithburn Valley* - small tight valley showed enhanced ^{137}Cs signals in the valley bottom. Field work was therefore performed in this area. The valley was centred about NS 330 620 and the topography of the valley is shown in figure 4.1.

The Raithburn valley is situated on the *Clyde Plateau Volcanic Formation* (Carboniferous: Dinantian) which predominantly comprises basic igneous rocks. More detailed geological maps (1:10,560) reveal olivine basalt to be interspersed with some trachytic and rhyolitic flow components to the geology. However, this was also the case for other valleys selected in the area. Generally, the structure dips to the east and the final area considered was relatively uniform in trachytic rock. The presence of this more intermediate to acidic igneous rock suggests that the concentration of the natural radionuclides, particularly ^{40}K and possibly ^{232}Th is likely to be higher than originally desired. However, the soil maps available, although less detailed, indicate the area to be dominated by a series of upland peaty soils which appear to be relatively uniformly distributed. This predominant soil type indicates an acidic (low pH) environment in which the mobility of the natural radionuclides is likely to be restricted with little assimilation into the overlying organic soil profile.

Topographic maps reveal a relatively tight geometry valley which gradually opens out towards the east. Nevertheless, the valley shoulder to shoulder distance is less than 1 km along the whole valley section selected, with the effective "V" of the valley ranging from 400 m across with 85 m depth in the west to 400 m across with 60 m depth in the east. This was chosen to enable the influence of the topographic anomaly with

Topography

Height in Feet

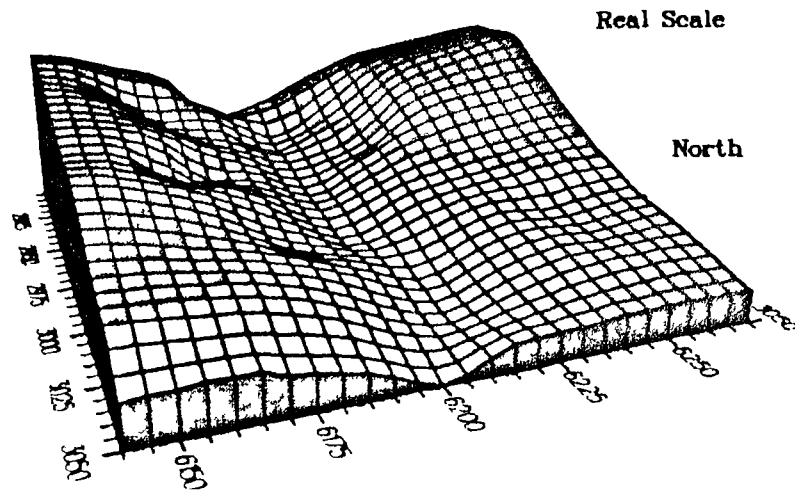
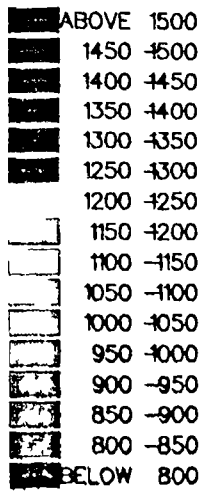


Figure 4.1 3 dimensional map representing the topography of the Raithburn Valley. *note the bi-linear interpolation smooths out the "V" of the valley bottom.*

changing valley geometry to be observed.

4.2 METHOD

4.2.1 Field Work Design and Method

The sampling equipment used for this work is described in Chapter 3. At the time of the field work the only corer available was the 38 mm diameter Leonard and Farnell corer. In addition, flight path positioning was based upon the Decca navigational system, whose positioning relied upon triangulation calculations between navigational beacons located around the UK's coastline. This had a nominal accuracy of between about 100 m to 150 m. Unlike the modern GPS system, the decca system provided no aids for navigational guidance.

A 1.4 km (E/W) by 1.4 km (N/S) area was selected within the Raithburn Valley. For field work, a theodolite, electronic distance meter (EDM), EDM targets and ranging

rods were used for positioning. Although the accuracy of these instruments is particularly good, sampling locations about these points are identified to a nominal accuracy of ± 5 m. An initial base point was selected on the southern side of the valley and positioned precisely in the field from trig points. Grid north was calculated from this position and a baseline constructed EW along the southern flank of the valley (along grid line 6144). 200 m positions were marked along this baseline with wooden stakes. The baseline formed the starting point for each subsequent NS transect across the valley.

The initial transects were spaced 400 m apart along the baseline, of which four were constructed. Along each transect, sampling positions spaced 200 m apart were determined by positioning with the theodolite and EDM. Where slope curvature obscured EDM and theodolite view, the equipment was moved and repositioned by back projection. A sample site, whose position was not controlled by the rigorous 200 m spacing of the grid, was also located at the valley bottom within each transect. A total of eight samples were collected along each transect.

Each sampling position was marked with a wooden stake, and at each site five random soil cores were collected at the standard 15 cm intervals to 30 cm depth (Cawse and Horrill 1986, Baxter *et al* 1989) within 5 - 10 m radius of the centre point. A single in-situ spectrum was collected with the 3"x3" NaI(Tl) detector, supported 1 m above the ground by a tripod and coupled to the Canberra Series 10^{plus} MCA.

Following completion of the four initial transects, the intermediate transects were sampled with the in-situ spectrometer only. This resulted in a total of seven transects giving a 200 m grid sampled with the in-situ spectrometer providing a total of 56 data points across the area. The four 400 m spaced transects with 200 m spaced samples provided a total of 32 soil samples, which were divided into 64 sub-samples by the two 15 cm depth intervals. The sampling positions are shown in figure 4.2. This is thought to satisfy the minimum number of data points required for an effective semivariogram analysis as defined by Russo (1984). The field work took over 2 months to complete.

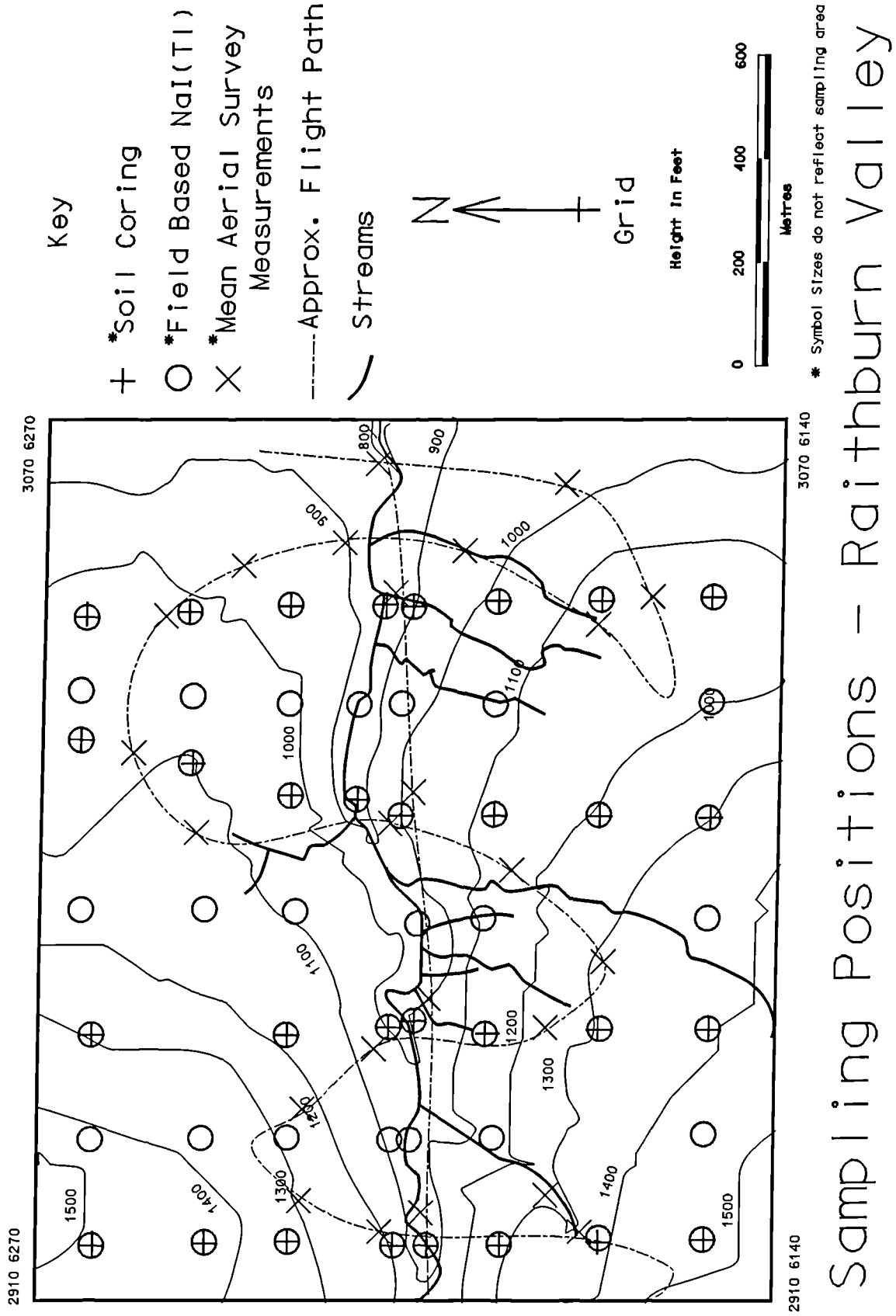


Figure 4.2 Sampling Plan within the Raithburn Valley, Lochwinnoch.

The Raithburn Valley was flown by free-flying, at an altitude of about 75 m \pm 15 m. This gave an effective field of view of approximately 200 m radius. 60 gamma ray spectra were collected over the Raithburn valley area over a 15 minute period. This data set was later reduced to 23 spectra by the constraints of the sampling area selected. This represents approximately 7 minutes of flying time (figure 4.2).

The soil samples were then processed in the manner described in chapter 3. A sample self absorption correction was later applied (chapter 5) and the corrected results are used here. This period of sample analysis took about 3 months of laboratory work. The in-situ and aerial survey measurements were processed also as described in chapter 3 and were calibrated later with sensitivity estimates derived from calibration sites sampled during the Ayrshire survey only (Appendices A and B). This enabled direct comparisons between in-situ and aerial survey activity estimates to be made.

Table 4.1 Mean Activity Estimates Derived from the 3"x3" NaI(Tl) and 16 Litre NaI(Tl) over the Raithburn Valley, Renfrewshire.

	¹³⁷ Cs	¹³⁴ Cs	⁴⁰ K	²¹⁴ Bi	²⁰⁸ Tl
3"x3" NaI(Tl) 1000 seconds integration time					
Stripped cps					
	12.1	1.17	2.07	0.201	0.307
Calibrated Equivalents					
	kBq m ⁻²	kBq m ⁻²	Bq kg ⁻¹	Bq kg ⁻¹	Bq kg ⁻¹
	5.16	0.52	232.9	6.14	2.9
16 litre NaI(Tl) 10 seconds integration time					
Stripped cps					
	73.2	12.2	43.4	2.8	7.9
Calibrated Equivalents					
	kBq m ⁻²	kBq m ⁻²	Bq kg ⁻¹	Bq kg ⁻¹	Bq kg ⁻¹
	8.22	0.99	404	3.4	5.8

Table 4.1 shows the mean counts per second and their calibrated equivalents for the

3"x3" NaI(Tl) detector and the aerial survey 16 litre NaI(Tl) detector across Raithburn Valley. By comparing these values both in cps and calibrated equivalents with tables 3.6 and 3.7, it can be seen that ^{134}Cs , ^{214}Bi and ^{208}Tl levels are below the limits of detection for the 3"x3" NaI(Tl) detector. For the aerial survey detector, ^{134}Cs and ^{214}Bi concentrations are below the limits of detection, whilst mean ^{208}Tl activity levels are just above the lower limits of detection. Thus effective comparisons can only be made for ^{137}Cs and ^{40}K .

The two data sets of ^{137}Cs and ^{40}K were compared through 2 and 3 dimensional graphical methods. Semivariogram analysis of the data was undertaken with Uniras-Unimap (*University Raster Based Mapping System*) which has kriging facilities. The models used to describe the semivariogram were fitted manually. However, a further discussion on semivariogram analysis is thought to be appropriate here, prior to the presentation of the results.

4.2.2 The Principles of Semivariogram Analysis

For a given bivariate data set (x,y,Z) where the attributes Z (the regionalised variable) are measured at (x,y) , the spatial variability of these attributes across the data set can be effectively quantified by semivariogram analysis. A comprehensive discussion of variogram or semivariogram analysis is provided in Huijbregts (1975), Burgess and Webster (1980), Zirschky (1985), Cressie (1989) and Conradson *et al* (1992). The theoretical semivariance $\gamma(h)$ is given by equation 4.1:

$$\gamma(h) = \frac{1}{2} E [(Z(\underline{u}) - Z(\underline{u} + h))^2] \quad (4.1)$$

where position \underline{u} is given by (x,y) anywhere within the data set, h is a defined distance or *lag* between points and E is the standard expectation operator. In this case $2\gamma(h)$ is the expected value of the total sum of squares of the differences or *variance* between the points for a given set of data spaced h apart, ie. for a given *lag*.

Since there is a finite number of points $N(h)$ with spacings h apart, the experimental

semivariance is given by equation 4.2:

$$\gamma(h) = \frac{1}{2N(h)} \sum_{\alpha=1}^{N(h)} [(Z(u_{\alpha}) - Z(u_{\alpha} + h))^2] \quad (4.2)$$

where $\alpha = 1$ to $N(h)$

Thus a semivariogram is calculated as the average value of the square difference between points for a range of lags h . The semivariogram model assumes that the attributes of points closer together tend to have a greater spatial dependence upon each other than those further apart. Thus $\gamma(h)$ is observed to increase with sample spacing, often to an asymptote. Beyond this point at distance h , no spatial dependence between points is observed and the distribution is effectively random. This level, or sill, will reflect the variance (σ^2) within the whole data set.

The semivariogram (or variogram) enables the nature of spatial variation to be quantified. It is used in the method of surface mapping or kriging which estimates attribute values at any given location by a weighted average of the points inside the associated domain in space. Kriging is discussed by Burgess and Webster (1980), Webster and Burgess (1980), Huijbregts (1975) and Zirschky (1985).

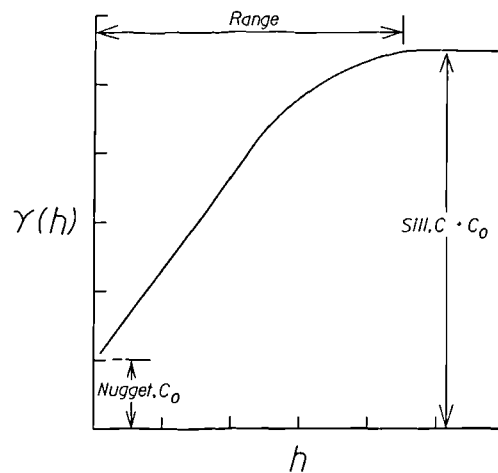


Figure 4.3 The Spherical Semivariogram Model

Figure 4.3 shows a typical theoretical semivariogram model, which depicts the characteristics of the regionalised variable and is known as the spherical model. The distance at which the samples become independent is the range and is the point when the sample variance is at a maximum called the sill. Error influences will introduce some uncertainty into the data. Theoretically, when $h = 0$, $\gamma(0) = 0$, however, the semivariogram will not always appear to tend to zero. This discontinuity is called the

nugget effect (C_0) and represents the component of the variance which may reflect the zero spaced sampling error in addition to random components of the experimental error.

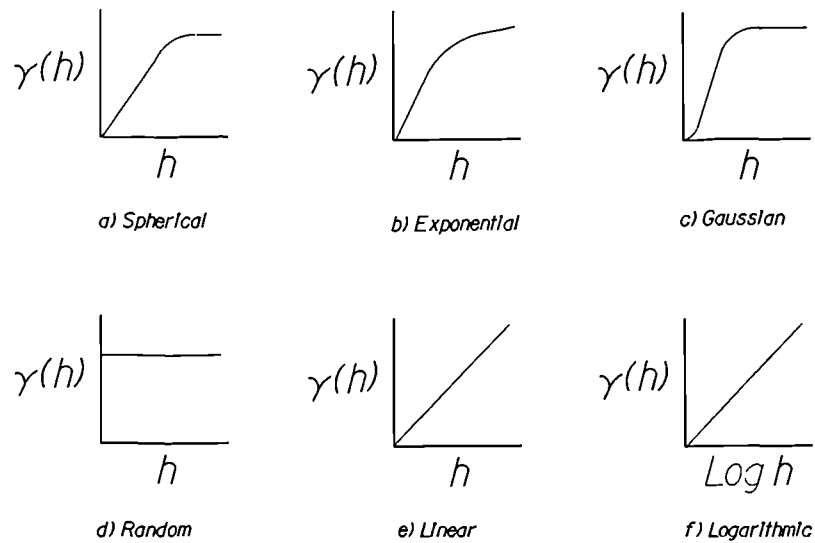


Figure 4.4 Semivariogram Models

Figure 4.4 illustrates the common semivariogram models. The spherical, exponential, gaussian and random models are all illustrations of transition models in which beyond some distance or *lag* (h) the samples become independent. The logarithmic and linear models are examples of non-transition models where sample variance increases indefinitely. Non-transitional models are often used to approximate spherical and exponential models where sample spacing is far less than the range (Zirschky 1985). One identified weakness of the approach is the need to construct a model for the observed semivariogram, which may not be appropriate for the observed distribution.

Semivariograms can be used to study the spatial variability for all possible directions at once. However, by restricting the analysis to defined orientations, *anisotropy* may be observed where spatial variability has a directional dependency.

4.3 RESULTS

The comparison between the three data sets; soil samples, in-situ spectroscopy and aerial spectroscopy measurements for ^{137}Cs , ^{134}Cs and ^{40}K is undertaken by: i) direct statistical analysis of the data. Further data analysis for ^{137}Cs and ^{40}K is achieved by: ii) three dimensional comparisons between the three data sets; iii) analysis by direct point to point comparison along transects; and vi) semivariogram analysis of each data set.

The first three approaches are used to make a straightforward comparison between the data sets and to determine the presence of a topographical anomaly and identify any other environmental controls which may influence the direct comparison between the techniques. The fourth approach is used to investigate spatial variability with measurement technique.

4.3.1 Data Statistics

The statistics on the soil sample, in-situ and aerial survey data are shown in table 4.2. On average the in-situ and aerial survey data sets for ^{137}Cs and ^{40}K agree within the limits defined by the standard error. However, comparisons with the soil sample data set show a lack of agreement, with the in-situ and aerial survey data under-estimating the ^{137}Cs and over-estimating the soil core derived ^{40}K activities. Little comparison can be made between the ^{134}Cs results derived through the three techniques because the majority of the ^{134}Cs results are below the mean estimated minimum detection limits of the in-situ and aerial survey detectors.

An empirical comparison of variability can also be made by calculating the coefficients of variation (*CV*) given by (*standard deviation/mean*). The *CV* for ^{134}Cs soil core inventories of 47 % is lower than the *CV* observed for ^{137}Cs (106 %) and ^{40}K (149 %), suggesting that ^{134}Cs is more uniformly distributed across the valley. As the effective sampling volume increases ie. with in-situ and aerial survey gamma spectrometry, the increased spatial averaging reduces the *CV* for ^{137}Cs and ^{40}K . For example, the *CV* for

Table 4.2 Statistical Results of the Soil Sample, In-Situ and Aerial Survey data sets.

	Soil Sample	In-situ NaI(Tl)	Aerial Survey
¹³⁷Cs			
Mean (kBq m ⁻²)	8.2	5.2	6.2
St. Dev. (1σ)	8.7	2.1	1.9
CV %	106	41	30
St. Error	1.6	0.29	0.76
Variance (σ ²)	76	4.5	3.5
Sample No.	31	54	23
Maximum	52.7	15.6	11.7
Minimum	2.26	3.35	4.08
¹³⁴Cs			
Mean (kBq m ⁻²)	0.51	0.52 (BDL)	0.74 (BDL)
St. Dev. (1σ)	0.24	0.21	0.34
CV %	47	40	46
St. Error	0.043	0.028	0.071
Variance (σ ²)	0.058	0.043	0.115
Sample No.	31	54	23
Maximum	1.12	1.27	1.48
Minimum	0.092	BDL	BDL
⁴⁰K			
Mean (Bq kg ⁻¹)	100	233	270
St. Dev. (1σ)	149	270	175
CV %	149	116	65
St. Error	27	37	36
Variance (σ ²)	22140	72950	73080
Sample No.	31	54	23
Maximum	694	1120	664
Minimum	BDL	BDL	BDL

BDL: Below Detection Limits

¹³⁷Cs falls from 106 % for soil samples (area 6x10⁻³ m²) to 41 % for In-situ (314 m²) to 30 % aerial survey (8x10⁴ m²).

It should be emphasised that ¹³⁴Cs soil core inventories are particularly low, indicating that the in-situ and aerial survey ¹³⁴Cs estimates are below the minimum detection limits.

4.3.2 Three Dimensional Comparison Between Data Sets.

The distribution of ^{137}Cs , ^{134}Cs and ^{40}K as estimated through the three measurement techniques (where appropriate), are spatially represented in 3 dimensional format in figures 4.5, 4.6 and 4.7 respectively. The data have been interpolated into 28 x 28 grid cells using a bi-linear interpolation. Activities are quantified in terms of kBq m^{-2} (^{137}Cs and ^{134}Cs) and Bq kg^{-1} (^{40}K) and expressed in terms of the colour scale and the magnitude on the Z-axis. However, interpretation of the results must take into consideration that the bi-linear interpolation may dilute some of the more exaggerated spatial variability through spatial averaging.

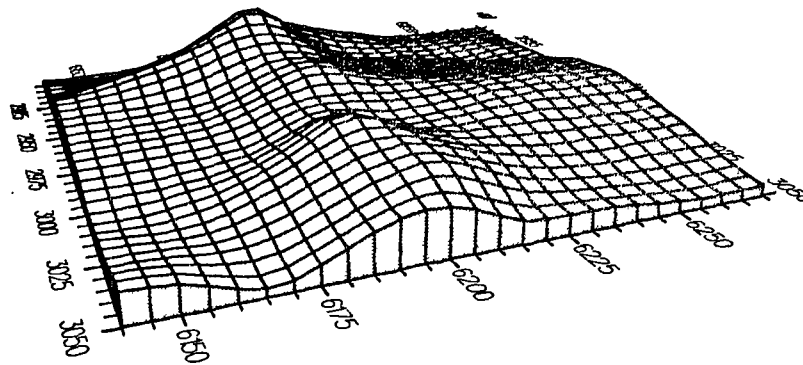
i) ^{137}Cs

The observed distributions of ^{137}Cs determined from the three monitoring techniques are shown in figure 4.5. The spatial observations of the distribution of ^{137}Cs across the valley are highly concordant and show that it is concentrated within the bottom of the Raithburn valley.

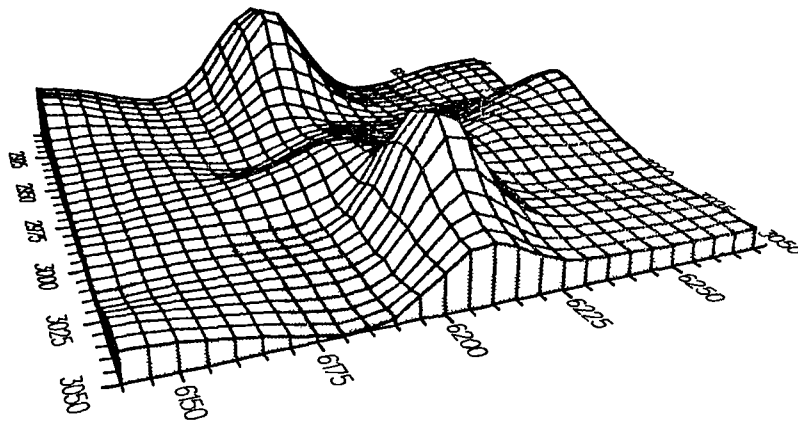
Soil sampling results exhibit a more exaggerated distribution of ^{137}Cs activity across the site, with data peaking at over 26 kBq m^{-2} (53 kBq m^{-2} from raw data) at NS 2920 6200. A similar distribution is observed with the in-situ 3"x3" NaI(Tl) detector measurements. However, the magnitude of activity observed in the valley bottom with the 3"x3" NaI(Tl) detector, although similar in the eastern end of the valley, markedly underestimates the soil core results in the western end of the valley, with activity estimates about 15 kBq m^{-2} (NS 2920 6200). On the valley sides and shoulders the activity estimates are highly concordant between the two monitoring techniques, with activity concentrations of about $6 \pm 3 \text{ kBq m}^{-2}$. In addition, both data sets indicate a zone of depletion on the southern valley side.

The aerial survey results show elevated signal strengths along the valley bottom. Here, values, although similar to the in-situ measurements, still underestimate the concentrations at the valley bottom determined by the soil core results. However, there

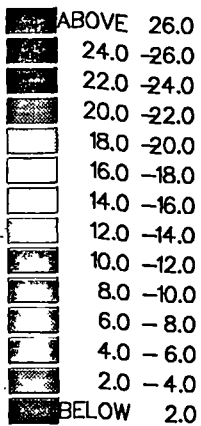
Aerial Survey



3"x3" NaI(Tl)



^{137}Cs kBq m⁻²



Soil Sample

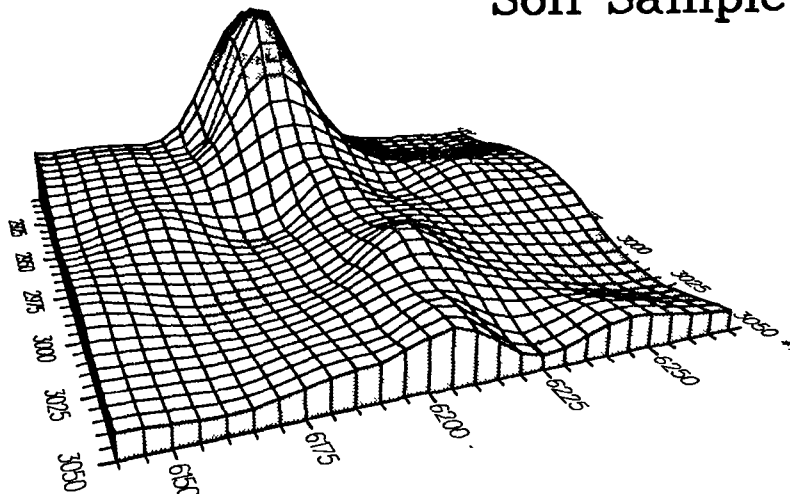


Figure 4.5 3 dimensional maps of ^{137}Cs activity (kBq m⁻²) across the Raithburn valley from soil samples (400 x 200 m grid), 3"x3" NaI(Tl) in-situ measurements (200 m grid) and aerial survey measurements.

is some indication of slightly enhanced ^{137}Cs values at the western end of the valley. The spatial extent of the distribution is very similar to that observed by both the ground monitoring techniques.

Activity estimates observed on valley sides and shoulders are highly concordant with those observed by the ground monitoring techniques. Although there is some loss of spatial detail, aerial survey measurements also indicate a zone of ^{137}Cs depletion on the southern side of the valley.

ii) ^{134}Cs

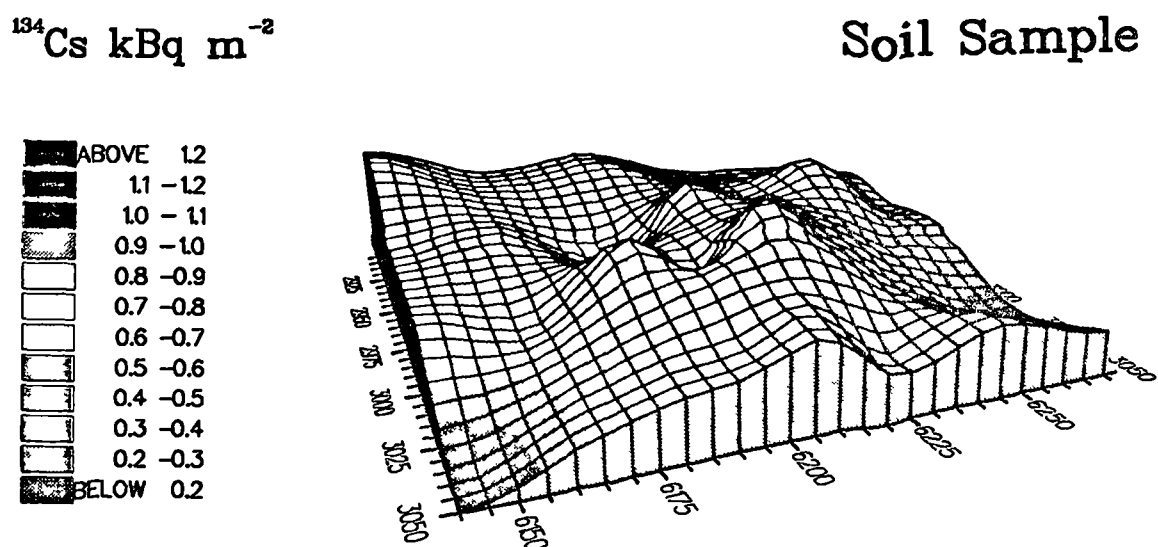
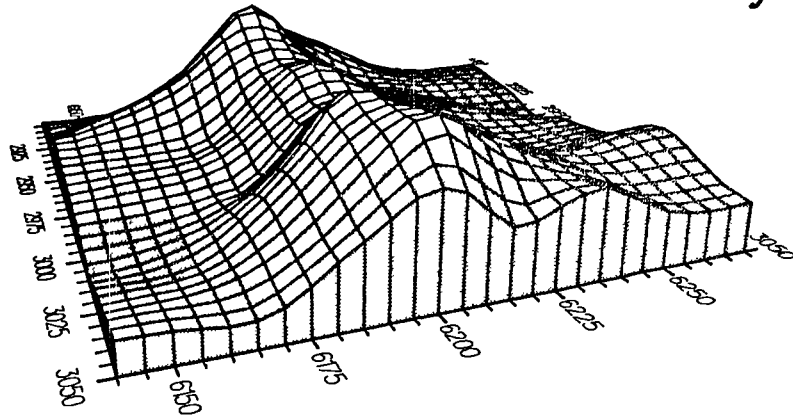


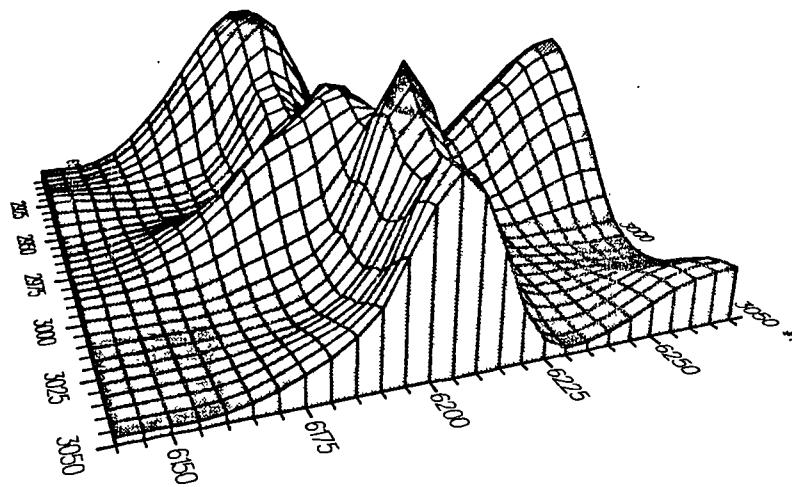
Figure 4.6 3 dimensional maps of ^{134}Cs activity (kBq m⁻²) across the Raithburn valley from soil samples (200 m x 400 m grid).

The soil sample derived ^{134}Cs estimated distribution across the valley is shown in figure 4.6. In contrast to ^{137}Cs , the distribution of ^{134}Cs displays no spatial distribution which can be related to the valley geometry. Although there is a slightly enhanced concentration at NS 3000 6210, no enhancement of activity is observed at NS 2920 6200, the area of particularly high ^{137}Cs activity concentration.

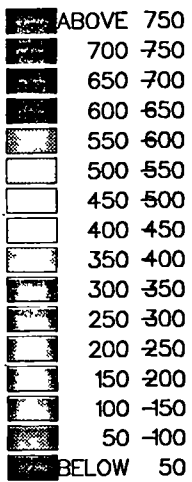
Aerial Survey



3"x3" NaI(Tl)



^{40}K Bq kg⁻¹



Soil Sample

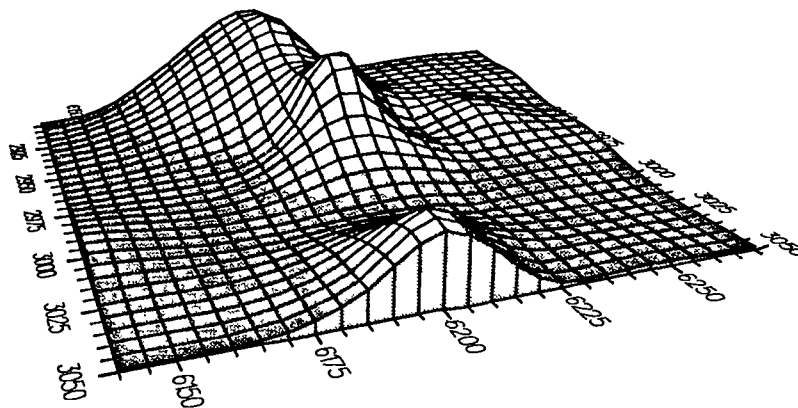


Figure 4.7 3 dimensional maps of ^{40}K activity (Bq kg⁻¹) across the Raithburn valley from soil samples (200 m x 400 m grid), 3"x3" NaI(Tl) in-situ measurements (400 m grid) and aerial survey measurements.

iii) ^{40}K

As with ^{137}Cs , ^{40}K determinations (Bq kg^{-1}) from all three techniques as shown in figure 4.7, have a strong spatial relationship with the Raithburn valley topography. The soil sample results provide inventories below 500 Bq kg^{-1} within the valley bottom which decrease to well under 100 Bq kg^{-1} on the valley sides and tops. Although the spatial distribution is very similar to that observed from the soil sample results, the in-situ $3" \times 3"$ NaI(Tl) detector determines values on the valley bottom to be of the order of 700 Bq kg^{-1} . In addition, there is a zone of increased ^{40}K activity concentration on the northern flanks of the Raithburn valley which is only marginally detected by the soil sample results.

As might be expected from the observations made with the ^{137}Cs results, the aerial survey measurements of ^{40}K distribution are again very similar in spatial structure to the soil core and in-situ results, and underestimate the activity concentration of the valley bottom compared with the in-situ measurements. However, as with the in-situ detector, the aerial survey observations provide higher estimates of ^{40}K concentrations than those determined through soil sample analysis.

4.3.3 Comparisons between transect data

Three transects were chosen which provided positionally favourable comparisons between soil samples, in-situ $3" \times 3"$ NaI(Tl) and aerial survey spectrometric results. Figures 4.8 to 4.13 show the three chosen transects for ^{137}Cs , ^{134}Cs and ^{40}K . These diagrams allow a point to point comparison to be made between the three monitoring techniques. Each figure also shows the topographic cross section of the valley.

The errors shown for soil sample results represent the analytical error associated with laboratory based analysis and are typically less than 5 % for ^{137}Cs and about 8 % for ^{40}K . The error estimates for in-situ and aerial survey gamma spectrometry are dependent upon the activity levels and sampling error observed across the calibration sites used to determine the sensitivity estimates. The error on the in-situ estimates are

dominated by the error on the regression used to calibrate each measurement (Appendix A). The following estimated errors also include the error on count rates. For ^{137}Cs , 69 data points were collected during the Ayrshire aerial survey (Sanderson *et al* 1990c) as discussed in Appendix A. The error on the mean activity levels (Table 4.2) are dominated by the error on the regression and estimated at about 20 %, increasing to about 40 % for the lower activity levels and decreasing to about 16 % for the highest. Similarly, ^{40}K estimates are determined from Appendix A, with a mean error estimate of about 16 % increasing to 100 % for *MDL's* and falling to about 10 % for the highest activities measured. For the aerial survey measurements, sensitivity estimates are derived from spatially matched calibration areas and are discussed in chapter 6 and shown in Appendix B. The error on ^{137}Cs is derived from the four Ayrshire calibration sites and is calculated at about 15 %. Similarly for ^{40}K , the error from the three sites (Table B.2) is about 10 %. As with the in-situ detector, for activity levels at *MDL's*, an error of 100 % is assumed. However, as the *MDL's* vary across the whole site, for simplicity the mean error is used for graphical comparison.

i) ^{137}Cs

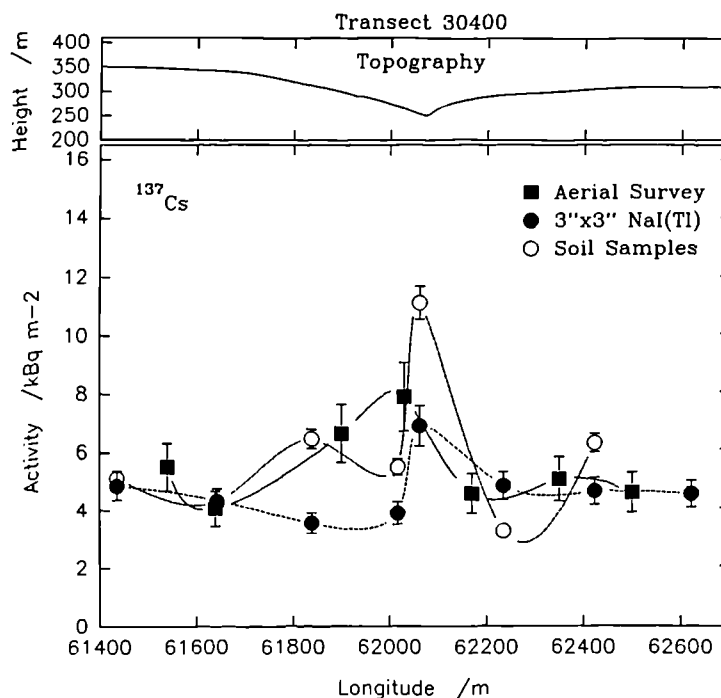


Figure 4.8 ^{137}Cs distribution across transect 30400.

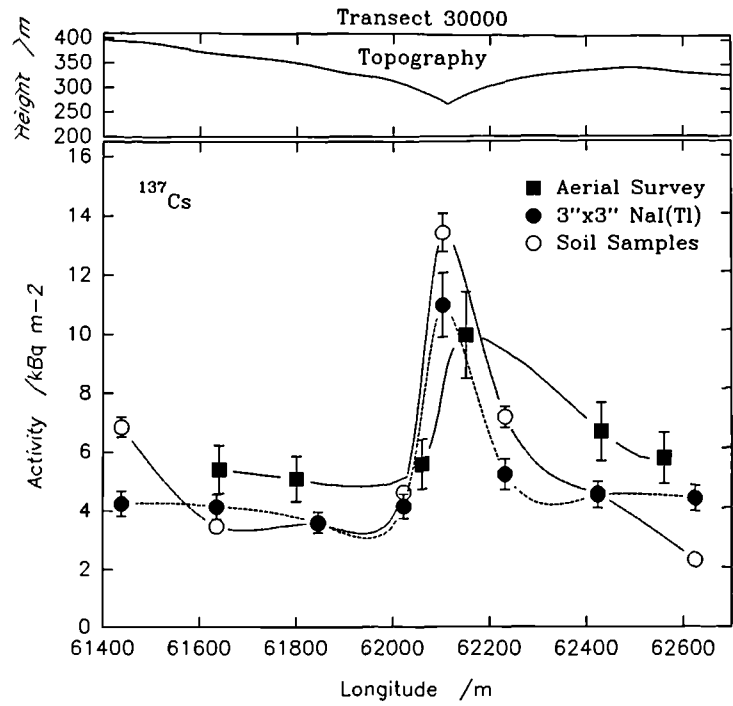


Figure 4.9 ^{137}Cs distribution across transect 30000

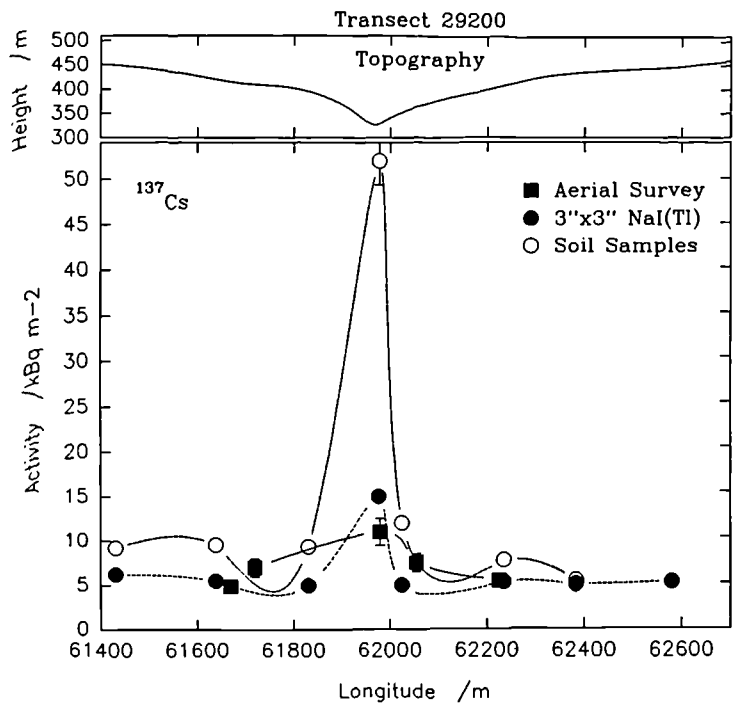


Figure 4.10 ^{137}Cs distribution across transect 29200.

Figures 4.8 to 4.10 show the three selected transects across the Raithburn Valley. All three figures show that ^{137}Cs inventories increase in the valley bottom. For the point to point comparison between the data sets, differences of more than a factor of two between inventory estimates appear at many of the points along the transects. There appears to be no systematic control in this variation on the valley sides, with the most exaggerated variations being observed within the soil sample data set. However, the mean result of the samples collected on the valley sides from each measuring technique provides a very similar answer ie. between 5 and 6 kBq m^{-2} . The exception is observed in measurements made in the valley bottom, where systematic differences in the observed activity estimates indicate soil core analysis consistently provides higher inventory estimates than those derived from in-situ or aerial survey estimates.

ii) ^{40}K

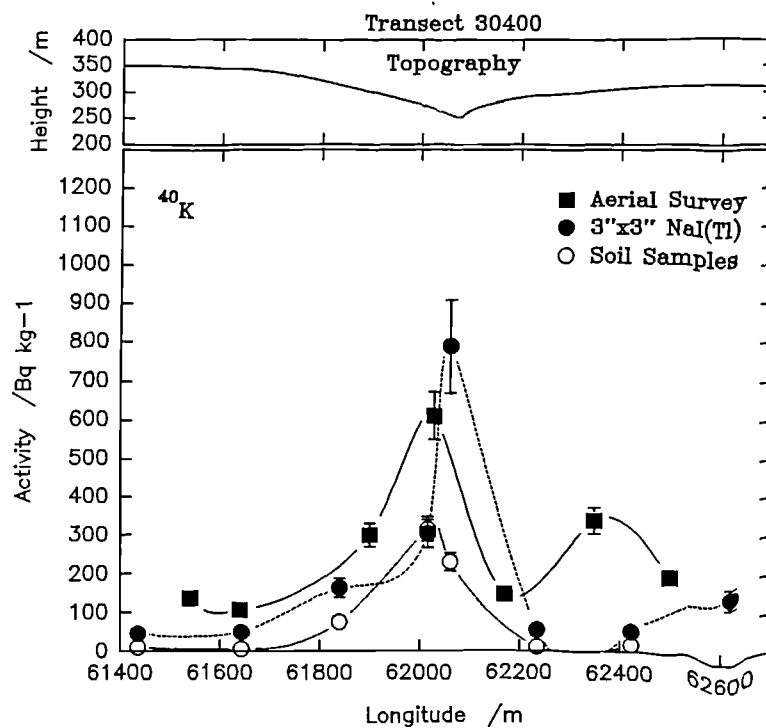


Figure 4.11 ^{40}K activity concentration across transect 30400

The distribution of ^{40}K along each transect is very similar to that of ^{137}Cs as illustrated in figures 4.11 to 4.13. The concentration of ^{40}K is at a maximum in the valley bottom, and this is shown by each of the monitoring techniques, except for the soil samples observed in figure 4.12 where very little ^{40}K activity is observed at all. In all transects

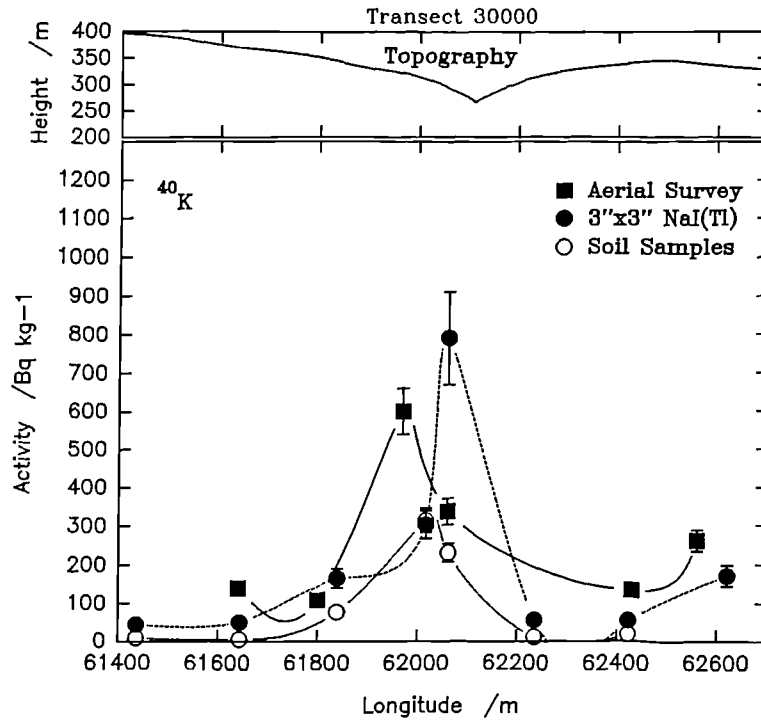


Figure 4.12 ^{40}K activity concentration across transect 30000

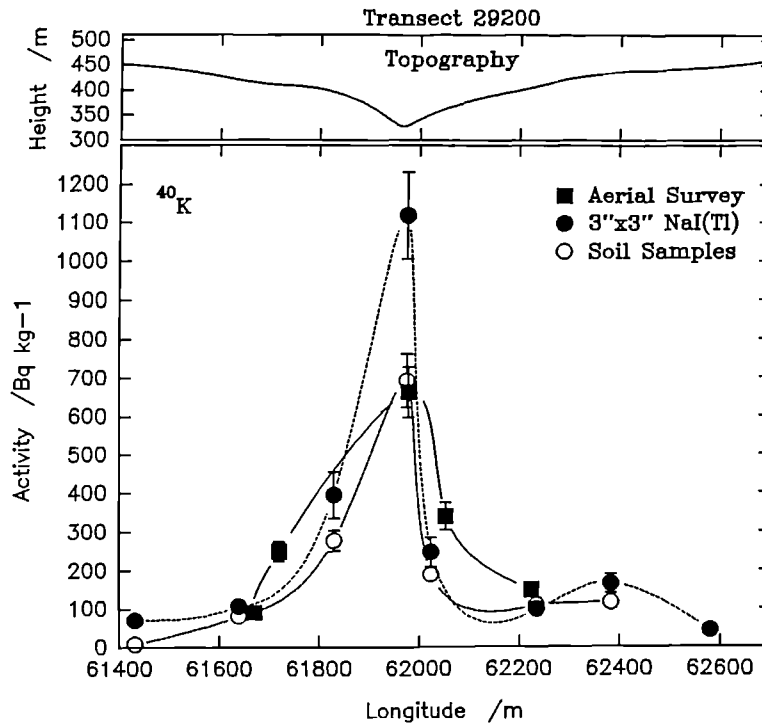


Figure 4.13 ^{40}K activity concentration across transect 29200

the soil sample results provide the lowest estimates of ^{40}K concentration across the valley. The in-situ 3"x3" NaI(Tl) detector provides the highest estimates of ^{40}K activity

estimates, particularly in the valley bottom. The aerial survey results in turn provide similar estimates to those observed by the in-situ detector on the valley sides but again exceed those estimates determined from soil samples. Figure 4.13 shows a good correlation between soil sample inventories, in-situ and aerial survey estimates of ^{40}K .

4.3.4 Semivariogram Analysis

Semivariogram analysis of the data for all directions across the data set was undertaken. In general, the results generated distributions that could be represented by spherical models. However, by looking at semivariograms in one direction only at a time (ie, 0° , 45° and 90°), anisotropy in the data set could be determined. The greatest anisotropy was observed between the 0° (EW) and 90° (NS) directional orientations. Lags of 200 m were chosen as this represents the dominant spacing between the sampling positions. The exception to this was a 400 m lag required in the EW orientation of the soil sampling data set. The finite data size leads to fewer observations being made at sample spacings of 1 km than at 200 m. A standard search tolerance of 10° was used.

The results are shown in figures 4.14, 4.15 and 4.16. In almost every case a spherical model described the spatial model observed in the EW orientation. Models were very difficult to fit to the NS orientated sampling plane and thus random models were chosen.

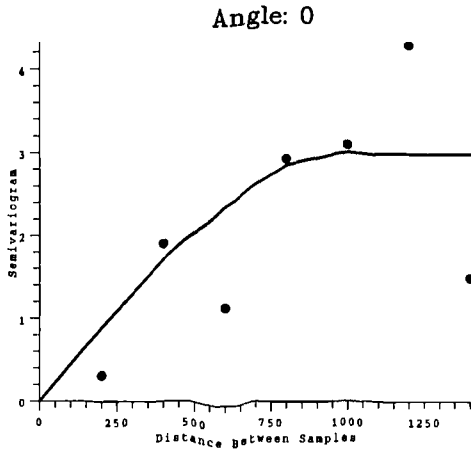
The ^{137}Cs semivariogram results for aerial survey, in-situ and soil sampling results are shown in figure 4.14 a to f. The aerial survey results (a. and b.) show a spherical model in the EW plane with a range of about 1 km and a sill value of about $3 \text{ (kBq m}^{-2}\text{)}^2$. This suggests that observations made in the EW plane which are less than 1 km apart are spatially dependent. However in the NS plane, a different distribution is observed. Here the semivariance is significantly higher at a small lag than at a large lag. This suggests that the sharp change in activity concentration observed in the valley bottom is smaller than the sample area (field of view) and thus observations on this scale appear to be random. However, with larger lags the semivariance falls

demonstrating a negative correlation or spatial dependency. This can only be described by a random model in semivariogram terms. However, the overall sample variance in both directions is $3 \text{ (kBq m}^{-2}\text{)}^2$, which is comparable with estimates in (table 4.2).

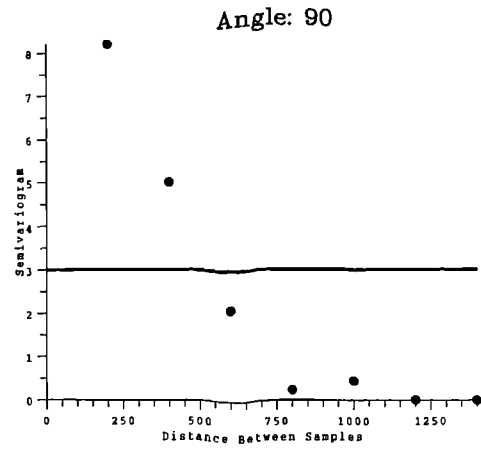
The in-situ (3"x3" NaI(Tl)) results (figure 4.14 c. and d.) demonstrate a spherical and random model. The EW orientated semivariogram has a range of about 1 km and a sill of about $7 \text{ (kBq m}^{-2}\text{)}^2$. The NS orientated variogram is more difficult to describe by a model. Although variability appears to increase with sample spacing initially, variability falls considerably at and after lags of 800 m. This is likely to be a function of the high activity concentrations within the valley bottom, which tends to be ignored at lags of 800 m or more, because of the finite spatial distribution of the sample set. Thus comparisons are made with data points either side of the valley. The overall variability is therefore determined to be about $3 \text{ (kBq m}^{-2}\text{)}^2$, although values of up to $6 \text{ (kBq m}^{-2}\text{)}^2$ are observed, and given a greater distribution of data, this value may be maintained as the sill value.

The ^{137}Cs soil sample data set also shows two different distributions in the NS and EW planes. In the EW plane only 3 semivariance points could be calculated due to the minimum sample spacing of 400 m. However, the distribution is not inconsistent with a spherical model with a range of about 1 km and a sill of about $160 \text{ (kBq m}^{-2}\text{)}^2$ which is greater than that observed in table 4.2. As with the in-situ results, the distribution in the NS plane is affected by the enhanced concentrations in the valley bottom, dominating the observed variance on the small lag scales. A mean variance is estimated in this plane of about $40 \text{ (kBq m}^{-2}\text{)}^2$, which is lower than that calculated in table 4.2. However, the combined average of the NS and EW planes would provide a mean variance estimate similar to that observed in table 4.2.

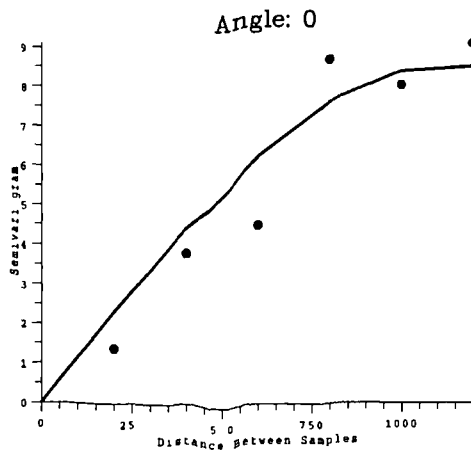
All the data sets for the NS orientated semivariogram data suggest that sample spacing is not appropriate to model accurately the rapid change in the distribution of activity across the valley. Whilst the field of view of the aerial survey detector may be too large to map the finer spatial detail, the sample spacing of the in-situ and soil corer is too great to determine the smaller scale of spatial dependency.



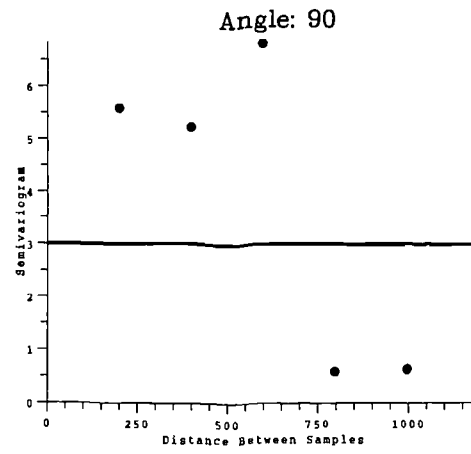
a. Aerial Survey ^{137}Cs E/W



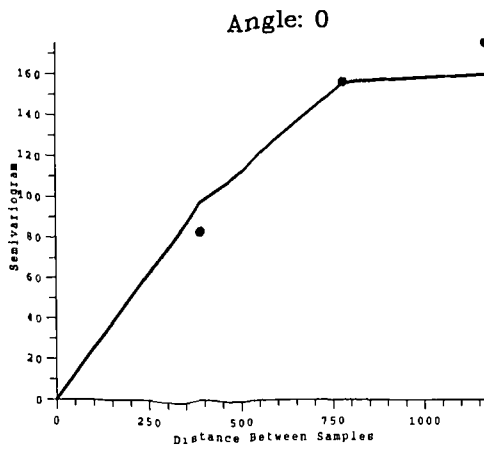
b. Aerial Survey ^{137}Cs N/S



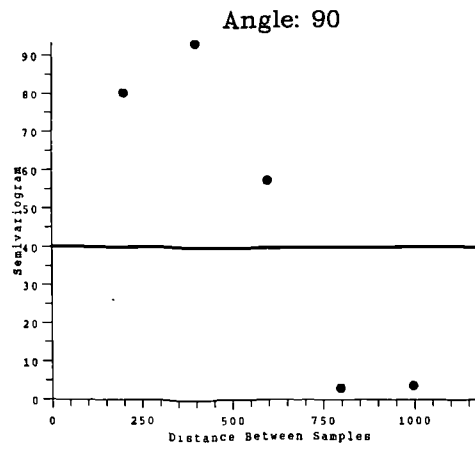
c. 3"x3" NaI(Tl) ^{137}Cs E/W



d. 3"x3" NaI(Tl) ^{137}Cs N/S

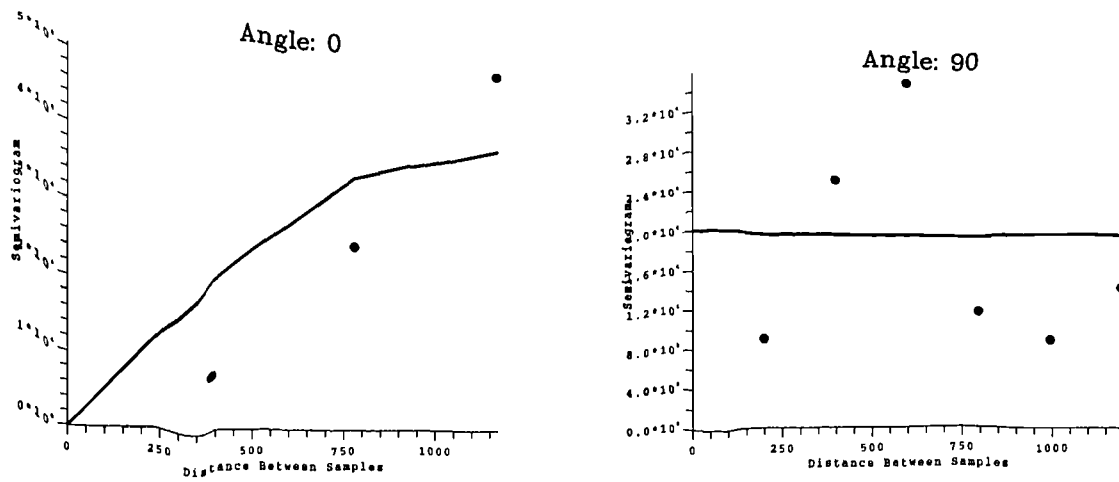


e. Soil Sample ^{137}Cs E/W



f. Soil sample ^{137}Cs N/S

Figure 4.14 ^{137}Cs Semivariograms (kBq m^{-2})² showing spatial variability at Raithburn



a. Soil Sample ^{134}Cs E/W

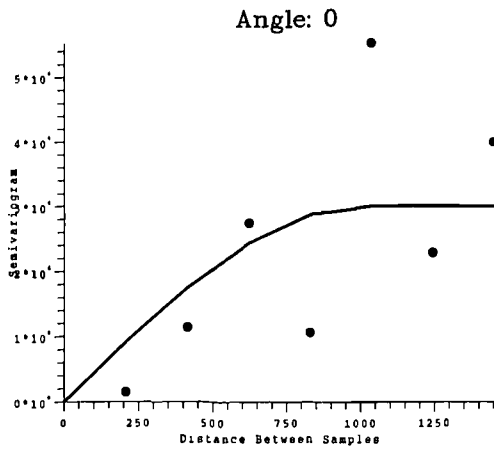
b. Soil Sample ^{134}Cs N/S

Figure 4.15 ^{134}Cs Semivariograms (Bq m^{-2})² showing spatial variability at Raithburn

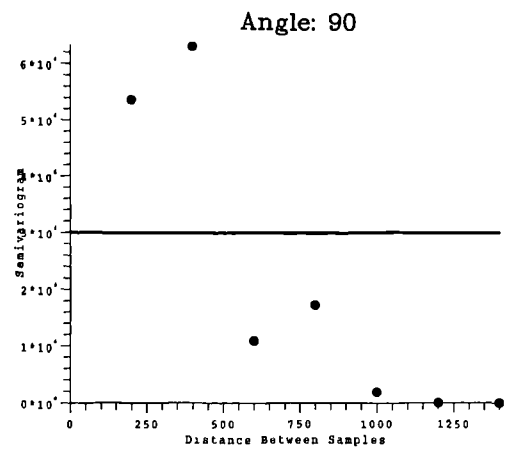
As with table 4.2, the overall degree of variance for ^{137}Cs increases with a decrease in the sampling area of individual measurements.

^{134}Cs semivariogram model observations (figure 4.15) for the soil sample results are very similar to those of ^{137}Cs although the sill values provide lower estimates of semivariance which are similar to those shown in table 4.2. As with ^{137}Cs , spherical models are used to describe the distribution in the EW plane for the ^{134}Cs results. Again in the NS plane, although there is evidence of some spatial dependence between the data at lags of 600 m or less, the values observed with lags of 800 m or more have a lower variance. Thus random models are again used to describe the distribution.

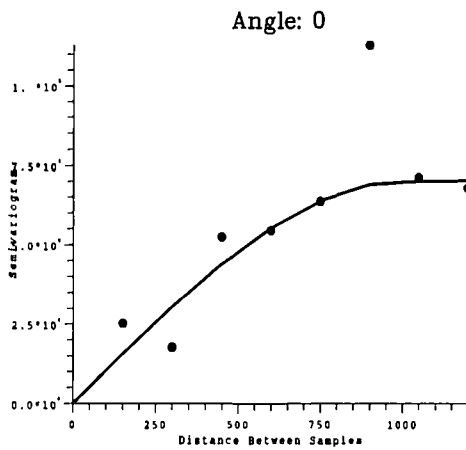
^{40}K semivariogram results are shown in figure 4.16. Again the structural descriptions of the semivariograms are very similar to those observed with ^{137}Cs . The sills observed for the aerial survey distributions are different to those predicted in table 4.2. However, the sill values and ranges observed with the in-situ and soil sample results are equivalent to those shown in table 4.2. The change in semivariance with sample spacing for the ^{40}K soil sample data, EW orientation (figure 4.16 e), is unlike ^{137}Cs and ^{134}Cs in that it does not necessarily demonstrate a spherical model and may be approximated by a random model.



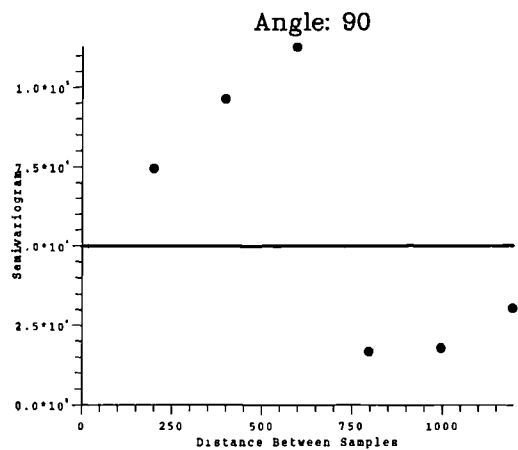
a. Aerial Survey ^{40}K E/W



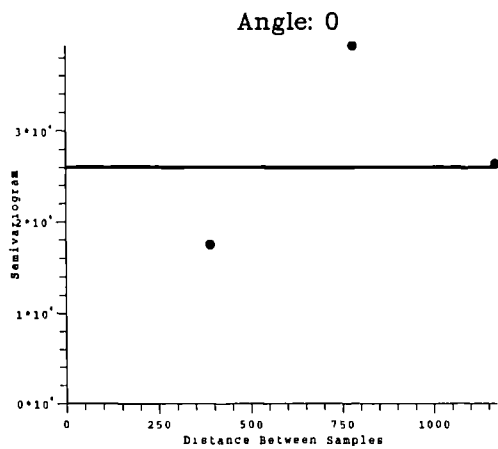
b. Aerial Survey ^{40}K N/S



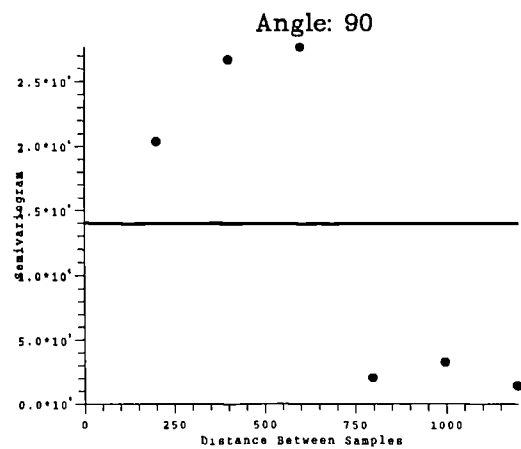
c. 3" x 3" NaI(Tl) ^{40}K E/W



d. 3" x 3" NaI(Tl) ^{40}K N/S



e. Soil Sample ^{40}K E/W



f. Soil Sample ^{40}K N/S

Figure 4.16 ^{40}K Semivariograms (Bq kg^{-1})² showing spatial variability at Raithburn

4.4 DISCUSSION

4.4.1 Discussion of the Main Distributional Characteristics

All three data set observations of ^{137}Cs , in both the three dimensional and transect representations, show that the valley bottom is acting as a capture area or sink for ^{137}Cs . As discussed in chapter 2, the highly organic nature of the soils, characteristic of the surrounding upland areas, are unable to fix and adsorb caesium as well as the inter layer sites of clay minerals associated with higher density soils. Thus the ^{137}Cs in this environment appears to be migrating down slope in particulate form although movement in solution may also occur. Much of the material is then caught in the clay rich sediments and sinks in the valley bottom. This behaviour of ^{137}Cs has been used to determine the erosional behaviour of radionuclides in drainage basins and has been discussed by many authors: Bonnett (1990), Pennock and De Jong (1987), Dominik *et al* (1987), Ritchie and McHenry (1977), Rogowski and Tamura (1970).

The movement and behaviour of ^{137}Cs and soils within the catchment area resulting in the depletion of ^{137}Cs from the slopes and deposition within the valley bottom, will lead to a different vertical activity profile across the drainage system. However, the experimental design and equipment used did not allow for the measurement of the vertical profile.

The distribution of ^{134}Cs (figure 4.6) from the data displays conflicting spatial characteristics to that of ^{137}Cs (figure 4.5). The ^{134}Cs soil sample data, clearly demonstrates that the distribution, although heterogenic, does not have any clear relationship with the valley topography, except perhaps in the eastern portion of the valley.

This contrast in ^{137}Cs and ^{134}Cs distribution may therefore be explained by two different depositional events. Typical weapons testing fallout across the UK, although regionally variable, is believed to be of the order of between 2 and 3 kBq m⁻² (Miller *et al* 1989). Thus about a third of the ^{137}Cs deposition in the upland areas (approximately 2 kBq m⁻²)

is likely to be attributed to weapons testing fallout and about two thirds (approximately 4 kBq m⁻²) to Chernobyl fallout. This provides a ¹³⁴Cs/¹³⁷Cs ratio at the time of Chernobyl (May 1986) of about 0.6. This is comparable to other findings (e.g. Miller *et al* 1989 and Cambray *et al* 1987). Thus given this relatively heterogenic, though random, distribution across the valley of ¹³⁴Cs, the spatial relationship of ¹³⁷Cs with the topography indicates that this must be associated with a separate depositional event. The movement of ¹³⁷Cs into the valley bottom must be dominated by the redistribution of weapons testing fallout prior to the deposition of the Chernobyl fallout. Therefore, from figures 4.10 and 4.13 (transect 29200), only 3.8 kBq m⁻² of the total 53 kBq m⁻² of ¹³⁷Cs can be accounted for by Chernobyl fallout. Also, from figures 4.8 and 4.11, 4.5 kBq m⁻² of the 12 kBq m⁻² of ¹³⁷Cs must be Chernobyl fallout within the base of the valley along transect 30400.

Thus, the data enables environmental change and in particular effects of the hydrology of the valley system to be investigated. The deposition of ¹³⁷Cs from weapons testing fallout began in the 1950's and so it has taken between 30 and 40 years for the movement of weapons testing fallout from the surrounding upland areas into the valley bottom. In addition, the rate of deposition has been clearly more rapid in the western portion of the Raithburn Valley than in the eastern end. However, the ¹³⁴Cs data appears to indicate a change in the redistributive pattern over the 4.5 years since Chernobyl, as the ¹³⁴Cs concentrations collected in the eastern portion of the valley are higher than observed in the west. This is also clearly observed when looking at the three dimensional soil core information as illustrated in figures 4.5 and 4.6. Although heterogeneity in the initial distribution must be considered, these results may suggest that the hydrological controls of the drainage system have also changed with time.

The distribution of ⁴⁰K across the drainage system is similar to that of ¹³⁷Cs with significant concentrations in the valley bottom. Although soil sample estimates underestimate the observations made by the in-situ and aerial survey detectors, the results are spatially concordant. The soil samples analysed provided additional information of soil type distribution across the valley. Generally, the soils on the valley sides are characteristically upland peats and monoliths, with an increasing gritty and

clay component towards the valley bottom. This is associated with corresponding changes in soil density from $< 1 \text{ g cm}^{-3}$ on the valley sides to $> 1 \text{ g cm}^{-3}$ on the valley bottom. In addition, soil acidity was observed to decrease, with the pH values increasing respectively from a pH of 3 on the valley sides to about 5 in the valley bottom. However, the clay and gritty soils were highly heterogenic and interspersed with organic soils and outcrops of the underlying trachytic and rhyolitic rock. The soils were generally thinner ($\leq 30 \text{ cm}$) in the valley bottom. In the upland parts of the valley, soil moisture content was often $> 80\%$ resulting in difficulties in sample retrieval with the standard soil sampling equipment.

The lower acidity and possible addition of glacial sediments has allowed more advanced soil types to develop with clay content from the underlying geology at the bottom of the valley. Thus the concentration of the natural radionuclides as a whole was significantly higher than that observed in the organic soils from the valley sides and upland areas. These higher estimates of ^{40}K derived from the in-situ and aerial survey measurements are discussed in section 4.4.2.

4.4.2 Identification of the Environmental Factors Controlling the Relationships Between Soil Sample, In-Situ and Aerial Survey Inventory Data

The comparative approach between soil sampling, in-situ and aerial survey methods of monitoring environmental radioactivity has enabled several important environmental factors to be identified. It was anticipated that activity estimates observed from in-situ and aerial survey measurements collected within the valley bottom would be greater than similar measurements made over an infinite flat plane. However, this feature was masked by the significantly enhanced concentrations of radionuclides in the valley bottom. It is difficult to deconvolute the contributions brought about by these enhanced concentrations due to the shortcomings or environmental factors which have influenced inventory estimations with all the techniques used. Since this experiment was undertaken, Schwarz *et al* (1992) describe a linear geometrical correction factor to correct for topographic effects which is not based on experimental observations and is yet to be verified. However, this experiment has enabled several environmental

influences for further investigation to be identified.

Spatial variability and spatial dependence has been observed. This is shown in table 4.2 and by the analysis of the semivariogram results. The coefficients of variation within the data sets decreased with increased sampling area (including detector field of view) of individual measurements, particularly for ^{137}Cs and ^{40}K . Also, the soil core analysis indicated that ^{134}Cs was relatively more uniformly distributed (*CV of 47 %*) compared with ^{137}Cs and ^{40}K (*CV of 106 and 149 % respectively*). The difference in the *CV* is attributed to the age of the deposition and the redistributive processes which have been acting upon the weapons testing component of ^{137}Cs in particular over the last 30 to 40 years. ^{40}K distribution is controlled by the natural pedological and geological variability and demonstrates a broadly similar distribution to ^{137}Cs .

The difference between the EW and NS orientated semivariograms demonstrated a high degree of anisotropy in spatial variability across the site. This is controlled by the distribution of activity within the valley bottom, and the sampling scales chosen were not ideal for the characterisation of this distribution. In addition, the finite size or range of the bi-variate distribution of the data set limited the inclusion of the valley bottom observations within the semi-variance calculations for observations with lags of 800 m or more. The EW semivariograms show that variance increases with sample spacing, with the maximum variance (*sill*) occurring at about 1 km, suggesting spatial dependence of the samples upon each other within 1 km spacings, and independence at lags greater than 1 km. Again, however, variance determined at lags of 1 km is based on fewer observations due to the dimensional limits of the data set and this must be allowed for in the interpretation. The verification of the estimated range would be achieved by extending the sample grid.

The NS semivariograms are dominated by very rapid spatial change, which occurs on a scale smaller than the field of view of the aerial survey detector. Thus small scale movement of the aerial survey detector results in large changes in the measured radioactivity. This led to a large semivariance on the small scale observations. However, with increased sample spacing, because of the restricted dimensions of the

survey area, variance calculations are based on valley shoulder to valley shoulder comparisons, and thus a smaller variance is observed with larger lag. This change is measured better with smaller sampling areas (small field of view), although sample spacing should also to be reduced.

Spatial variability was also observed in the point to point comparisons between soil sample results with in-situ and aerial survey results. In particular, the scatter of soil sample results about the in-situ and aerial survey estimates of radionuclide inventories makes direct comparison difficult. This is likely to be attributed to sampling errors and poor spatial comparability between the three techniques. Single small and randomly collected samples have little spatial relationship with the field of view of in-situ detectors. Both soil samples and in-situ measurements have little spatial relationship with aerial survey measurements.

It is this poor spatial representability which has helped mask the topographic anomaly, particularly for ^{137}Cs . In addition, because the enhanced activity concentrations present a small linear feature, perhaps tens of metres wide compared to the field of view of the airborne detector which is perhaps 350 m wide, the aerial survey measurements will spatially dilute the higher inventories observed by smaller scale measurements. This can be overcome by either flying lower, slower and reducing the detector integration time. However, this is unlikely to fully explain why in-situ spectrometric measurements underestimated the ^{137}Cs inventories observed in the valley bottom relative to soil core observations.

The degree of soil type variability across the valley was also quite considerable with densities ranging from 0.5 g cm^{-3} to 1.3 g cm^{-3} . This was accompanied by a significant change in soil composition from a highly organic and water bound peaty soil to highly mineral rich gritty soils. As discussed in section 4.4.1, these characteristics were controlled by valley structure. However, this change in composition and density must have an influence on the calibration of in-situ and laboratory based measurements due to the changes in the soil's self absorption characteristics. In particular, with laboratory based gamma spectroscopy, such changes in soil composition are likely to have an

influence on the detector calibrations and, although clearly energy dependent, should be accounted for when making inventory estimates.

In addition, this change in soil type must influence the self absorption characteristics of the soil itself with regard to in-situ and aerial survey measurements. Of particular importance here is the vertical distribution or stratification of radionuclides within the soil profile. For the anthropogenic radionuclides which have undergone redistribution processes, the changes in the vertical profiles of caesium must be quite considerable, particularly between areas of caesium removal and redeposition. Such changes in the vertical profile will influence the photon emission or fluence rate observed at the soil surface. This effect is compounded when soil type and density change. This would therefore explain the good correlation between the three techniques in the upland areas but would underestimate ^{137}Cs activities observed in the valley bottom by in-situ techniques. This effect may also contribute to underestimations made by aerial survey measurements.

The degree of contribution that a change in source depth within the field of view can make to aerial survey measurements is dependent upon the spatial extent of these different source characteristics in relation to the field of view of the detector. The aerial survey detector has a centrally weighted field of view of perhaps 400 m in diameter, and is distorted to an ellipse when the platform is moving. Thus, if the change in source depth characteristics dominate this centrally weighted field of view, the expected photon fluence will be altered accordingly. However, if such features are small, it is likely that their influence will be much less. From semivariogram analysis, the activity concentration in the valley bottom was small, resulting in significantly different estimates of the activity concentrations at low lag.

The source burial effect may also explain the variation in ^{40}K estimations. In almost every case, particularly in the valley basin environment, ^{40}K inventory estimates were greater with the in-situ and aerial survey techniques. This can also be explained by source burial in the upland areas in particular, where lack of assimilation of ^{40}K into the soil profile, particularly the top 30 cm, has led to low ^{40}K estimations from soil core

analysis. However, the 1462 keV photon signal from ^{40}K is still likely to be able to penetrate through the low density organic soil profile from the underlying geology and can thus be detected by both in-situ and aerial survey measurements. Thus the 30 cm soil sample does not provide a representative sample of the natural radionuclide activity estimations in these environments and for their comparison with in-situ and remote sensing forms of gamma spectrometry. There is also considerable exposure of the underlying geology from stream erosion in the valley bottom. Thus, although soil samples collected contain significant amounts of the ^{40}K available, the rock exposures and coarse stream and glacial sediments present a greater ^{40}K source signal to the detectors. This renders the samples less representative.

Again, ^{40}K determined by aerial survey underestimates the distribution determined by in-situ gamma spectrometric techniques. As with ^{137}Cs , this distribution can be explained by the spatial averaging of the aerial survey detectors. This is caused by the field of view of the airborne detector being considerably larger than the source dimensions. Semivariogram analysis of the aerial survey observations of ^{40}K and ^{137}Cs across the valley suggest that the source is small compared to the field of view of the detector, thereby rendering each successive observation in the NS plane almost independent and thus random. To map the spatial distribution more precisely the detector should be flown at lower heights to reduce the field of view. Alternatively, in-situ or soil sampling techniques should use a finer sampling grid.

It is interesting to note that stripping residuals were observed within the ^{134}Cs window for both the in-situ and aerial survey gamma spectrometric measurements. Although difficult to prove by regression analysis, given the inherent association within this environment of caesium with potassium rich soils and sediments, these residuals do spatially relate to the distribution of ^{40}K , thus providing a significant contrast to the distribution of ^{134}Cs determined from soil sample estimates. These stripping residuals are likely to have been brought about by the changes in the scattering characteristics of the radiation field due to: i) valley geometry; and ii) ^{40}K source stratification within the soil profile, thus rendering the stripping coefficients inappropriate.

Quantification of any one of the environmental factors indicated here is made difficult by the fact that they are all acting at the same time. Thus a series of experiments is required to enable these environmental factors to be separately determined and quantified, since in the present case they appear to be more important than the influence of the topographic shape on in-situ and aerial survey measurements.

4.5 SUMMARY AND CONCLUSIONS

The results of measurements of the distribution of radioactivity across the Raithburn valley have demonstrated the probable movement of radionuclides in a dynamic environment and illustrate the use of environmental radioactivity monitoring to measure environmental processes.

This experiment has demonstrated the capability of soil sampling and laboratory based analysis, in-situ and aerial survey analysis to map the distribution of ^{137}Cs and ^{40}K across a tight geometry valley. The results for the distribution of ^{137}Cs and ^{40}K are clearly concordant although absolute magnitudes of activity within the valley bottom are variable. ^{134}Cs results are less well matched between the techniques as a consequence of low activity levels.

These results have demonstrated that further research is required to enable the experimental relationships between soil sample analysis, in-situ and aerial survey measurements to be understood more fully. Experimental work was therefore designed to isolate and quantify these environmental factors. The environmental factors which will receive further attention in the following chapters are categorised as follows:

- 1) Soil type and its variability in composition and density. These factors influence the self absorption characteristics of the soil, which will be photon energy dependent. The influence on laboratory based gamma spectrometry is investigated and the soil sampling depth required for effective comparison with in-situ and aerial survey based gamma spectrometry determined.

2) Spatial variability not only occurs on the macro scale but, as indicated by poor spatial correlation between soil samples, in-situ and aerial survey estimates, also occurs on the micro scale. Spatial variability has an influence on the results derived from soil sampling and thus the representability of a sample. In addition, spatial averaging associated with the fields of view of in-situ and aerial survey, controlled by their height above ground, photon energy and source characteristics, requires spatially representative ground sampling to make effective comparisons for calibration and verification purposes. Such spatially representative sampling is required to enable an effective study of other environmental controls influencing the relationship between these techniques.

3) Source burial effects for both natural and anthropogenic radionuclides need to be considered for the interpretation of in-situ and aerial survey measurements. This has an influence not only on primary photon attenuation, observed as a reduction in the spectral photo-peak area, but also on the scattering characteristics within the environmental radiation field which are observed in the detector response characteristics. In addition source burial is not only brought about by soil and peat, but also by increase in the air path length between source and detector. Thus detector response characteristics for stripping and photo-peak response are investigated.

5. SELF ABSORPTION CHARACTERISTICS OF SOILS AND THEIR INFLUENCE ON GAMMA SPECTROMETRY

5.1 INTRODUCTION

During the course of the Raithburn Valley investigation, a considerable variation in soil type and density was observed across the site. The consequences of this change upon in-situ and, in particular, laboratory based gamma spectroscopy, are investigated in this chapter. The calibration corrections derived for this density variation, particularly in laboratory based gamma spectroscopy, are also discussed here and traced to IAEA and NBS standards.

It is generally recognised that the attenuation of gamma rays in matter is subject to the density and atomic number Z of the medium through which photons travel. The effect of the atomic number is quantified in terms of the mass attenuation coefficient, which is made up of contributions from incoherent (Compton) scattering, coherent scattering (Rayleigh), the photoelectric effect and pair production (Coppola and Reiniger 1974).

The mass attenuation coefficient (μ_m) has long been used as the basis for determining sample density and water content (Stroosnijder and DeSwart, 1974; Saksena *et al*, 1974; Mudahar and Sahota, 1986). However, such experiments using low energy photons below 150 keV (e.g. ^{241}Am), where the photoelectric effect predominates, have been hampered by variations in the soil's chemical composition. Mudahar and Sahota (1986) suggest a 5% variation in μ_m for 662 keV determined from a few selected soils.

Having demonstrated the importance of the soil's chemical composition on the attenuation of photons, Mudahar and Sahota (1988a) attempted to show the dependence of μ_m on soil particle grain size and/or particle geometry. This is contradictory to expected observations for gamma ray energies well above those dominated by the photoelectric effect. Coppola and Reiniger (1974) and Hubbell (1982) demonstrated the influence of sample atomic number and photon energy on μ_m . Coppola and Reiniger (1974) examined four soils, principally loam and clay types, and determined that μ_m was

dependent on sample chemical composition below 150 keV.

In the knowledge of the effect of sample chemistry on μ_m , radionuclide inventory estimates made with laboratory based high resolution gamma spectroscopy seldom consider the importance of μ_m on the sample activity determinations. Whilst the solid angle Ω remains constant for a standard geometry size, Galloway (1991a) showed the *effective* solid angle to be dependent upon the attenuating properties of the sample. Thus as μ_m or density increases or photon energy

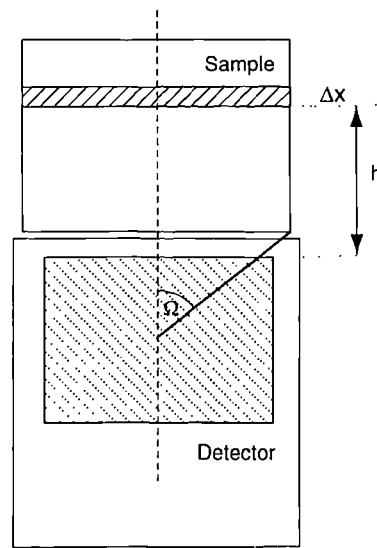


Figure 5.1 Diagram showing the detector-sample geometry

decreases, then the photons detected will originate predominantly from the front of the sample, resulting in a change in the effective solid angle. Thus the magnitude in change of photon contribution from a layer Δx (figure 5.1) with distance h will be dependent upon μ_m and sample density. The absolute detection efficiency must therefore also change with sample composition and density. Galloway (1991a) describes an effective method for accounting for changes in self absorption characteristics of samples. Galloway also demonstrates an analytical approach used to correct for geometrical variations in sample geometry, in particular under filling of containers (Galloway 1991b, 1993). This chapter describes an empirical method for sample self attenuation correction.

The effect of variations in soil self attenuation also has implications upon in-situ and aerial based gamma spectrometry. Representative soil cores should be collected, where the sample depth cored represents the depth from which the majority of the photon flux at the soil surface originates. This variation in the analytical depth in the field may also affect the response to layered anthropogenic sources. The consequences of this variation are also discussed here.

An experiment was set up to measure the linear (μ) and mass attenuation (μ_m) coefficients of a range of soils from across the U.K. The importance of the chemical composition of soils on μ_m was then demonstrated by calculating μ_m for a series of geostandard reference soils (Govindaraju, 1989). The conclusions from these results are examined for in-situ and laboratory based gamma spectroscopy. First, estimates of soil density variations are made.

5.2 CHANGES IN SOIL DENSITY AS AN ENVIRONMENTAL VARIABLE

Table 5.1 Typical density ranges observed through soil sampling

	Wet Soil	Dry Soil	Ground Dry Soil
Raithburn Valley Investigation			
Mean (kg m ⁻³)	800	249	783
St. Dev. (1 σ)	171	229	254
St. Err.	22.1	29.6	32.8
Max.	1285	1020	1512
Min.	372	52.9	300
Ayrshire Calibration Site Samples			
Mean (kg m ⁻³)	591	146	752
St. Dev. (1 σ)	178	142	233
St. Err.	15.6	12.5	20.5
Max.	1156	781	1472
Min.	249	8.42	296
Caerlaverock Salt Marsh Calibration Samples			
Mean (kg m ⁻³)	1504	940	1358
St. Dev. (1 σ)	162	207	123
St. Err.	18.4	23.4	13.9
Max.	1956	1540	1591
Min.	882	358	992

The density ranges observed within the Raithburn Valley investigation and subsequent Ayrshire and Caerlaverock Calibration site sampling are shown in table 5.1 and figure

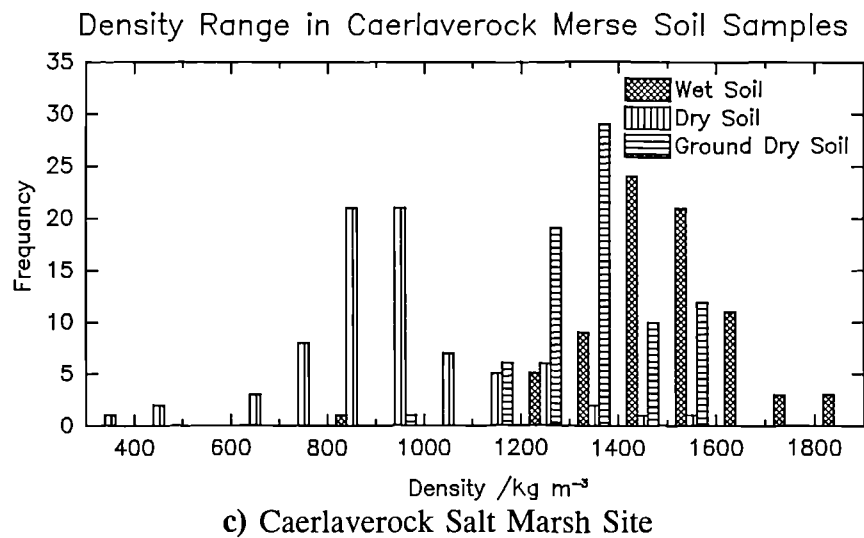
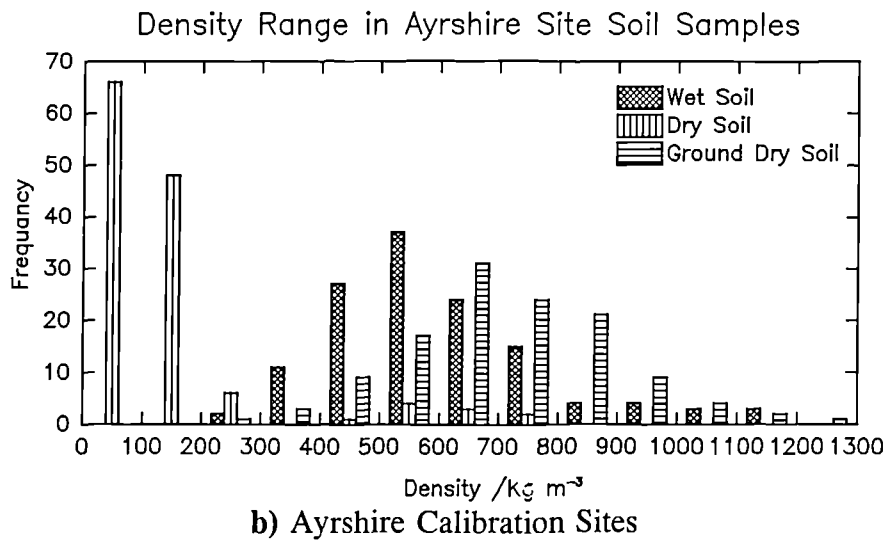
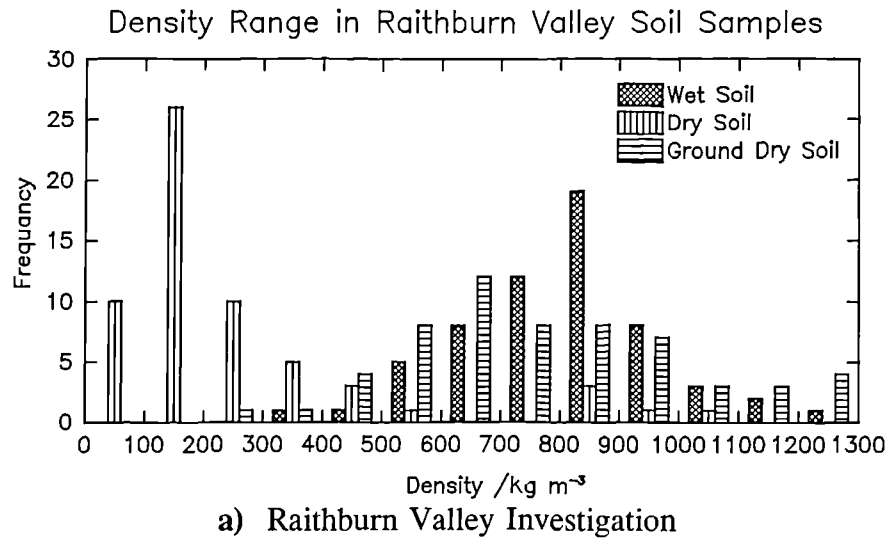


Figure 5.2 Density Ranges Observed Across and Within Soil Sample Site Investigations

5.2. The Raithburn and Ayrshire sites are predominantly organic rich whilst the saltmarsh sediments at Caerlaverock are of higher density. These sites, discussed further in chapter 6, demonstrate the range of soil densities which were encountered in the field. A range from 250 kg m^{-3} to 2000 kg m^{-3} . Drying soils reduces the soil density considerably, particularly within the organic rich samples, as observed in the majority of the Ayrshire sites (figure 5.2b). However, once ground and homogenised, pore spaces are lost and soil sample densities increase to levels higher than those observed in the field for the organic samples, or slightly lower with clay and sediment rich samples. The ground soil density variations are also quite considerable, from 300 kg m^{-3} to 1600 kg m^{-3} .

Thus this natural environmental variable, soil density, is likely to have considerable influence on the calibration of laboratory based detectors. In the field the influence of variations in water content are likely to lead to enhanced variations in the analytical depth observed for in-situ gamma spectrometry.

5.3 THE MEASUREMENT OF THE MASS ATTENUATION COEFFICIENT OF A RANGE OF BRITISH SOILS

5.3.1 Objective

This experiment was devised to determine the importance of sample density and the mass attenuation coefficient on the absorption and scattering of gamma photons of different energy. The results formed the basis of determining whether sample self absorption was important and whether correction would be required in the absolute efficiency calibration of detectors to compensate for the variation in sample types typically found in the environment.

5.3.2 Method

Thirty soil and sediment samples which included soils from across the UK, and two IAEA reference standards were selected. The samples were all ground within a Tema

mill to about 30 micron particle size and placed into a standard 150 cc container geometry. The sample weight, thickness and densities were measured.

Three Amersham point reference sources were chosen to provide a selection of energies across the spectrum of interest. The sources used were ^{241}Am (59.54 keV, 429 GBq), ^{137}Cs (661.7 keV, 425 GBq) and ^{60}Co (1173.3 and 1333 keV, 435 GBq). Figure 5.3 shows the apparatus set up. The reference sources were placed above a 40 mm thick lead collimator (5 mm diameter hole) at a distance of about 100 mm from the top of a coaxial HPGe detector. This ensured a pencil like beam would penetrate the sample and minimize the complicating influence a *broad beam* would have. Thus equation 5.1 is applied:

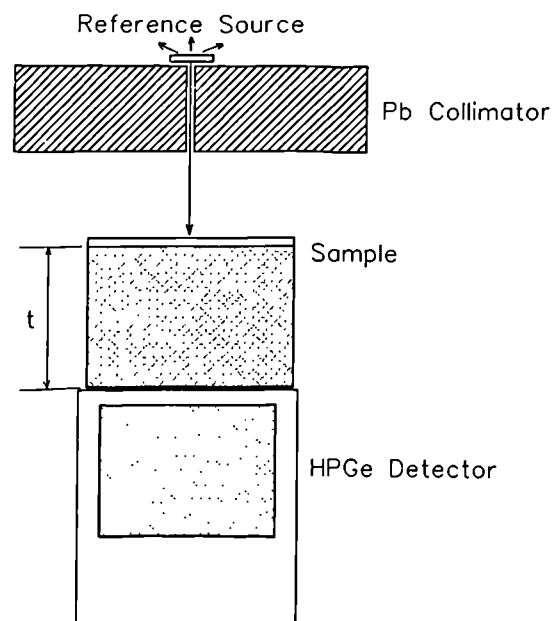


Figure 5.3 Apparatus used to determine μ and μ_m of soils

$$I_s = I_o e^{-\mu_s t} \quad (5.1)$$

For each mono-energetic gamma ray source, I_o was determined using an empty 150 cm³ container followed by a series of I_s determinations for the selected soils. After each series of measurements, I_o was first determined for the next mono-energetic photon source and verified throughout the series of measurements.

Thus from the measurements of I_o and I_s , μ_s could be determined from equation 5.2 and μ_m from equation 5.3.

$$\frac{I_s}{I_o} = e^{-\mu_s t} \quad (5.2)$$

$$\mu_m = \frac{\mu}{\rho} \quad (5.3)$$

where ρ = sample density, μ = linear attenuation coefficient and μ_m = mass attenuation coefficient of the soil sample.

From these measurements the dependence of μ and μ_m on photon energy and sample density could readily be determined.

5.3.3 Results

The measurements for I_s and I_o were made with between 1 and 2 % counting statistics. The sample thickness and density estimates were made with an estimated 5 % accuracy. These analytical errors are shown in figure 5.5.

The results for μ and μ_m and their dependence upon the photon energies of ^{241}Am , ^{137}Cs and ^{60}Co for the thirty soils are shown in figure 5.4 a and b and tabulated in Appendix C. Figure 5.4.a shows a variation in μ for all energies measured. A large scatter particularly at low energy (59.6 keV) is observed. However, sample density is also a factor and when accounted for as in figure 5.4.b, the dependence of μ_m with photon energy is clearly seen. At low energy the scatter in μ_m is appreciable and must be associated with variations in sample composition. Three examples of the soils used are shown in figure 5.4: an organic rich soil (peat); IAEA soil-6; and a heavy mineral soil from the Lizard in Cornwall. The largest changes in μ and μ_m with energy are observed in soils with a much higher mineral content such as the Lizard sample.

The relative dependence of μ on sample density is shown in table 5.2 where a marked change is observed between μ and μ_m especially for higher energy photons. However, as demonstrated, there is almost a 10 % variation in μ_m for energies associated with ^{137}Cs and ^{60}Co . The dependent nature of μ_m on sample composition is shown in figure 5.5. The magnitude of the scatter is higher for 59.54 keV photons as demonstrated in table 5.2. This scatter is independent of sample density and is therefore attributed to sample chemical composition. Figure 5.5.a suggests a possible relationship with increasing μ_m and density, which may reflect a relationship between sample composition and sample density. However, the overall random scatter probably reflects the

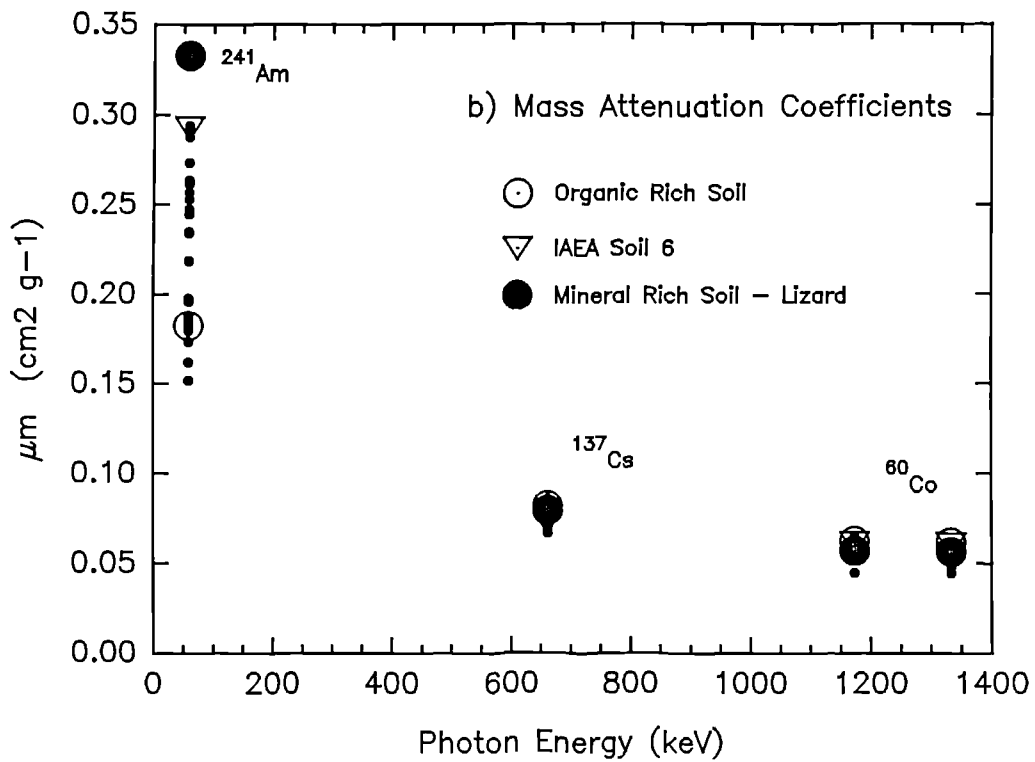
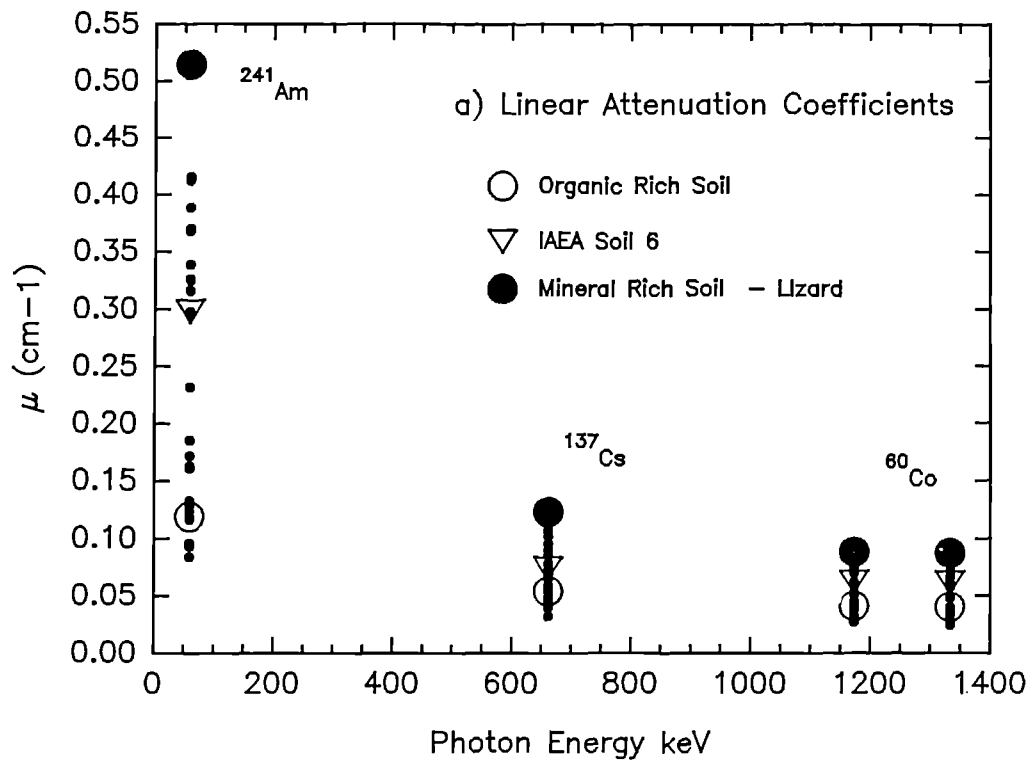


Figure 5.4 The dependence of a) μ and b) μ_m on the photon energies associated with ^{241}Am , ^{137}Cs and ^{60}Co for a range of soils.

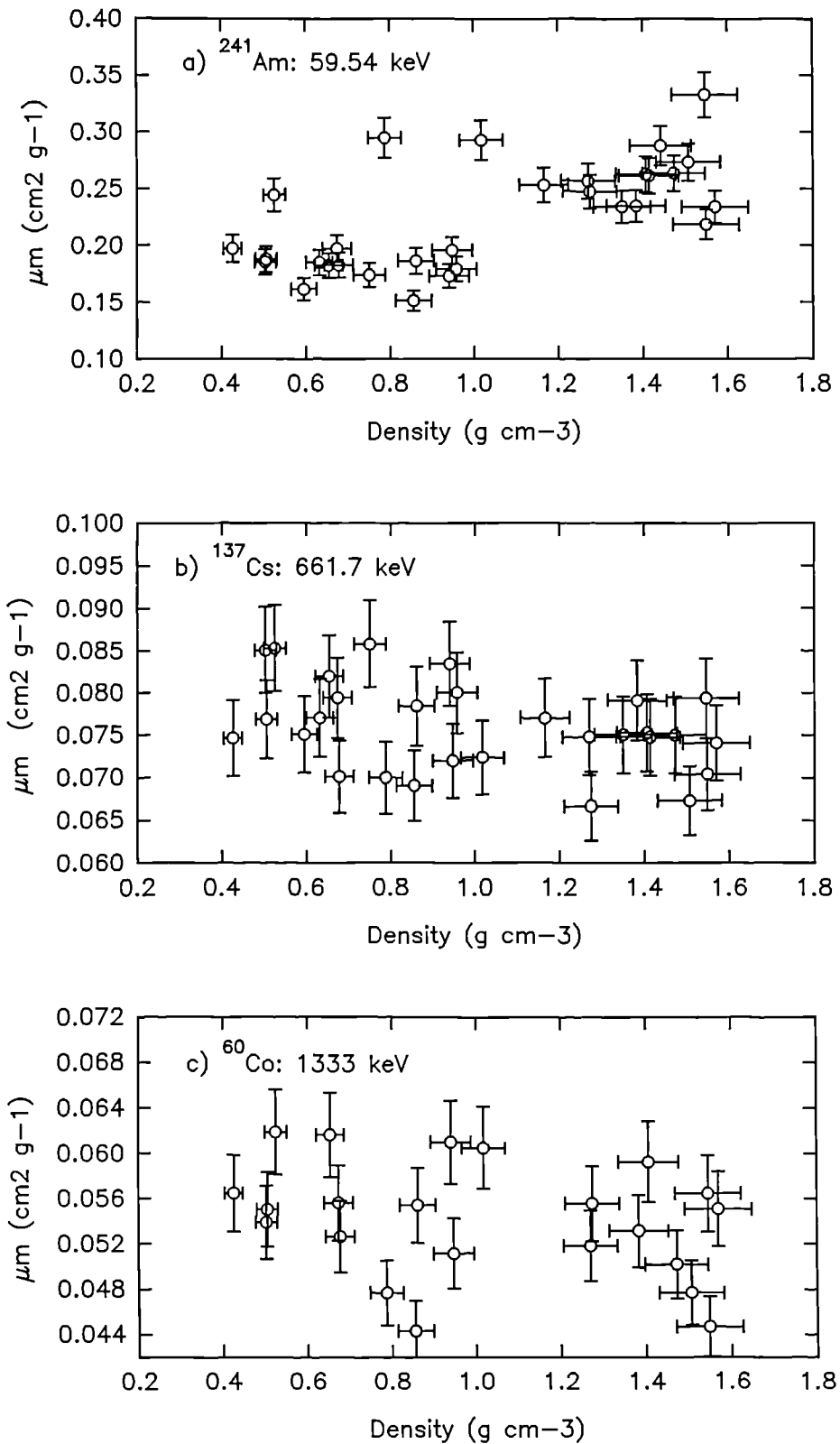


Figure 5.5 The scatter of μ_m with density and thus the dependence of μ_m on the chemical composition of the sample as well as gamma ray energy, a) 59.54 keV; b) 661.7 keV; and c) 1333 keV.

Table 5.2 The variation of μ and μ_m with photon energy and expressed in terms of the coefficients of variation (CV). Dry soil density used.

	²⁴¹ Am (59.54 keV)	¹³⁷ Cs (661.7 keV)	⁶⁰ Co (1333 keV)
Mean Density (g cm ⁻³)	1.022	1.022	1.018
Density Std Dev 1 σ	0.373	0.373	0.383
CV (1 σ /mean)	36.6	36.6	37.6
	μ	μ	μ
Mean	0.240	0.0759	0.0546
Std Dev 1 σ	0.122	0.0268	0.0202
CV (1 σ /mean)	50.9	35.3	37.0
	μ_m	μ_m	μ_m
Mean	0.2222	0.0754	0.0539
Std Dev 1 σ	0.0475	0.0064	0.0052
CV (1 σ /mean)	21.4	8.44	9.55

dependence of μ_m on sample composition.

Table 5.3 shows the importance of the variation in the linear attenuation coefficient μ on half depth, where half depth ($D_{1/2}$) is given by:

$$D_{1/2} = \frac{\ln 2}{\mu}$$

A considerable difference in $D_{1/2}$ occurs between organic and mineral rich soils, driven mainly by their contrasting bulk densities. This has important implications in the absolute efficiency calibration of laboratory based detectors as well as soil sampling depth for direct comparison with in-situ and aerial based gamma spectroscopy.

5.3.4 Summary

The experiment has demonstrated the dependence of the linear attenuation coefficient (μ) on a combination of sample density, chemistry and photon energy. The mass attenuation coefficient is dependent upon sample chemistry and photon energy.

Table 5.3 The variation in half depth with energy.

$\frac{1}{2}$ Depth	^{241}Am 59.54 keV	^{137}Cs 661.7 keV	^{60}Co 1173.3 keV	^{60}Co 1333 keV
Mean /cm	3.99	10.9	14.4	15.4
Std. Dev. 1σ	2.19	4.70	6.00	6.57
Max. (Peat) /cm	8.24	22.8	26.0	28.8
Min. (Lzd soil)/cm	1.35	5.65	7.78	7.94

Low density organic rich soils show a smaller change in μ and μ_m with energy than the mineral rich, reflecting the dependence on the photoelectric component of the mass attenuation coefficient at low energy. Thus chemical composition and density would appear to be important factors in the absolute efficiency calibration of laboratory based detectors for low energy photons (e.g. ^{241}Am), whilst sample density would also appear to be a major factor which will potentially affect the efficiency calibration of higher energy photons.

However, without examining the composition of the soils, one can only qualitatively illustrate the variation of μ_m with possible composition. In addition, this experiment has not shown clearly where the photoelectric effect loses its dominance over μ_m and thus the importance of μ_m with photon energy. Finally, although a spectrum of soils was chosen with a potentially wide range in oxide content to be sure of the maximum range of μ_m with photon energy, μ_m should be calculated from a broad spectrum of soils with known composition.

5.4 CALCULATION OF THE MASS ATTENUATION COEFFICIENTS OF A RANGE OF SOILS

5.4.1 Objectives

The objectives of this section are to calculate the individual photon fractions associated with coherent, incoherent, photoelectric and pair production interactions and total mass attenuation coefficients relative to changes in atomic number and photon energy. In addition, these are to be calculated with respect to a variety of the world's soils chosen

from the Geostandards News Letter (Govindaraju, 1989) which provides the major and trace elemental composition of soils as well as other reference materials. Thus Z_{mean} is calculated along with μ_m for these media and μ_m is compared with energy and composition. This is important in accounting for changes in sample chemical composition and photon energy in laboratory based gamma spectroscopy, as well as being particularly important when using photon transport equations to calculate fluence rates and fields of view in environmental gamma ray spectroscopy (section 3.8). In this latter respect, part of this work was initially undertaken jointly with Allyson (1994) to identify the maximum likely variation in μ_m with energy for ICRU (1993) (SURRC 1992). This has provided the most comprehensive investigation into the variation of μ_m with sample composition and photon energy yet undertaken.

5.4.2 Method

Previous authors (e.g. Beck *et al* 1972, Beck 1978, Mudahar and Sahato 1988a,b) have typically taken a selection of the dominant oxides in soils to calculate μ_m for a single soil composition. However, in order to demonstrate the effect of changes in Z_{mean} on μ_m , this section includes calculations of μ_m with minor trace elemental contributions.

Soil compositions were selected from the Geostandards News Letter (Govindaraju 1989) and compared with other sources as illustrated in table 5.4. This provides the major weight percent oxide of soils, which includes SiO₂, Al₂O₃, Fe₂O₃, FeO, MnO, MgO, CaO, Na₂O, K₂O, TiO₂, P₂O₅, H₂O, and CO₂. To this C was also added as a major soil component.

For completeness, trace elements were also selected for the calculation. However, in order to save computational time, the trace elements included were rationalised to those with a potential for making a significant contribution to changes in μ_m . Thus those "more abundant" elements with a Z greater than 50 were selected. These included parts per million (ppm) concentrations of Ar, Ba, Bi, Ce, Cu, Dy, Eu, Er, Gd, Hf, Ho, La, Lu, Nd, Os, Pb, Pt, Sn, Th, U, and W. In addition, N and S were also included.

Table 5.4. List of soil samples and references for chemical composition used in the calculation of μ_m .

Soil Compositions from Geostandards News Letter (Govindaraju 1989)

- | | | |
|-----|------------------|---|
| 1. | 24 GXR-2 | Soil from Park city, Utah, USA |
| 2. | 27 GXR-5 | Soil (B zone) Sommerset, County, Maine, USA |
| 3. | 28 GXR-6 | Soil B Zone, Davidson County, N. Carolina, USA |
| 4. | 36 SO-1 | Regosolic Clay Soil, Hull, Quebec, Canada |
| 5. | 37 SO-2 | Podzalic B Horizon Soil, Montmorency Forest, N. of Quebec City, Canada. |
| 6. | 38 SO-3 | Calcareous C Horizon Soil, Guelph, Ontario, Canada |
| 7. | 39 SO-4 | Chermozemic A horizon Soil, N.E. Saskatoon, Saskatchewan Canada |
| 8. | 98 SP-1 | Black Earth, Kursk, Russia |
| 9. | 99 SP-2 | Moscow Podzol Soil, Russia |
| 10. | 100 SP-3 | Bright Chestnut Coloured Soil (Caspian), Russia |
| 11. | 181 GSS-1 | Dark Brown Podzolic Soil, Yichun, Heilongjiang, China. |
| 12. | 182 GSS-2 | Chestnut Coloured Composite Soil, Semi Arid Region, Bainimias, Neimuggo, vicinity of copper deposit, China |
| 13. | 183 GSS-3 | Yellow-Brown Soil, Temperate country, Shandong, vicinity of Gold Mine, China |
| 14. | 184 GSS-4 | Limy-Yellow Soil, Subtropical, Yishan, China |
| 15. | 185 GSS-5 | Yellow-Red Soil, Humid Area of Quibaoshan, Polymetallic Ore Field, Hunan, China |
| 16. | 186 GSS-6 | Yellow-Red Subtropical Soil, Yangchun, Guangdong, China Copper, tin, tungsten, antimony and arsenic mineralization in region. |
| 17. | 187 GSS-7 | Lateritic Tropical Soil, Leizhou Peninsula, China |
| 18. | 188 GSS-8 | Loess Soil, Louchan, Shaanxi Province, China |
| 19. | 196 K-3 | Tropical Composite Soil, Western Suriname |
| 20. | 197 CS-1 | Tropical Composite Soil, Central Suriname |
| 21. | 198 SAu-1 | Gold Bearing Soil from Central Suriname |
| 22. | 199 SUR-1 | Composite Soil, Central Suriname |
| 23. | 210 S-1 | Cu-Ni-Co rich soil from western bank of Sterkstroom |

Other Soil Compositions

- | | |
|-----|---|
| 24. | Beck Composition. Harold L. Beck, Joseph DeCampo, Carl Gogolack, 1972. In situ Ge(Li) and NaI(Tl) Gamma-Ray Spectrometry. HASL-258, Atomic Energy Commission, USA. |
| 25. | Mudahar and Sahota Composition. 1988. Effective Atomic Number Studies in Different Soils for Total Photon Interaction in the Region 10-5000 keV. Appl. Radiat. Isot. Vol. 39, No. 12 pp.1251-1254. |
| 26. | Peat Dry. Typical organic composition: C=56.8%, H=5.49%, N=1.75%, O=34.74%, S=1.22% |
-

The contributions of coherent and incoherent scattering, photoelectric effect and pair production contributions and total μ_m were tabulated in a spread sheet for the above elements from Storm and Israel (1970) with later contributions from Hubbell (1982). The oxide fractions were then split by weight in order to provide their concentrations in ppm. Elemental compositions of individual soils were then tabulated and the individual photon interactions and total μ_m were calculated by weighting each elemental photon interaction and total μ_m appropriately for each elemental member of the soil as shown in equation 5.5:

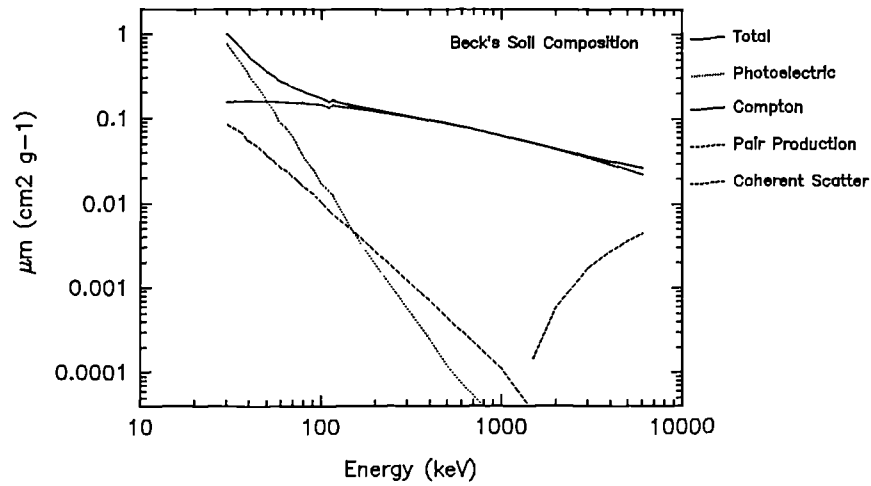
$$\mu_m = \sum_{i=1}^N w_i \mu_{mi} \quad (5.5)$$

where μ_{mi} is the mass attenuation coefficient of element i , N is the number of elements present in the soil fraction, w_i represents the abundance by weight of the i th element, such that the sum of $w_i = 1$. Z_{mean} of the soil was also calculated simply by the weighted average of the individual Z 's.

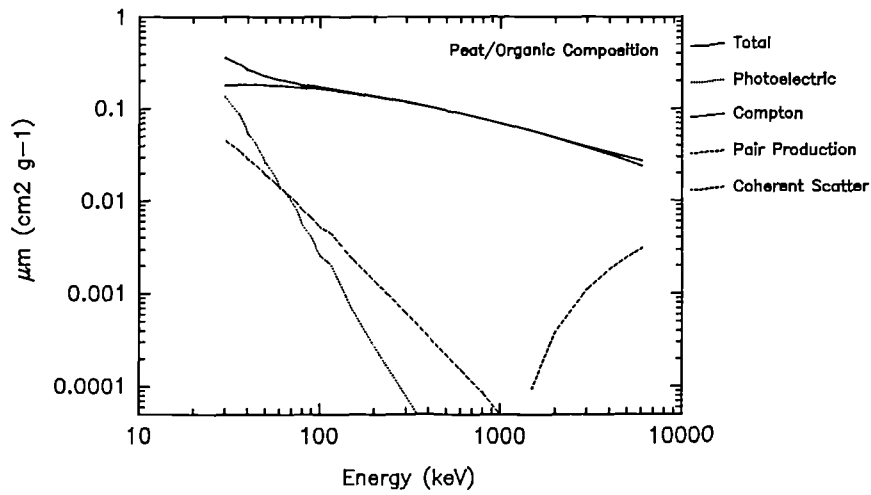
5.4.3 Results and Discussion

Figure 5.6 shows the contributions of coherent and incoherent scattering, photoelectric absorption and pair production on the total mass attenuation coefficient for energies between 30 and 6000 keV. The photoelectric effect dominates μ_m at low energies (< 200 keV approx.). This is linked to the chemical composition of the soil. For energies greater than about 200 keV, the total μ_m is broadly similar between the three examples due to similar scattering coefficients.

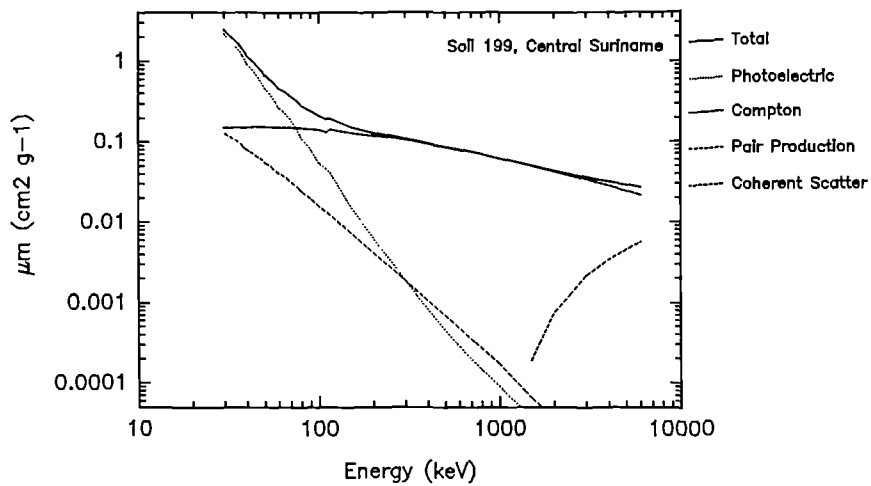
Beck's soil (Beck *et al* 1972) has been used by many others to determine the value of μ_m for soils. However, figure 5.6 suggests that for low energies the assumption that Beck's soil is representative is likely to be inaccurate. By dividing the total μ_m for each soil composition by total μ_m of Beck's soil, a comparison of μ_m can be made between the soils. This is illustrated in figure 5.7. There is a broad distribution of μ_m for soils at low energies which increases with reduction in energy. From figure 5.6 this is dominated by the photoelectric effect and all reference soils provide values of μ_m that



a) Beck's Soil



b) Organic Composition



c) Soil 199, Central Suriname, Georeference Material

Figure 5.6 The contribution of scattering and absorption to the total μ_m for a) Beck's soil and two extreme soil compositions; b) organic; and c) mineral rich.

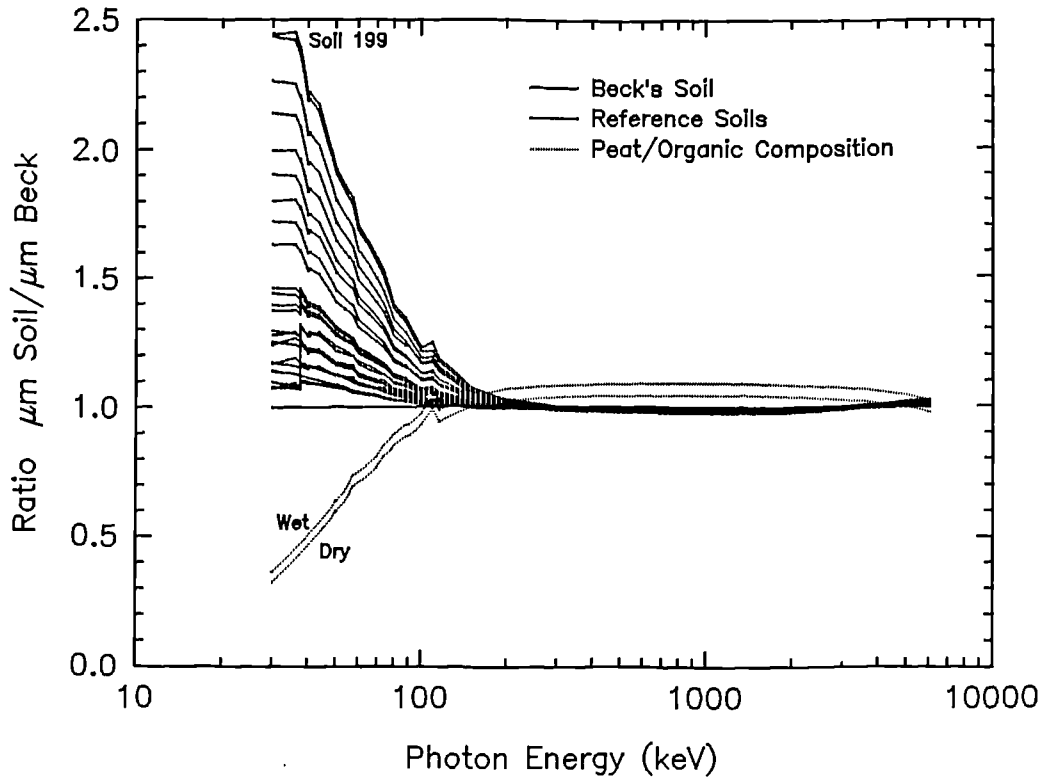


Figure 5.7 Comparison of μ_m relative to Beck's soil composition, with energy.

are greater than predicted by Beck's soil. The pure organic peat results in very much lower values for μ_m than indicated by Beck's soil. However, the reference soils contain no organic component, due to ashing of samples during preparation for analysis. In the real world, where organic contents in soils range from 0 to almost 100 %, the spread of the potential values of μ_m as indicated in figure 5.7, probably reflects reality. However, the mean μ_m is likely to be close to that represented by Beck's soil.

At energies above 150 keV (approx.), incoherent scattering dominates the μ_m , and very minor differences between the Beck soil and the geostandard reference soils are apparent. However, the organic soil shows the largest difference from Beck's soil. Again, given that most soil contains some quantity of organic matter, the range of μ_m likely to be observed would be represented by the *organic soil* and *soil 199*. This suggests a natural variation of about 5 % for μ_m for dry soils and up to 10 % for wet soils.

From this data base, it is also possible to establish how μ_m will vary with chemical composition. Table 5.5 gives the calculated mean atomic number Z_{mean} , and the

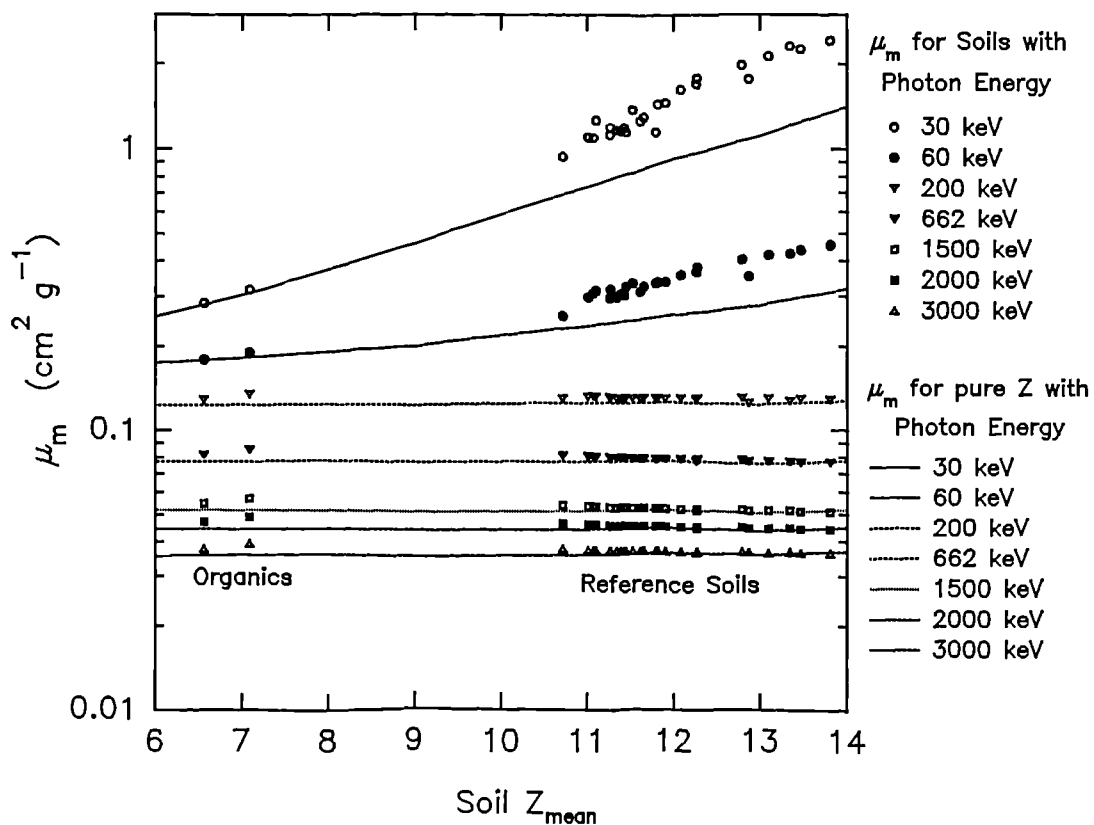


Figure 5.8 The relationship between μ_m and Z_{mean} for soils (*symbols*) and also for pure elements of Z (*solid line*).

associated μ_m with different photon energies for the soils. Z_{mean} was calculated by weighting each elemental component of the soil by its concentration in ppm. Figure 5.8 also plots the change in μ_m with Z_{mean} for the soils (*symbols*) and with pure Z (*lines*) for given energies.

For the lower energy gamma photons there is a marked difference in μ_m between the values obtained from Z_{mean} and Z . At low energy (e.g. 30 keV and 60 keV gamma photons) this is particularly marked. Mudahar and Sahato (1988b) argue this as resulting in an *effective atomic number* (Z_{eff}) from similar earlier reports by Hine (1952). The Z_{eff} can be determined from the interception of μ_m of a soil with the pure Z line for the given energy. Thus, for example from figure 5.8, at 60 keV, soils with a Z_{mean} of between 11 and 14 would result in a Z_{eff} of between 13 and 16. It can also be seen from figure 5.8 that the Z_{eff} will vary with photon energy, particularly in the energy region where the photo electric effect predominates (<200 keV).

Table 5.5 The variation in μ_m with selected energies and composition.

Sample	Z_{mean}	μ_m (cm ² g ⁻¹)		
		60 keV	662 keV	1500 keV
1. 24 GXR-2	11.07	0.2956	0.07749	0.05157
2. 27 GXR-5	11.27	0.3057	0.07738	0.05151
3. 28 GXR-6	11.45	0.3148	0.07749	0.05158
4. 36 SO-1	11.79	0.3278	0.07733	0.05147
5. 37 SO-2	11.53	0.3263	0.07730	0.05145
6. 38 SO-3	11.10	0.3024	0.07749	0.05161
7. 39 SO-4	11.01	0.2851	0.07756	0.05164
8. 98 SP-1	11.43	0.2934	0.07728	0.05145
9. 99 SP-2	11.26	0.2848	0.07733	0.05148
10. 100 SP-3	11.61	0.3044	0.07721	0.05140
11. 181 GSS-1	11.82	0.3314	0.07750	0.05156
12. 182 GSS-2	11.65	0.3182	0.07747	0.05156
13. 183 GSS-3	11.39	0.2954	0.07741	0.05153
14. 184 GSS-4	12.27	0.3771	0.07754	0.05159
15. 185 GSS-5	12.79	0.4025	0.07738	0.05146
16. 186 GSS-6	12.08	0.3536	0.07761	0.05164
17. 187 GSS-7	13.34	0.4211	0.07691	0.05135
18. 188 GSS-8	11.91	0.3328	0.07744	0.05154
19. 196 K-3	12.26	0.3618	0.07674	0.05106
20. 197 CS-1	13.47	0.4344	0.07656	0.05091
21. 198 SAu-1	13.10	0.4164	0.07655	0.05091
22. 199 SUR-1	13.81	0.4554	0.07651	0.05087
23. 210 S-1	11.34	0.2867	0.07734	0.05147
	Mean	11.51	0.3403	0.07725
	Std. Dev.	2.29	0.0515	0.00034
24. Beck Composition.	10.71	0.2436	0.07791	0.05202
25. Mudahar and Sahota	12.87	0.3491	0.07650	0.05109
26. Dry Peat.	6.56	0.1798	0.08155	0.05451
27. Wet Peat.	7.09	0.1891	0.08513	0.05682

From Knoll (1989) the probability of photoelectric absorption can be approximated by equation 5.6:

$$\mu_{pe} \cong \text{constant} \times \frac{Z^n}{E_\gamma^{3.5}} \quad (5.6)$$

where n varies from between 4 and 5 and E is the gamma ray energy of interest. Thus

from equation 5.5, this will result in a linear summation of μ_{pe} to determine the total μ_{pe} for a given soil. Thus, small changes in the amount of a given element present within the compound or soil will result in significant changes in μ_{pe} for that soil and therefore also in μ_m at energies where the photoelectric absorption predominates. As a result, for higher gamma photon energies (>200 keV) out of the energy region dominated by the photoelectric effect, the values of μ_m for soils resemble those associated with pure elements and thus $Z_{eff} \approx Z_{mean}$.

Figure 5.8 and table 5.5 demonstrate that μ_m for the geostandard reference soils do not vary as markedly as was suggested by the experiment described in section 5.3. However, this can be explained by the preparation of the geostandard materials for analysis. These samples were ashed thus burning off the organic components of the sample. Organic compositions, as indicated in figure 5.8 and table 5.5, result in μ_m of significantly different values, particularly at low energy. Thus naturally occurring soils with variable organic content will lead to greater observed variation in μ_m than indicated here and as shown in figures 5.4 and 5.5.

Note also that for 60 keV photons, the variation in soil chemistry resulted in a range in values of μ_m from $0.284 \text{ cm}^2 \text{ g}^{-1}$ to $0.455 \text{ cm}^2 \text{ g}^{-1}$ giving a standard deviation of only 15%. Measurements of a variety of soils which include different amounts of organic content led to observed variations in μ_m with ^{241}Am of up to 21.4 % as given in table 5.2. Again, this can be accounted for by the addition of the organic component to natural soils. Table 5.5 shows that μ_m at 60 keV may be as low as $0.180 \text{ cm}^2 \text{ g}^{-1}$ for organic rich soils. Adding this organic component to mineral rich soils at concentrations from 0 to 100 % will effectively change the observed μ_m for all energies. Thus, for low energy photons, the amount of organic content in the soil can also be a controlling factor on the final μ_m observed.

5.5 DISCUSSION AND IMPLICATIONS OF SOIL SELF ABSORPTION

5.5.1 Summary

From both experimental observations in sections 5.3 and 5.4, as expected, the photoelectric effect dominates observed values of μ_m at low energies (< 200 keV approx.). The degree to which this controls μ_m for soils has been quantified. At low energy the photoelectric effect results in μ_m estimates for soils to be higher than for pure elements. In compounds such as soils, Z_{mean} is not related to orbital electron density as with neutral atoms. As a result, μ_{pe} which is proportional to Z^{4-5} is likely to be influenced by some of the heavier elements present.

At higher energies (> 200 keV approx.) the observed and calculated variation in μ_m is far smaller. In this region where incoherent scattering of photons dominates μ_m , variations are estimated to be significantly less than 10%. Most of this variation above 200 keV may be explained by the amount of organic matter present.

5.5.2 Implications for Laboratory Based Gamma Ray Spectrometry

The implications of this work for laboratory based gamma spectroscopy suggest that for energies above 200 keV the variation in sample self absorption and scattering is dominated principally by sample density, and to a lesser extent by the amount of organic matter present in the sample. At energies below 200 keV, photoelectric absorption dominates the attenuation characteristics of the soil which in turn are determined by the chemical composition of the sample. Although, changes in sample density may account for some of the attenuating characteristics of the sample, it is still the chemical composition which predominantly controls μ_m at low photon energy.

Thus by accounting for sample density one can correct for the consequential changes in detector efficiency for energies above 200 keV, whilst only partly doing so for energies below 200 keV. This is discussed further in section 5.6.

5.5.3 Implications for In-situ and Airborne Gamma Ray Spectrometry

As discussed in section 5.2, the half depth observed from differing values of μ has particular implications on in-situ gamma ray spectroscopy. From the half depth we can estimate the soil sampling depth required for effective comparison with in-situ and aerial survey gamma spectrometric techniques. As the primary photon contribution to photon fluence decreases exponentially with depth, there is a trade off with the depth of soil core required to be representative. The *effective sampling depth* can be defined as three times the half depth. Thus, if we assume that the activity distribution is uniform, then 87.5 % of the primary gamma photons from the ground can be accounted for.

For energies below about 200 keV, e.g 59.6 keV, the mean half depth observed for dry soils is about $4 \text{ cm} \pm 2.2 \text{ cm}$. Although this value varies considerably (table 5.2), it does suggest that 87.5 % of the primary photon fluence for ^{241}Am originates from about the top 12 cm of the soil profile. In contrast, at 662 keV, the mean half depth is about $11 \text{ cm} \pm 4.7 \text{ cm}$, depending primarily on soil density. Thus, on average about 87.5 % of the primary photon fluence originates from an integrated depth of about 33 cm. For higher photon energies, such as at 1333 keV, the half depth is $15.4 \text{ cm} \pm 6.6 \text{ cm}$. At these energy values, 87.5% of the photon fluence will originate from depths of over 45cm.

The variation in μ with soil type is an example of an environmental factor or variable which has implications for the effective sampling depth required to make direct comparisons with in-situ and aerial survey gamma ray spectrometry. The half depth for ^{137}Cs can vary from about 30 cm in peaty locations to 4.6 cm in very high density salt marsh sediments. Further more, this factor is complicated by the stratification of source distribution. Fortunately, for these peaty sites, most (>90 %) of ^{137}Cs is found in the top 30 cm of the soil profile. However, in coastal salt marsh environments, examination of the vertical stratification reveals the development of the subsurface maxima within and below the typical 30 cm soil sampling depth. This degree of source burial will lead to a significant amount of primary photon attenuation resulting in increased secondary scattered photons. Thus for an extreme example, activity buried

within a narrow layer at 30 cm depth, only 12 % of the primary photon fluence originating from this level would reach the surface. This environmental factor for in-situ gamma spectrometry is discussed further in chapter 7.

However, difficulty is observed when sampling for higher energy photon emitting radionuclides (^{40}K , ^{214}Bi , ^{208}Tl) particularly in highly organic rich sites. At energies of 1500 keV, for example, observed half depths may vary from 43 cm (peat) to 6.5 cm (sediment). This causes problems when activity is quoted in terms of activity per unit area (Bq m^{-2}), as the integrated sampling depth will be dependent upon photon energy and soil type characteristics. If the distribution of activity is uniform with depth and activity is measured in concentration (Bq kg^{-1}), then the *effective* sampling depth is not constrained by depth requirements. However, if the source distribution is not uniform with depth, then further attention must be given to the *effective* sampling depth. The importance of this was demonstrated with ^{40}K within the Raithburn Valley investigation where the highly acidic organic soils, effective in breaking down clays, reduce uptake of ^{40}K into the soil column. For photon energies of about 1500 keV with low soil densities, between 60 % ($\rho \approx 300 \text{ kg m}^{-3}$) and 25 % ($\rho \approx 800 \text{ kg m}^{-3}$) of the primary photon fluence observed at the soil surface may originate from below typically the 30 cm soil sampling depth, particularly if the activity was concentrated just below the sample depth e.g. from underlying geology. Consequently the potential variation in density with water content, particularly in peaty soils, will result in variations in the attenuation of the primary photon fluence, which therefore leads to temporal changes in the *effective* sampling depth. This is also discussed further in chapter 7.

The influence of μ_m on low energy (<200 keV) in-situ gamma spectrometry complicates the in-situ estimation of ^{241}Am activity. Here, in addition to density, the effect of soil composition, and thus μ_m will influence the effective sampling depth. This may make absolute quantification of detected photon fluence rates difficult.

5.6 SAMPLE SELF ABSORPTION CORRECTION FOR ABSOLUTE EFFICIENCY CALIBRATION OF LABORATORY BASED DETECTORS

5.6.1 Objectives

As already demonstrated, density effects and changes in sample composition can result in marked changes in the linear attenuation coefficient associated with changes in soil type. At lower energies this is dominated by the photoelectric effect which in turn is controlled by changes in sample composition. At higher energies ($> 150 - 200$ keV) density and to a lesser extent soil composition, dominated by changes in organic content, results in changes in the linear attenuation coefficient.

Thus, corrections for sample self absorption for laboratory based gamma spectroscopy are determined here empirically. This should account for potential changes in sample density and composition for energies above 200 keV, whilst only partly accounting for such variations for energies below 200 keV. To account for changes in sample self absorption for energies below 200 keV, a calibration associated with the linear attenuation coefficient would be more appropriate.

The degree of influence of changes in μ_m and density on the absolute efficiency calibration is also influenced by the geometry size of the sample with respect to the detector crystal size. A coaxial Ge(Li) and HPGe detector and 50% relative efficiency GMX Detector were calibrated with this technique.

5.6.2 Method

To achieve a correction for self absorption and scattering, a range of samples of differing densities was required. To achieve this, two ground and homogenous samples of very different composition were used. The first was a sediment collected from several metres depth with a relatively high density of 1.5 g cm^{-3} (Elginhaugh soil). The second was a monolithic peat sample collected at 1.5 metres depth with a density of 0.53 g cm^{-3} (Ilkley Moor monolithic peat). Both samples were checked to be free of

anthropogenic radionuclides. By mixing these two samples in different proportions, any number of hybrid samples could be made with varying densities ranging from the minimum of 0.53 g cm^{-3} to 1.5 g cm^{-3} with corresponding variations in organic content.

Section 3.5.6 discusses the two methods used for spiking soils with radionuclides. The absolute efficiencies for the natural radionuclide energies are determined by interpolation between the anthropogenic calibration points with polynomial equations.

5.6.3 Results and Discussion

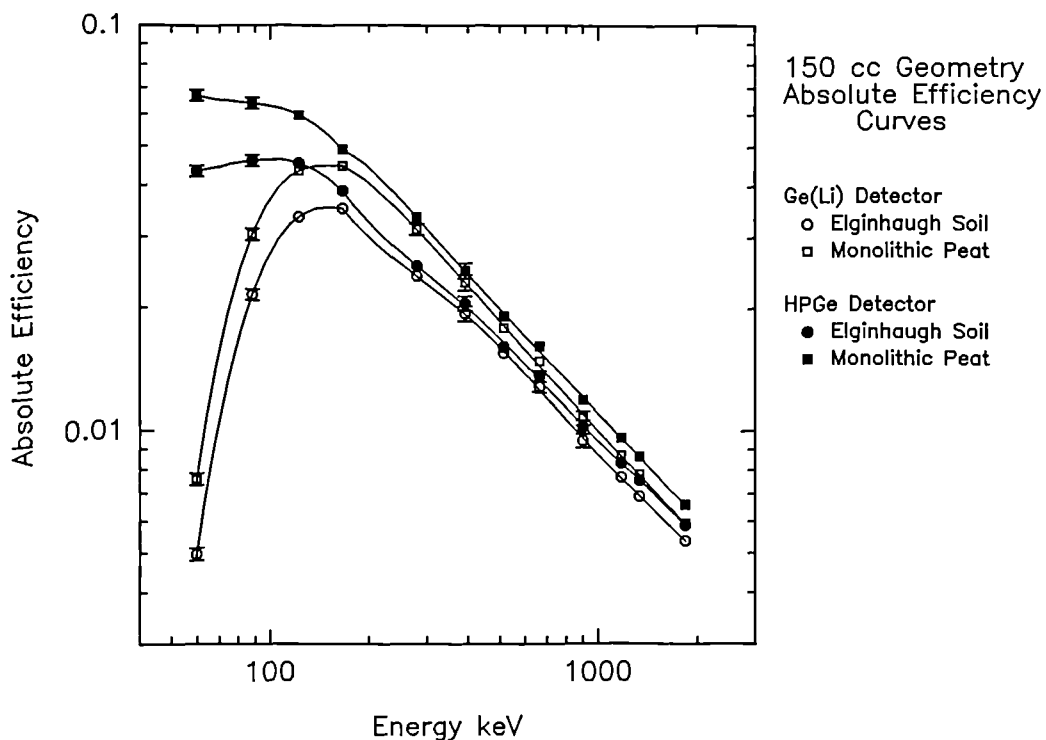


Figure 5.9 The change in absolute efficiency with energy and sample density (Elginhaugh Soil = 1.5 g cm^{-3} , Monolithic Peat = 0.53 g cm^{-3}).

For the two extremes in sample density, figure 5.9 demonstrates the magnitude of change in detector absolute efficiency with energy. The data are tabulated in Appendix D. The difference in absolute efficiency for the two soils is greatest at low energy. This is caused by changes in the *effective* sample geometry, or *effective* solid angle exposed to the detector which is brought about by the change in μ_m as well as by a change in density. Polynomial equations are fitted to these points either side of the 165.8 keV point.

These two curves for each detector clearly suggest the need for a density corrected absolute efficiency calibration. Thus absolute efficiency curves were determined for a suite of hybrid soils of varying density. From the polynomial equations derived from the subsequent efficiency curves with photon energy, absolute efficiencies could be derived for photons from the primordial radionuclides.

Table 5.6 The Photo-peaks used in Density Correction Efficiency Calibration

Nuclide	Energy keV	% Yield
²⁴¹ Am	59.5	36.3
¹³⁷ Cs	661.7	85.2
¹³⁴ Cs	604.74	97.6
⁴⁰ K	1460.6	10.7
²¹⁴ Bi	1764.79	16.4
²⁰⁸ Tl	583.0	86.0

In this study the anthropogenic radionuclides of particular interest are ²⁴¹Am, ¹³⁷Cs and ¹³⁴Cs and the primordial radionuclides of interest are ⁴⁰K, ²¹⁴Bi and ²⁰⁸Tl. The tabulated data are given in Appendix E. The Canberra Spectran AT software has the capability of using as many of the photo-peaks available per radionuclide of interest to determine the activity concentration. However, this approach was simplified in order to determine a density correction. Single photo peaks were chosen which could not be confused in the spectrum and which had a relatively high photon yield. Table 5.6 shows the photo peaks chosen for density correction and radionuclide inventory analysis.

The efficiency calibration was based on the wet spiking technique as described in section 3.5.6. Figures 5.10 and 5.11 show the calibration lines for 150cc containers on a Ge(Li) detector for the energies of interest as shown in table 5.6. The equations of each line are given in table 5.7. From figure 5.10.a, ²⁴¹Am demonstrates a linear regression with absolute efficiency and sample density. Similarly figure 5.10.b shows the simple linear regression through the calibration points of the hybrid soils for ¹³⁷Cs.

To verify this calibration technique the procedure was repeated three times for the pure Elginhaugh soils and twice for the pure peat samples. As shown in figures 5.10 and 5.11, no significant variation in detector response was observed from these multiple samples for the energies of interest.

Table 5.7 Absolute Efficiency Calibration Equations For Sample Self Absorption. Errors include error on calibration curve and absolute efficiency.

Eff = Absolute detector Efficiency, D = Sample density (g cm^{-3})

Coaxial Ge(Li) Detector

150 cm³ Geometry ($\phi = 6.5$ cm, $t = 4.7$ cm)

Nuclide	Equation of line of best fit	Range in Error %	Change $Eff.$ % $\rho=0.5-1.5$
²⁴¹ Am	$Eff = 0.009125 - 0.002916 \cdot D$	3.9 - 4.5	61.38
¹³⁷ Cs	$Eff = 0.015284 - 0.002076 \cdot D$	4.0 - 4.3	17.06
¹³⁴ Cs	$Eff = 0.016360 - 0.002057 \cdot D$	3.9 - 4.3	15.52
⁴⁰ K	$Eff = 0.007386 - 0.000735 \cdot D$	1.5 - 2.6	11.70
²¹⁴ Bi	$Eff = 0.006252 - 0.000558 \cdot D$	2.8 - 4.2	10.30
²⁰⁸ Tl	$Eff = 0.016938 - 0.002160 \cdot D$	4.0 - 4.6	15.77

75 cm³ Geometry ($\phi = 5.0$ cm, $t = 3.9$ cm)

²⁴¹ Am	$Eff = 0.010992 - 0.002470 \cdot D$	4.2 - 4.8	33.90
¹³⁷ Cs	$Eff = 0.018318 - 0.002219 \cdot D$	4.2 - 4.5	14.80
¹³⁴ Cs	$Eff = 0.020129 - 0.002619 \cdot D$	4.3 - 4.5	16.17
⁴⁰ K	$Eff = 0.008778 - 0.000974 \cdot D$	2.0 - 2.7	13.31
²¹⁴ Bi	$Eff = 0.007310 - 0.000586 \cdot D$	3.0 - 4.0	9.11
²⁰⁸ Tl	$Eff = 0.020893 - 0.002775 \cdot D$	4.2 - 4.7	16.59

Coaxial n-type HPGe Detector, 150 cm³ Geometry

²⁴¹ Am	$Eff = 0.07950 - 0.025990 \cdot D$	3.5 - 4.0	64.15
¹³⁷ Cs	$Eff = 0.01680 - 0.002320 \cdot D$	4.0 - 4.5	17.42

50 % GMX n-type HPGe Detector, 150 cm³ Geometry

²⁴¹ Am	$Eff = 0.09571 - 0.026420 \cdot D$	3.5 - 4.0	45.97
¹³⁷ Cs	$Eff = 0.02384 - 0.002280 \cdot D$	3.5 - 4.0	11.17

A separate pure ¹³⁷Cs Amersham spike was then used to spike soils collected in the environment which had very low concentrations of ¹³⁷Cs. The dry spiking technique was used. The activity of spike used was between 200 and 300 times the soil's natural activity. Even so, the activity present was taken into account in the analysis, although its contribution was almost negligible. Figure 5.10.b shows that both spiking techniques agree with each other.

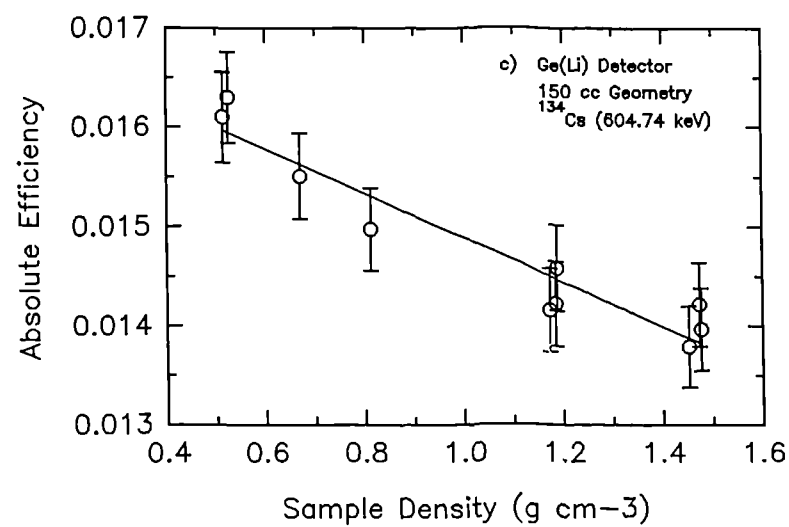
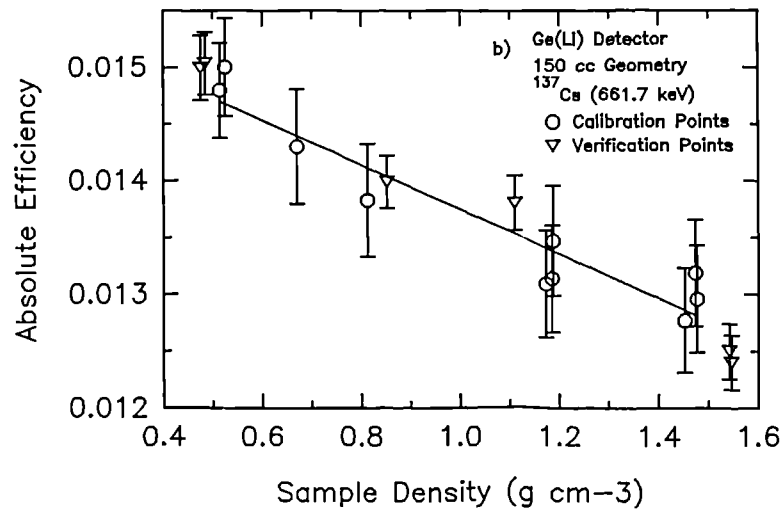
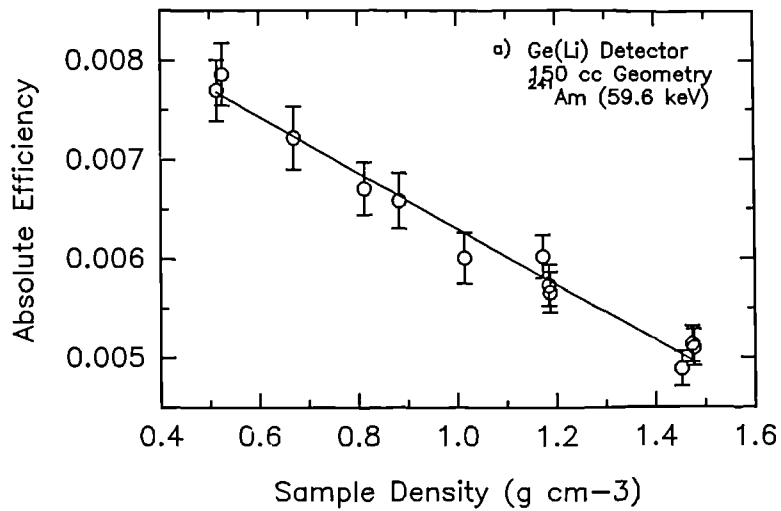


Figure 5.10 The change in absolute efficiency with sample density for anthropogenic radionuclides with 150cc geometry containers (data in Appendix E).

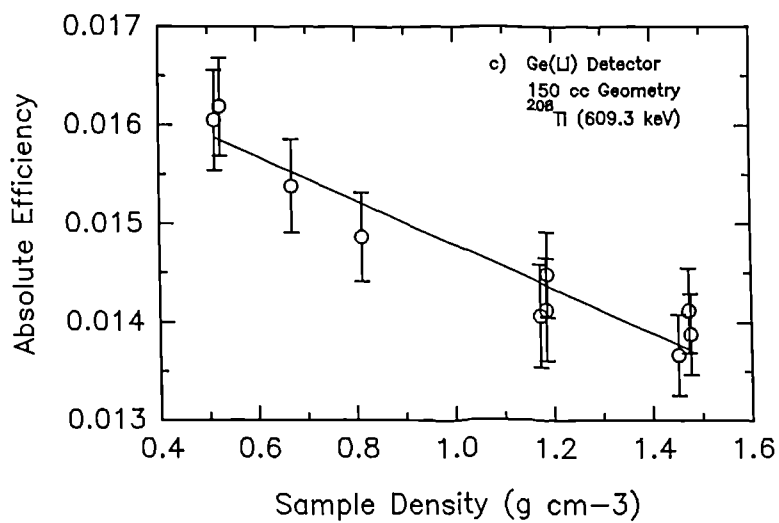
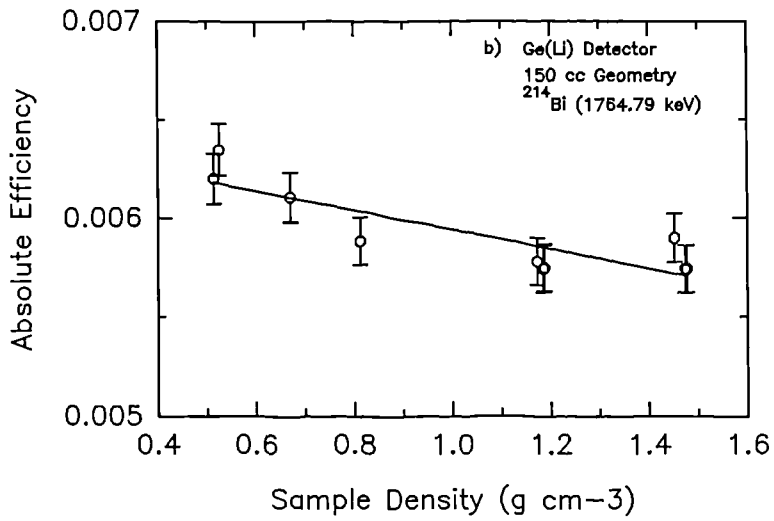
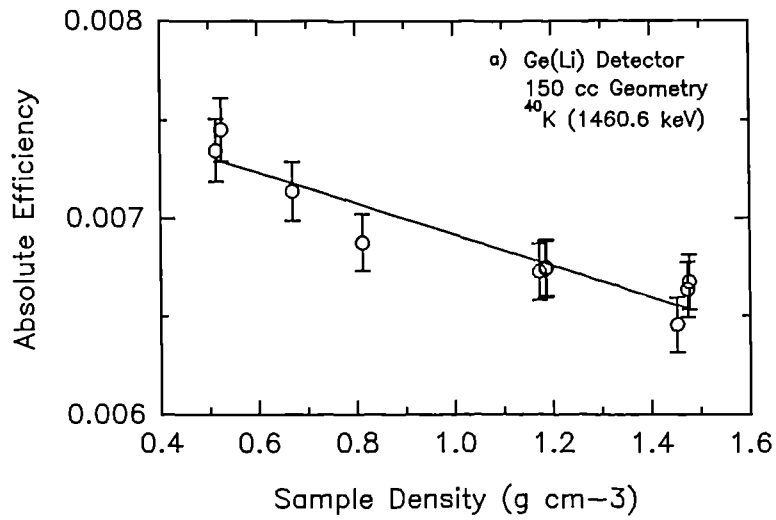


Figure 5.11 The change in detector absolute efficiency for primordial radionuclides in 150cc geometry containers (data in Appendix E).

The linearity in detector response with activity concentration was also verified. Samples analyzed during this study had a typical activity range of between 3 and 3000 Bq kg⁻¹. Thus a single sample of density 1.17 g cm⁻³ was spiked three times in succession with the wet spiking method. No systematic variation was observed and the slight scatter on the graph can be attributed to slight changes in sample mass and density in addition to analytical errors.

Analytical errors brought about by changes in sample weight, ie under/over filling of the detector geometry were examined. The results of consecutively

under-filling the Elginhaugh 150 cc geometry are demonstrated in figure 5.12. Very little variation is observed for ²⁴¹Am detection efficiency with up to a 30 % reduction in sample within the geometry. Clearly, the majority of the ²⁴¹Am photons originate from the lower portions of the sample. For higher energy photons, such as ¹³⁷Cs as shown in figure 5.12.b, the same reduction in sample content leads to a considerable increase in detection efficiency. This is because the detector geometry is changing and the mean sample-source position is moving closer to the detector. However, from such observations, sample weight variations of up to ±10 % could be tolerated. Galloway (1991b and 1993) describes a method to correct for under filling of standard sample containers. He also shows that small variations in sample filling are effectively compensated for by the changes in self absorption characteristics.

¹³⁷Cs calibration is clearly corroborated by the two spiking techniques used and by the use of different soil types including a variety of peats from a range of depths and locations, clay and mineral rich soils from Cambourne and the Lizard. Any possible

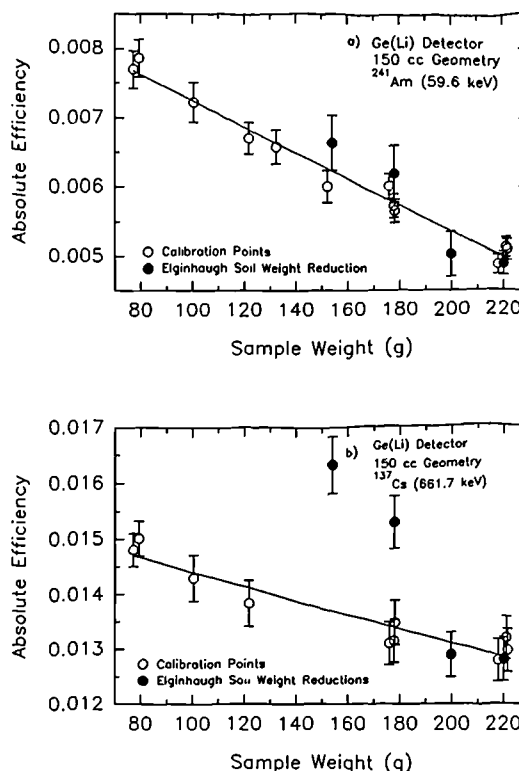


Figure 5.12 The change in detection efficiency with sample weight reduction i.e. sample under-filling.

contribution brought about by minute changes in μ_m , are likely to be accounted for by the scatter about the line of best fit. A contribution to the scatter of points is also likely to have been introduced by pipetting errors during the spiking procedure. These errors have been determined to be better than 2 %. From figure 5.10 a linear approximation to the relationship between absolute efficiency and sample density is used. However, the higher energy photon calibration curves in figure 5.11 (e.g. ^{40}K and ^{214}Bi) indicate a non-linear relationship. Further examination of the ^{137}Cs graph (figure 5.10) shows a contradiction in this non-linear trend by the verification points (pure ^{137}Cs spike). Further detailed experimental work with higher precision absolute efficiency estimates would be useful to determine the nature of this relationship. However, given that the majority of the samples analysed fell outside the 0.8 to 1.2 g cm^{-3} density range, a linear approximation was used.

Figures 5.10 and 5.11 and table 5.7 also show the decrease in gradient with increasing photon energy. The mass attenuation coefficient decreases with increasing energy and changes in sample density result in smaller changes in the absolute efficiency of the detector for the 150 cm^3 sample container.

The errors involved in the analysis include the random and systematic errors provided with the spike certification, counting statistics, the pipetting error and the error about the regression for the line of best fit. The sum of these errors was calculated simply as the square root of the sum of the squares of the fractional error components. These are given in table 5.7. This demonstrates the need to take into consideration the errors in the efficiency calibration in the final inventory analysis. All too often figures are quoted to single percent precision levels with no consideration of calibration error.

Over 90% of the soil sample analyses were performed with the 150 cm^3 geometries. The smaller geometries were used when the quantity of sample available was not sufficient to fill the larger 150 cm^3 geometries. Fewer calibration points were used in the determination of the 75 cm^3 and petri dish calibration resulting in an overall larger error estimate. By observing the relative change in efficiency with sample density (e.g. density change from 0.5 to 1.5 g cm^{-3} ; table 5.7), comparisons can be made between

sample-detector geometry and absolute efficiency measurements. For 150 cm³ geometries, there is a very similar sample-detector geometry relationship resulting in similar relative changes in absolute efficiency calibration for the coaxial detectors. For the larger GMX detector, similar changes in sample density result in smaller changes in detector absolute efficiency. In addition, as shown for the Ge(Li) detector, when geometry size decreases the absolute efficiency of the detector increases.

The change in calibration gradient with sample size is dependent upon: i) sample density, ii) surface area exposed to the detector, and iii) sample volume. Table 5.7 shows how with smaller container geometries, the change in efficiency calibration across the density range (0.5 g cm⁻³ to 1.5 g cm⁻³) decreases.

A similar calibration was carried out on coaxial and 50% GMX HPGe detectors. The calibration equations for ²⁴¹Am and ¹³⁷Cs are illustrated in table 5.7. Clearly the absolute efficiency for ²⁴¹Am is much higher for the HPGe detectors than the Ge(Li) detector, and ¹³⁷Cs is significantly higher on the 50 % GMX HPGe detector. The gradient of the calibration curve for ²⁴¹Am is very much greater for the HPGe detectors than the Ge(Li) detector and is likely to be related to the change in effective detector geometry. In addition comparisons between efficiency determinations for 30 cm³ ($\phi = 4.8$ cm, $t = 1.65$ cm) sized sample geometries on the 50 % GMX detector suggest that density corrections required for both ²⁴¹Am and ¹³⁷Cs are negligible.

5.6.4 The variation of μ and μ_m for environmental samples from that associated with the calibration soils for 59.6 keV photons.

Figure 5.13 shows the change in the linear attenuation coefficient (μ) at 59.6 keV with density for the hybrid samples used for detector efficiency calibration. Several samples collected at various depths and locations across the Caerlaverock salt marsh and an IAEA sample are also shown in figure 5.13. There is a good correlation between the hybrid samples used for calibration and the Caerlaverock samples. This suggests that the hybrid sample compositions are similar to the Caerlaverock samples. The IAEA sediment 306 sample however does not correlate well with the calibration samples.

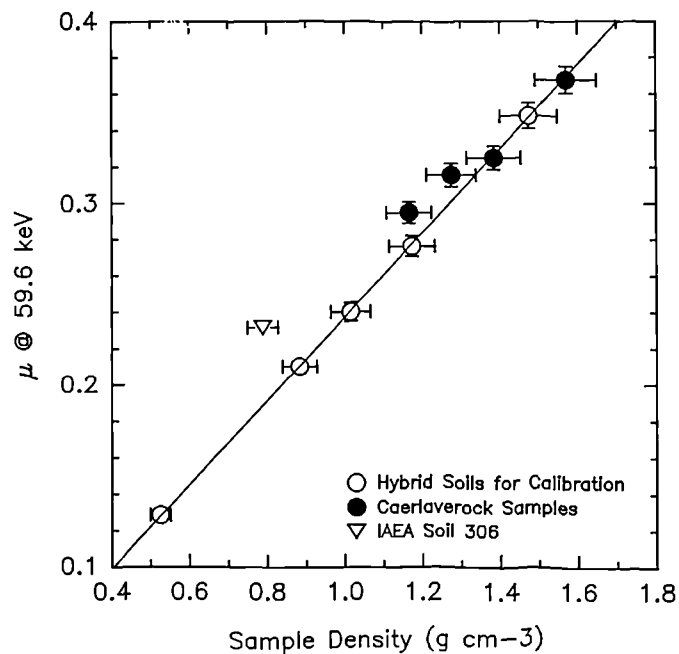


Figure 5.13 The change in the linear attenuation coefficient with sample density for the calibration samples, Caerlaverock samples and IAEA 306 Standard

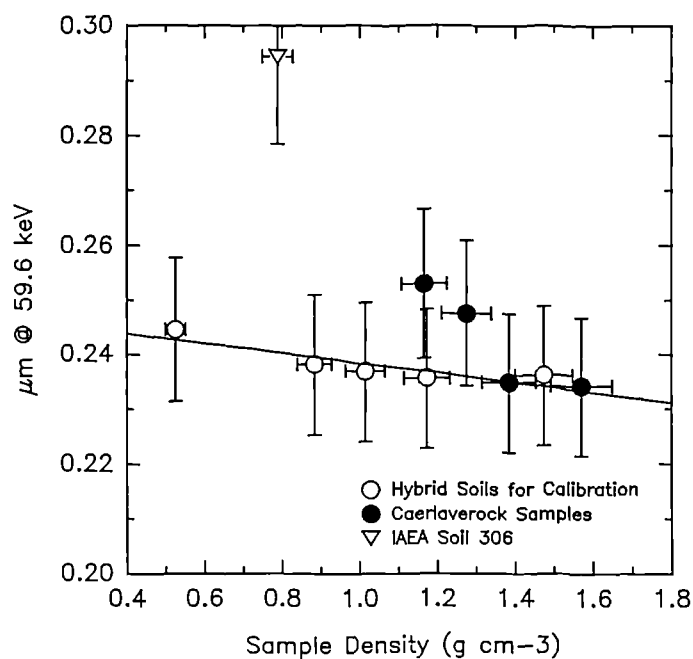


Figure 5.14 The variation of μ_m with sample density for the calibration samples, Caerlaverock samples and IAEA soil 6.

From figure 5.10.a an efficiency calibration of approximately 8% lower than that indicated by the sample density would be more appropriate.

Figure 5.14 demonstrates that the variation in the mass attenuation coefficient is consistent with the calibration samples. The Caerlaverock samples generally agree with this trend although there is evidence of a slight deviation from this trend with the lighter more organic rich samples. For the IAEA sediment 306 sample, there is a clear difference between the mass attenuation coefficients measured and those of the Caerlaverock and hybrid samples.

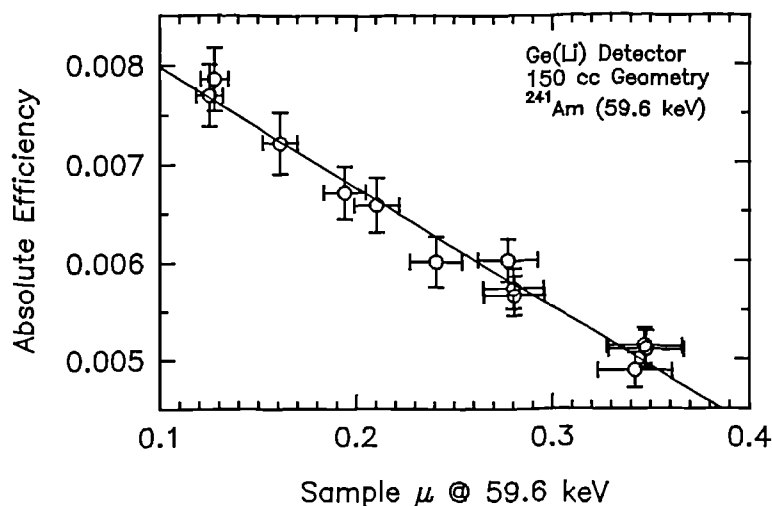


Figure 5.15 ^{241}Am detector calibration correction based on changes in sample μ at 59.6 keV.

These relationships corroborate the calibration for ^{241}Am soil core inventories for the Caerlaverock site. The results, however, suggest that ^{241}Am calibration correction should be based upon linear attenuation coefficients (μ) of the samples for 59.6 keV photons as illustrated in figure 5.16. Here the calibration correction for 150 cm³ containers would be based upon equation 5.7:

$$Eff = 0.0092 - 0.01222 \cdot \mu \quad (5.7)$$

5.6.5 Verification and Quality Assurance

Verification of this calibration can only be brought about with reference to international standards. Table 5.8 shows the standards used and the results obtained. Cross comparison of inventory estimations across geometry sizes is illustrated in the following

Table 5.8 Quality Assurance and Calibration Verification

Activities quoted in Bq kg⁻¹. Concentrations in () are in ppm
 Errors/Measured Range quoted at 1 σ . *BDL* = Below Detection Limits

IAEA Soil 6

150 cc Geometry Size

Nuclide	Reference		Measured	
	Value	Range	Value	Range
¹³⁷ Cs	53.65	51.45 - 57.9	51.389	48.72 - 54.06

IAEA Primordial Reference Material

75 cc Geometry Size

⁴⁰ K	13700 (52.4)	14700 (56.5) \pm 3 %
²³⁸ U _{eq} (²¹⁴ Bi)	4820 (400)	4970 (412.3) \pm 3 %
²³² Th _{eq} (²⁰⁸ Tl)	2960 (800)	2930 (791.9) \pm 4.5 %

NBS Standard SRM 4353

75 cc Geometry Size

¹³⁷ Cs	17.6 \pm 4.5%	16.8 - 18.4	15.7 \pm 7%	14.7 - 16.8
²⁴¹ Am	12.5 \pm 7.3%		<i>BDL</i>	
⁴⁰ K	723 \pm 9.6%	653 - 792	688 \pm 3%	674 - 702
²³⁸ U	38.9 \pm 5.1%	38.9 - 40.9	40.3 \pm 7%	37.4 - 43.3
²³² Th	69.3 \pm 5.1%	65.8 - 72.8	63.6 \pm 5%	60.7 - 66.5

Refer to table 6.1 for inventory comparison across geometry sizes

chapter in table 6.1. In addition, to ensure the quality of results over time, a bulk sample has been repeatedly counted as demonstrated in figure 6.2.

Table 5.8 provides a comparison between internationally derived inventory estimates for reference materials and inventory estimates using the above determined calibrations. There is a good comparison for the primordial radionuclides for all standards and for ¹³⁷Cs in IAEA soil 6. However, there is a slight underestimation of the ¹³⁷Cs in the NBS standard SRM 4353. Given the good correlation between geometry sizes (table 6.1) and the likely insignificant change between μ_m of the two sample standards at 662 keV, there is a suggestion of inconsistency between the standards. Sample composition

used in the calibration procedure must be particularly important in determining this reference value for ^{241}Am . Verification of ^{241}Am calibration has been hampered by low detection efficiency for low energy photons with the Ge(Li) detector.

5.7 SUMMARY AND CONCLUSIONS

The experiments and calculations observed here clearly indicate that sample self absorption is dictated by the mass attenuation coefficient (μ_m) and sample density. For energies below 200 keV, μ_m is highly dependent upon sample chemical composition, whilst above about 200 keV sample density dominates the attenuating characteristics of soil. These observations have significant implications on both laboratory based and in-situ gamma ray spectrometry.

Given the dependence of self attenuation upon sample composition, any calibration of laboratory based detectors for radionuclides with energies below 150 keV e.g. ^{210}Pb (46.52 keV), ^{234}Th (63.28 KeV) and ^{241}Am (59.6 keV) should take this into consideration. One possible means of measuring μ , as demonstrated in this chapter, is to measure the photon absorption with collimated point sources thus enabling an appropriate absolute efficiency calibration to be used.

For energies above 150 keV, sample self absorption is less dependent upon variation in μ_m . Any variation in μ_m appears to be controlled by the amount of organic content, with the maximum expected variation in μ_m observed to be a little over 5 % at 662 keV. Photon scattering at these energies is dominated by changes in sample density. Observed changes in the linear mass attenuation coefficient revealed large changes in the half depths of soils encountered which also changed with photon energy and soil density. Such variations may lead to changes in the *effective* sample-detector geometry and thus also changes in the absolute efficiency calibration of the detector. The calibration correction required is dependent upon the original size of the sample container and detector geometry.

Density corrected calibration curves have been determined to account for changes in

sample self absorption due to changes in sample density. For energies above 150 keV, the calibration has been verified with IAEA and NBS standards. Verification of inventory estimates below 150 keV must take into consideration changes in sample composition. Density correction of these samples only performs part of the correction required. The effects of large changes in μ_m may be avoided by designing sample containers which have a thickness t that is very small compared with the minimum half depth of the sample so far encountered e.g. 1.3 cm for ^{241}Am , thus essentially making the sample non-self absorbing. Alternatively, if a calibration is designed to be dependent upon the samples μ , then subsequent measurement of unknown samples could be preceded by a determination of μ with a similar experiment as described in section 5.2.

The use of these systematic self absorption corrections provide better levels of precision on sample activity estimation. Failure to account for sample self absorption may lead to significant systematic errors. Alternative techniques to overcome the difficulties imposed by changes in sample characteristics would be to use containers which are thin and small compared to photon half-depth. Thus changes in the effective geometrical shape due to changes in the sample's density and μ_m would be minimised. However, smaller samples require longer counting times and the representability of the sub-sample of the whole is in doubt unless homogeneity is accounted for. Such sub-sampling errors may contribute considerably to the overall estimate of precision on the activity estimate. The influence of sample size on sampling error is investigated in chapter 6.

The influence of variation in μ have significant implications on the integrated sampling depth for comparison with in-situ and airborne gamma ray spectrometry. For uniform sources and with activities expressed in terms of activity per unit mass (Bq kg^{-1}) this has little relevance. However, as discussed in section 5.5.3, for anthropogenic sources which are stratified with depth as observed in both terrestrial and salt marsh environments (chapter 7), the influence of μ on photon fluence and its change with soil and sediment type as well as with water content are quite considerable. The vertical stratification and its influence on photon fluence controlled by μ must be an important environmental factor which influences in-situ and airborne gamma spectrometry.

6. ACCOUNTING FOR SOIL SAMPLING ERRORS, SPATIAL VARIABILITY AND FIELDS OF VIEW IN ENVIRONMENTAL GAMMA RAY SPECTROSCOPY

6.1 INTRODUCTION

The Raithburn valley project demonstrated the problems associated with estimating environmental radioactivity and its spatial distribution using techniques with very different spatial sampling characteristics. This problem is highlighted when comparisons between these techniques are required. As discussed in chapter 1, for the environmental scientist and geologist, interpretation of in-situ and airborne gamma ray spectrometry is aided when the calibration relates directly to soil and sediment sample data rather than fixed artificial calibration standards. Thus calibration, verification and interpretation of environmental gamma ray spectrometry measurements may be best achieved when related spatially with soil sample derived estimates.

Sampling and sub-sampling errors are rarely acknowledged in the reporting of environmental radionuclide inventory estimations from soil sample analysis. The problem of spatial variability has received little more than a tacit recognition by environmental scientists. In contrast, since at least 1915, when Harris observed the variability within soil strata, the problems of pedological spatial variability have been recognised by the soil scientist. Although the problem still remains today, e.g. with site variability obscuring temporal variability (Frankland *et al* 1962), spatial variability has received considerable attention by soil scientists (e.g. Burgess and Webster 1980; Cameron *et al* 1971; Cambell 1979,1978; McBratney and Webster 1986; Schimmack *et al* 1987; Wilding and Drees 1983) and geochemical sampling errors by geochemists (e.g. Gy 1967; Ingamells *et al* 1972; Ingamells 1974 a,b; Visman 1969, 1972).

This chapter examines the problems that environmental heterogeneity imposes on sampling and sub-sampling of soils for radionuclide activity estimation. The heterogeneity of radionuclides in soils is caused by the interaction of many environmental factors such as the depositional and emplacement mechanisms and

assimilation controls within the soil profile, coupled with the soil's own natural heterogeneity. Quantifying the heterogeneity of radionuclides in soils is also important when trying to spatially relate soil samples with the fields of view of in-situ and aerial survey detectors. It is of particular importance to account for spatial variability for a range of detector altitudes for the determination of height correction coefficients.

6.1.1 Spatial Variability

The lack of recognition of the influence of spatial variability and sampling errors on inventory estimation is surprising, since, for example, ^{137}Cs soil activities of between 3 and 3000 Bq/kg typically correspond to concentrations of between 10^{-15} to 10^{-12} parts by weight. This small fraction coupled with different depositional mechanisms may lead to highly heterogenic distribution of activity in soils. The extent of spatial variability can be appreciated when considering the differences which may be expected between water borne and aerial deposition, both from the stratosphere and troposphere, of anthropogenic sources. The degree of spatial variability will depend on the depositional pathway. Subsequent weathering and re-mobilization of the radionuclides within the soil matrix, which itself has heterogenic characteristics (Livens and Baxter 1988 a and b), will add to the horizontal spatial and vertical distribution of radionuclide concentrations.

Similarly, the soil concentrations of naturally occurring U, Th, and their daughters and ^{40}K are governed by the underlying geology, weathering, erosion and deposition and the chemical behaviour and mobility of these elements with different soil types as summarised in chapter 2. The subsequent spatial variability of radionuclides due to bed rock or lithospheric variability may range considerably from a nanometre scale within U rich minerals to a centimetre scale in areas of intense mineralization, such as the Needles Eye area (Miller and Taylor 1966) to a kilometre scale in areas of relatively uniform geology.

Therefore, one might expect micro (soil sampling level) and macro variability (variation between soil sample sites or in-situ spectrometric measurements) to be a significant

factor in environmental inventory estimation. Against this, although many papers have been written on the distribution and concentration of radionuclides in contrasting sites and site material (e.g. Ritchie et al 1970; Bunzl and Kracke 1988), only a few site specific studies of spatial variability have been undertaken. These have tended to be along transects (e.g. Sutherland and de Jong 1990) although Parkinson and Horrill (1984) used both transect and some grid sampling plans to examine sample site variability of anthropogenic radionuclides in vegetation on the salt marsh and pasture fields of Cumbria. However, single transects whilst allowing variability in one direction to be observed, do not allow spatial anisotropy (directionality in spatial trends) to be estimated.

Parkinson and Horrill (1984) recognised the problem of sampling error with vegetation sampled from Sellafield contaminated grazed and ungrazed salt marsh areas and pasture fields. They studied the variation of actinide inventory estimation due to laboratory and field conditions. They recognised an error of between 7.9 % and 9.2 % from replicate analysis with careful laboratory procedure. Parkinson and Horrill recognised that field variability is controlled by sampling technique and "inherent variability within the site itself". Their paper concentrates on sampling error determined from grid and transect data and found site variability ranged from 47.2% for an ungrazed salt marsh to 95.7% for a grazed salt marsh area for $^{239} + ^{240}\text{Pu}$ analysis and 35% for ^{137}Cs on the ungrazed salt marsh. However, by dividing the samples into discrete vegetation classes and thus stratifying the sites accordingly, the coefficient of variation dropped, for example, from 35% to 16% for ^{137}Cs . Parkinson and Horrill also calculated that between 23 and 44 samples were required for the mean inventory estimate to fall within 10% of the true mean at a 95% confidence level.

A similar study was undertaken by Drichko *et al* (1977) and Drichko and Lisachenko (1984) for the distribution of the natural radionuclides ^{226}Ra , ^{228}Th and ^{40}K in a range of cultivated Russian soils, grains and potatoes. Although no spatial dependence was assumed or accounted for, the distributions of radionuclide concentrations in agricultural plants followed closely that of the soil, with ^{40}K demonstrating a normal frequency distribution, whilst ^{226}Ra and ^{228}Th showed a log-normal frequency distribution. Poisson

statistics are usually assumed to apply in soil sampling, although gaussian distributions are often used to simplify ideas and results.

Recognising the lack of investigation into the problem of radionuclide spacial variability Sully *et al* (1987) and Sutherland and de Jong (1990) undertook transect studies to investigate this phenomenon. Sully *et al* discussed the sampling strategy and data analysis required to characterise natural radionuclide specific activities in soil. 100 m transects were sampled at 1 m intervals at a depth of 25 - 35 cm for undisturbed soil in an area of "uniform" geology. The coefficients of variation of the sample results for ^{226}Ra , ^{228}Ra , were less than the analytical error and thus variability can be accounted for by analytical or measurement error. Sutherland and de Jong (1990) successfully used autocorrelation analysis to study the distribution of anthropogenic (weapons testing ^{137}Cs) and natural (^{40}K , ^{238}U and ^{232}Th series) γ emitting radionuclides in three fields of Saskatchewan. Autocorrelation analysis was applied to 240 m length transects with 20 equally spaced data points. At each point three 5.4 cm diameter cores were collected in 0-15 cm and 15-30 cm intervals. Generally, no serial correlation was found within distances of between 12.5 m and 125 m and thus each sample did not replicate information and was independent. The coefficients of variation (CV) for the natural radionuclides ranged from 2.3% to 10% whilst for ^{137}Cs , the CV ranged from 18% to 23%. Again, the number of sample locations required to estimate the ^{137}Cs inventory to within 10% of the true mean at 95% confidence was between 12 and 20.

Much work has been undertaken on spatial variability associated with Nuclear test sites with or for the Nevada Applied Ecology Group (NAEG) / Desert Research Institute University of Nevada System. Fowler *et al* (1974) and Gilbert *et al* (1974) discussed the philosophy of soil sampling and sampling design in application to plutonium distribution measurements in the Nevada test site. A technique of stratified random sampling was employed. Initially, a NaI field spectrometer was used to map the spatial distribution of ^{241}Am to predict ^{239}Pu concentration. These results were stratified into activity concentrations and used to guide random soil sampling within each stratified unit. However, attempts to calibrate the NaI field spectrometer for ^{241}Am and thus also ^{239}Pu mapping were not so successful.

Barnes (1978), Barnes *et al* (1980) and Gilbert and Simpson (1985) applied semi-variogram and variogram geostatistical techniques, traditionally applied to geoexploration and pedological variability, to the distribution of bomb testing fallout in the Marshall Islands and Nevada test site.

Barnes developed the kriging technique for radionuclide inventory area estimation of the Frenchman Lake region of the Nevada test site (Barnes *et al* 1980). Site characterisation was undertaken for isopleth estimation for ^{241}Am , ^{155}Eu , ^{152}Eu , ^{137}Cs , ^{60}Co and ^{239}Pu with a collimated in-situ HPGe detector attached to a four wheel drive vehicle. Grid sample spacings were at least 100 feet apart and were based around the ground zero (GZ) positions. Extensive sampling was undertaken in the Small Boy GZ area. Variogram analysis of the plume areas displayed anisotropic characteristics though a single spherical model was fitted to the data with a typical range of 1000 feet. Each radionuclide displayed similar distribution characteristics. For non-plume areas, a linear model was appropriate for variogram distributions except for ^{60}Co where a spherical model was applied. This was attributed to the lack of ^{60}Co observations. Other GZ areas were sampled and similar distribution characteristics were observed.

Gilbert and Simpson (1985) discussed the limitations of kriging for global, regional and sub-regional applications and found that the influence of change in support (sample volume, shape and orientation) can affect the shape of semivariograms. They applied a log-normal model to a data set of ^{241}Am samples from the nuclear site 201 on the Nevada test site. Sample spacing was least where concentrations were highest and most variable, notably at the GZ locations. This produced a skewed data set. The data demonstrated the importance of not ignoring the change in semi-variogram model over space for the estimation of the spatial distribution of activity.

Very little work, however, appears to have been carried out in the quantification of radionuclide spatial variability in the environment resulting from different sources of input, ie. atmospheric or marine to land transfer. The major problem for such a detailed study is the time and expense required in soil sample analysis. However, given a correctly calibrated and understood detector system, in-situ or aerial gamma ray

spectrometric measurements provide a relatively cheap and rapid means of monitoring spatial variability on different scales of study. Such data can be analysed both qualitatively through mapping and quantitatively through semivariogram analysis.

However, as discussed in section 3.8, the spatial response of the in-situ and aerial survey detector is centre weighted. Although this feature is generally recognised (IAEA 1991), few people have attempted to overcome this problem and the consequences of not doing so are not generally appreciated. Barnes (1978) illustrates a simple sampling plan for collimated in-situ detectors.

This chapter therefore discusses techniques and solutions for relating soil samples with in-situ and aerial survey gamma spectroscopy measurements. This involves the understanding of soil sampling and sub-sampling errors, the calculation of *circles of investigation* or *fields of view* (section 3.8), and the development of sampling plans which spatially match these fields of views at various platform heights and account for radionuclide spatial variability within the field of view of the detectors.

6.1.2 Sampling and Sub-sampling Errors in Radionuclide Inventory Estimation

The problems of sampling and sub-sampling errors have long been recognised by the geochemists (e.g. Gy 1967; Ingamells et al 1972; Ingamells 1974 a,b). Sampling error often exceeds analytical error and in rock or mineral analysis can amount to or exceed 100% (Ingamells *et al* 1972). There are three principle contributions to data error: i) the heterogeneity of the site being sampled, ii) sampling technique, and iii) errors in the analysis. Careful laboratory procedure and sample homogenisation should enable systematic and random errors in the laboratory to be controlled. However, the collection of representative samples in the field is governed by the heterogenic nature of the site and the number and size of samples collected.

Ingamells proposed a laboratory sampling constant, expressed in terms of the relative deviation (R, per cent) in a series of determinations using sub-samples of weight w . This is given in equation 6.1

$$K_s = R^2 w \quad (6.1)$$

where K_s describes the sampling characteristics of an unsegregated mixture with respect to the element of interest. K_s is the weight of the sample in grams which must be taken, to give with 68% confidence, a relative sampling error of 1% or less. The $\sqrt{K_s}$ is numerically equal to the coefficient of variation expected for a series of results. This applies for a homogenous sample and the expected relative error in analytical results for that constituent using sub-samples of mass w can be predicted from equation 6.2

$$R = \sqrt{\frac{K_s}{w}} \quad (6.2)$$

Thus from equation 6.1, if W is a larger sub-sample mass, then the new relative deviation R can be expected to be given by equation 6.3

$$R = \sqrt{r^2 \cdot \frac{w}{W}} \quad (6.3)$$

where r is the relative deviation associated with samples of mass w .

Sampling statistics rarely behave in a Gaussian fashion and Poisson statistics usually apply. In the sub-sampling of bulk samples in geochemical analysis, to account for the skewed distribution, Gy (1967) developed a sampling constant which took account of weights and dimensions of the sample fragments to describe the non gaussian behaviour of the sub-sample estimates. In the sampling of areas with heterogenic and segregated distributions, Visman (1969 and 1972) developed an optimum sample weight theorem. However, since, the radionuclides form chemical associations with clays and organic complexes in the field are ground and homogenised in the laboratory, these more complicated statistical descriptions have little application. For simplicity 6.1 to 6.3 will be referred to.

Ingamells (1974a) produced a sampling model determined by repetitive sampling and measuring the content of X with sample weight. For a given set of sampling constants,

the uncertainty of the X content can be given by equation 6.3.

Figure 6.1 shows an example of Ingamells' model calculated from equation 6.3. It also illustrates the *most probable results* discussed by Ingamells. As the sample weight diminishes, the scatter of concentration estimates increases. Ingamells (1974a) suggests that where mineral grains for geochemical analysis are large in number for all constituent types, then the distribution of the analytical results is approximated by Gaussian statistics.

However, where mixtures contain only a small number of grains of interest in a sample, the Gaussian distribution breaks down and the Poisson statistics apply. Moreover, this produces a highly skewed distribution and too few determinations will yield an average which is often too low. This is illustrated in figure 6.1 as the *probable result*. There is a very strong analogy to this theory with homogenised samples for radionuclide inventory estimation. In particular, the results of Fowler *et al* (1974a) and Oughton (1992) on hot particle sampling have analogous results with the *probable result* leading to an underestimation of the sample mean.

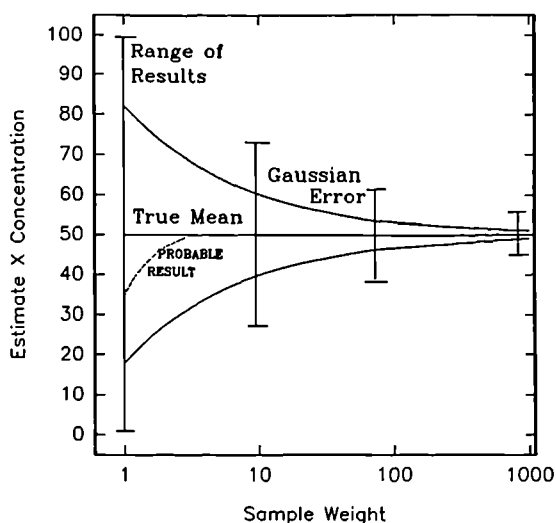


Figure 6.1 Ingamells' Sampling Model - adapted from Ingamells (1974a)

6.2 SUB-SAMPLING ERRORS AND SAMPLE REPRODUCIBILITY - EXPERIMENTAL PRECISION

6.2.1 Objective

To determine the reproducibility of activity estimates from sub-sampling of homogenised material and thus its implications on experimental precision.

6.2.2 Method

Following the grinding and homogenisation process discussed in section 3.2, typically a sub-sample of about 150 g is taken from a 1 kg sample. To determine the representability of such sub-samples, a number of samples were taken from a 1.5 kg salt marsh sediment sample which had been ground and homogenised in the usual way. Six 150 cm³ containers were filled and counted on a high resolution Ge(Li) detector. Following this, six 75 cm³ and six 30 cm³ containers were filled with sub-samples and counted in a similar fashion, though with longer counting times to reproduce the counting statistics associated with the 150 cm³ containers. The results from these sub-samples are given table 6.1.

As part of the quality assurance procedure, a 4 kg Chernobyl contaminated sample was collected from Broughton Mains (Solway) and processed in the normal way. Sub-samples were taken from this sample periodically over the three year research period. These results are also described and discussed.

6.2.3 Results and Discussion

From table 6.1, except for ⁴⁰K and ²¹⁴Bi, all the sampling errors (as quantified by the *coefficient of variation %*) are less than or comparable with the analytical errors (*Exp. Err. %*). Although "identical" containers were used for each measurement, filling different geometries with the same soil to determine the sub-sampling error will also account for slight distortions in container geometry shape and variations in sample weight and density. In addition, although each container was placed in almost exactly the same position on the detector, the slight irregularities in detector response over its surface area (Knoll 1979, 1989) must also be accounted for in these sub-sampling errors. However, these errors were all found to be negligible when compared with the analytical error.

Table 6.1 shows a high degree of reproducibility for the anthropogenic radionuclides ¹³⁷Cs and ²⁴¹Am, in particular for the 75 cm³ and 150 cm³ containers. The estimates for

Table 6.1 The Sub-sampling Errors of a Homogenised Gley Sediment

	²⁴¹ Am	¹³⁷ Cs	Activity Bq/kg ⁴⁰ K	²¹⁴ Bi	²⁰⁸ Tl
30 cm³					
Range	564-659	3052-3164	651-722	14.6-29.6	15.4-18.9
Mean	592	3107	669	21.1	17.3
Std. Dev. 1σ	34	34	28	4.6	1.1
Std. Err.	14	14	11	1.9	0.5
CV %	5.7	1.1	4.1	21.8	6.4
Exp. Err. %	5.9	4.5	3.4	15.1	10.1
75 cm³					
Range	464-506	3145-3302	642-747	20-30.7	17.7-20.9
Mean	487	3230	682	25.2	19.8
Std. Dev. 1σ	14	54	34	3.5	1.0
Std. Err.	5.7	22	14	1.4	0.4
CV %	2.8	1.6	5.0	13.9	5.1
Exp. Err. %	6.1	4.5	3.5	13.3	9.9
150 cm³					
Range	450-480	3143-3268	645-665	19.3-33.8	16.6-19.5
Mean	465.6	3207	632	28.7	18.6
Std. Dev. 1σ	10.8	43	8.0	4.7	1.0
Std. Err.	4.4	18	3.3	1.9	0.4
CV %	2.3	1.3	1.3	16.4	5.4
Exp. Err. %	4.9	4.0	2.6	9.7	8.1

²⁴¹Am and ¹³⁷Cs for the 30 cm³ samples appear to be statistically significantly high and low respectively. This is likely to be attributed to the cruder estimate of the sample density correction coefficients. However, for all these samples, the coefficient of variation is significantly less than the analytical or experimental error. Thus the samples are effectively homogenous and any increase in sample size does not appear to benefit the sample analysis in any way other than to reduce the counting time on the detector.

In contrast, the only significantly different CV from the experimental error is ²¹⁴Bi for the 30 cm³ and 150 cm³. This can be explained by the leakage of ²²²Rn, the U daughter and parent of ²¹⁴Bi. It is significant that the 75 cm³ container demonstrates a coefficient

of variation equal to the experimental error. This is an improvement over the other containers and suggests that the 75 cm³ container is better for ²²²Rn sealing. In contrast ²⁰⁸Tl estimates show a smaller CV than indicated by the experimental error. This suggests that the sample is essentially homogeneous with respect to ²⁰⁸Tl.

The results from a similar series of analysis for sub-samples from a 4 kg sample of Chernobyl contaminated soil from Broughton Mains (Solway) are shown in table 6.2 and figure 6.2. Table 6.2 shows the results for all measurement estimates for: 1) all container sizes on the two principal detectors used over the research period, 2) for the 150 cm³ and 75 cm³ container sizes on the two detectors used over the research period, 3) for the 150 cm³ and 75 cm³ container sizes on the Ge(Li) detector only used over the research period, 4) for the 150 cm³ geometry over the research period on the Ge(Li) detector, 5) for one particular sample (170.3 g) over the research period on the Ge(Li) detector, and 6) for one particular sample (199.9 g) consecutively over a period of a few days on the Ge(Li) detector.

¹³⁷Cs shows a high degree of consistency over the 3 year period of measurements with CV only slightly greater than the experimental error. This concordance is improved when the container geometry is isolated (4) and when the sample remains the same (5 and 6). For ¹³⁴Cs this improvement is observed only when the sample remains the same (5 and 6).

The coefficient of variation for ⁴⁰K with time is observed always to be considerably greater than the experimental error, except for those measurements made with the same sample consecutively. However, measurements made with the same sample over a longer time period shows a larger CV than experimental error. For individual samples this may be explained by sample heterogeneity. However, clearly another factor of perhaps slightly changing background may be responsible, even though the background is periodically remeasured and shown to be relatively consistent.

As with table 6.1, table 6.2 shows ²¹⁴Pb with a greater CV than experimental error. This is illustrated in all but the repeat measurements of the same sample (5 and 6),

Table 6.2 Statistics for Broughton Mains Bulk Sample over a 3 Year Period.

		¹³⁷ Cs	¹³⁴ Cs	⁴⁰ K	²¹⁴ Bi	²⁰⁸ Tl
1) Statistics for all Measurements n = 22 Both HPGe and Ge(Li)	Mean	291.1	144.1	475.6	17.6	10.5
	Std. Dev. 1σ	12.0	10.0	58.6	2.7	0.94
	Std. Err.	2.6	2.1	12.8	0.6	0.20
	CV %	4.1	6.9	12.5	15.3	9.0
	Exp. Err. %	3.6	4.7	4.2	8.6	8.5
2) Statistics for 75 and 150 cm ³ geoms n = 19 Both HPGe and Ge(Li)	Mean	290.3	144.5	477.7	17.1	10.6
	Std. Dev.	12.5	10.3	44.0	2.3	0.8
	Std. Err.	2.9	2.4	0.9	0.5	0.2
	CV %	4.3	7.1	9.2	13.4	7.9
	Exp. Err. %	3.6	4.7	4.2	8.6	8.5
3) Statistics for 75 and 150 cm ³ geoms on Ge(Li) only n = 15	Mean	287.3	142.8	475.0	17.3	10.3
	Std. Dev.	11.2	7.4	50.9	2.4	1.0
	Std. Err.	2.9	1.9	13.1	0.6	0.3
	CV %	3.9	5.1	10.7	13.8	9.4
	Exp. Err. %	3.6	4.7	4.2	8.6	8.5
4) Statistics for 150 cm ³ , Ge(Li) Includes mean of repeat measures. n = 7	Mean	289.3	143.8	487.3	16.6	10.5
	Std. Dev.	7.7	10.0	35.0	2.5	0.7
	Std. Err.	2.9	3.8	13.2	0.9	0.3
	CV %	2.6	7.0	7.2	15.1	6.6
	Exp. Err. %	3.7	4.9	6.6	11.8	9.0
5) Statistics for 170.3g samples on detec. 1.1 over 3 years, Ge(Li) n = 5	Mean	295.0	143.4	500.0	17.1	11.1
	Std. Dev.	3.0	1.9	43.4	1.98	0.69
	Std. Err.	1.3	0.9	19.4	0.89	0.31
	CV %	1.0	1.3	8.6	11.6	6.2
	Exp. Err. %	3.5	4.9	4.5	12.1	7.9
6) Statistics for 199.9g on Detec. 1.1 consecutively Ge(Li) n = 6	Mean	280.2	136.3	475.0	22.3	10.3
	Std. Dev.	1.89	1.94	7.23	1.71	0.78
	Std. Err.	0.77	0.79	2.95	0.70	0.32
	CV %	0.67	1.4	1.1	7.7	7.6
	Exp. Err. %	4.1	5.5	3.8	11.3	7.4

where the CV is equivalent to the experimental error. This indicates the problem of sample sealing, particularly for ²²²Rn equilibration across samples. Temporal fluctuations with indoor radon may contribute to the overall estimate of precision. ²⁰⁸Tl has a CV equivalent to the experimental error with all sample container estimates suggesting that ²⁰⁸Tl must be homogeneously distributed in the bulk sample.

Broughton Mains Bulk Sample Data

Reference Date: 6th May, 1986

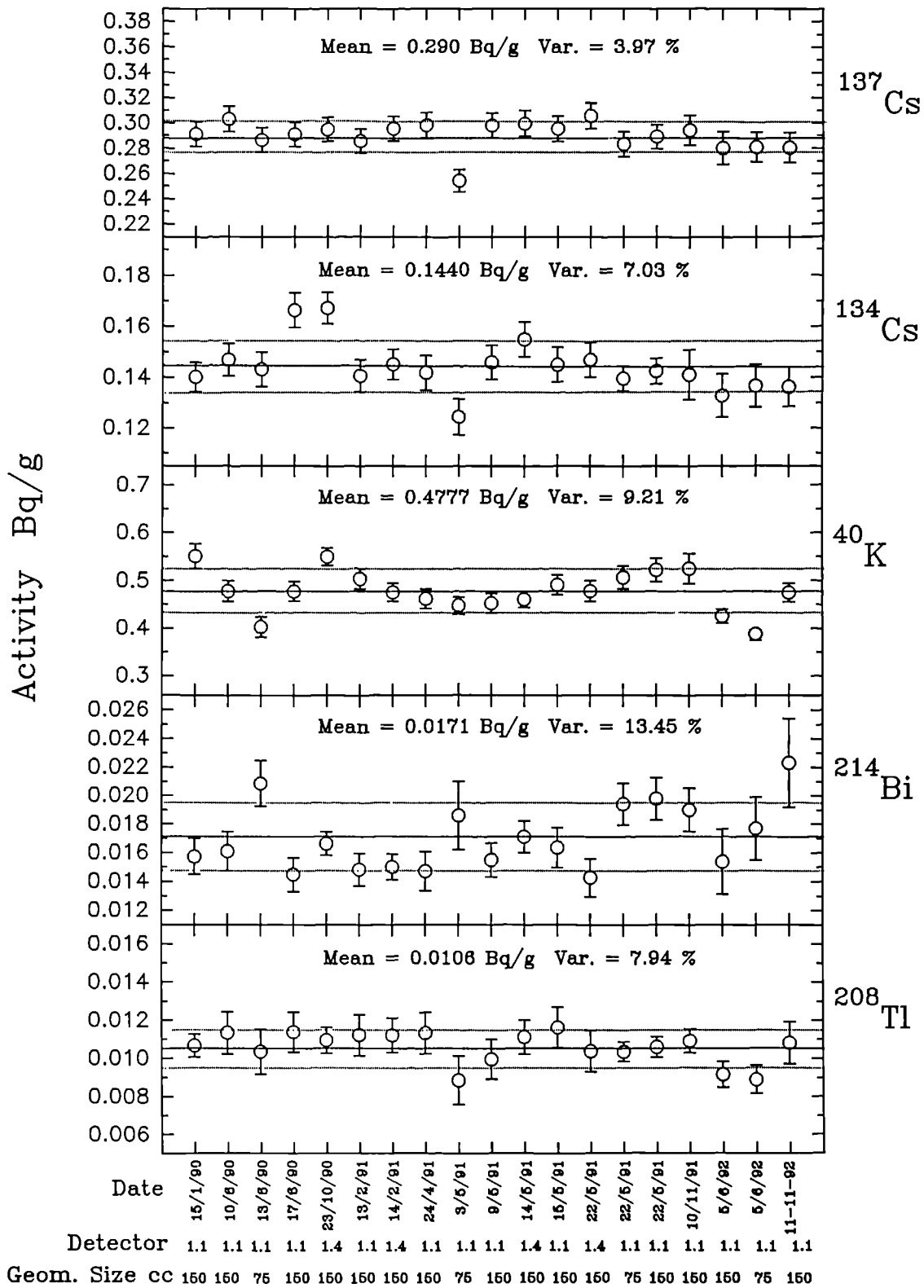


Figure 6.2 The Reproducibility of the Broughton Mains Bulk Sample with Time. (1.1 = Ge(Li) Detector; 1.4 = HPGe Detector)

6.2.4 Conclusions

The results from tables 6.1 and 6.2 show a high degree of reproducibility and therefore experimental precision. Comparison of activity estimates across container sizes indicates lower levels of precision than is suggested by the analytical errors, although this is only marginally so for the two caesium radionuclides.

Of greater significance is the problem of sealing the containers to allow ^{222}Rn equilibration with its daughter ^{214}Bi , used to determine ^{238}U concentrations. Verification of equilibration within the sample can be obtained by determining ^{226}Ra (186 keV) and ^{234}Th (63.3 keV) concentrations although care must be taken to check for ^{235}U interference (185 keV). However, the use of these lower γ photon emitters is hampered by the problem of variations in μ_m although periodic checks with standard geometries have indicated agreement in these values.

When comparing soil sample derived inventories, it is important to take into consideration the possible effects caused by changes in sample geometry, sample heterogeneity, and the escape of ^{222}Rn . When comparing inventory estimates from samples measured over a considerable time period (years), it may be more appropriate to use precision estimates indicated by table 6.2.1.

6.3 FIELD SAMPLING ERRORS

6.3.1 Objective

Initially, the Cawse and Horrill (1986) technique of random sampling within a specified area was adopted in this study. However, the representability of the sample is unknown, and thus an attempt to determine the effectiveness of this technique and to quantify the sampling error is made.

6.3.2 Method

To determine the effectiveness of the sampling technique, an area contaminated predominantly with Chernobyl derived anthropogenic radionuclides, close to the Reactor Centre site at East Kilbride was sampled.

A 2 x 2 m grid was constructed in which 9 individual samples were collected at 1 m spacings (figure 6.3) with the Leonard Farnell corer (38 mm diameter) described in chapter 3.2. Each sample was extracted in 15 cm intervals, bagged individually and processed in the manner described.

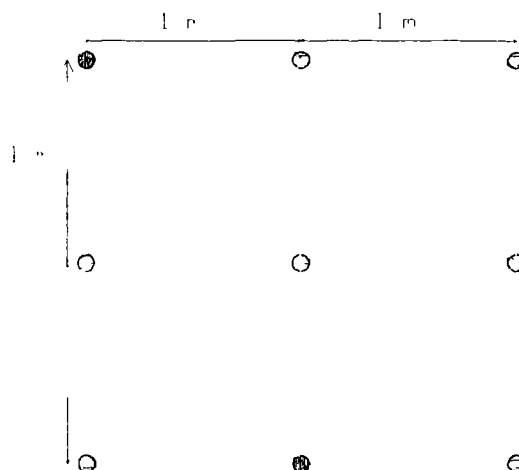


Figure 6.3 2m x 2m Sampling Grid

6.3.3 Results and Discussion.

Table 6.3 shows the results obtained. The sampling error, estimated as the *CV*, is in all cases considerably greater than the experimental error (associated with counting error, errors on absolute efficiency, sample weight and core dimension). Of particular importance is the anthropogenic radionuclide variation, with ^{137}Cs varying by almost a factor of 3 within a 4 m² area giving a *CV* of about 30 %. In contrast, ^{40}K varies by

a factor of 1.2 with a *CV* of less than 10 %.

Table 6.3 Radionuclide inventory analysis from SURRC 2m x 2m Sampling Grid. Samples taken with 38mm corer (November 1989).

	kBq m ⁻²		St.Dev		St. Err		Experiment	
	Range of Values	Mean	1 σ	CV.%	1 σ	%	Error	(%)
¹³⁷ Cs	5.82-14.23	8.61	2.49	(29)	0.94	(11)	0.30	(3.5)
¹³⁴ Cs	0.816-2.19	1.36	0.29	(21)	0.11	(8)	0.06	(4.2)
⁴⁰ K	98.9-120.1	109.1	8.81	(8)	3.33	(3)	3.50	(3.2)
²¹⁴ Bi	6.88-10.6	8.81	1.08	(12)	0.41	(4)	0.27	(3.1)
²⁰⁸ Tl	2.66-4.61	3.89	0.54	(14)	0.21	(5)	0.14	(3.6)

The heterogeneity of the distribution of anthropogenic radionuclide distribution far outweighs that associated with the natural radionuclides and must be associated with depositional processes, subsequent absorption within the soil profile and the remobilisation of caesium attached to particles or in solution within the soil profile.

This sampling technique is clearly not satisfactory for sampling Chernobyl radiocaesium distribution unless a substantially larger number of samples is collected. Assuming Gaussian statistics, equation 6.8 can be used to predict the number of samples (*n*) required for the experimental average to be within *f* % of the true mean with 95% confidence:

$$2. \frac{SD}{\sqrt{n}} = f\bar{x} \quad (6.8)$$

where *f* is the fraction of the mean required and \bar{x} is the overall average. The results for the SURRC site are shown in table 6.4.

Given that nine soil cores were sampled, the results shown in table 6.4 suggest that the Leonard Farnell corer is suitable for natural radionuclide inventory estimation to be 95% confident that the experimental average will be within 10% of the true mean.

Table 6.4 Number of samples required for mean result to be within 5 and 10% of the true mean.

	¹³⁷ Cs	¹³⁴ Cs	⁴⁰ K	²¹⁴ Bi	²⁰⁸ Tl
Number of Cores Required					
For 95% confidence (5% of mean)	133	71	10	24	31
(10% of mean)	33	18	3	6	8

However, for ¹³⁷Cs and ¹³⁴Cs, there is a considerable problem even if estimations are required to within 10% of the true mean, and to be within 5 % of the true mean (level of accuracy usually quoted in the literature) over 130 samples would be required for ¹³⁷Cs determination.

6.4 IMPROVEMENT IN SAMPLING ERROR

6.4.1 Objective

Given the poor sample representability described in section 6.3, an attempt must be made to improve sampling error. Instead of increasing the number of samples to reduce sampling errors, Ingamells' (1974a) approach is to increase the sample weight. A larger soil corer was bought as illustrated in section 3.2. The new 105 mm diameter sampler enables 7.6 times more material to be collected than the 38 mm diameter sampler. Thus from equation 6.3, one might expect a reduction in sampling error from 28.9% to 10.5% for ¹³⁷Cs and from 21.1% to 7.6% for ¹³⁴Cs for Chernobyl contaminated soils.

This hypothesis was tested on two new sampling sites with contrasting environmental depositional characteristics: i) Chernobyl contamination dominated land near the Solway at Longbridgemuir Farm, Dumfries, and ii) Sellafield contaminated salt marsh at Caerlaverock, Dumfries.

6.4.2 Method

Seven equidistant samples were collected with the 38 mm corer and the 105 mm corer on a 2 m spacing hexagonal sampling plan to a depth of 45cm (peat) and 30 cm

(sediment).

Two sites of contrasting depositional mechanisms were selected. The first site of Chernobyl derived deposition from the atmosphere was at Longbridgemuir farm (Solway), an area of basin and valley peat. The natural radionuclide concentrations were below the limit of detection of the Ge(Li) detector in the laboratory and were thus excluded from the analysis. The second site consisted of Irish Sea sediments contaminated with Sellafield derived radionuclides. These well mixed sediments were sampled at the Caerlaverock National Nature Reserve (Dumfries).

6.4.3 Results and Discussion

As with the SURRC site, a factor of 3 was observed in the range of results for the caesium inventories, as shown in table 6.5 with the 38 mm corer. The 105 mm corer reduces the CV (sampling error) by about 10% to between 25% and 28% but does not follow the prediction from Ingamells' equation 6.3, predicting a sampling error of 12.6%. This is likely to be due to the highly heterogenic nature of Chernobyl fallout and subsequent interaction and assimilation within a naturally heterogenic media giving the distribution a spatial component.

The same procedure was carried out in an area of contrasting depositional environment at Caerlaverock salt marsh, an area dominated by Sellafield contaminated sediments. Both the ^{137}Cs and ^{134}Cs might have a Chernobyl component. The different origins of these radionuclides suggests that the distribution within the sediment profile will be characteristic of their dominant origin.

The Caerlaverock results are given in table 6.6. Here, where the activity within the sediment is well mixed, a considerably smaller sampling error was observed, although the sampling error for the natural radionuclides is considerably greater than that observed at the SURRC site. The standard error of the mean for the salt-marsh site is comparable to the experimental error for the anthropogenic radionuclides, although the CV (sampling error) is considerably greater than the analytical error for the 38 mm

Table 6.5. Longbridgemuir Basin and Valley Peat Inventory Results from a 2m Hexagonal Sampling Plan. 45cm deep soil cores Inventories (1992)

Nuclide	Range of Values	kBq m ⁻²			St. Err. of mean (%)	Experiment Error 1σ (%)
		Mean	St. Dev. 1 σ	CV%		
38 mm Corer						
¹³⁷ Cs	7.37-19.0	12.4	4.33	(35)	1.64 (13)	0.37 (3.0)
¹³⁴ Cs	0.34-0.99	0.59	0.23	(38)	0.085 (15)	0.04 (6.5)
105 mm Corer						
¹³⁷ Cs	6.53-14.4	9.92	2.73	(28)	1.03 (10)	0.03 (3.0)
¹³⁴ Cs	0.40-0.93	0.67	0.17	(25)	0.06 (10)	0.04 (6.5)

Table 6.6. Caerlaverock Salt Marsh Inventory Results (1992), 2m Hexagonal Sampling Plan. Inventories for 30 cm deep soil cores.

Nuclide	Range of Values	kBq m ⁻²			St. Err. of mean (%)	Experimental Error 1σ (%)
		Mean	St. Dev. 1 σ	CV%		
38 mm Corer						
¹³⁷ Cs	77.1-94.9	81.2	8.42	(10)	3.18 (4)	2.8 (3.5)
¹³⁴ Cs	0.59-1.04	0.79	0.13	(17)	0.05 (6)	0.06 (8.2)
²⁴¹ Am	11.8-14.97	13.4	0.95	(7)	0.36 (3)	1.03 (7.7)
⁴⁰ K	109-145	125	18.3	(15)	6.9 (6)	3.75 (3.0)
²¹⁴ Bi	2.16-4.9	3.7	0.94	(26)	0.36 (10)	0.22 (6.0)
²⁰⁸ Tl	1.6-2.2	1.8	0.28	(15)	0.11 (6)	0.10 (5.2)
105 mm Corer						
¹³⁷ Cs	79.1-90.2	84.3	4.9	(6)	1.8 (2.2)	2.95 (3.5)
¹³⁴ Cs	0.72-0.97	0.83	0.08	(9)	0.03 (3.4)	0.06 (6.8)
²⁴¹ Am	12.7-16.24	14.9	1.24	(8)	0.5 (3.2)	0.67 (4.5)
⁴⁰ K	100-162	133	17.6	(13)	6.7 (5)	4.00 (3.0)
²¹⁴ Bi	2.7-5.5	4.2	0.77	(18)	0.3 (7)	0.15 (3.5)
²⁰⁸ Tl	1.4-2.0	1.7	0.25	(15)	0.1 (5.5)	0.06 (3.5)

corer results. This error is considerably reduced for caesium with the 105 mm sized corer reducing the sampling error from 10.4% to 5.8% for ¹³⁷Cs, and from 16.6% to 9.1% for ¹³⁴Cs. This magnitude of change is less than that predicted by equation 6.3

which may be due to the heterogenic nature of the distribution in the sediment.

This section has demonstrated the magnitude of sampling error in different depositional contexts, and has shown that sampling error can be reduced by sampling larger cores and homogenisation of the sediment.

6.5 MATCHING SAMPLES TO FIELDS OF VIEW OF IN-SITU AND AIRBORNE GAMMA SPECTROMETERS

6.5.1 Objective

The problem of sampling error and spatial variability is compounded when having to relate spatially soil samples with in-situ and airborne γ ray detectors. For example, a detector 1 m above the ground 'samples' about 10^5 times more material than a typical 2 or 3 kg soil sample, whilst a detector at 100 m above the ground 'samples' about 10^7 times more material.

Knowing the spatial representation of a single in-situ gamma spectrometric measurement, calibration of this spectral data from soil core data requires that the soil samples collected must relate spatially to these measurements. In-situ gamma spectroscopy spatially averages the activity of an area within the field of view of the detector and measures the activity from a volume of soil several orders of magnitude greater than can be practically measured by soil sampling. Thus, the samples collected must be: a) spatially representative of the activity within the field of view of the detector, requiring a centre weighted sampling plan to match the circles of investigation, and b) quantify the variability of activity within the field of view. Thus irrespective of the homogeneity of the site, the sampling plan will be able to provide a spatially weighted activity estimate of the site with fewer samples.

6.5.2 Principles and Method - A Simple Centre Weighted Sampling Plan

For the Ayrshire Aerial Survey (Sanderson *et al* 1990c), four areas were set up for the calibration of aerial survey measurements. For these areas, the circle of investigation for ^{137}Cs and for a detector at 100 m altitude was estimated (figure 3.12) and a sampling plan was determined as shown in figure 6.4. 17 locations were sampled per site. At each sample locality 10 soil cores were randomly collected within a 3 m or 4 m radius, with the 38 mm soil corer to a depth of 30 cm at 15 cm intervals. In

addition, some random samples were taken to 45 cm depth, where possible, to estimate the depth of ^{137}Cs and ^{134}Cs penetration. In addition, at the centre of each sampling point a single spectrum was collected with the 3" x 3" NaI(Tl) detector and Canberra Series 10^{plus} MCA.

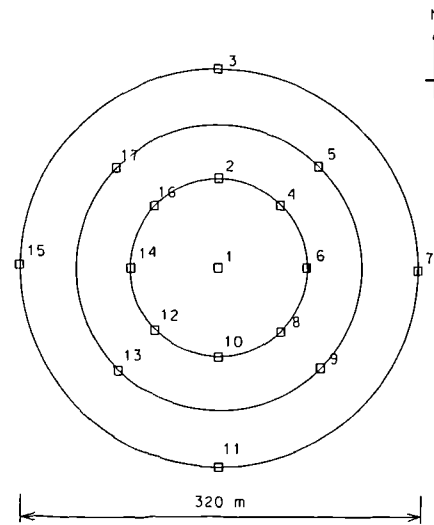


Figure 6.4 Ayrshire Ground Sampling Plan.

Given the finite sample number, the spatial distribution of these samples was determined to spatially match the field of view of a detector at 100 m height. This was achieved by placing a fraction of the total number of samples at a radial distance from the centre of the area that was equivalent to the same fraction of γ photon flux originating from that area for a detector at 100 m altitude as described by the circle of investigation (figure 3.16).

The results from the weighting and spatial matching are given in table 6.7. Thus the mean of the sample inventories collected on each site would represent the spatially averaged mean activity measured by the detector at 100 m altitude with an appropriate sampling error associated with the heterogeneity of activity distribution of the site.

The four localities chosen were in topographically flat terrain, situated on contrasting

Table 6.7. Calculation of Radial Sampling Pattern for Prismatic Detector at 100m Altitude for ^{137}Cs

No. of Samples	Cumulative Number	Per Cent of Total	Radial Distance m	Per Cent of total γ fluence
1	1	5.9	0	0
8	9	52.9	70	50
4	13	76.5	115	70
4	17	100	160	90

Table 6.8 Calibration Area Site Selection

Site	Grid Ref	Soil	Geology/ Topography	Radionucl. Concent.*
Eaglesham Moor	NS 570 462	Peat/Myre	Basaltic lavas rolling hills	Chern-High Nats-Low
Lochwinnoch	NS 307 626	Variable peat/mineral	Basalt/Andasite Upland site	Chern-Mod. Nats-Low
Leana Hill	NX 124 787	Upland peat	Slates/shales Upland Valley	Chern-Low Nats-Mod
Lakin Farm	NR 898 307	Lowland peat/mineral	Felsite-acidic Lowland	Chern-Low Nats-High

*Chern: ^{134}Cs and ^{137}Cs . Nats: *Naturals* (^{40}K , ^{214}Bi and ^{208}Tl)

geological rock formations and soil type. These areas were chosen by studying geological, soil and topographical maps, as briefly described in table 6.8, and selected to attempt to represent the typical range of the conditions flown over during the aerial survey. Final location choices were also dictated by access and availability.

6.5.3 Results and Discussion

The results from the calibration areas are illustrated in tables 6.9 to 6.13. From the random 30-45 cm measurements, the estimated fraction of the total inventory was calculated and the 0-45 cm integrated depth was estimated. There is a high degree of compatibility between the mean soil core activity estimates and the mean activity estimates derived through in-situ gamma spectroscopy measurements (in-situ calibration described in Appendix A).

Table 6.9 Myres Hill Calibration Area Data, Eaglesham Moor. Comparison between Soil Core Inventories and 3" x 3" NaI In-Situ Measurements

	¹³⁷ Cs	¹³⁴ Cs	Activity kBq m ⁻²		
			⁴⁰ K	²¹⁴ Bi	²⁰⁸ Tl
NaI(Tl) Results					
Mean	6.93	0.86	<i>BDL</i>	<i>BDL</i>	<i>BDL</i>
Standard Dev.	1.02	0.42			
Standard Error	0.24	0.10			
C.V. %	14.7	48.8			
Core 0-45 cm Results (Estimated)					
Mean	7.12	0.802	1.77	0.144	0.064
Standard Dev.	1.41	0.143	0.822	0.081	0.021
Standard Error	0.38	0.038	0.22	0.022	0.006
C.V. %	19.8	17.8	46.4	57.1	32.8
Activity Bq wet kg⁻¹					
NaI(Tl) Results					
Mean	--	--	<i>BDL</i>	<i>BDL</i>	<i>BDL</i>
Standard Dev.	--	--			
Standard Error	--	--			
C.V. %					
Core Results					
Mean	--	--	21.77	2.48	0.93
Standard Dev.	--	--	12.77	1.31	0.19
Standard Error	--	--	3.10	0.32	0.05
C.V. %			58.7	52.8	20.4

BDL: Below Detection Limits

The coefficient of variation associated with the soil samples is in all cases (tables 6.9 to 6.12) greater than those associated with in-situ gamma spectrometric readings, particularly for ¹³⁷Cs. This demonstrates that soil sampling errors are a significant contribution to the overall site variability, whilst in-situ gamma spectrometry spatially averages the activity within its field of view, thereby eradicating the contribution to the variability from soil sampling errors. This is illustrated graphically by plotting the distribution of ¹³⁷Cs and ¹³⁴Cs in a two dimensional plane as shown in figures 6.5 and 6.6. Figures 6.5 and 6.6 both show that the in-situ NaI(Tl) detector measured activity levels in the centre of the calibration area significantly higher than those determined through soil sampling estimates. Conversely, an area of high activity to the north of the area is determined by soil sample analysis, but not detected by the in-situ detector.

Table 6.10 Lochwinnoch Calibration Pad Data. Comparison between Soil Core Inventories and 3" x 3" NaI In-Situ Measurements.

	¹³⁷ Cs	¹³⁴ Cs	Activity kBq m ⁻²		
			⁴⁰ K	²¹⁴ Bi	²⁰⁸ Tl
NaI(Tl) Results					
Mean	4.73	0.41	13.1*	0.89*	0.04
Standard Dev.	0.68	0.08	9.05	1.25	0.18
Standard Error	0.16	0.02	2.19	0.30	0.04
C.V. %	14.4	19.5	69.1	>100	>100
Core 0-45 cm Results (Estimated)					
Mean	4.58	0.4	4.2	0.171	0.104
Standard Dev.	1.08	0.09	5.05	0.098	0.079
Standard Error	0.262	0.022	1.23	0.024	0.02
C.V. %	23.6	22.5	>100	52.9	76.0
Activity Bq wetkg⁻¹					
NaI(Tl) Results					
Mean	--	--	58.82*	3.3*	1.39
Standard Dev.	--	--	52.02	1.99	1.09
Standard Error	--	--	12.62	0.48	0.27
C.V. %	--	--	88.4	60.1	78.4
Core Results					
Mean	--	--	57.37	3.05	1.17
Standard Dev.	--	--	21.30	3.20	0.37
Standard Error	--	--	5.17	0.78	0.09
C.V. %	--	--	37.1	>100	31.6

* At or Below Detection Limits

This detailed spatial mis-match in activity estimates is likely to be related predominantly to sampling error, as described earlier in this chapter.

There is also a high degree of compatibility between in-situ measurements and soil sample derived measurements of the natural radionuclides when quantified in terms of Bq wetkg⁻¹ (tables 6.11 to 6.12) and when activity levels are above the estimated minimum detection limits. The exception is observed at Lakin Farm (table 6.12), where the NaI(Tl) detector appears to overestimate the ²¹⁴Bi activity by a factor of 3. This may be the result of several environmental factors acting at once: i) the organic rich and porous soils at Lakin Farm allowed ²²²Rn emanation from the underlying felsite rock; ii) the passage of a cold weather front allowed further ²²²Rn emanation on the

Table 6.11 Leana Hill Calibration Pad Data. Comparison between Soil Core Inventories and 3" x 3" NaI In-Situ Measurements.

	¹³⁷ Cs	¹³⁴ Cs	Activity kBq m ⁻²		
			⁴⁰ K	²¹⁴ Bi	²⁰⁸ Tl
NaI(Tl) Results					
Mean	3.25	0.24*	12.4*	0.83*	0.11
Standard Dev.	0.39	0.06	7.01	0.78	0.20
Standard Error	0.10	0.02	1.81	0.20	0.05
C.V. %	12.0	25.0	56.5	94.0	>100
Core 0-45 cm Results (Estimated)					
Mean	2.81	0.203	4.12	0.171	0.126
Standard Dev.	0.72	0.061	3.30	0.128	0.116
Standard Error	0.18	0.015	0.83	0.030	0.028
C.V. %	25.6	30.0	80.1	74.9	92.0
			Activity Bq _{wet} kg ⁻¹		
NaI(Tl) Results					
Mean	--	--	55.62*	2.90*	1.32
Standard Dev.	--	--	16.51	2.01	0.43
Standard Error	--	--	4.26	0.52	0.11
C.V. %	--	--	29.7	69.3	32.6
Core Results					
Mean	--	--	51.72	2.96	1.61
Standard Dev.	--	--	29.90	1.14	0.55
Standard Error	--	--	7.72	0.29	0.14
C.V. %	--	--	57.8	38.5	34.2

* At or Below Detection Limits

second day's sampling, particularly as the mean count rate increased by a factor of 2 on the second day; iii) ²¹⁴Bi photon penetration through the soil profile from the underlying rock; and iv) ²¹⁴Bi concentrated at the base of the vertical soil profile. In addition, the lack of ²²²Rn equilibration within the soil sample container due to failure in the sealing procedure may lead to underestimation of ²¹⁴Bi activity.

Figures 6.7 and 6.8 show very similar distribution for ⁴⁰K between the soil core inventories and in-situ gamma spectrometric measurements in terms of both Bq m² and Bq_{wet} kg⁻¹. In both figures 6.7 and 6.8 there is a slight mis-match of data. Where the soil sample provides a higher reading than the detector, this suggests that the soil sample contained more than a representative sample of the underlying felsite rock. Conversely, where the soil sample underestimates the detector response, this suggests

Table 6.12 Lakin Farm Calibration Pad Data, Isle of Arran. Comparison between Soil Core Inventories and 3" x 3" NaI In-Situ Measurements.

	¹³⁷ Cs	¹³⁴ Cs	Activity kBq/m ²		
			⁴⁰ K	²¹⁴ Bi	²⁰⁸ Tl
NaI(Tl) Results					
Mean	3.20	0.34*	64.1	5.61	0.72
Standard Dev.	0.28	0.07	35.3	3.84	0.44
Standard Error	0.07	0.02	9.44	1.03	0.12
C.V. %	8.75	20.6	55.1	68.5	61.1
Core 0-30 cm Results					
Mean	3.593	0.197	35.41	0.776	0.369
Standard Dev.	0.93	0.055	27.89	0.710	0.330
Standard Error	0.24	0.015	7.45	0.187	0.088
C.V. %	25.9	27.9	78.8	91.5	89.4
Activity Bq wetkg⁻¹					
NaI(Tl) Results					
Mean	--	--	177.4	15.2	2.63
Standard Dev.	--	--	83.14	9.85	0.95
Standard Error	--	--	3.10	2.63	0.25
C.V. %	--	--	46.9	64.8	36.1
Core Results					
Mean	--	--	212.6	5.72	2.08
Standard Dev.	--	--	133.4	2.80	0.28
Standard Error	--	--	35.64	0.75	0.07
C.V. %	--	--	62.7	49.0	13.5

* At or Below Detection limits

that the single photons arrived at the detector from the underlying geology in disproportionate amounts to that represented by the sample.

The variability across each site exceeds a factor of three for the anthropogenic radionuclide with a CV of about 30 % which was a characteristic of all sites surveyed containing Chernobyl deposition on both a sampling scale and large scale across these calibration sites. This is likely to be largely associated with sampling errors, as the site variability associated with in-situ gamma spectrometry is smaller. For the natural radionuclides the variability is considerably larger. This may be related to the highly heterogenic nature of the soils themselves across the site as well as to the variable nature of the uptake of the natural radionuclides into the soil. This may be illustrated by the CV of 48% in the soil bulk density on the Lakin Farm site (Arran).

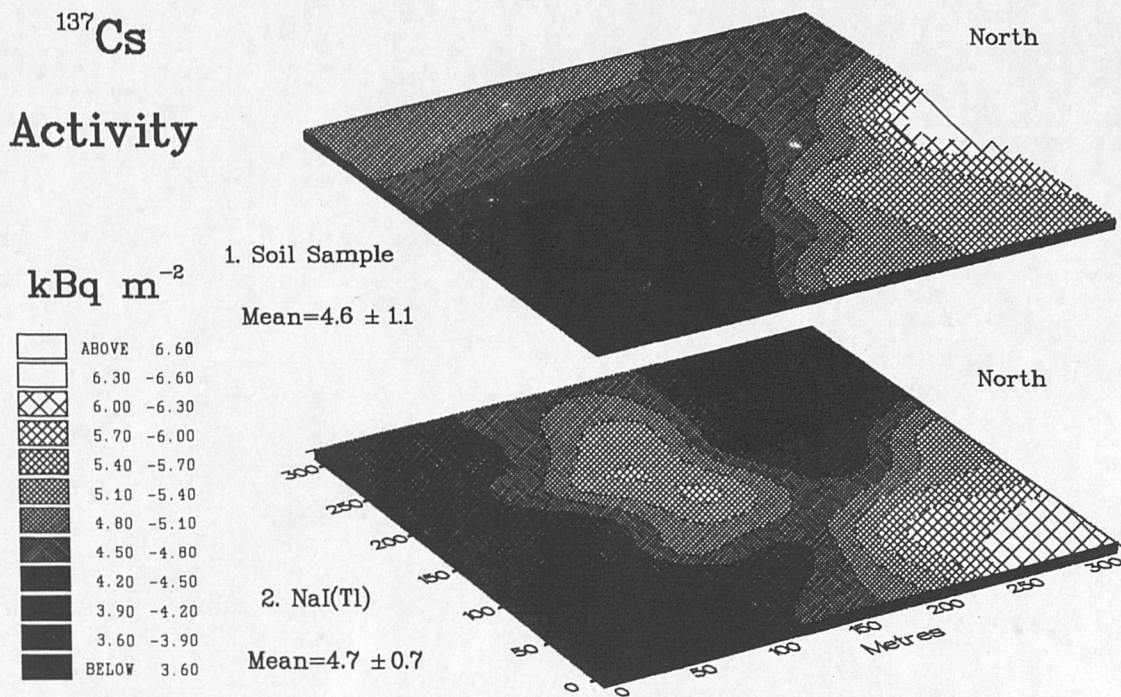


Figure 6.5 Comparison between ¹³⁷Cs activity determinations from soil samples and in-situ gamma spectroscopy at the Raithburn Calibration site, Lochwinnoch.

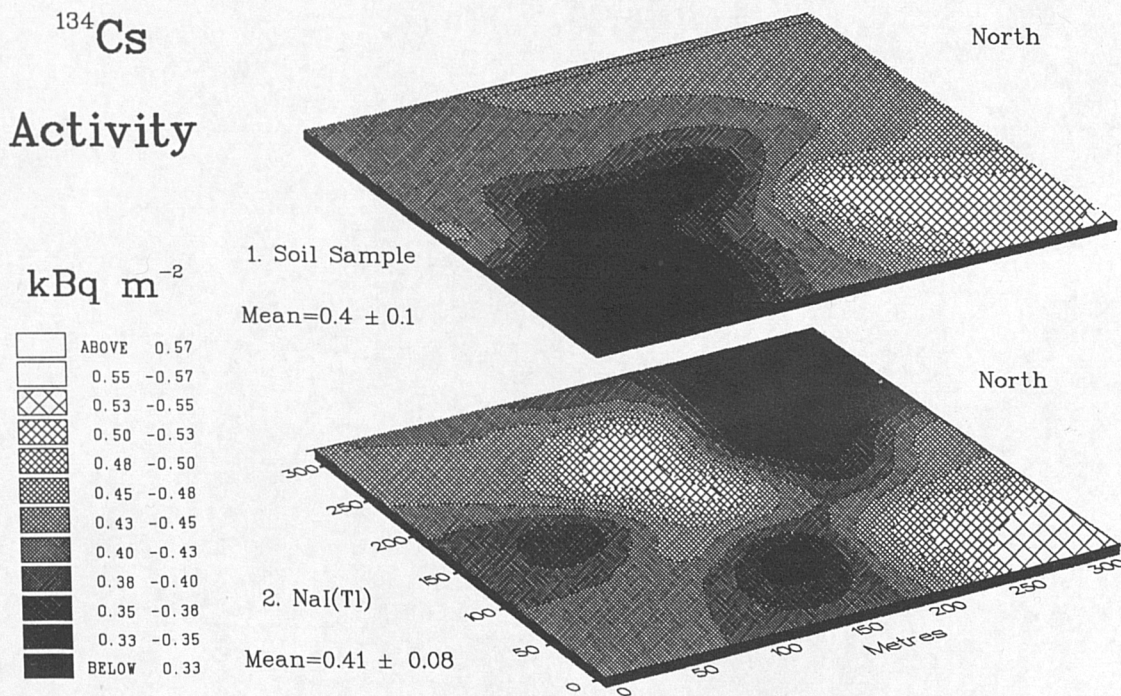


Figure 6.6 Comparison between ¹³⁴Cs activity determinations from soil samples and in-situ gamma spectroscopy at the Raithburn Calibration site, Lochwinnoch.

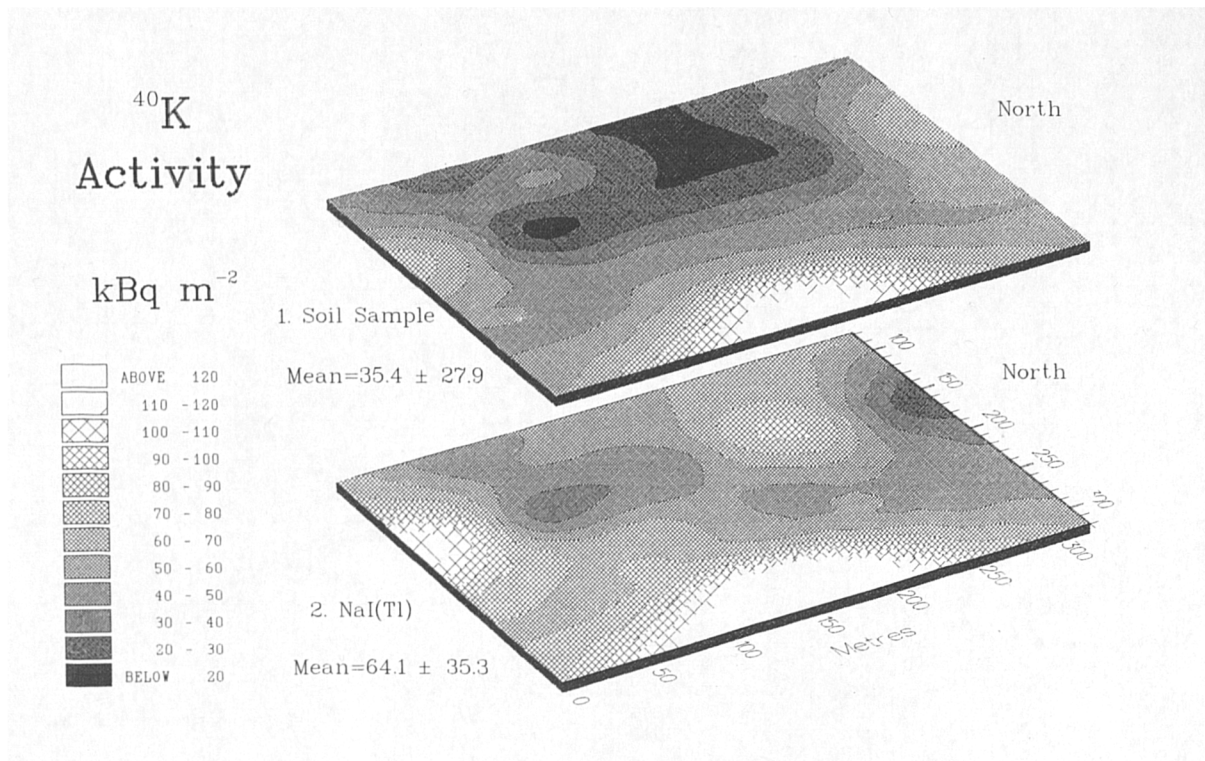


Figure 6.7 Spatial 2 dimensional comparison of ⁴⁰K activity (kBq m⁻²) estimation at Lakin Farm, Arran.

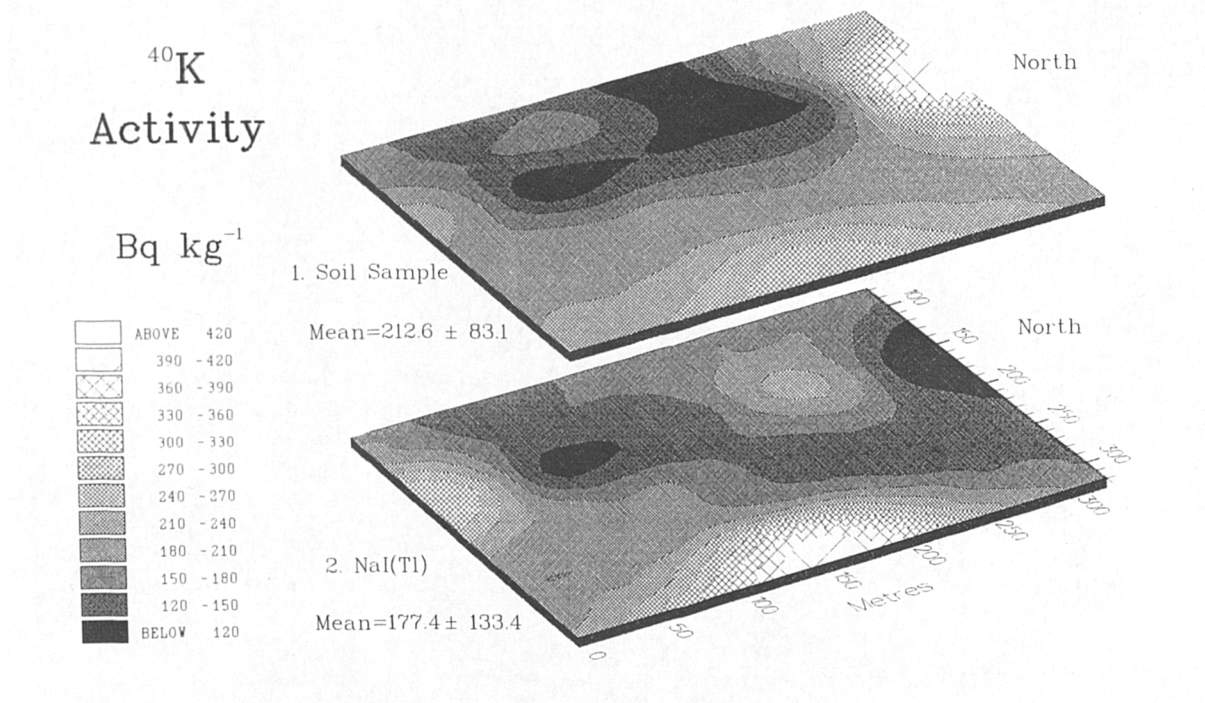


Figure 6.8 Spatial 2 dimensional comparison of ⁴⁰K activity (Bq kg⁻¹) estimation at Lakin Farm, Arran.

These sites were useful for calibrating detectors at a fixed height and for observing sample variability within that field of view. Although site variability has been quantified simply by the overall CV, knowledge of the spatial distribution of activity would be useful to enable detector calibration at various platform altitudes. As was quantitatively shown for the Lochwinnoch and Lakin Farm sites, the spatial distribution of activity may be concentrated in such a way as to influence the determination of the height correction coefficients. For example, at the Lakin Farm site ^{40}K estimates were higher towards the edges of the site. Thus as the detector height increased over the site, the photon fluence detected was greater than expected. Taking account of such spatial distribution would ensure that the height correction coefficients are spatially corrected.

6.6 ACCOUNTING FOR WITHIN SITE VARIABILITY AND VARIABLE DETECTOR HEIGHT FOR IN-SITU AND AERIAL SURVEY CALIBRATION

6.6.1 Objective

Although the calibration facilities described in section 6.5 proved useful, the sampling plan was inflexible for the determination of detector calibration constants for any other height other than 100 m. Spatially weighted activity estimates would also be useful for a range of detector altitudes to: a) account for spatial variability, and b) determine spatially corrected height correction coefficients. A new calibration sampling plan was therefore designed and applied.

6.6.2 Solution - The Expanding Hexagon Sampling Plan

The expanding hexagon sampling plan was developed for site characterisation to enable:

1. Field based detector calibrations to be carried out for various platform heights.
2. Potential errors on detector calibration due to soil sampling errors to be reduced.
3. Spatially corrected height correction coefficients to be calculated.
4. Spatial variability to be quantified for different radionuclide spatial

characteristics.

Figure 6.9 shows the expanding hexagonal sampling plan. The design can be altered to expand on any scale required either x2, x3 or x4. Figure 6.9 gives two examples of x4 expanding sample spacing. Thus, as the hexagonal radial distance increases, the sample spacing increases by the same amount, providing seven samples for each set of sample spacings.

EXPANDING HEXAGONAL SAMPLING GRID

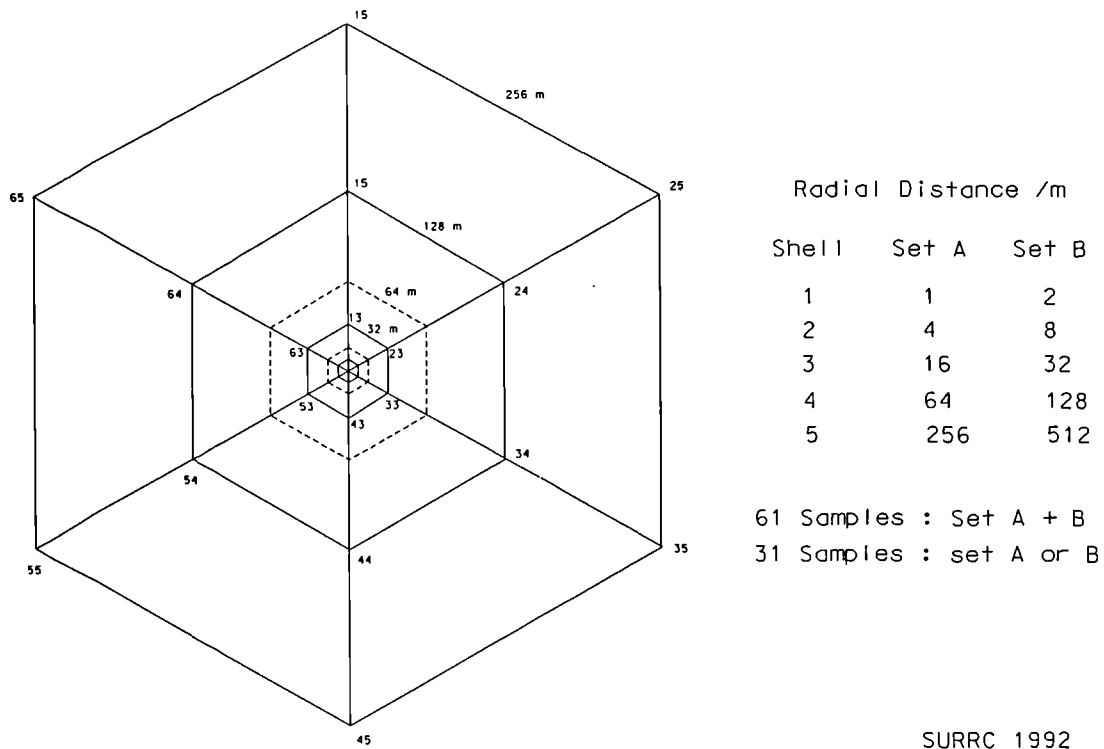


Figure 6.9 Illustrates the Expanding Hexagonal Sampling Plan and Typical Sampling sets

Table 6.13 shows a x2 format, sample spacing and the percent proportion of the total samples with given sampling radius. By changing the weighting for each sampling radius, the sampling plan can be altered to match the appropriate field of view for a given detector height.

Table 6.13 The Natural Spatial Sample Weighting of a x2 Expanding Hexagon

Radius metres	No. of Samples	Cumulative Total	Per Cent of Samples
0	1	1	1.8
1	6	7	12.7
2	6	13	23.6
4	6	19	34.5
8	6	25	45.5
16	6	31	56.4
32	6	37	67.3
64	6	43	78.2
128	6	49	89.1
256	6	55	100

6.6.3 Method

The expanding hexagon was used to describe the spatial variability of the anthropogenic radionuclides across two contrasting sites: i) a Sellafield contaminated site; and ii) an atmospherically derived Chernobyl contamination dominated site. For this purpose a salt marsh area at Caerlaverock on the Solway coastline and an organic rich site at basin valley peat site at Longbridgemuir, near Dumfries was chosen.

The Caerlaverock site was chosen for the calibration of in-situ detectors at variable platform heights for the Chapelcross Aerial survey (Sanderson *et al* 1992) and the Longbridgemuir site for the Scottish Office Aerial Survey (Sanderson *et al* 1993a and 1994). To reduce the sampling and sample processing time a x4 expanding hexagon was chosen as illustrated in table 6.14.

Figure 6.10 illustrates the relationship between the natural weighting of the hexagonal sampling plan (thin solid line) with the circles of investigation for ^{137}Cs with a mass relaxation depth of 14.5 g cm^{-2} at various platform heights. Clearly the "natural" weighting of the sampling plan does not correspond exactly to any of the circles of investigation calculated. However, by applying the additional weighting to each hexagonal shell, then the shells can be made to pass through the appropriate circle of investigation. This is shown in figure 6.10.

Table 6.14 The Natural Spatial Sampling Weighting for the Caerlaverock

Radius metres	No. of Samples	Cumulative Total	Natural % Weighting
0	1	1	3.2
2	6	7	22.6
8	6	13	41.9
32	6	19	61.3
128	6	25	80.6
256	6	31	100

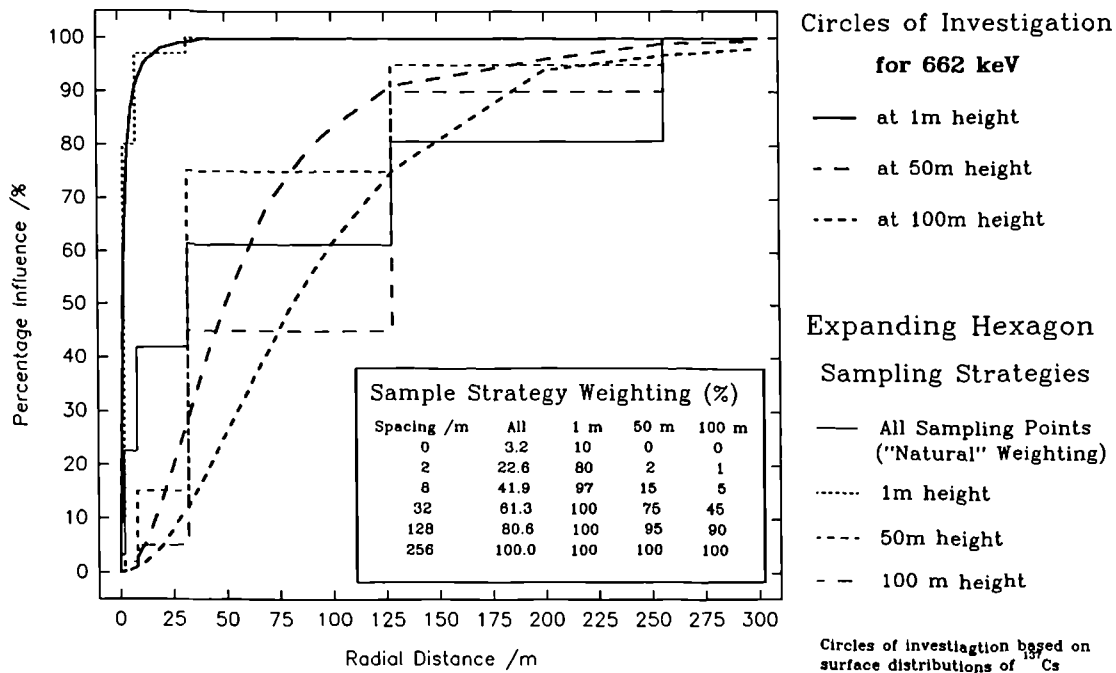


Figure 6.10 The Relationship between the Circles of Investigation for ¹³⁷Cs and the Hexagonal Sampling Strategies.

As demonstrated in figures 6.7 and 6.8, the distribution of ⁴⁰K activity appears to increase towards the edges of the circular calibration site. This spatial change in the activity concentrations may interfere with the determination of the height correction coefficients. The calculation of the height correction coefficients is discussed in section 3.7.5. Incorporation of the expanding hexagon into the determination of the height correction enables influences of spatial change on activity estimation to be corrected for.

6.6.4 Spatially Weighted Results

Table 6.15 gives the appropriate weighting for mean activity determination for a detector at 1 m, 50 m and 100 m height platforms using the weighting illustrated in figure 6.10. The calibration site was centred on an area of higher anthropogenic activity. Thus as the detector altitude increases, the field of view increases, viewing the areas of lower activity at the edge of the site. Without spatially matching the sampling strategy with the detector field of view, this variation in the calibration may not have been observed. The errors were calculated by weighting the errors for each shell with the same weighting used for the mean weighted activity calculation. As the importance of the outer shells of the hexagon increases for the weighted activity calculation, so the error on the mean also increases. This is due to the larger sample spacing and increasing variability across the site with ^{137}Cs distribution.

The expanding hexagon applied to the peaty Longbridemuir calibration site is shown in table 6.16. Here the spatially weighted activity does not appreciably change with detector height. The ability to estimate the activity with given levels of precision for a range of detector heights is useful and ensures that the spatial variability within the field of view is accounted for and quantified. Note, however, that the overall error does not change markedly with detector altitude above the ground with an estimated error of about 10 % precision on the mean activity for a range of detector altitudes. This indicates that spatial variability is similar on the micro and macro scales.

6.6.5 Results. Spatial Variability.

A brief look at sample variability within each shell of both the Caerlaverock (table 6.15) and Longbridgemuir (table 6.16) sites demonstrates the problem of spatial variability. By plotting the range and standard deviation of inventory estimation with sample spacing as shown in figure 6.11, a spatial radial structure can be clearly observed. For example, ^{137}Cs and ^{241}Am distribution shows little variability at the centre of the calibration site with sample spacings within 32 m. Above this spacing, the spatial structural characteristics of the site associated with ^{137}Cs and ^{241}Am

Table 6.15 The Spatially Weighted Mean Activities for ^{137}Cs at Caerlaverock Sampling site.

Radius metres	Percent Weighting	Cumulative Percentage	Activity Bq/m ²	St. Dev. 1 σ	St. Err. of Mean
Detector Height 1 m					
0	10	10	86020	1727	1727
2	70	80	84039	5189	2118
8	17	97	83376	7515	3068
32	3	100	83360	7140	2915
		Weighted Mean	84104	5502	2301
Detector Height 50 m					
2	2	2	84039	5189	2118
8	7	9	83376	7515	3068
32	48	55	83360	7140	2915
128	35	90	78754	33594	13715
256	10	100	39375	19907	8127
		Weighted Mean	79031	21531	8790
Detector Height 100 m					
2	1	1	84039	5189	2118
8	3	2	83376	7515	3068
32	32	35	83260	7140	2915
128	45	80	78754	33594	13715
256	20	100	39375	19907	8127
		Weighted Mean	73299	25272	10040

distribution from sediment deposition, become increasingly important and thus increase the activity inventory range and error. This distribution is likely to be controlled by a combination of historical changes in discharges from Sellafield and tidally controlled sedimentation which itself is structurally orientated with the coast. In the salt marsh environmental context, the presence of ^{134}Cs can be attributed to both the presence of Chernobyl deposition and Sellafield contaminated sediments. The different structural trends in the coefficient of variation across the site with sample spacing of ^{134}Cs with respect to both ^{137}Cs and ^{241}Am suggest that ^{134}Cs may be dominated by Chernobyl deposition. Thus it would appear that the Chernobyl derived deposition provides a moderate coefficient of variation uniformly across the site. In contrast, ^{241}Am shows a considerable increase in CV across the site with increasing sample spacing. ^{137}Cs also

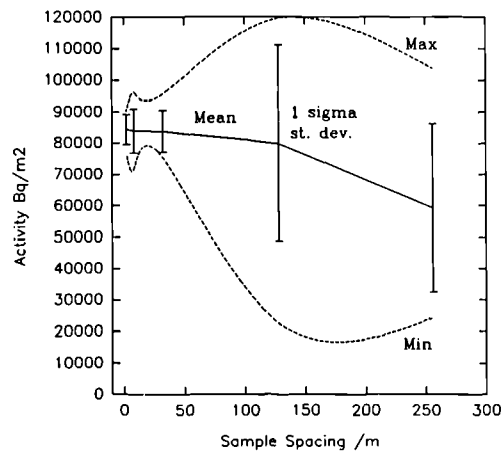
Table 6.16 The Spatially Weighted Mean Activities for ^{137}Cs at Longbridgemuir Sampling site.

Radius metres	Percent Weighting	Cumulative Percentage	Activity Bq/m ²	St. Dev. 1 σ	St. Err. of Mean
Detector Height 1 m					
0	10	10	9178	184	184
2	70	80	9972	3325	1357
8	17	97	7821	1875	765
32	3	100	9622	2427	990
		Weighted Mean	9516	2737	1117
Detector Height 50 m					
2	2	2	9972	3325	1357
8	7	9	7821	1875	765
32	48	55	9622	2427	990
128	45	100	9681	2128	869
		Weighted Mean	9722	2108	860
Detector Height 100 m					
2	1	1	9972	3325	1357
8	3	2	7821	1875	765
32	32	35	9622	2427	990
128	65	100	9681	2128	869
		Weighted Mean	9706	2249	918

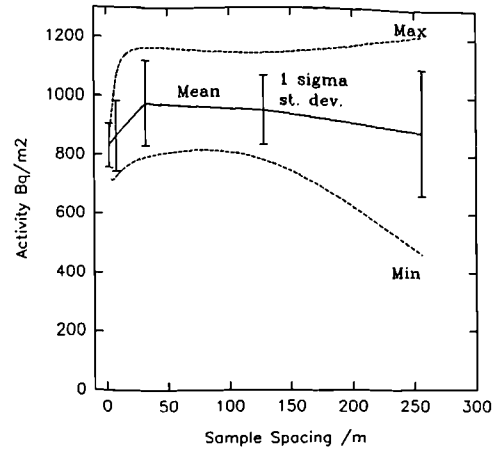
shows this effect, although not with quite such an exaggerated appearance. This is shown in figure 6.12 which shows the change in the coefficient of variation with sample spacing across the Caerlaverock salt marsh site.

The primordial radionuclides show a different pattern. The sampling error does not change systematically with an increase in sample spacing. This is demonstrated in figure 6.11, for ^{40}K , ^{214}Bi and ^{208}Tl . This indicates a uniform nature of the distribution of these radionuclides within the range demonstrated.

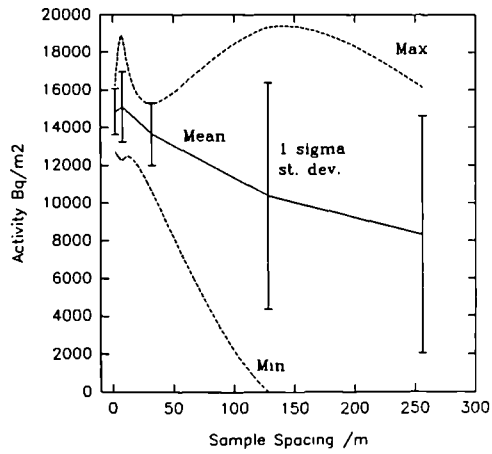
Figure 6.13 suggests a more random component in the activity distribution across the site with coefficients of variation for ^{40}K , ^{214}Bi and ^{208}Tl being as great at 2 m sample spacing as at 256 m sample spacing. Great care was taken to seal the containers for



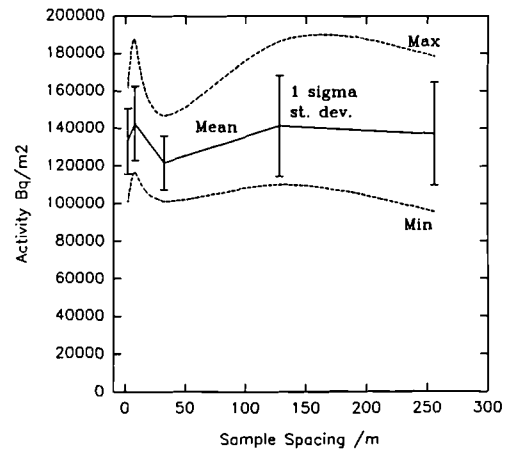
a. ^{137}Cs



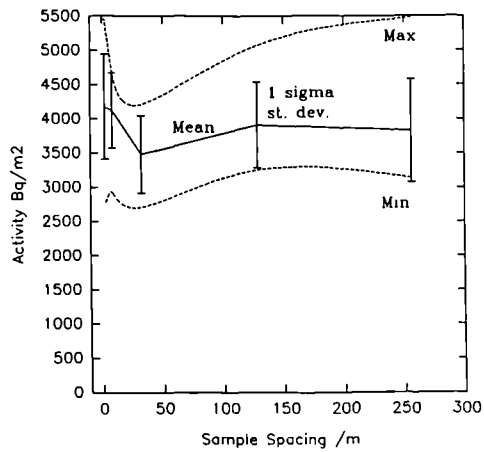
b. ^{134}Cs



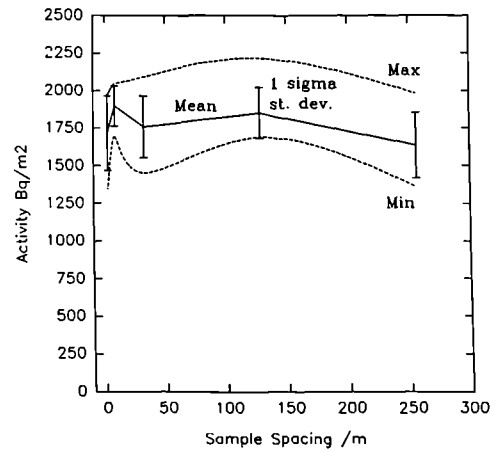
c. ^{241}Am



d. ^{40}K



e. ^{214}Bi



f. ^{208}Tl

Figure 6.11. Variation of Sampling Error with Radionuclide within each Hexagonal Shell Sampled at Caerlaverock

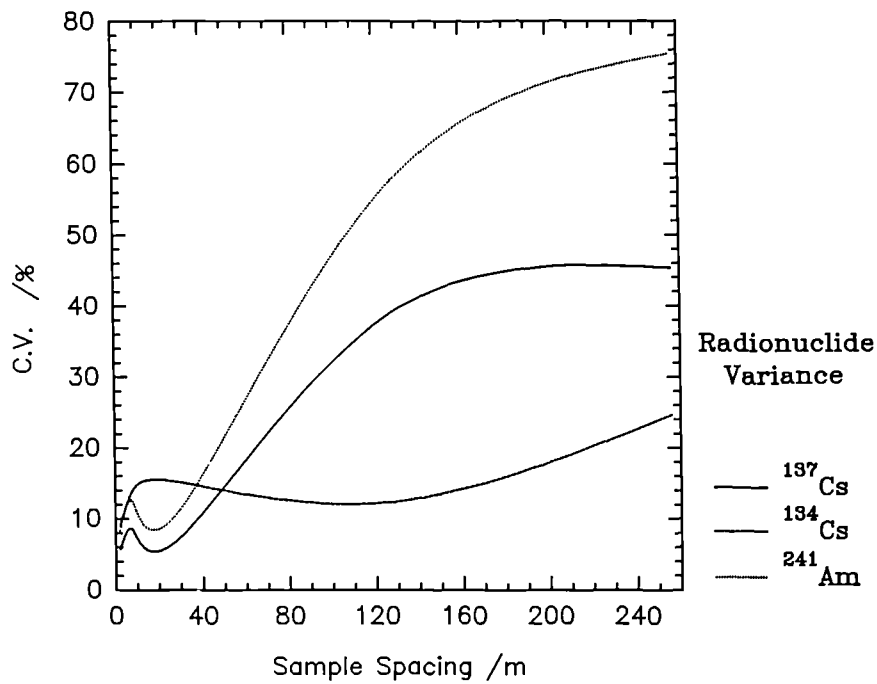


Figure 6.12 Coefficient of Variation (CV) of Anthropogenic Radionuclides across the Caerlaverock Salt Marsh with Sample Spacing.

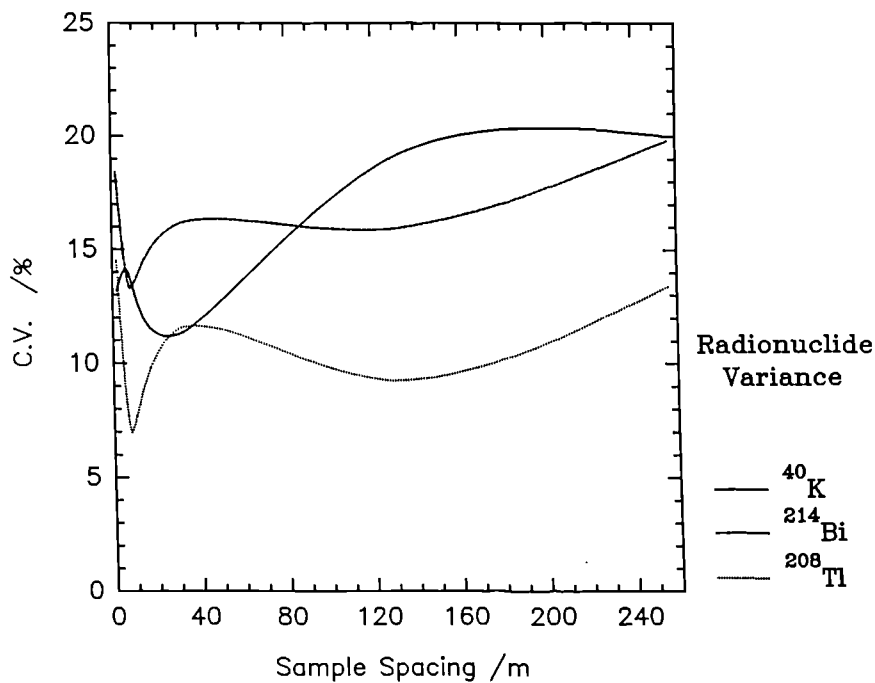


Figure 6.13 Coefficient of Variation (CV) of Primordial Radionuclides across the Caerlaverock Salt Marsh with Sample Spacing

laboratory based analysis of ^{214}Bi , allowing equilibration with ^{222}Rn . Thus the greater coefficient of variation associated with ^{214}Bi is likely to be one associated with the chemical and physical mobility of U distribution factors on the site. Generally for the primordial radionuclides, sampling errors (or CV) appear to be uniform across the site irrespective of sample spacing, especially for ^{214}Bi and ^{208}Tl , and do not appear to exceed 20 % at 1σ .

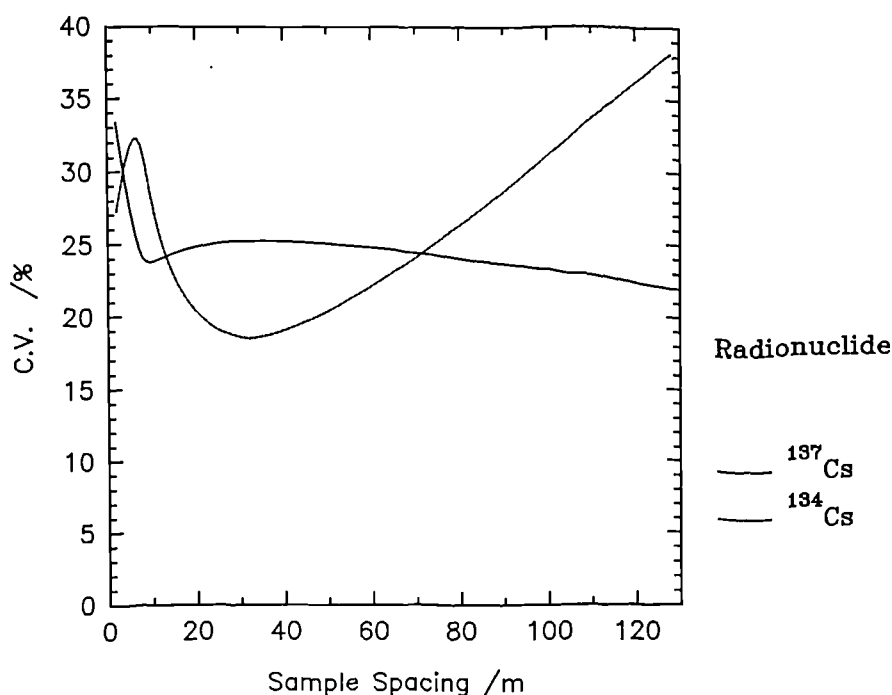


Figure 6.14 Coefficients of variation with sample spacing at the Longbridgemuir Calibration site.

The distribution of atmospherically derived anthropogenic radionuclides is shown in figure 6.14 for the Longbridgemuir site. ^{137}Cs has both weapons testing (about 30 %) and Chernobyl (about 70 %) components whilst ^{134}Cs is derived purely from Chernobyl. Both distributions show a high coefficient of variation, between 20 and 35 %, and tend to be uniformly independent of sample spacing. These values are clearly similar to those observed in section 6.3, 6.4 and 6.5. This is a demonstration of the consequences of precipitation scavenging of radioactive plumes on the distribution of anthropogenic radioactive fallout. The difference between the ^{137}Cs and ^{134}Cs at Longbridgemuir probably indicates a combination of different depositional events, ie. weapon's testing and Chernobyl fallout.

6.6.6 Determination of Height Correction Coefficients

The change in detector response with altitude is demonstrated in figures 6.15 and 6.16 for ^{137}Cs and ^{134}Cs at the Myres Hill calibration site. The figures also illustrate that the results are highly reproducible, with two sets of measurements demonstrated from the beginning and end of the Ayrshire aerial survey (Sanderson *et al* 1990c). As discussed in section 3.7.5, the relationships can be approximated by an exponential form. The *height correction coefficients* (a) are given in tables 6.17 and 6.18 for each site and radionuclide of interest.

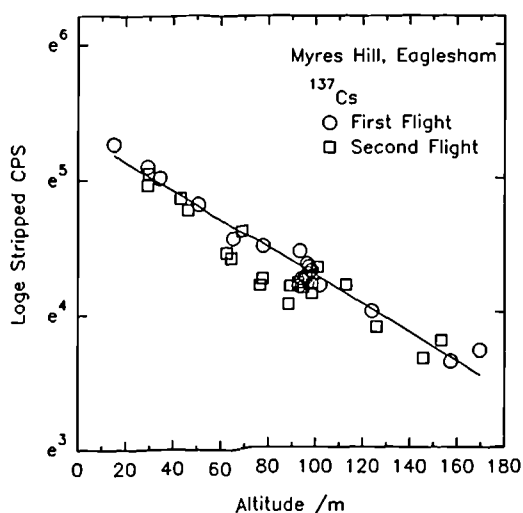


Figure 6.15 ^{137}Cs detector response with Altitude at Myres Hill

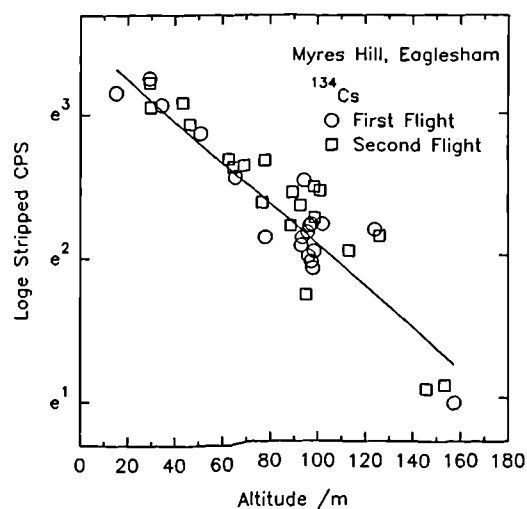


Figure 6.16 ^{134}Cs Detector response with altitude at Myres Hill.

The magnitude of the height correction coefficient (a) is dependent upon photon energy, detector height and the change in the field of view (change in the solid angle Θ ; figure 3.10). However, spatial variability in source distribution can have an additional influence on (a). For example, the spatial distribution indicated by qualitative mapping of Lochwinnoch calibration area (figure 6.5) suggested an enhanced ^{137}Cs activity region at the centre of the site. This would suggest that the spatially weighted mean activity observed by the detector with increasing altitude would decrease. However, the design of the circular sampling plan does not allow sufficient flexibility to quantify and correct for this effect. Such changes in the spatial distribution in ^{137}Cs activity are likely to lead to the most significant error contributions on the determination of (a) for ^{137}Cs .

With such fixed facilities, the best estimate of (a) can be achieved only by averaging (a) for a number of such calibration sites.

The expanding hexagonal sampling plan provides a means for correcting for changes in the spatial distribution of activity. This can be illustrated by the examples of the Caerlaverock, Warton, Wigtown and Longbridemuir calibration sites. Figures 6.17 and 6.18 show the uncorrected and corrected determinations of (a) with coefficients given in table 6.17. Reproducibility of this data was determined to be better than 5 % from a second flight one year later (Sanderson *et al* 1993a).

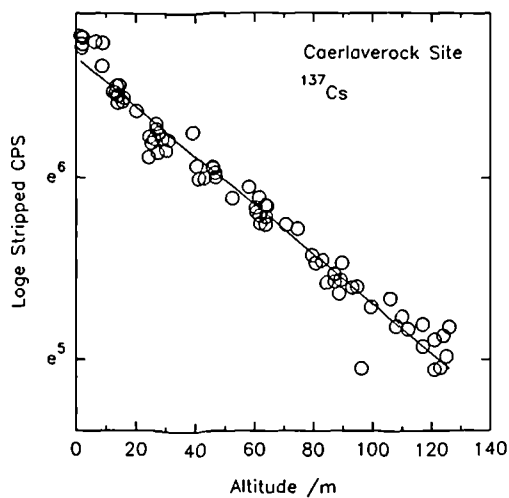


Figure 6.17 Variation of detector response for ^{137}Cs at Caerlaverock

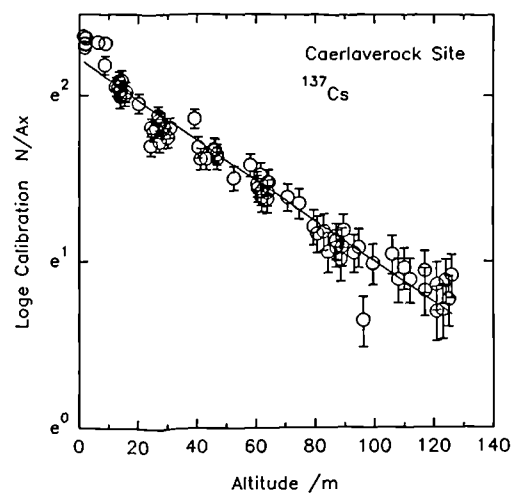


Figure 6.18 The spatially corrected variation of detector response with height for ^{137}Cs at Caerlaverock.

The correction is achieved by calculating the detector response function (N/A_x) for the detector at each altitude. The appropriate weighted activity A_x for each detector altitude and the stripped count rate N is calculated. In this way the detector response is spatially determined at each altitude. Thus determination of (a) for N/A_x with altitude is automatically spatially corrected. The largest proportion of the error is attributed to the weighted mean activities used to calculate N/A_x . Taking account of spatial variability in this way also allows for helicopter drift over the calibration site.

Errors brought about by change in the stripping coefficients with detector altitude have

Table 6.17 Height Correction Coefficients (I_o and a) for Radiocaesium (^{137}Cs and ^{134}Cs). I_o is the count rate at 0 m altitude.

Sampling Site	^{137}Cs Height Correction Coef.		^{134}Cs Height Correction Coef.	
	I_o	a	I_o	a
<i>Fixed Circular Calibration Sites</i>				
<i>Terrestrial Sites</i>				
Myres Hill	193.25	-0.0104	37.08	-0.01509
Leana Hill	57.47	-0.00863		
Lakin Farm	61.874	-0.00918		
Raithburn	132.69	-0.01004	17.59	-0.01119
Mean (working value)		-0.00956		-0.01314
standard deviation (1σ)		± 0.0007		± 0.00280
<i>Expanding Hexagon Calibration Sites</i>				
<i>Terrestrial Sites</i>				
Longbridgemuir	196.47	-0.01117	24.66	-0.01375
<i>Salt Marsh Sites</i>				
Caerlaverock	785.1	-0.01360	31.6	-0.00710
Warton Bank	1953	-0.01507	165.1	-0.01966
Wigtown Bay	1193	-0.00957	85.6	-0.00984
<i>Spatially corrected coefficients</i>				
Caerlaverock	9.217	-0.01222		
Warton Bank	6.845	-0.01340		

not been accounted for. The change in stripping with altitude is discussed in chapter 7 and Appendix J. ^{40}K stripping within the ^{137}Cs window is shown to be the most vulnerable to changes in detector altitude as demonstrated in Appendix J. This error contribution, given that nominal stripping ratio's at 100 m altitude are used, is likely to be at a maximum at ground level. The activity levels on the salt marsh sites are high providing high count rates. Thus at Caerlaverock the error contribution at ground level is about 3.5 % and at Warton Bank the error contribution is about 1.4 %. These maximum errors are smaller than those simply attributed to sampling error.

Having corrected for the spatial change in activity across the site, the change in the

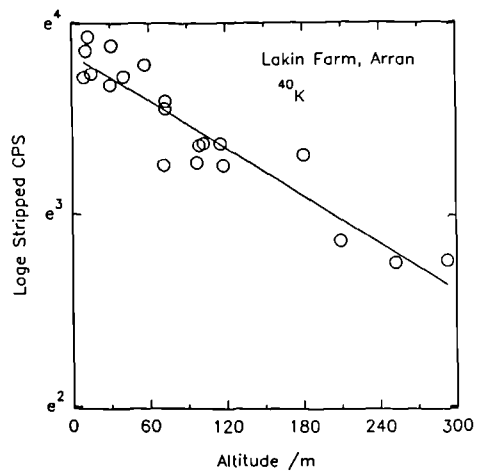
Table 6.18 Height Correction Coefficients (I_o and a) for ^{40}K , ^{214}Bi and ^{208}Tl . I_o is the count rate at 0 m altitude.

Sampling Site	Height Correction Coefficients		IAEA (1991)	Grasty (1976)
	I_o	a	a	a
^{40}K				
Lakin Farm	46.75	-0.00412		
Caerlaverock	101.2	-0.00872		
Wigtown	111.6	-0.00847		
			-0.0082	-0.00797
^{214}Bi				
Lakin Farm	5.246	-0.00576		
Caerlaverock	11.648	-0.00683		
Wigtown	11.2	-0.0109		
			-0.0084	-0.00678
^{208}Tl				
Lakin Farm	6.650	-0.00204		
Caerlaverock	17.335	-0.01009		
Wigtown	24.91	-0.0077		
			-0.0066	-0.00673

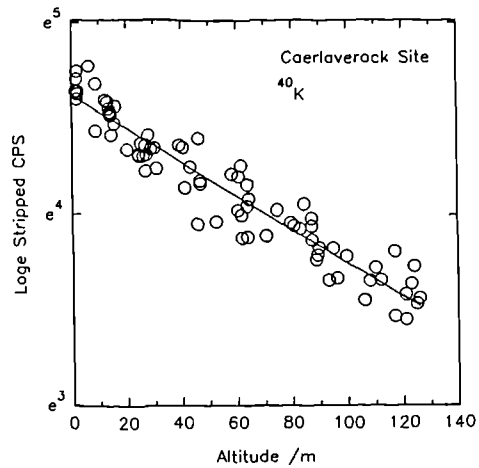
height correction coefficients are not significantly high, suggesting that the salt marsh sites are not too variable. However, the magnitude of (a) may now be related to the source burial. Note from table 6.17, that the *height correction coefficient* (a) for ^{137}Cs are markedly higher for the salt marsh sites than the terrestrial calibration sites.

The considerable variability in (a) between sites for ^{134}Cs is not only a function of source burial and lateral distribution, but is also due to the activity concentrations which are close to and/or below the lower limits of detection. Consequently, the data are also exposed to the effect of the possible changes in stripping coefficients with altitude.

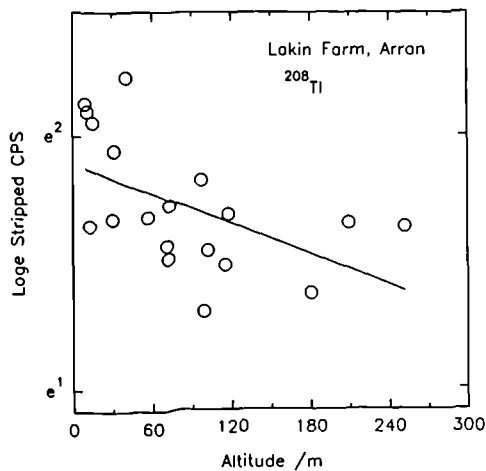
The problem of source distribution in measuring the height correction coefficient is not restricted to anthropogenic radionuclides alone, but also to the natural radionuclides. Figures 6.7 and 6.8 suggest that the ^{40}K distribution appears to increase towards the



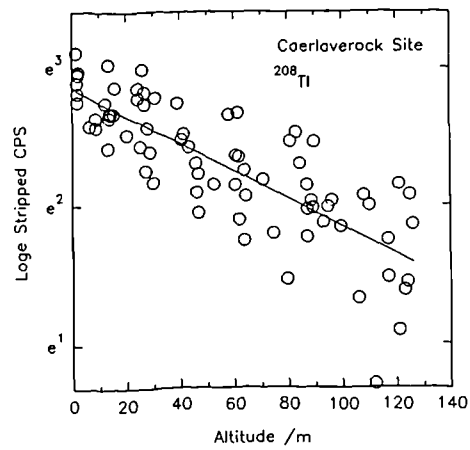
a) ^{40}K at Lakin Farm



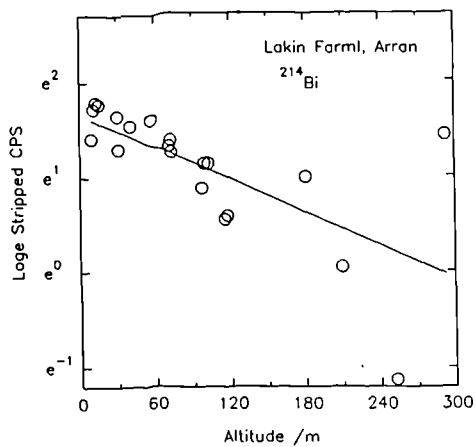
b) ^{40}K at Caerlaverock



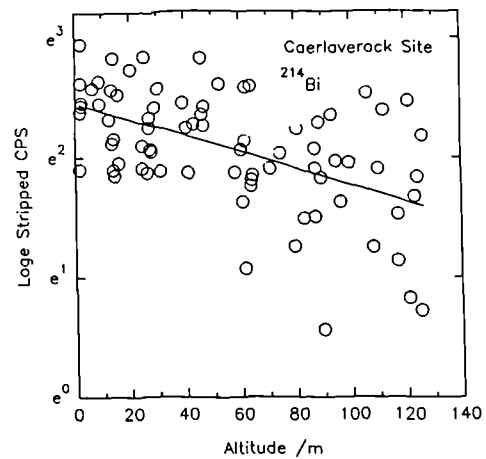
c) ^{208}Tl at Lakin Farm



d) ^{208}Tl at Caerlaverock



e) ^{214}Bi at Lakin Farm



f) ^{214}Bi at Caerlaverock

Figure 6.19 Change in detector response with altitude at Lakin Farm and Caerlaverock.

edges of the calibration site at the Lakin Farm (Arran). This would suggest that, as the detector height increases, the contribution from the outer parts of the calibration area will distort the height correction coefficient determined. This is indicated in table 6.18 by a markedly lower estimation in (*a*) for the Lakin Farm site than the relatively homogeneously distributed salt marsh sites. Application of the expanding hexagon to such a site would enable a spatial correction to be determined. Ideally, uniform areas of activity distribution should be chosen to determine (*a*). The salt marsh sites approximate such areas as verified by analysis of the data provided by the expanding hexagon (figures 6.11, 6.13). Thus comparison of the height correction coefficients (table 6.18) provided by the different sites illustrates the problems in determining (*a*) if spatial variability cannot be accounted for.

Table 6.18 also shows a favourable comparison of (*a*) determined from these calibration sites with values of (*a*) given by IAEA (1991) and Grasty *et al* (1976).

Figure 6.19 shows the change in detector response with altitude for the natural radionuclides at Lakin Farm (Isle of Arran) and Caerlaverock Salt Marsh. As the count rate decreases, the amount of scatter about the height correction line due to random statistical component increases. This requires more observations to be made across the range of altitudes to estimate the height correction coefficient (*a*) to an appropriate level of precision. This is particularly well observed with ^{40}K and ^{208}Tl . However, the scatter increases considerably for ^{214}Bi , and the determination of (*a*) is problematic. This increased scatter is brought about by the contribution of ^{214}Bi from airborne ^{222}Rn , which is particularly well observed at Caerlaverock.

6.7 DISCUSSION

This chapter demonstrates the need to take into account sampling errors and spatial variability in determining overall precision levels of environmental radionuclide activity estimation. Given the existence of spatial variability in the environment, it is of paramount importance to account for this variability when sampling and making spatial comparisons between different environmental monitoring techniques.

An investigation into the improvement of sub-sampling error was undertaken. Although some improvement is seen in sub-sampling errors with increasing geometry size, generally sub-sampling errors tend to be negligible when counting statistics and errors on efficiency calibration are accounted for. However, the results indicate the need for careful hermetical sealing of sample containers for ^{222}Rn equilibration. Comparisons with data collected between different detectors and sample containers and over longer time scales must take into consideration slight differences in detector performances.

These sample processing errors described tend to be negligible when compared with sampling errors and the consequences of spatial variability. In addition to the macro scale, spatial variability occurs on the micro (1 or 2 m) scale and this influences soil sampling errors. Micro spatial variability for primordial radionuclides varies depending upon the soil type and its ability to assimilate elements of the underlying geology either through a liquid phase or mechanical phase.

Micro spatial variability of anthropogenic radionuclides is dependent upon the deposition pathway. Typically, fallout from the troposphere, such as from Chernobyl, is characterised by large soil sampling errors, whilst in water borne well mixed sediments such as that associated with Sellafield, sampling errors are significantly smaller.

Improvement in sampling errors for both the natural and anthropogenic radionuclides was observed with the implementation of a larger 105 mm soil corer. Whilst an improvement in sampling error was observed, it was not as substantial as predicted by geochemical soil sampling theory (Ingamells *et al* 1972, and Ingamells 1974 a and b). This is likely to be due to a non-normal distribution of activity caused by some spatial component.

On a larger scale, ie. between sampling localities, primordial radionuclide variability is additionally dependent upon climate, underlying geological variation, sedimentary depositional characteristics, slope and aspect. Spatial variability has been observed to be considerable in peaty sites whilst very much less within salt marsh areas. Spatial

variability of anthropogenic radionuclide deposition is dependent upon the depositional pathway. As demonstrated at Longbridgemuir, the coefficient of variation does not change significantly with sample spacing, and thus spatial variability for atmospheric deposition of radionuclides is similar on both the micro and macro scale of sampling and tends to be spatially independent with a typical coefficient of variation of between 20 and 30 %. This uniformly high coefficient of variation is likely to be a result of precipitation scavenging mechanisms and absorption into soil with its own heterogenic characteristics, which tends to lead to variability occurring on a scale smaller than the sampling area of an individual soil core. In contrast, areas of anthropogenic contamination from the deposition of water borne well mixed sediments of the Irish Sea, ie. salt marsh sites, demonstrated relatively homogeneous micro scale (<2 m scale) sampling. However, as sample spacing increased, variability also increased on the Caerlaverock salt marsh. Above about 40 m sample spacing, variability of both ^{137}Cs and ^{241}Am exceeded the levels associated with Chernobyl outfall (i.e. CV of 30 %). It is interesting to note, that at Caerlaverock, the CV for ^{134}Cs remained similar to that associated with Chernobyl fallout. On a micro scale however, observations on Warton Bank (Sanderson *et al* 1993 b) indicated that small scale variability and sampling error can be increased with proximity to other structural controls in the merse environment, such as proximity to drainage channels.

Given the inherent spatial variability, sampling error and the considerable spatial averaging of in-situ and aerial survey gamma spectroscopy measurements, soil sampling plans have to be spatially weighted to account for the variability within the field of view of an in-situ or airborne detector. Simple spatially weighted sampling strategies tend to be inflexible. However, the *expanding hexagon* allows a large number of samples to be collected in a realistic time scale and provides the flexibility for spatially matching soil sample inventories with various detector platform heights as well as accounting for the within site variability with realistic sampling error estimates. The expanding hexagon has the additional advantage of accounting for spatial change in the determination of height correction coefficient (a). These observations have also indicated the problem associated with airborne ^{222}Rn components in making a determination of (a) and sensitivity estimates for ^{214}Bi difficult (Appendices A and B).

Having accounted for the within site variability and spatial matching of soil sample inventories with in-situ and aerial gamma ray spectroscopy measurements, an important second factor has to be taken into consideration which may affect the detector response between different sites. This factor is the influence of source burial, quantified in terms of the source mass depth distribution which takes into consideration the activity and density distribution of the soil with depth. This has a significant influence on photon fluence from the surface and is observed in detector response characteristics. The influence of source burial is investigated in chapter 7.

7. RADIONUCLIDE DEPTH DISTRIBUTION PROFILES AND IN-SITU GAMMA SPECTROSCOPY.

7.1 INTRODUCTION

The calibration of laboratory based detectors relies upon a fixed standard container geometry for which, as was demonstrated in chapter 5, the correction for self absorption can be readily accounted. In contrast, in-situ and airborne gamma ray spectrometry has a variable source geometry. In particular source burial complicates the source to detector relationship. Having accounted for lateral spatial variability in the field and collected representative samples for in-situ and airborne detector calibration, the primary photon signal strength and secondary photon scattering characteristics attributed to source burial can be investigated and quantified. Source burial represents an important environmental factor which affects activity estimation and comparisons between in-situ and soil core estimates. Representative samples of source burial are required for effective comparison with in-situ techniques. For example, shallow sampling in salt marsh environments to 15 cm depth (e.g. McKay *et al* 1991) may severely underestimate the total gamma photon contribution from ^{137}Cs in salt marsh sediment profiles.

Section 2.5 discusses the distribution of anthropogenic and primordial radionuclides in the environment. The vertical distributions of the radionuclides within the soil profile is dependent upon the depositional or emplacement mechanisms, and the chemical and physical behaviour and mobility of the radionuclide. Of particular interest in this chapter is the vertical distribution of caesium in the soil, although the distribution of the natural radionuclides are also investigated. The influences these have on the detection and quantification of activity from in-situ detectors is explored through experimental modelling.

Much work has been undertaken in measuring and understanding the mechanisms which control the distribution of caesium within soils and sediments. Deposition of caesium from the atmosphere, i.e. from weapons testing or Chernobyl fallout, leads to a fresh

deposition of caesium on the surface of the soil. However, diffusion, advective and leaching mechanisms re-mobilize the caesium with a general movement down the soil profile. Many laboratory based experiments with lysimeters, batch column experiments or similar (e.g. Ohnuki and Tanaka 1989, Veen and Meijer 1989, Fahad *et al* 1989, Miyahara *et al* 1990, Burns *et al* 1991, Coughtrey 1988) have demonstrated that the activity distribution from atmospheric deposition decreases rapidly with depth and consequently has often been described by a negative exponential. Models developed to explain this behaviour tend to include migration of caesium in ionic form, non-ionic form and in particulate form by quasi-diffusion and the addition of a velocity transfer factor. Caesium can be quickly absorbed and fixed in clay matrices, or adsorbed onto organic and mineral complexes, and/or attached to silt and clay particles which move through the soil column. Alternatively caesium may stay in solution often with the aid of humic acids, undergo leaching, ion exchange and diffusion with upward, downward and lateral direction in stagnant water within the soil. A complicated interaction of a number of processes has been observed to control the distribution of caesium. Thus the caesium profile observed is dependent upon the soil's physical and chemical characteristics, the amount of water infiltration, movement and time.

The ability of the soil to retain radionuclides is often expressed in terms of the K_d value which is defined in equation 7.1:

$$K_d = \frac{\text{amount of radionuclides sorbed per gram of soil}}{\text{amount of radionuclide per millilitre of solution}} \quad (7.1)$$

K_d values are often determined in the laboratory. However, their application to the "real world" is seldom completely accurate in predicting the behaviour of radionuclides in the field due to other processes such as the advective upward, downward and lateral movement of water in the soil column. However, the observed changes in K_d with depth can serve as an indication of the influencing controls on the caesium depth distribution profile (Bachauer *et al* 1982).

There are conditions under which true exponential profile can occur. For example, an exponential profile may result from the diffusion of activity from the surface layers of

a soil profile, or the continuous deposition of freshly contaminated sediments in accretionary areas in conjunction with ageing. However, these processes rarely occur uniquely. Observations in the field (Bachauber *et al* 1982, Silant'ev and Shkuratova 1988, El Fawaris and Knaus 1984) and prolonged laboratory and lysimeter experiments (Veen and Meijer 1989, Bachauber *et al* 1982) have demonstrated that the assumption of an exponential profile is not valid, particularly for aged deposits. A subsurface maximum often develops as a result of a humus rich surface layer which cannot fix caesium permanently and which with the addition of meteoric water allows a slow leaching and transfer of caesium downwards (Veen and Meijer 1989, Bachauber *et al* 1982). In addition soil acidity and the chelating capacity of dissolved humics can maintain trace metals in solution (Torgessen and Longmore 1984) and caesium is only permanently fixed within soil horizons with clay, particularly the montmorillonite (micaceous) group (Francis and Brinkley 1976, Bachauber *et al* 1982, Fahad *et al* 1989). Thus a subsurface maximum can occur due to the subsurface absorption of caesium as well as the general downward leaching processes. A subsurface maximum may also occur under a surface maximum due to aged caesium from weapons testing fallout having moved down the soil profile followed by a subsequent fresh deposition of caesium on the soil surface. Thus the depth distribution profiles observed may often be a superposition of two separate events. This has been observed in relatively uniform organic rich soil. Similar processes have been observed in lake bed sediments although here sediment inundation is an additional controlling factor (Irlweck 1991, Bonnett and Cambray 1989, Torgessen and Longmore 1984). Additional factors such as erosion and redistribution, growth and decay of plant matter and bioturbation may lead to more complicated soil profiles.

In addition the depth distribution profile can be altered by the erosion and depositional processes associated with slopes and drainage and catchment areas (Ritchie and McHenry 1990). Also subsurface movement of water down-slope may account for mass transfer of caesium (Burns *et al* 1991) particularly in an organic rich environment such as upland areas of Scotland, as demonstrated in the Raithburn Valley (chapter 4). Thus, subsurface maxima may be removed or enhanced by sideways or down-slope movement of surface or subsurface caesium either in particulate or dissolved form.

Following deposition, the subsequent movement of caesium within the soil profile will be highly dependent upon local factors of soil type and composition, slope aspect and the amount of meteoric water input and its subsequent movement within the soil profile. Thus with time, the depth distribution profile is likely to differ considerably between and within sites due to the inherent variability in soil type, and climatic and topographic controls.

In the marine and intertidal environment of the Irish Sea, Sellafield discharges have provided a locally significant source of anthropogenic radionuclides (Chapter 2). The radionuclide contaminants are well mixed in sediments at the bottom of the Irish sea of which some have been moved through strong currents to coastal locations around the Irish Sea Basin (McKenzie *et al* 1987, McDonald *et al* 1990, 1992a) and collected in areas of sediment accumulation, usually in salt marsh accretionary environments, but also within man made harbours. Detailed studies here and by Allen (1994) of salt marsh environments have shown that sediments deposited with activities associated with peak Sellafield discharges in the early to mid 1970's (BNF 1990,1991) have subsequently been buried by lower activity sediments. Thus the distribution of activity with depth may have a historical relationship with discharge levels and sedimentation rates. In the salt marsh localities, the depth of the profile is related to frequency of tidal cover and sediment deposition. Thus a subsurface maximum has been created with depth of burial directly related to the proximity to the near shore environment. Deposition of caesium from solution directly within the salt marsh sediments may be a factor influencing depth distribution. Post depositional movement may also be important.

Thus the assumption of an exponential decrease of activity with depth is a generalisation which is more often than not inaccurate, particularly for long lived radionuclides such as ^{137}Cs . The application of in-situ gamma spectroscopy to the measurement of ^{137}Cs has often involved the assumption of an exponential decrease of activity with depth (ICRU 1993, Zombori *et al* 1992, Winkelmann *et al* 1987, Miller *et al* 1990, Rybacek *et al* 1991, Dickson *et al* 1976, Beck *et al* 1972). Although ICRU 1993 acknowledges the difficulties of this assumption, estimates of exposure rates dependent upon the

assumption of the exponential profile were made. With these estimates, real deviations from the assumed profile have been small. Zombori *et al* (1992) attempts to account for the subsurface maximum within photon fluence equations by the adoption of a positive and negative exponential. However, such subsurface maximum shapes can rarely be described by exponential relationships, and mathematical description of these shapes requires further examination.

The distribution of primordial radionuclides in soil is discussed in chapter 2. The distribution is also dictated by the chemical and physical properties of the soil as well as the activity concentrations of the underlying geological material. In addition, complications occur as a result of disequilibrium in the uranium and thorium decay series particularly by emission of radon and thoron. In summary, Hanson and Stout (1968) observed that Th concentrations tend to be higher in the lower B and C horizons of the soil, whilst U being more mobile is often found in higher concentrations in the top soil. However, in areas of organic rich terrain, very little assimilation of the underlying primordial radionuclides is observed in these often very highly acidic environments which result in the breakdown of clays. In contrast, the distribution of U, Th and K is observed to be uniform with depth in salt marsh environments. In environmental gamma ray spectroscopy, the distribution is often assumed to be uniform with depth and hence concrete calibration pads are used for detector calibration.

This chapter explains the problems of soil core smearing and the need for special coring tools to minimise smearing, and enable cores to be sampled rapidly. Having demonstrated the success of the new tool, soil profiles measured from areas of contrasting environmental characteristics are discussed. The problems of quantifying source burial are explored with different soil profiles with particular emphasis on source attenuation, and thus mass depth is explained and demonstrated. Source burial is quantified in terms of *mean mass depth* (β , g cm⁻²).

Having quantified source burial by β , particularly for ¹³⁷Cs, the spectral characteristics of in-situ NaI(Tl) detectors are examined experimentally. Following Zombori *et al's* (1992) observations, with HPGe detectors, of increases in forward scattering with

primary photon attenuation due to increased point source burial under a tank of water, an experiment with extended layered sources is demonstrated with a NaI(Tl) detector to model the relationship between source burial and the photopeak to valley ratio. Having modelled this relationship in a controlled environment, the application to environmental gamma ray spectrometry is explored. The need for full spectral stripping required experimental verification of the change in stripping coefficients with source burial (simulating low activity organic and water overburden). A similar experiment was undertaken with aerial survey detectors to model the change in stripping coefficients with air path length. Having verified these parameters, a salt marsh environment was examined where the change in source burial was measured from soil samples. Full spectral stripping was undertaken for the in-situ spectra collected at these sites, and a relationship determined between β and the increase in forward scattering relative to photopeak attenuation observed in the spectrum. This relationship was then applied to predict β at other points on the site and used to determine a spectral derived calibration correction factor. This results were compared with soil sample estimates.

7.2 SOIL SAMPLING AND THE DEPTH DISTRIBUTION PROFILE

7.2.1 Objectives

In order to interpret the in-situ gamma-ray spectra collected, an understanding of the radionuclide distribution within the soil column is required. The objective is to determine the depth distribution profile of radionuclides in differing environments and to demonstrate the limitations of using small diameter and sample length corers.

7.2.2 Method

Chapter 2.2 discussed the sampling technique and chapter 5.5.3 the sampling depth required for effective comparison with in-situ and airborne gamma spectrometry. A solution to the sampling depth problem is simply achieved by sampling to 30 cm depth in high density soils and 45 cm in low density organic rich soils. This is adequate for ^{137}Cs activity estimation, as usually most of the activity is found within the top 15 cm

to 30 cm of the soil horizon in terrestrial environments. The exception to this is in salt marsh environments where source burial can be significant, although the contribution to the primary gamma photon fluence at the surface from below 30 cm of the soil is small. For primordial radionuclides, the depth distribution is assumed to be uniform with depth, and thus a 30 cm length sample collected and quantified in terms of Bq kg⁻¹ should provide a representative sample. The problem arises when the activity is buried in low density soils, such as those observed at the Raithburn Valley. Samples of bed rock are not collectable with the available coring tools.

Direct comparisons are made between soil samples collected with the two different coring tools to demonstrate the limitations of the 38 mm diameter corer, particularly when determining the depth distribution profile. In order to make direct comparisons between sites of differing soil compositions, radionuclides and unequal depth intervals, inventory concentrations are expressed as activity per unit mass (Bq g⁻¹).

7.2.3 Results

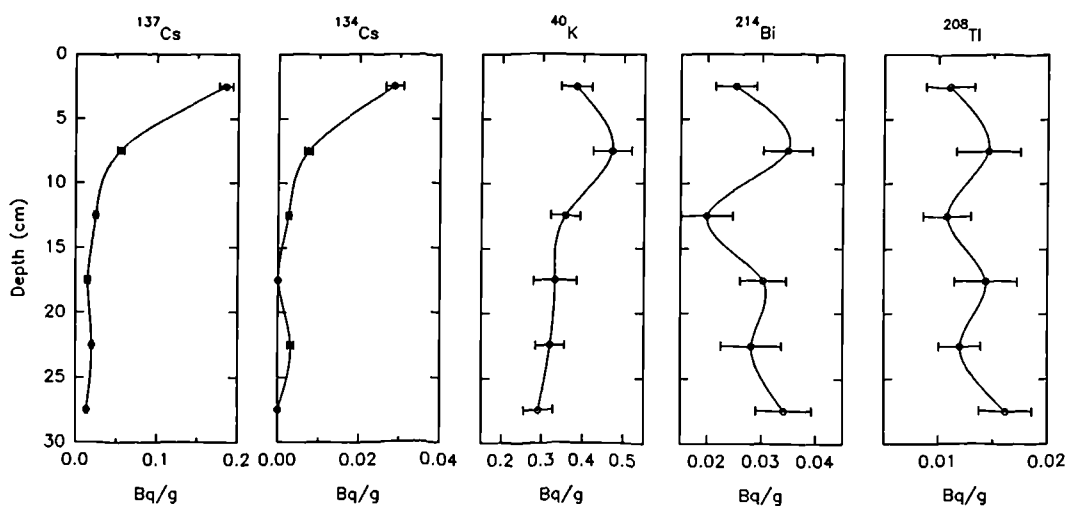


Figure 7.1 Depth distributions of ¹³⁷Cs, ¹³⁴Cs, ⁴⁰K, ²¹⁴Bi and ²⁰⁸Tl for grassland site, SURRC (23/2/90). Samples collected with a 38 mm Leonard Farnell corer.

Figure 7.1 shows the depth distribution profile of ¹³⁷Cs, ¹³⁴Cs, ⁴⁰K, ²¹⁴Bi and ²⁰⁸Tl in loamy soil of a grassland area close to SURRC sampled with the 38 mm diameter corer. The depth distribution profile of ¹³⁷Cs and ¹³⁴Cs clearly demonstrates a rapid decrease

in activity with depth. The increase in activity of ^{134}Cs between 20 and 25 cm depth indicates contamination originating from the upper portions of the soil as a result of a certain amount of smearing in the soil profile. However, generally ^{137}Cs levels appear to have penetrated to greater depths which indicates the presence of aged ^{137}Cs originating from weapons testing fallout of the 1960's and 1970's. For the natural radionuclides the distribution with depth is relatively uniform, with the scatter accounted for by the analytical error.

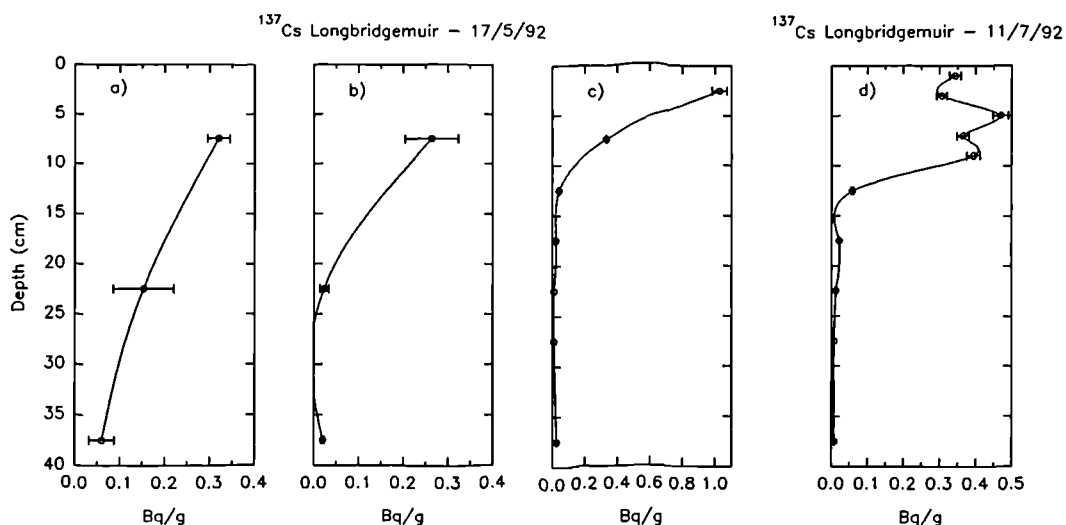


Figure 7.2 Depth distribution profiles of ^{137}Cs in peat determined from a) 38 mm corer - 15 cm intervals, b) 105 mm corer - 15 cm intervals, c) 105 mm corer - 5 cm intervals, d) 105 mm corer - 2 and 5 cm intervals.

Observations from eight separate cores collected within the 2 m x 2 m grid shown in figure 6.3 taken in 15 cm intervals, suggest that except for the surface of the soil column (O horizon < 2 cm) these random fluctuations in the activity with depth are consistent with a uniform activity distribution.

Figures 7.2 and 7.3 display depth distribution profiles obtained from the basin valley peat area at Longbridgemuir. The site as discussed in section 6.2.2 demonstrated considerable localised variability. Figures 7.2 a and b, and 7.3 a and b, show the average of four depth distribution profiles determined at 15 cm interval samples from the 38 mm and 105 mm diameter corers respectively. This demonstrates quite a considerable amount of smearing down the soil profile by the 38 mm corer leading to overestimates of the total inventory originating from below 15 cm. This may lead to

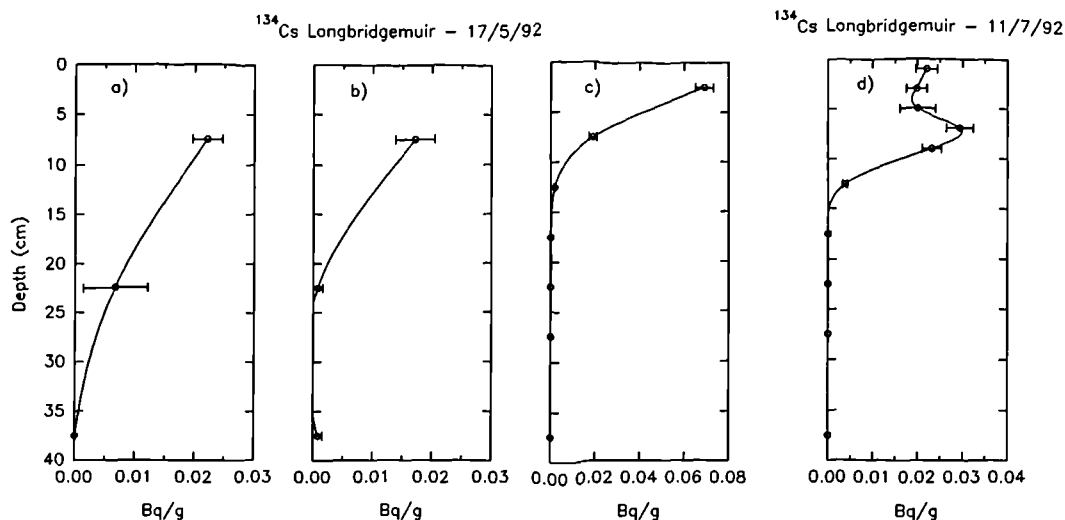


Figure 7.3 Depth distribution profiles of ^{134}Cs in peat determined from a) 38 mm corer - 15 cm intervals, b) 105 mm corer - 15 cm intervals, c) 105 mm corer - 5cm intervals, d) 105 mm corer - 2 and 5 cm intervals.

overestimation of caesium depth penetration and total inventories. In contrast, figures 7.3.b and 7.3.c show that over 90 % of the caesium is found within the top 15 cm of the peat profile.

Choice of the vertical sampling interval is also important in determining this profile accurately. The 15 cm interval suggests a gradual decrease in activity with depth. However, the 5 cm depth interval show that the activity declines quickly within the first 15 cm. A core sample collected 2 months later in dry conditions (figures 7.2 d. and 7.3 d.) and divided into 2 cm intervals showed the presence of a subsurface maximum to between 5 and 10 cm depth from which it declines rapidly to about 15 cm depth. Such detailed depth distributions in peaty environments can be explained by a sequence of processes. The initial deposition of atmospherically derived caesium is followed by diffusion and adsorption. New growth and decay of plant material assimilates the underlying activity into new fresh horizons overlying the original deposition, leading to the production of a subsurface maximum. Comparison of figures 7.2.d and 7.3.d suggests a more complicated history for ^{137}Cs than ^{134}Cs , with multiple depositional events with time. Thus the exponential like decrease with depth suggested in figures 7.2 c and 7.3 c does not result. The magnitude in variation in activity concentrations between the two graphs is an additional consequence of spatial variability due to

deposition and the soil/peat characteristics.

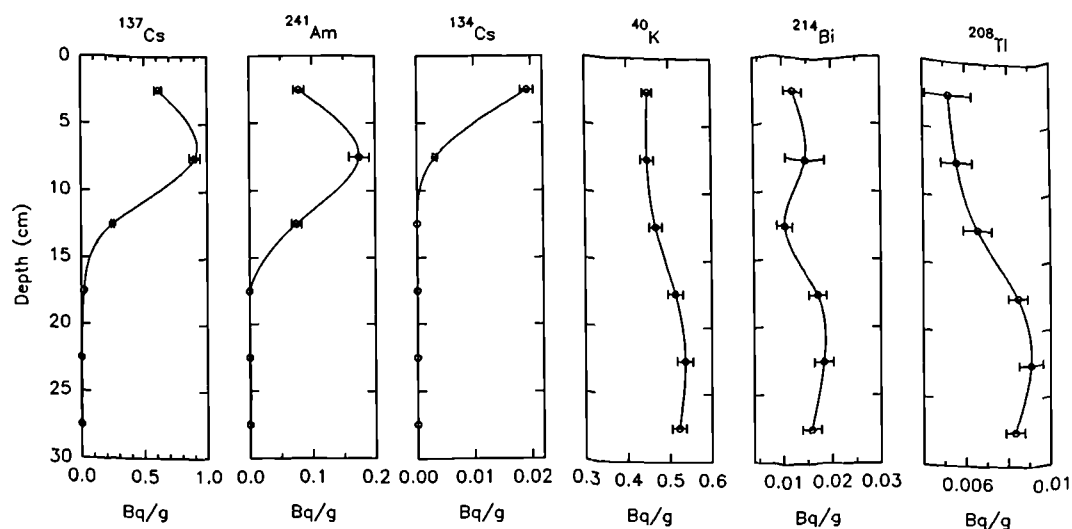


Figure 7.4 The depth distribution profiles of ^{137}Cs , ^{241}Am , ^{134}Cs , ^{40}K , ^{214}Bi , ^{208}Tl at the centre of the Caerlaverock hexagonal sampling site. Position 01. (2/92)

Buried source profiles of anthropogenic radionuclides are observed in salt marsh environments around the Irish Sea coastline. Figure 7.4 shows the source depth profile of ^{137}Cs , ^{241}Am and ^{134}Cs . Clearly the source profile of ^{134}Cs displays an activity concentration similar to that observed from Chernobyl fallout, although there may be a Sellafield component within this which is likely to have decayed away given 10 half lives since the peak Sellafield discharges (BNF 1991). ^{137}Cs and ^{241}Am demonstrate subsurface maxima due to burial of higher contaminated sediments by lower activity sediments in the coastal environment. The maxima represents a remnant of sediments contaminated from peak discharge rates from the Windscale plant in the 1970's subsequently been deposited in salt marshes.

These subsurface maxima in the intertidal zone are observed to vary across the site with proximity to the coast. Figure 7.5 shows the sub-surface maxima for ^{137}Cs and ^{241}Am determined from finer depth intervals, indicating that most of the activity is buried beneath 15 cm depth. The detail of the depth distribution of ^{241}Am is more pronounced than ^{137}Cs , which may be due to the greater chemical mobility of ^{137}Cs .

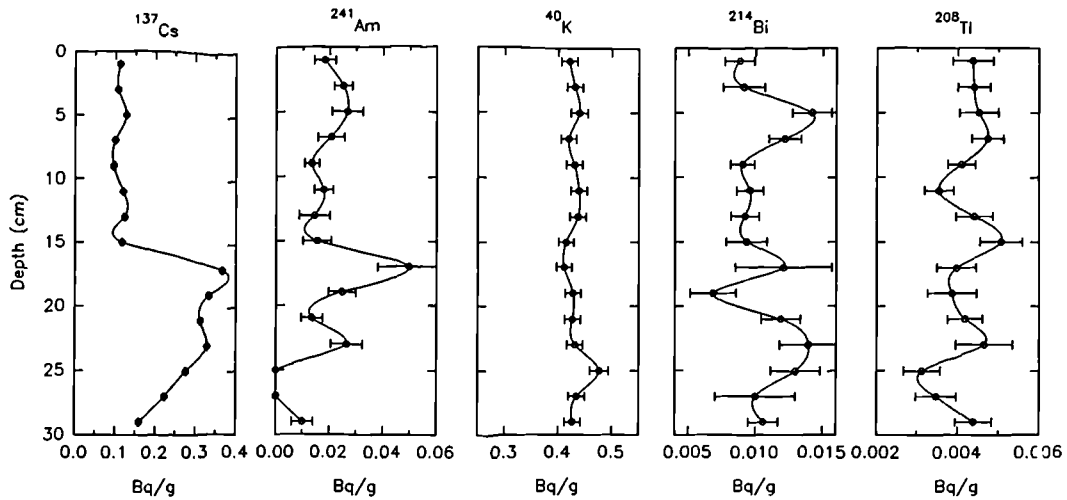


Figure 7.5 The depth distribution profiles at Caerlaverock (position 44) for ^{137}Cs , ^{241}Am , ^{40}K , ^{214}Bi and ^{208}Tl .

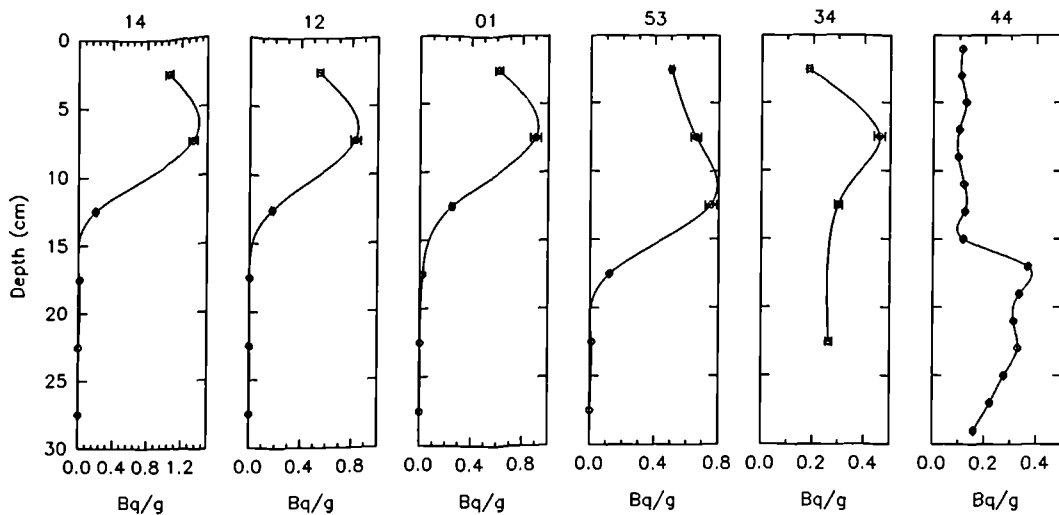


Figure 7.6 Demonstrates a range of ^{137}Cs soil core profiles across the Caerlaverock Calibration area. The sample positions are indicated in figure 4.15.

To demonstrate the variation in subsurface maxima across salt marsh environments figure 7.6 shows ^{137}Cs depth distribution profiles selected across the Caerlaverock site to demonstrate the range in profiles. The sample positions for the cores identified in figure 7.6 are shown in figure 6.15. These results suggest that subsurface maxima exist across the site and become deeper in the soil profile towards the higher energy intertidal area. Also activity concentrations within any single horizon decrease as a whole as the profile becomes deeper, while the total activity concentration is very similar for all

similar for all these locations suggesting that the activity is spread over a greater depth range in the higher energy, greater sediment accretionary rate, intertidal deposits. This is demonstrated in figure 7.7 with samples collected at 128 m spacings across Warton Bank on the Ribble Estuary (Sanderson *et al* 1993b). It also suggests a complex but systematic change in source burial geometry across salt marsh environment.

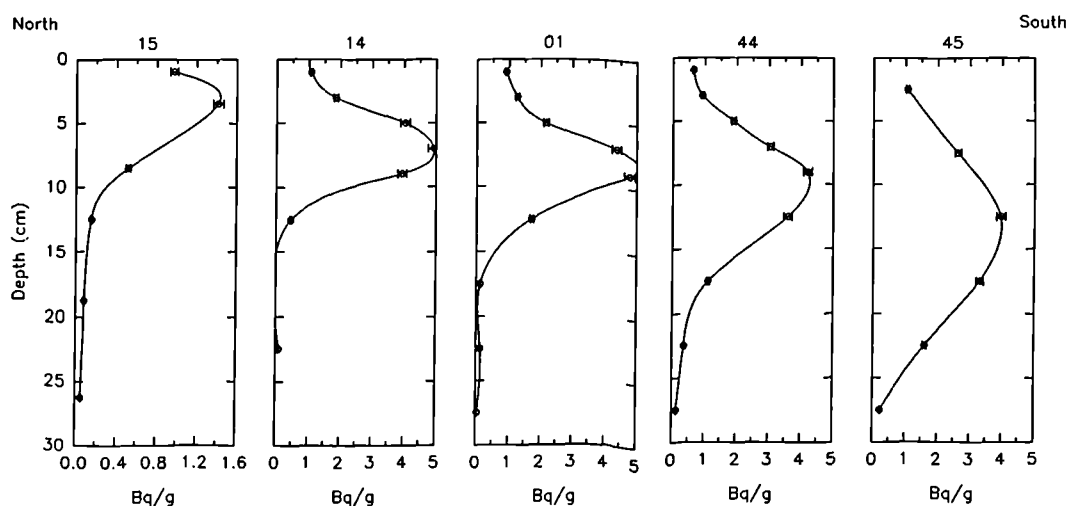


Figure 7.7 The depth distribution profiles of ^{137}Cs across Warton Bank (Ribble Estuary). 128 m spacing between sampling points.

Figures 7.4 and 7.5 show a fairly uniform ^{40}K distribution with depth. ^{214}Bi and ^{208}Tl are more variable although much of this variation is accounted for by analytical error. Thus, as with the SURRC site, a uniform depth distribution was assumed.

7.2.4 Discussion

The sampling technique and tool used are fundamental to the measurement of depth distribution profiles. By comparison with the 105 mm soil corer, the 38 mm corer is proved to be of little use in determining depth distribution profiles and leads to an over estimation of source depth due to smearing and cross contamination between sample depths. This, may lead to overestimation of soil core inventories through resampling at greater depths. Contamination of the corer from the upper levels of the soil profile becomes an inevitability.

The depth intervals chosen for coring with the 105 mm corer are also important for determining depth distribution profiles. Clearly 15 cm intervals are of very little use when the bulk of the atmospherically derived anthropogenic radioactivity is concentrated within the top 15 cm of the soil column. Smaller depth increments of 5 cm show an "exponential like" decrease of activity with depth, whilst 2 cm intervals show the depth profile to be more complicated than would otherwise be suggested.

In salt marsh environments, the depth distribution profile is complicated by its change with proximity to the near shore environment. This leads to a complex source geometry and suggests that the activity associated with peak Sellafield discharges is being continually buried at a rate which is also dependent upon proximity to the coast and the energy of the depositional environment. The shape of the subsurface maxima broadens nearer the coastal edge of the salt marsh. Depth divisions of 5 cm appear to optimise the description of the depth distribution profile, whilst 2 cm depth divisions provide finer detail which is useful for sedimentological investigations.

The primordial radionuclides do show some variability with depth. For the sites illustrated here, the random nature of the variability with depth which is almost within experimental error, suggests that spatially the activity can be assumed to be uniform with depth. On terrestrial locations, only the first two or so centimetres may be assumed to have lower concentrations of primordial activity due to a higher organic content from decaying matter.

Soils on sites with high organic content such as Lakin Farm on the Isle of Arran (Section 6.5) have demonstrated that very little of the underlying activity has been assimilated into the organic rich soil. Activity detected in the soil has been concentrated in the 15-30 cm component of the soil column (sampled with the 38 mm Leonard and Farnell corer). Hence uniform depth distribution cannot be assumed for these sites.

7.3 CALCULATION OF MASS PER UNIT AREA (MASS DEPTH) AND THE MEAN MASS DEPTH (β)

7.3.1 Objective and Theory

This section describes the depth distribution profiles particularly for ^{137}Cs , to enable comparisons to be made and understood with primary photon fluence rates and in-situ spectroscopy between sites with different depth distribution characteristics.

The primary photon fluence rate in soils is a function of the soil density in addition to source depth z . For relating exposure, dose and in-situ gamma spectroscopy with source burial, it is more appropriate to determine depth distribution functions in terms of mass per unit area given by ρz , rather than linear depth (ICRU 1993, Rybacek *et al* 1991). Given that the soil density ρ varies with depth, and the depth intervals selected also tend to vary, and the combined effect will lead to further variations in z , activities should be expressed in terms of activity per unit mass (Bq g^{-1}). Thus the function mass per unit area, defined as x is given by equation 7.2:

$$x = \int_0^z \rho(z') dz' \quad (7.2)$$

where x is the total mass depth or effective mass per unit area (g cm^{-2}) for the soil sample depth provided.

If the activity distribution can be assumed to be a negative exponential with depth, from ICRU (1993) and Rybacek *et al* (1991) the activity distribution with depth $A(x)$ (Bq g^{-1}) is given by equation 7.3:

$$\begin{aligned} A(x) &= A_o \cdot e^{\left(\frac{-x}{\beta}\right)} \\ \ln A(x) &= -\ln A_o \cdot \frac{x}{\beta} \\ \therefore \text{slope} &= -\frac{1}{\beta} \end{aligned} \quad (7.3)$$

where A_o is the activity concentration (Bq g⁻¹) at the surface.

β is the relaxation mass per unit area (g cm⁻²) or mean mass depth.

From Beck *et al* (1972), Miller *et al* (1990), Helfer and Miller (1988), density is assumed to be constant with depth and β is equivalent to ρ/α , where α is the reciprocal of the relaxation length (cm⁻¹) (equation 3.14). However, often considerable change in density is observed with depth in the soil profile. As β will be derived with changes in soil density taken into consideration, the activity per unit area A_a may be obtained by an integration of the specific activity $A(x)$ over the mass per unit area, resulting in equation 7.4 (ICRU 1993, Rybacek *et al* 1991):

$$A_a = \beta \cdot A_o \quad (7.4)$$

As discussed in section 7.2, a subsurface maximum often develops from aged caesium deposits derived from atmospheric deposition and from buried source layers in salt marsh environments. Thus a description of the depth characteristic is required which should ideally be related to previous work and β . Zombori *et al* (1992) proposed a solution to this by combining a positive and negative exponential to describe such buried features. However, the shape of the distributions observed is unlikely to fit exponential profiles. From the discussion thus far:

$$\beta = \left(\frac{\rho}{\alpha} \right) = \frac{x_{1/2}}{\ln 2} = \text{mean mass depth} \quad (7.5)$$

By fitting a polynomial to the subsurface maximum and integrating with respect to mass depth, the mean mass depth can be estimated from equation 7.6:

$$\beta = \frac{\int_0^{\infty} x \cdot A(x) dx}{\int_0^{\infty} A(x) dx} \quad (7.6)$$

where x is the mass depth (g cm⁻²)

$A(x)$ is the activity per unit mass (Bq g⁻¹)

This can be solved by fitting a polynomial curve to the depth distribution $A(x)$ and calculating the mean mass depth from the area under the curve. However, given equal mass depth intervals, this could be simplified to equation 7.7:

$$\beta = \frac{\sum_0^x A(x) \cdot \Delta x}{\sum_0^x A(x)} \quad (7.7)$$

where $A(x)$ can be expressed in Bq g^{-1} and Δx are equal mass depth intervals in g cm^{-2} .

7.3.2 Results and Discussion

The depth distribution profiles are given in terms of mass depth (g cm^{-2}). Characteristic Chernobyl contaminated areas are given by figures 7.8 and 7.9. Figure 7.8 shows the open grass land loamy soil sampled at SURRC. There is a clear decrease in activity with mass depth which when plotted in terms of log activity initially displays an exponential decrease with depth. However, below 20 g cm^{-2} ^{137}Cs is still measurable in significant quantities. ^{134}Cs is also present at 22.5 g cm^{-2} depth which, given its pure Chernobyl origin suggests some smearing within the soil column through sampling with the 38 mm soil sampler.

Given that in terms of activity per unit area, almost 90% of the activity is derived from within the top 20 g cm^{-2} and the potential consequences of core smearing, the exponential was fitted through the top 4 depth intervals giving a mean mass depth of 5.9 g cm^{-2} . Similarly with ^{134}Cs , a mean mass depth of 4.0 g cm^{-2} was calculated. The higher mean mass depth associated with ^{137}Cs suggests a contribution of older and deeper weapons testing fallout within the soil profile.

Figure 7.9 illustrates the mass depth distributions associated with the organic rich basin peat of Longbridgemuir farm. When plotted in terms of mass depth, the lower density soils effectively raise ^{137}Cs in terms of the soil profile.

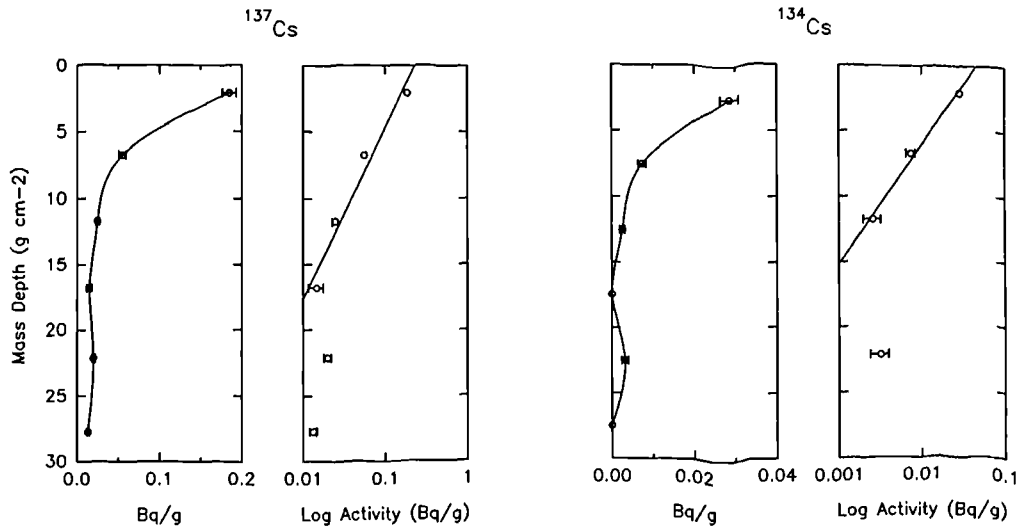


Figure 7.8 SURRC mass depth distribution profiles for ^{137}Cs (5.9 g cm^{-2}) and ^{134}Cs (4.0 g cm^{-2}).

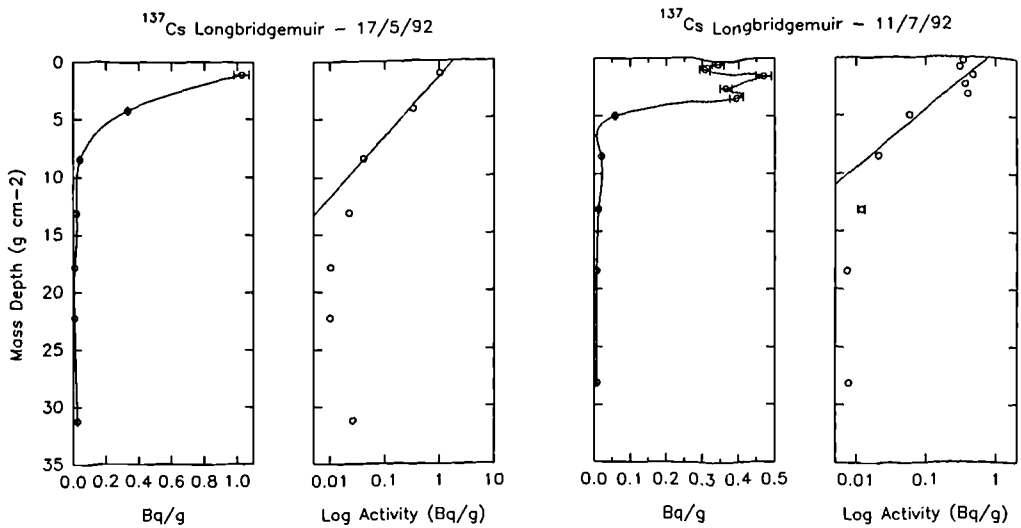


Figure 7.9 Longbridgemuir mass depth distribution profiles for ^{137}Cs on 17/5/92 (2.3 g cm^{-2}) and 11/7/92 (2.6 g cm^{-2}).

As with the SURRC site, when plotted in terms of log activity concentration, the 17/5/92 profile initially displays a rapid decrease in activity with depth (figure 7.9). However, ^{137}Cs activity is still significant at lower depths which must be attributed to weapons testing fallout as well as Chernobyl derived caesium which has not been adsorbed onto organic surfaces. Nevertheless, over 90% of the activity is found in the top 10 g cm^{-2} . Thus the exponential profile is fitted to the top three points providing a mean mass depth of 2.3 g cm^{-2} . However, figure 7.9 shows that a second exponential

could be used to describe the deeper parts of the activity distribution.

The second detailed profile collected later in drier conditions within 8 m of the above core on 11/7/92 and divided into 2 cm sections displays a subsurface maximum within the first 5 g cm⁻². The activity then decreases very rapidly with depth. This is again illustrated in terms of log activity (figure 7.9). By fitting the exponential line through the surface points from which over 90% of the activity is concentrated, a mean mass depth of 2.6 g cm⁻² can be approximated. The sub-surface maximum occurs at about 2 g cm⁻², which suggests that about 14 % of the photon originating from this layer will be attenuated. Above and below 2 g cm⁻², lower activity concentrations are observed, and although a reasonable regression is fitted, this can only approximate the observed depth distribution profile. Such observations do illustrate that the depth distribution profile is more complicated than suggested by the simple exponential depth distribution profile, and although such subsurface maxima influences may be small in such organic rich areas, similar observations in higher density soils are likely to be more important. Within site variability of mean mass depth was also observed at the Longbridegmuir calibration site. As with spatial variability of activity estimation, mean mass depth (β) was also observed to vary from 2.27 g cm⁻² to about 4.83 g cm⁻² sampled at 128 m spacing. This provided a mean β of about 3.55 ± 1.2 g cm⁻². Similar observations by Bachhuber *et al* (1985) showed that the K_d values for ¹³⁷Cs and other radionuclides varied significantly within a 150 m x 100 m area, leading to a significant variation in the depth distribution profile.

The effect of the subsurface maxima can be vividly observed in salt marsh environments. Figure 7.10 illustrates the mass depth profiles for the Caerlaverock samples as given in figure 7.6. Similarly the mass depth distribution profiles across the Warton Bank site are shown in figure 7.11. The incorporation of density effectively lowers the distribution in the soil profile as sediment density is generally greater than 1 g cm⁻³.

The depth distribution intervals were not equal and with the added consequence of changing soil density, polynomial curves were fitted to each depth distribution. By

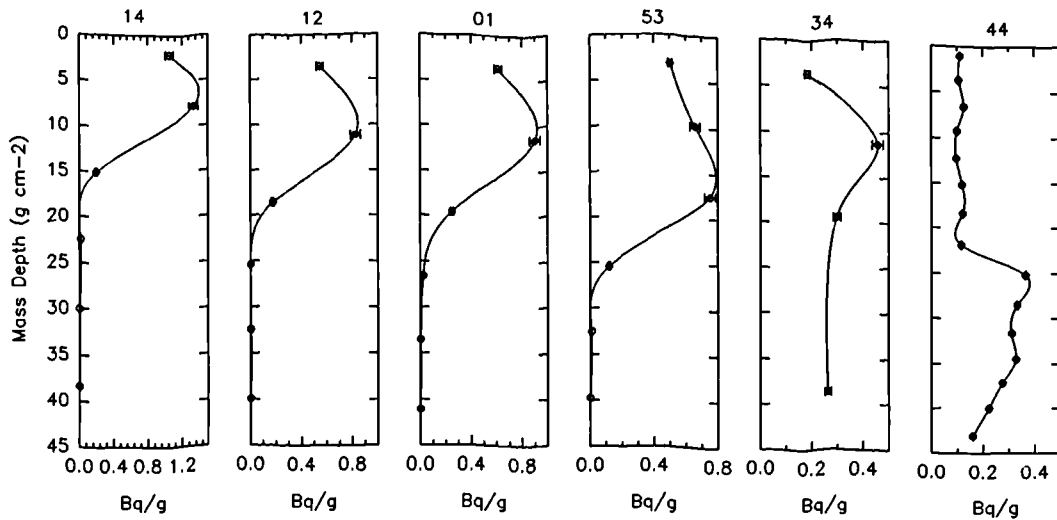


Figure 7.10 Caerlaverock mass depth ^{137}Cs profiles: 14 (7.20 g cm^{-2}), 12 (10.78 g cm^{-2}), 01 (11.24 g cm^{-2}), 53 (13.23 g cm^{-2}), 34 (20.7 g cm^{-2}) and 44 (26.50 g cm^{-2}).

implementing log fits and 4th or 5th order polynomials, curves can be fitted to almost any depth distribution shape although there are exceptions such as Caerlaverock sample 44. However, polynomial curves often underestimate activity between points with large depth intervals, leading to underestimation of the mean mass depth. Simple curves such as that illustrated in figure 7.11 sample 45 require no log relationships.

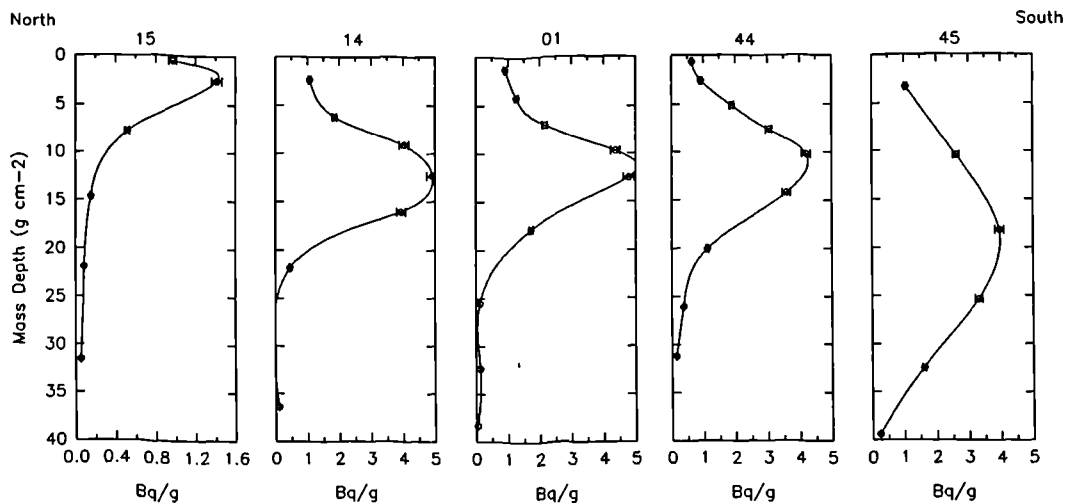


Figure 7.11 Warton Bank mass depth ^{137}Cs profiles: Sample 15 (7.69 g cm^{-2}), 14 (12.97 g cm^{-2}), 01 (12.66 g cm^{-2}), 44 (13.17 g cm^{-2}), 45 (19.74 g cm^{-2}).

However, in almost all cases, given the complex profile shapes, the mean mass depth was calculated graphically. Although slightly subjective, this provided a simplified

means of describing the more complex depth distribution profiles. The results are given in figures 7.10 and 7.11.

7.3.3 Summary

The shape of the subsurface maximum varies considerably with mode of ^{137}Cs deposition and within sites, particularly in salt marsh environments. Quantification of the subsurface maximum requires careful sampling techniques. Fluence rates observed at the surface are dependent upon source burial which has been quantified here in terms of *mean mass depth* (β , g cm^{-2}) which takes into consideration soil density which provides a defined parameter important for making comparisons of effective source burial between environments. The parameter β is, however, restricted in that it is unable to parameterise a second important function of source burial, that of profile shape. Source burial and profile shape are likely to have a significant influence on fluence rates.

7.4 MEAN MASS DEPTH AND PRIMARY PHOTON FLUENCE RATE

7.4.1 Objective and Theory

This section demonstrates the change in the primary gamma photon fluence from the surface of the soil profile with changes in the mean mass depth, water content and the shape of the depth distribution profile. The consequences of changes in the mean mass depth on detector response are demonstrated. Much of this investigation is applied to salt marsh environments. Given the smaller sampling errors (described in chapter 6) and significant changes in source burial, salt marsh environments were chosen to demonstrate the influence of source burial on photon fluence.

To demonstrate the dependence of detector response on the mean mass depth, a portable NaI(Tl) gamma spectroscopy system described in section 3.5, was used at 1 m above the ground. A spectrum was collected with times of between 600 to 1000 seconds providing counting statistics of better than 2 %. At each site a core was collected with

the 105 mm diameter soil corer to a depth of 30 cm. Several of these cores were subdivided into 2 and 5 cm intervals. At Caerlaverock six cores were chosen at random across the calibration site. At Warton Bank, the cores were collected in sequence to provide an estimate of the change in the mean mass depth across the site. A single core and in-situ measurement were collected at the Kirkconnel salt marsh (River Nith, Dumfries). The remaining 25 cores at Caerlaverock were divided into 15 cm intervals and an in-situ spectrum was collected at each position. Additional cores collected at Longbridgemuir and SURRC are also used in this comparison.

Sampling errors measured on the salt marsh are considered to be of the order of 10 %, although as measured at Warton Bank, this can be dependent upon proximity to drainage channels, where sampling errors of as much as 20 % were measured (Sanderson *et al* 1993b). Spatial matched inventories observed at Caerlaverock provide sampling errors of the order of about 12 %. The errors on stripping coefficients due to slight variations in the primordial source burial characteristics are assumed to be negligible, given the relatively uniform depth distribution of the natural radionuclides observed in section 7.2. The error on the mean mass depth is estimated to be better than 5%.

The detector sensitivity τ (or calibration coefficient) is calculated as:

$$\tau = \frac{\text{Detected stripped counts per second (CPS)}}{\text{activity concentration per unit area (kBq m}^{-2}\text{)}} = \frac{N}{A_x} \quad (7.8)$$

Thus as the source is buried in the soil or sediment profile, the fluence rate will be reduced through self absorption. There is therefore likely to be a relationship with the mean mass depth (β) as calculated in section 7.3. In addition, the shape of the source profile must also have a bearing on the relationship between τ and β . Thus given a set of site characteristics in terms of source burial, this section will illustrate the combined use of detector and soil inventories to predict the mean mass depth across a merse site.

In addition, the change in soil water content and its influence on the mean mass depth is briefly examined and discussed. The subsequent change in detector response with

mean mass depth is also examined. Appendix F also discusses the temporal change in detector response with changes in soil moisture content.

7.4.2 Results and Discussion

The results from the Caerlaverock National Nature Reserve *mass-depth* distribution profiles and detector response are shown in figure 7.12. The error estimates on the detector response functions are dominated by the sampling errors observed at the centre of the site. Although these sampling errors may vary, they are assumed to remain at about 10% for the purposes of this discussion.

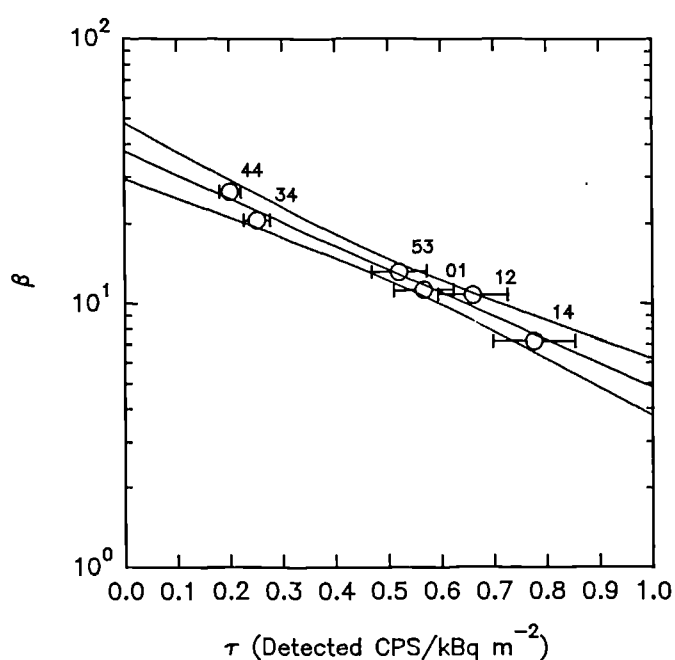


Figure 7.12 The detected activity with the log of *mean mass depth* (β) of ^{137}Cs at Caerlaverock Salt Marsh.

A relationship between the sampling points and in-situ detector response can be best described by an exponential as shown in figure 7.12. Given an estimated error on τ of about 10 % (1σ), the relationship demonstrated in figure 7.12 provides a good description of the behaviour of τ with respect to β and can be described by equation 7.9:

$$\begin{aligned} \log \beta &= \log \beta_o + m \cdot \tau \\ &= 1.58 - 0.892 \cdot \tau \end{aligned} \tag{7.9}$$

where τ is the detector response and β is the mean mass depth (g cm^{-2}). This relationship suggests that at a mean mass depth of 37.7 g cm^{-2} , no primary photon fluence would be detected at the sediment surface.

Given this relationship, a comparison with other salt marsh sites can be made. A soil sample and in-situ spectrum were collected from Kirkconnel Salt Marsh on the River Nith. The soil sample was sub-divided into 2 and 5 cm depth intervals and the depth distribution profile is shown in figure 7.13. The subsurface maximum is broader and "squarer" than previously observed at the Caerlaverock sites, although this sample has more detailed sampling divisions. The calculated mean mass depth for this core is 9.02 g cm^{-2} . From equation 7.9, the predicted value is 7.33 g cm^{-2} . This suggests that the broader subsurface maxima observed at Kirkconnel, as might be expected, provides a higher detectable fluence rate. However, when plotted with the Caerlaverock site, as shown in figure 7.14, the overall result is in close agreement with the equation 7.9, especially when soil sampling errors are taken into consideration.

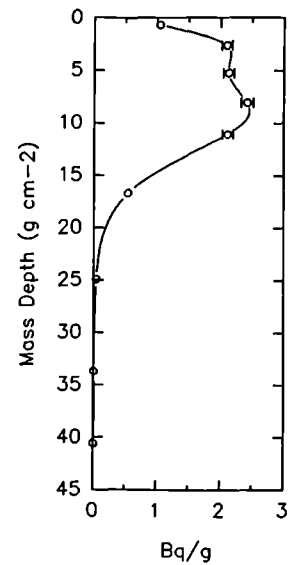


Figure 7.13 ¹³⁷Cs Mass Depth Profile at Kirkconnel.

Figure 7.14 also shows the relationship between the Warton Bank data set and the Caerlaverock sites. Only two of the Warton sampling sites correspond with the Caerlaverock sample set. This can however, be explained by the torrential rain during the sampling period and rising tide experienced during the middle of the day, creating areas of standing water. Thus a greater attenuation of the primary gamma fluence is observed. The Warton sites which do correlate with the Caerlaverock data set were sampled at the beginning and end of the sampling day.

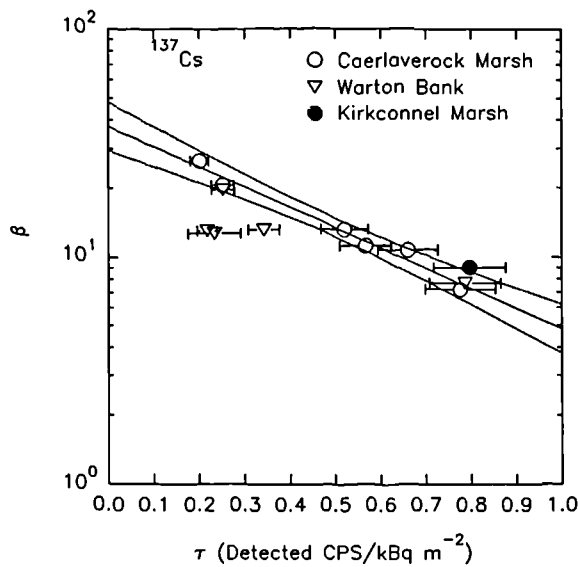


Figure 7.14 The correlation between Caerlaverock, Kirkconnel and Warton Bank salt marsh characteristics.

based gamma spectrometric analysis. The other sampling sites at Caerlaverock were subjected to this method and table 7.1 gives the results. The results show the mean mass depth increases as one approaches the near shore environment of the Solway coast. Transect 1 represents the data from the centre of the salt marsh heading north inland, and the decrease in the mean mass depth indicates shallower source burial. Similarly, transect 4 represents the observations from the centre of the salt marsh south towards the Solway coastline, and the mean mass depth increases. Only position 45 (transect 4: hexagon 5) has a lower mean mass depth than suggested by the geographical trend. This sample was collected within the marine sediments outside the salt marsh itself and is likely to have different source burial characteristics. The sampling plan as shown in figure 6.9 demonstrates how the other four transects corroborate these observations.

The results in table 7.1 suggest that the mean mass depth does not significantly change until the sample spacing reaches 128 m. This may therefore have a bearing on aerial survey calibration. These data can be used to predict the mean mass depth (β) for each aerial survey detector observation over the calibration site.

Given this exponential relationship which provides estimates of the mean mass depth, it is possible to predict the mean mass depth at other salt marsh locations given the stripped photopeak counts of the portable gamma ray spectrometer and the total activity per unit area (kBq m^{-2}), determined from soil samples, for each sampling location. This facility saves valuable time in determining mean mass depth through soil core sectioning and laboratory

Table 7.1 The Change in Mean Mass Depth (g cm^{-2}) across the Caerlaverock Calibration Site.

Transect No.	Hexagonal Shell No : Spacing m					
	0:0	1:2	2:8	3:32	4:128	5:256
1	11.75	10.87	9.71	9.68	7.64	4.28
2		11.45	10.99	10.83	7.96	6.29
3		10.4	13.86	12.54	22.47	20.79
4		12.47	11.72	14.09	25.43	16.49
5		12.07	11.38	12.94	19.64	25.45
6		12.23	11.02	10.43	1.58	6.31
Mean	11.75	11.58	11.45	11.75	14.12	13.27
1 σ	1.2	0.75	1.25	1.55	8.81	8.10
St.Err.		0.31	0.51	0.63	3.60	3.31

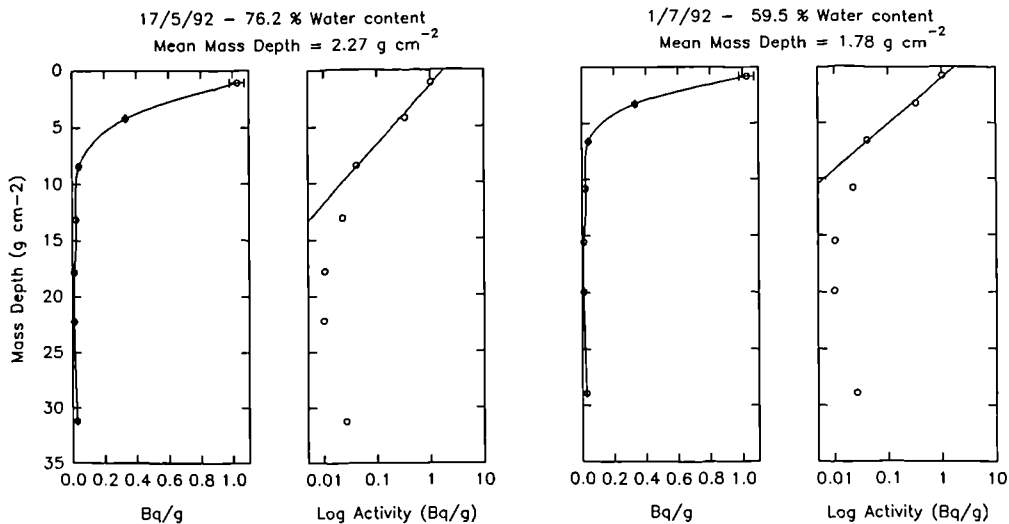


Figure 7.15 The change in mean mass depth with 0-15 cm water content at the centre of the Longbridgemuir calibration area.

Water content in soil contributes to the soil density and thus also the mean mass depth of activity distribution in the soil. As water content increases, bulk density increases until the soil saturation levels are reached. However, soil water content which reaches soil saturation is rarely achieved apart from during or immediately after torrential rainfall has been absorbed into the surface layers of the soil. Two mass depth observations are shown in figure 7.15 for the Longbridgemuir basin peat calibration area. The two soil cores were taken on the dates indicated. The first core was divided into 5 cm intervals and the water content was calculated after drying. The second

sample was collected about 1.5 months later and within a few centimetres of the first and divided into 15 cm intervals and the water content calculated after drying. The inventory was calculated for the 0-15 cm component of the two cores and found to be equivalent. However, the water content for the 0-15 cm components of the soil column was quite different, whilst the 15-30 cm component was essentially the same (about 84 %). The water content of the second core was used to estimate the new β for the first core under similar conditions, resulting in a reduction in β from 2.27 g cm⁻² to 1.75 g cm⁻². Given the inherent site variability, this value probably carries a 20 % error, although it does serve to illustrate the potential change in value of the mean mass depth.

However, the change in water content from 76.2 % to 59.5 % produced a change in detector response from 16.75 to 23.83 stripped cps. This is shown in figure 7.16.

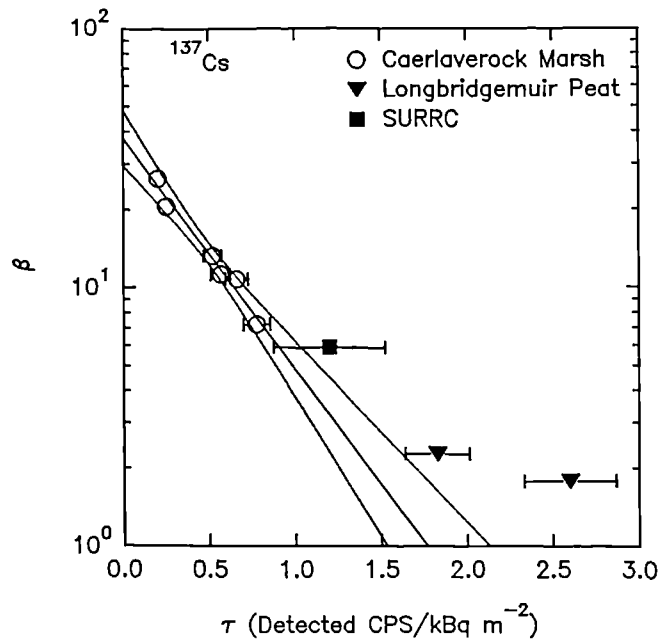


Figure 7.16 The relationship between soil profiles with "exponential" mass depth distributions with those of subsurface maxima.

The detector response associated with the SURRC site is also demonstrated in figure 7.16. The detector response characteristics are clearly different from those associated with subsurface maxima of salt marsh environments. Under such circumstances, the depth at which most of the primary gamma photons are attenuated can be predicted after a certain maximum mass depth β has been passed by the subsurface maxima, assuming

a certain maximum mass depth β has been passed by the subsurface maxima, assuming no activity in the overlying sediments. A definite maximum detector response can be expected for a surface distribution ($\beta = 0 \text{ g cm}^{-2}$). However, if β tends to infinity because of a uniform depth distribution, a definite minimum detector response can be predicted. Thus the shape of the source distribution profile is important, and as indicated by figure 7.16, the incorporation of other distributional profiles as β tends to zero, suggests that the relationship between τ and β may not be simply log linear. Further detailed investigations are required to determine these possible relationships.

Given the wide potential variation of soil type and the added complications of migration of radionuclides within the soil profile with the age of the deposit, the mean mass depth is likely to be highly variable as demonstrated here and by other authors such as Miller *et al* 1990 and Zombori *et al* 1992. Changes in water content in temperate climates such as the UK's, suggest that β will have a temporal dependence. The extent of this temporal change is likely to depend on soil type, pore space and water holding capacity. Hence peaty soils are likely to have a greater temporal change than clay rich soils. The likely variation of detector response with soil moisture content can be simply determined by plotting a series of in-situ measurements taken in the same location with time, rainfall and atmospheric temperature measurements. Such observations have been made and are discussed in Appendix F.

7.5 EXPERIMENTAL MODELLING OF IN-SITU SPECTRAL OBSERVATIONS WITH BURIED SOURCES

7.5.1 Objective

This section characterises the change in detector spectral response with simulated source burial. This will enable primary photon attenuation and scattering characteristics of the secondary photons through the detected spectral response characteristics to be used to determine changes in the radiation field and in particular, the prediction of source burial and thus the mean mass depth from spectral observations. This could ultimately lead to calibration corrections.

7.5.2 Principles

As demonstrated in section 7.4, relative changes in the photopeak attenuation can be directly related to source depth characteristics such as the mean mass depth β . In principle, because the linear attenuation coefficient (μ) decreases with increasing photon energy, a change in the ratio of two preferably energetically distant photo-peaks from the same radionuclide would indicate a change in source burial characteristics. Much work has already been undertaken in this field particularly with in-situ HPGe detectors (Rybacek *et al* 1991). The use of in-situ HPGe detectors greatly facilitates this application because of their high energy resolution and the lack of interference between photopeaks. The 662 keV photopeak of ^{137}Cs and the 32 keV X-ray of its daughter product $^{137\text{m}}\text{Ba}$ have been used successfully in the determination of source burial. Rybacek *et al* (1991) determined a relationship between the depth parameter α (cm^{-1}) and the ratio between the 662 keV and 32 keV photo-peaks. However, as discussed in chapter 5, the mass attenuation coefficients (μ_{m}) for photopeak energies below 200 keV are particularly vulnerable to changes in the chemical composition of soils. Thus at best, the application of the technique described by Rybacek is likely to be highly site specific. This approach may only be useful in the surface layers of the soil due to rapid attenuation of the 32 keV X-ray.

As a consequence of source mass depth burial, or increase in the air path-length, a reduction in the primary gamma photon flux will result in a build up of the scattered photons within the radiation field and can thus be observed in the gamma ray spectrum. Figure 7.17, as also discussed in chapter 3.7, is a schematic representation of a gamma spectrum typical of a single photon energy emitting radionuclide such as ^{137}Cs or ^{40}K . The spectrum is made up of three principal components, the photopeak, the Compton continuum and the forward scattering component.

Zombori *et al* (1992) used the photopeak to valley height (forward scattering component) ratio to determine a relationship with point source burial. He used a HPGe detector for his experimental observations. The advantage of using a semiconductor detector over scintillation detector principally lies with the better energy resolution. As

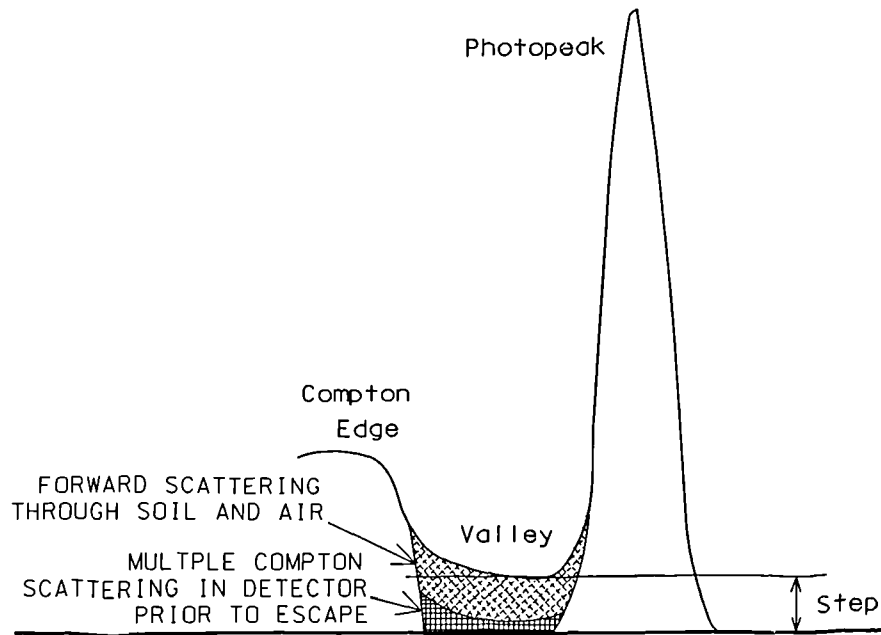


Figure 7.17 Schematic representation of gamma ray spectrum observed from a pure source such as ^{137}Cs or ^{40}K .

the valley is attributed to the scattering within the soil, air and can, then with constant air path (eg. at 1 m above ground) an increase in source depth will result in a relative increase in valley height with respect to photopeak height.

This section demonstrates the spectral-source behaviour characteristics through experimental observations with a NaI(Tl) detector and an extended layered ^{137}Cs source, to determine whether spectral derived relationships can be determined to quantify source burial.

7.5.3 Method

The installation of the concrete calibration pads used for these experiments is discussed in Appendix G. The design and construction of the ^{137}Cs extended layered source is described in Appendix H. The choice and description of absorber material from a variety of plastics, wood and gypsum plaster board required for these experiments to simulate water, peat and/or air column is given in Appendix I. Perspex was chosen as the most appropriate absorber material as it provided very similar μ_m properties to that

of peat, water and air and Beck's soil composition (Beck *et al* 1972) for energies above 150 keV and is easily defined chemically.

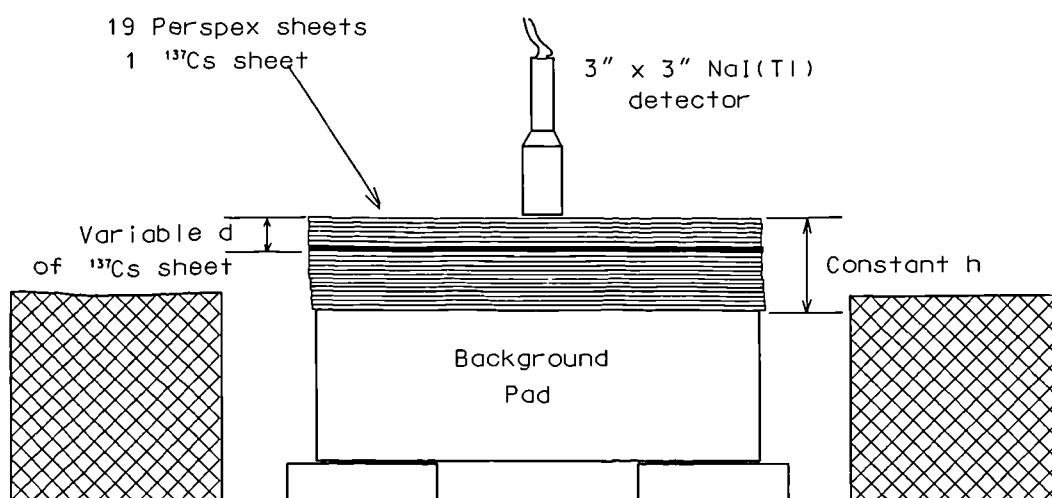


Figure 7.18 The method for measuring the change in detector response with source burial.

Figure 7.18 illustrates the experimental set up. The 3" x 3" NaI(Tl) detector was kept at the centre and at a constant height of 20 cm above the background calibration pad. A background spectrum was collected with 20 perspex sheets (total thickness 20 cm) separating the detector from the pad. The top sheet was then removed and replaced by the ^{137}Cs sheet and another spectrum collected from the same position. The ^{137}Cs sheet was then moved down one sheet in the profile so that it was covered by one perspex sheet and another spectrum was collected. This was repeated until the ^{137}Cs sheet was buried by 19 perspex sheets.

After each spectrum was collected, the region of interest data for the ^{137}Cs window was noted to determine counting statistics. The counting time was chosen to keep counting statistics below 3%. The background spectrum was then subtracted from each spectrum so that the pure ^{137}Cs spectra could be analysed.

The experiment is limited in that the source does not represent an infinite plane as experienced in the field, although the use of an extended layer source is a considerable improvement over a point source. However, its principal aim is to determine the

possibility of using the photopeak/valley-step ratio to characterise source burial. Also, by summing the contributions with appropriate weighting from each depth interval, the spectral characteristics associated with different source depth profiles can be modelled.

7.5.4 Results and Discussion of the Determination of Source Burial from Spectral Characteristics

The background spectrum was subtracted from each spectral measurement with source depth. The results for the spectral response below 1000 keV are given in figure 7.19. As expected, as the source is buried within the profile there is an increase in the overall attenuation of the photopeak and scattered portion of the spectrum. However, as shown the scattered portion of the spectrum increases relative to the photopeak. This is shown when plotting the spectra with a normalised photopeak and is shown in figure 7.20.

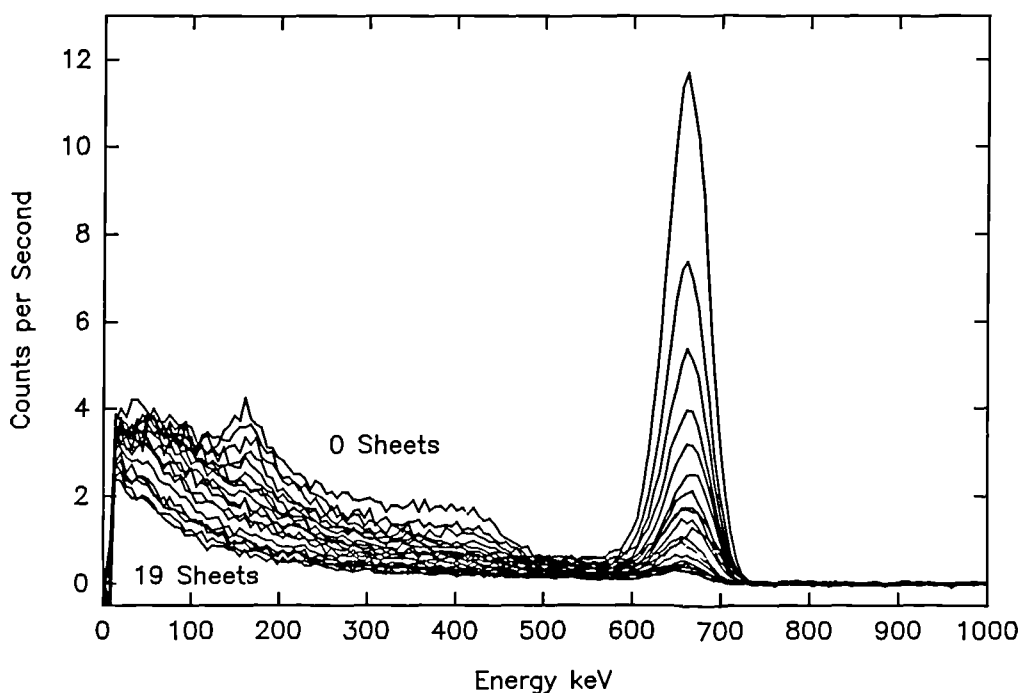


Figure 7.19 The true net spectral response from the ^{137}Cs sheet with burial

Figure 7.20 shows the increase in the valley component of the spectrum relative to the photopeak as the sheet source is buried beneath the perspex sheets. From this evidence, a relationship between photopeak/valley-step ratio and source burial may be found.

The valley height was calculated as the difference between the mean counts collected

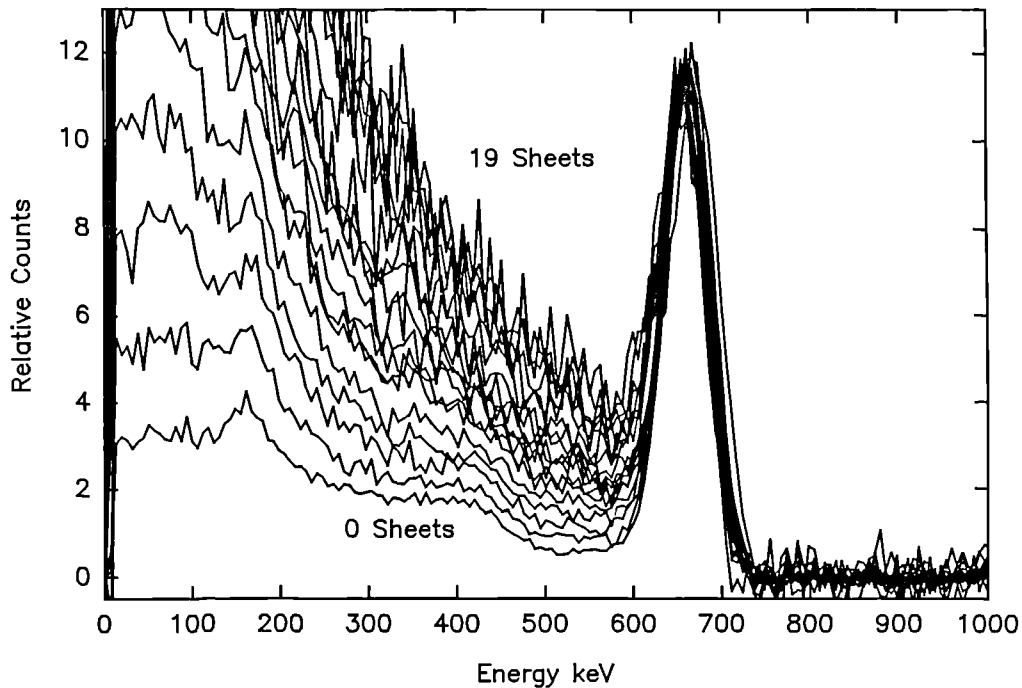


Figure 7.20 The change in spectral characteristics with increasing source burial relative to the photopeak.

per channel between channels 88 to 100 (500 to 575 keV) in the valley, and channels 126 to 130 (736 to 760 keV) in the region to the right of the photopeak. The error on these values was calculated as the standard deviation (1σ) within each region. The errors range from 10 to 20 % for the mean valley estimate and up to 300 % for the estimate of the plateau to the right of the photopeak. The total error on the valley step size was calculated as the sum of these absolute errors. This resulted in an error estimate ranging from about 11 to 27% on the step size. The error on the photopeak was calculated in terms of counting statistics and ranged from 0.6 to 2.5%.

The results of the photopeak/Valley-step ratio against source burial (number of sheets) are illustrated in figure 7.21. There is a clear exponential relationship described by equation 7.10:

$$\text{Log}N = 1.495 - 0.0133 \cdot \frac{P}{S} \quad (7.10)$$

where N is the number of sheets and P/S is the photopeak/valley-step ratio.

Thus clearly the photopeak/valley-step ratio has a direct relationship with source burial

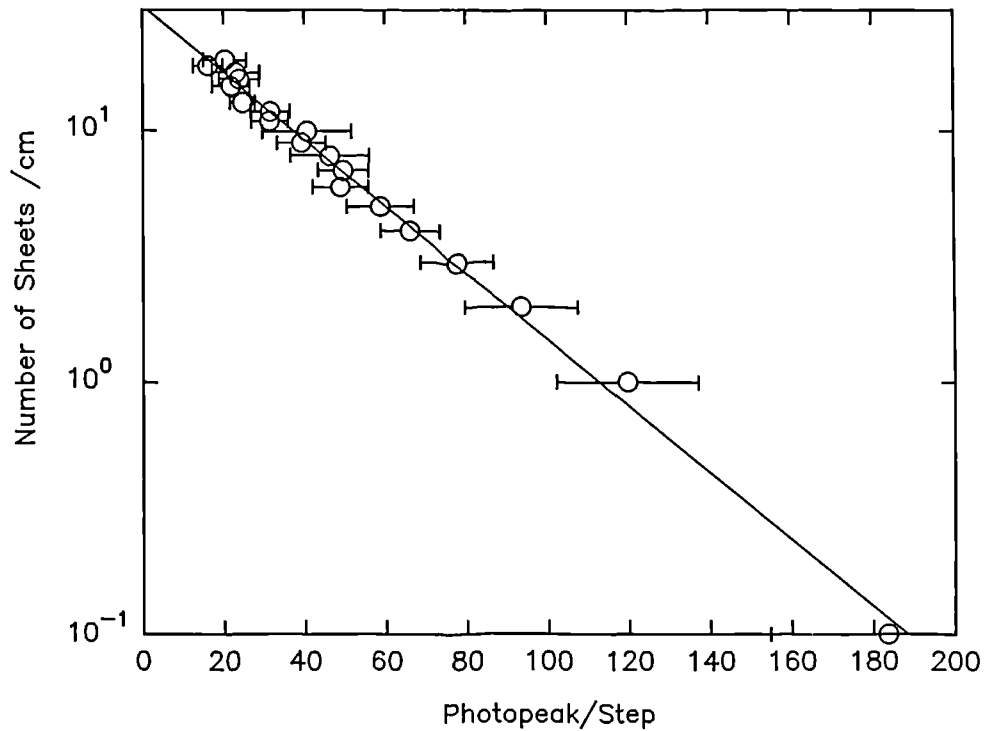


Figure 7.21 The change in the photopeak/valley step ratio with number of perspex absorber sheets. *n.b. for 0 sheets a cover of 1 mm paint was assumed.*

characteristics in the field for constant detector height.

The same data set can be used to determine the change in the detector response with change in source burial shape characteristics. Figure 7.22 shows two different source distribution characteristics, both with a mean depth of 4.215 cm. A total of 406.5 kBq is distributed with depth as shown.

The resultant accumulated detector response is shown in figure 7.23. The subsurface maximum leads to a greater scattered portion of the spectrum compared with the photopeak than that observed with the exponential distribution of activity with depth. An infinite source plane is likely to exaggerate this difference. However, this clearly shows that the shape of the source depth characteristics is important in determining the source depth characteristics from spectral information. Thus each spectral shape is unique and dependent upon source activity and burial characteristics.

However, given particular environmental contexts, such as salt marsh environments, where depth and shape of subsurface maxima are dependent upon structural controls

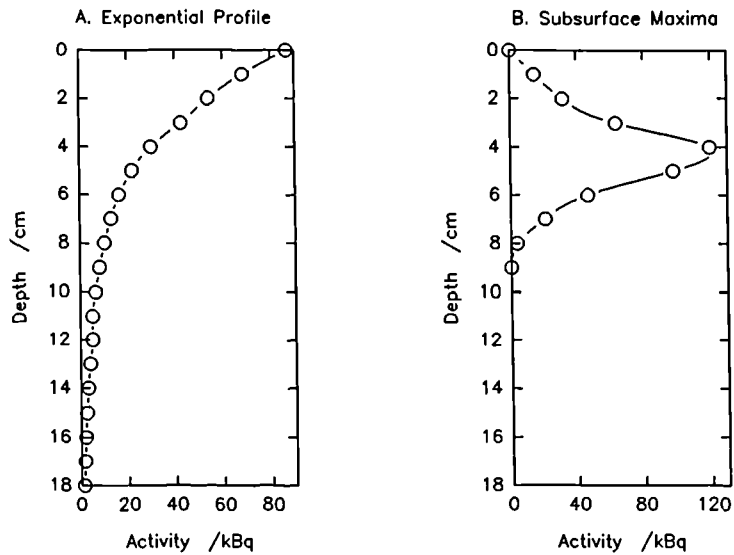


Figure 7.22. Two different depth distributions, both totalling 406.5 kBq and with mean depths of 4.215 cm.

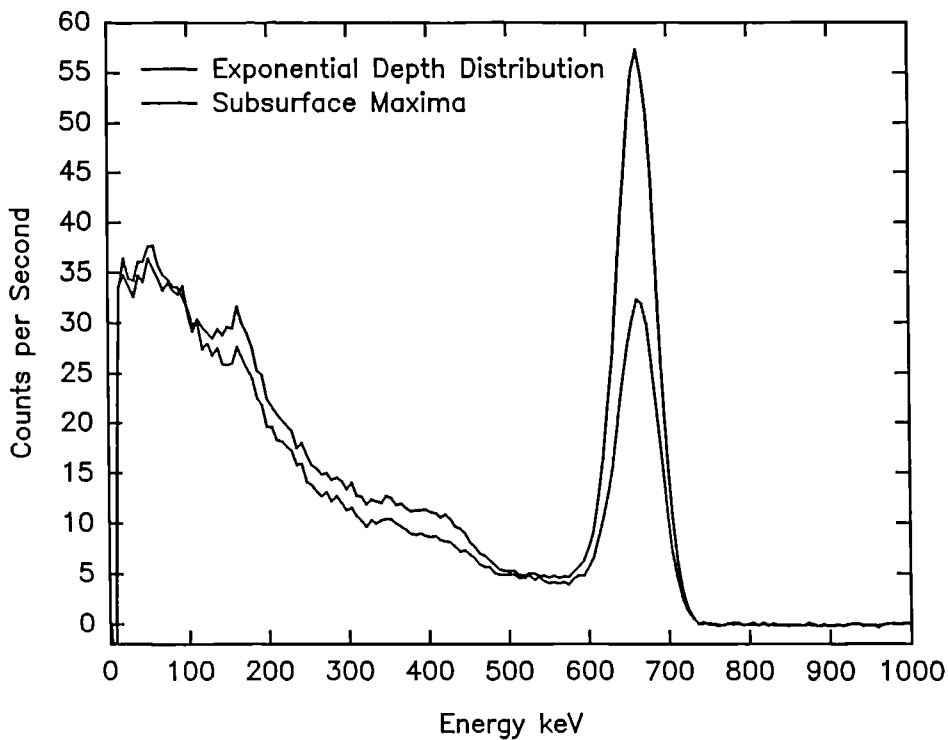


Figure 7.23. Both profiles have a mean depth = 4.215 cm. Total activity distribution 406.5 kBq. Note the greater scattering relative to the photopeak associated with the subsurface maximum.

dictated by site parameters (ie. tidal), it should be possible to determine the change in the mean mass depth from spectral information. However, such investigations are dependent upon a zero background. Alternatively, the background has to be subtracted

and spectral interferences have to be stripped away from the total spectrum to leave the ^{137}Cs net spectrum. The stripping of the primordial radionuclide and ^{134}Cs contributions from the spectra in the correct proportions is important and thus its dependency on source characteristics such as overburden and air path length needs to be investigated to verify its application to full spectral stripping.

7.6 EXPERIMENTAL MODELLING OF THE CHANGE IN STRIPPING COEFFICIENTS WITH SOURCE BURIAL

7.6.1 Objective

To determine whether it is possible to estimate mean mass depth from NaI(Tl) spectral derived data for particular environmental contexts it is beneficial that full spectral stripping can be accomplished. To verify the validity of such stripping aims, the change in stripping characteristics with source burial should be investigated. The change in μ with photon energy suggests that the stripping coefficients used to deconvolute spectral information with NaI(Tl) scintillation detectors are likely to change when absorbing media such as peat and/or water cover the geological substrata or when there is an increase in the air path-length. This section investigates the degree of change and thus the tolerance of the stripping coefficients for in-situ detectors. A similar experiment was also undertaken for aerial survey detectors to simulate air pathlength and is discussed in Appendix J.

In addition, these experiments show the dependency of the stripping ratios for ^{137}Cs and ^{134}Cs with ^{40}K , and thus the influence that changes in source burial can have on the quantification of the anthropogenic radionuclides. This demonstrates the stripping dependency of the observations made in the Raithburn valley.

7.6.2 Method

The installation of the calibration pads and choice of absorber materials is discussed in Appendices G and I. Figure 7.24 shows the experimental set up. The source does not

represent an infinite field and hence direct linear comparison between the number of sheets and source burial in the environment cannot be made.

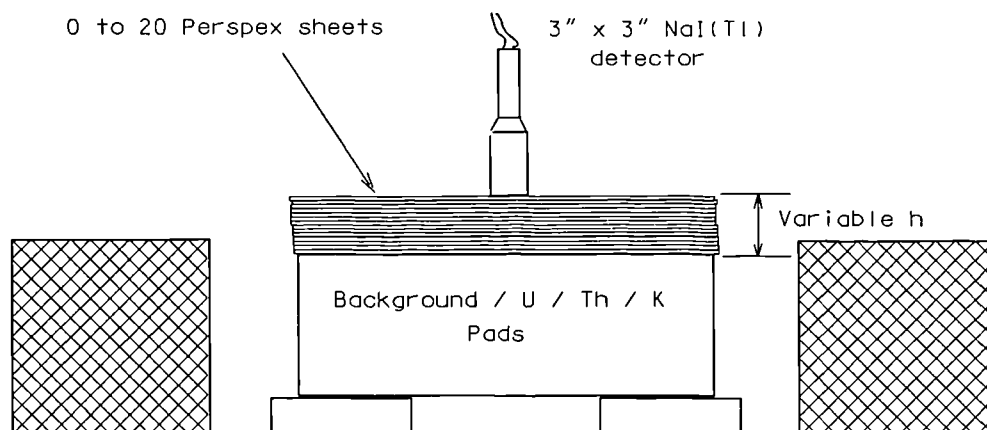


Figure 7.24 The experimental set up used to simulate the change in stripping coefficient with increasing peat/water overburden.

The experiment demonstrates the relative change in the stripping coefficient with overburden on the calibration pad. The detector was placed at the centre of each calibration pad and a spectrum collected with the 3" x 3" NaI(Tl) detector. One perspex sheet was then placed between the detector and pad and another spectrum was collected. This was repeated for 2, 3, 4, 6, 8, 10, 12, 15, and 20 sheets. The variable height was chosen to simulate the environment, i.e. as the source in the underlying geology is buried by low activity peat it is effectively moved further away from the detector.

The counting error was monitored for each region of interest and was better than 5%. The appropriate background spectrum for each overburden thickness interval was subtracted from the equivalent spectrum collected on each of the spiked pads. This allowed the change in stripping coefficients to be measured.

7.6.3 Results and Discussion of the change in stripping coefficients with absorber perspex sheets to simulate low activity organic rich geological overburden.

The change in photopeak contributions with increase in the number of absorber sheets is shown in figure 7.25 for the U calibration pad, figure 7.26 for Th calibration pad and

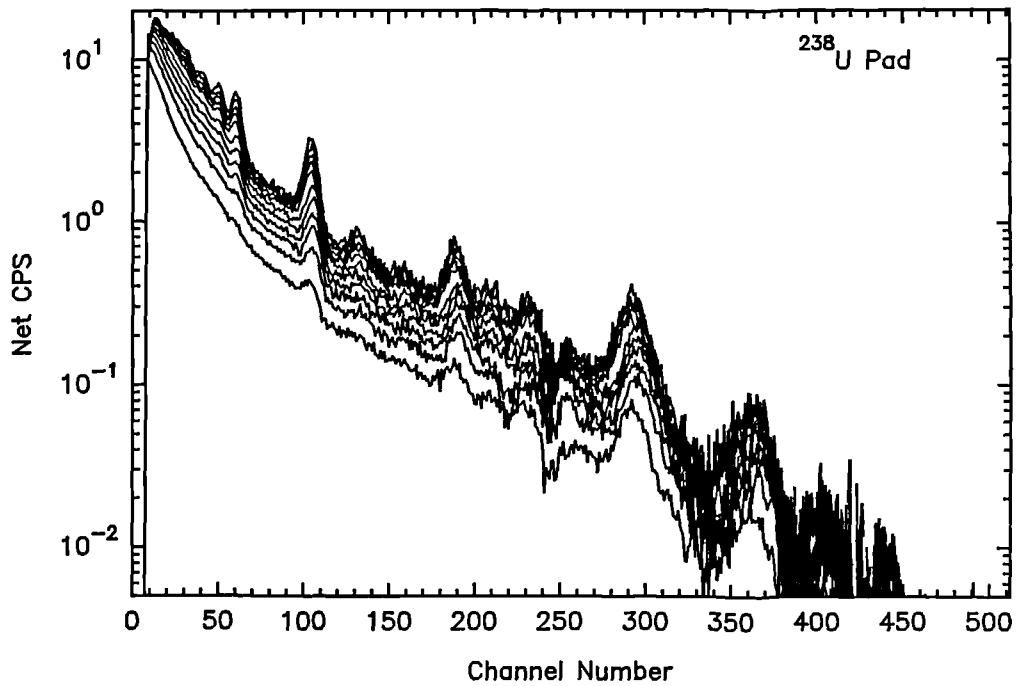


Figure 7.25 The change in relative peak intensities for ^{238}U calibration pad with source burial. 0, 1, 2, 3, 4, 6, 8, 10, 12, 15, 20 sheets used.

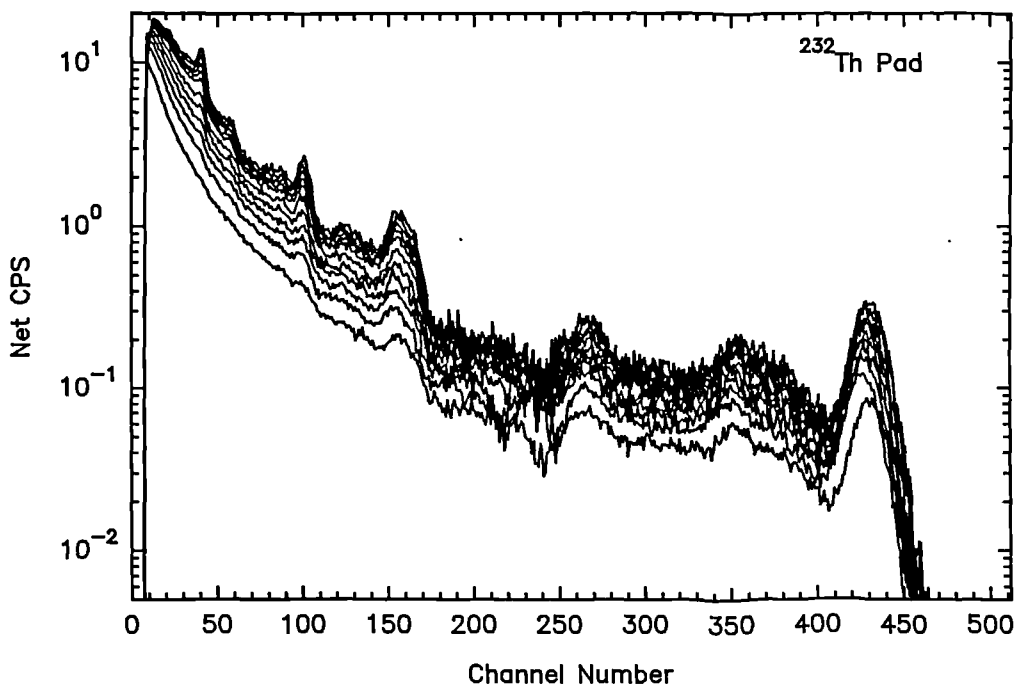


Figure 7.26 The change in peak intensities for the ^{232}Th calibration pad with absorbing media. 0, 1, 2, 3, 4, 6, 8, 10, 12, 15, 20 sheets used.

figure 7.27 for the K calibration pad. As expected, the lower energy photo-peaks such as the ^{214}Bi 609 keV (Channel 100) are attenuated more rapidly relative to the ^{214}Bi 1764

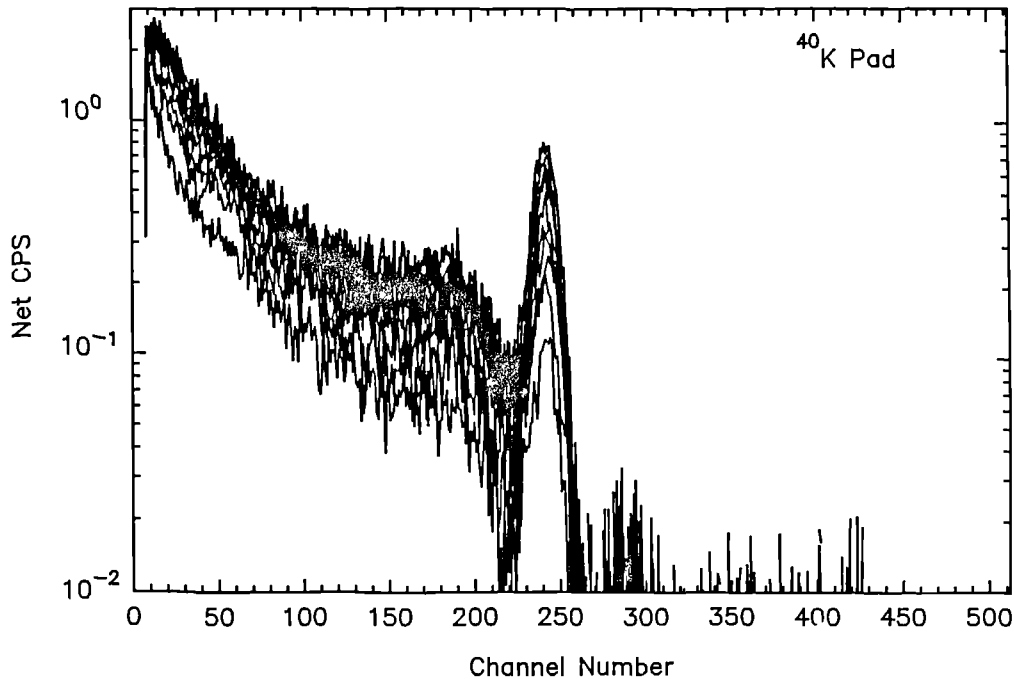


Figure 7.27 The change in photopeak intensities and scattering associated with the ^{40}K calibration pad with attenuating media. 0, 1, 2, 3, 4, 6, 8, 10, 12, 15, 20 sheets used.

keV (Channel 290) peak and this is clearly reflected in the reduction of the ^{137}Cs window stripping coefficient. However, the change in the stripping coefficient is not as rapid as would be expected (figure 7.28). This is due to the build up of secondary photons in the spectrum as a consequence of the increase in photon scattering due to the increase in the number of perspex absorber sheets. This is reflected in the slight increase in the U stripping coefficients as shown in figure 7.28 for ^{134}Cs .

The change in the thorium spectrum is shown in figure 7.29. As with uranium, the thorium spectrum demonstrates a more rapid attenuation of the photopeaks in the lower energy portion of the spectrum (eg. ^{228}Ac :270 keV and ^{208}Tl :277 keV at channel 42, ^{228}Ac :338 keV at channel 62 and ^{208}Tl :583 keV in channel 105) relative to the higher energy ^{208}Tl photopeak at 2620 keV at channel 427. Again this is reflected in a slight reduction in the ^{137}Cs window and stripping coefficient whilst the other coefficients remain almost constant (figure 7.29).

The ^{40}K spectrum in figure 7.27 shows similar characteristics to those demonstrated

with the ^{137}Cs sheet as shown in figures 7.19 and 7.20. There is a build up in the secondary scattered photons as the primary photons in the photopeak are scattered with an increase in the number of absorber sheets. This is demonstrated by a marked increase in the ^{137}Cs and ^{134}Cs window stripping coefficients.

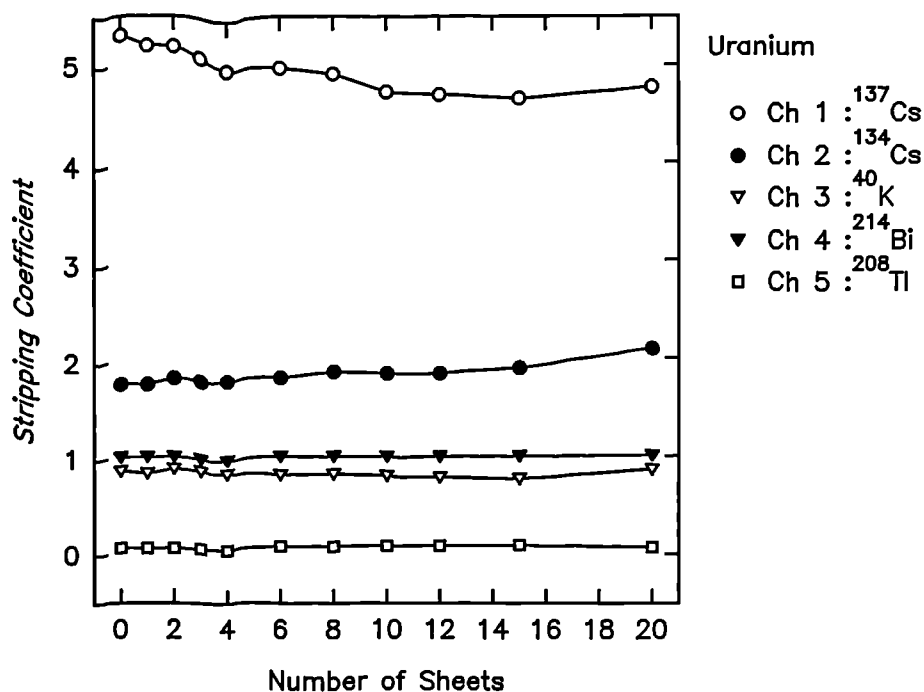


Figure 7.28 The change in stripping coefficients with number of absorber sheets

As discussed, the change in stripping coefficients is shown in figures 7.28 to 7.29. The depth distribution profiles (figures 7.4 and 7.5) for salt marsh environments suggest that there is negligible variation of ^{214}Bi , ^{208}Tl and ^{40}K in the soil profile with depth. As the stripping coefficients do not change significantly for uranium and thorium pads with the first 2 or 3 absorber sheets and the ^{40}K can be assumed to be constant with depth, the stripping coefficients associated with the concrete calibration pads (chapter 3) need not be altered.

Accounting for the influence of low activity overburden for detectors with wide angled fields of view is difficult from calibration pads which do not represent infinite source planes and thus the scattered photon contribution to the spectrum is likely to be underestimated. Whilst these experiments are not entirely representative of the environment, they demonstrate the potential change in stripping with source burial. No

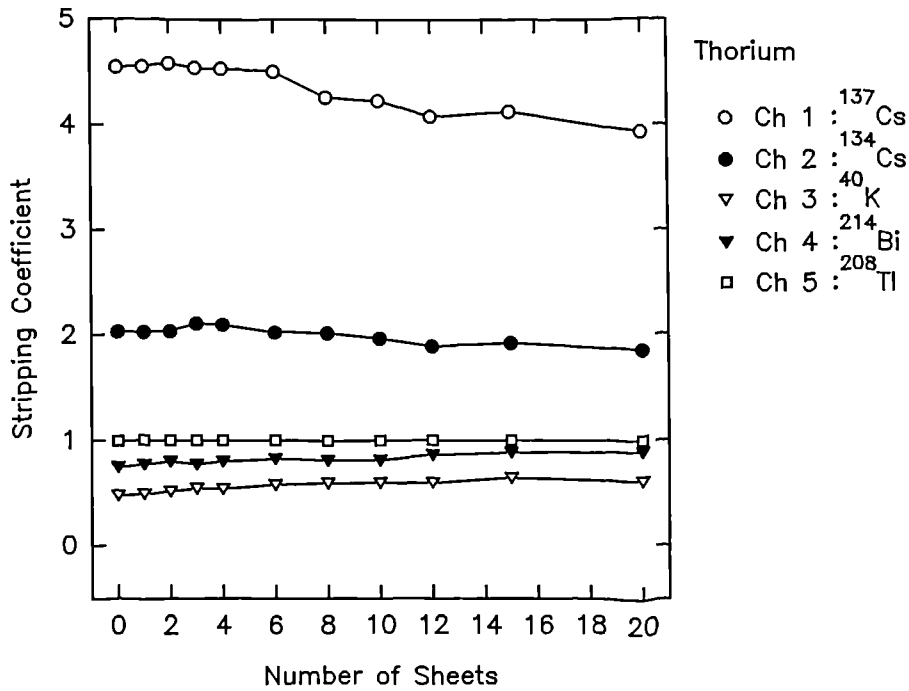


Figure 7.29 The change in stripping coefficients for ^{232}Th with attenuating media.

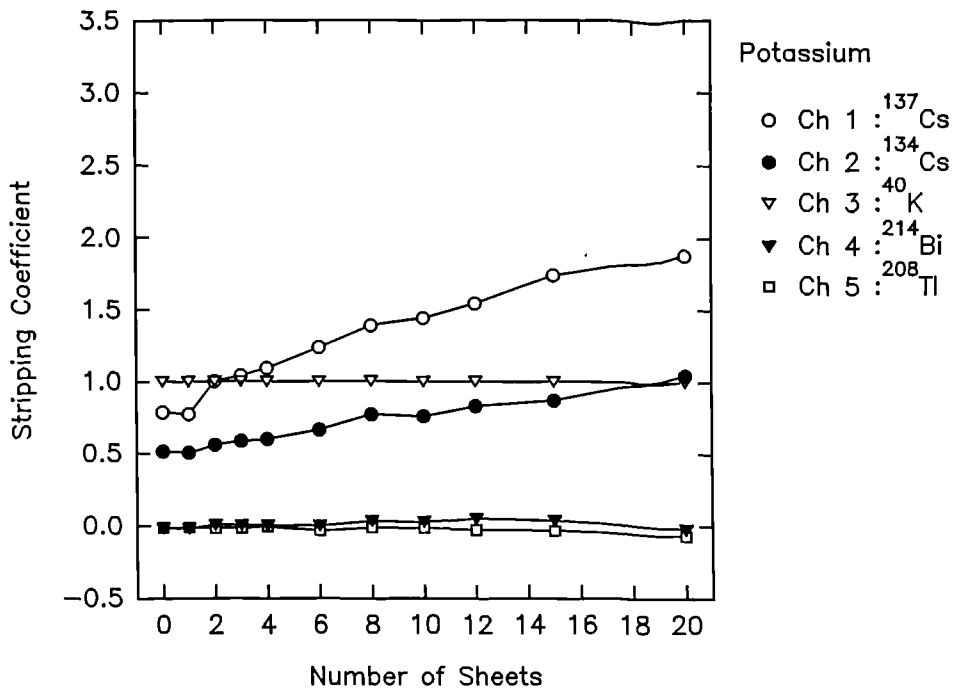


Figure 7.30 The change in stripping coefficients for ^{40}K with attenuating media

direct relationship between the number of absorber sheets and thickness of overburden can be made. Failure to account for changes in stripping coefficients could lead to over or under-stripping of ^{40}K contributions leading to residuals in the ^{137}Cs and ^{134}Cs

windows, whilst the ^{214}Bi and ^{208}Tl windows remain relatively unaffected.

However, in environments where bedrock of high primordial radionuclide concentration is covered with a blanket of peat with typically high concentrations of water, the stripping coefficients may need to be modified to account for the overburden's scattering properties particularly with ^{40}K . This is likely to apply to the Raithburn Valley. However, the need for this change also depends upon the relative activities of ^{137}Cs , ^{134}Cs and ^{40}K . For example, ^{137}Cs usually provides good counting statistics and whilst there is some compensation for ^{40}K over-stripping by ^{214}Bi and ^{208}Tl , from table 3.6, this is likely to lead to less than 7% residual contribution in the ^{137}Cs window. Conversely, in the ^{134}Cs window, because of its very low activity in the Raithburn Valley environment, residuals from under-stripping of ^{40}K are likely to contribute as much as 100 % of the ^{134}Cs window counts. The consequences of this have been discussed in chapter 4.

7.7 THE DETERMINATION OF MEAN MASS DEPTH (β) FROM IN-SITU SPECTRAL INFORMATION.

7.7.1 Objective

The objective is to examine the capability of estimating the mean mass depth of ^{137}Cs activity burial in salt marsh environments purely from spectral information collected in-situ with the 3" x 3" NaI(Tl) detector at 1 m above the ground. The benefit over the method based on photopeak attenuation and total soil core inventories described in section 7.4 is that it potentially requires no further information input after calibration, and can ultimately be used as a calibration correction factor, thus surmounting the main disadvantage of in-situ gamma spectrometry. The procedure is tested in salt marsh environments due to the significant systematic change in the depth distribution across these sites. In addition the concentrations of ^{134}Cs , which can complicate the application for NaI(Tl) detectors due to the need for stripping, are low compared to ^{137}Cs concentrations. Verification through soil sampling benefits from the relatively small sampling errors experienced on these sites as demonstrated in chapter 6.

7.7.2 Method

Spectra were collected at the Caerlaverock calibration site as previously described in this chapter and in chapter 6. Spectra collected from the concrete calibration pad facility and from a point ^{134}Cs source were used to determine the stripping coefficients as described in chapter 3 and verified in section 7.6 for the purposes of full spectral stripping.

The regions of interest data from the Caerlaverock spectra were used to apportion the amount of deconvolution of the pure natural series, starting with the ^{232}Th series. The region of interest for ^{238}U was then re-calculated and the ^{238}U spectrum was stripped away in the appropriate proportions. This procedure was followed for ^{40}K and then for ^{134}Cs stripping.

The spectrum associated with ^{134}Cs was derived from a point source. This presented problems with obtaining a stripping ratio appropriate to that observed in the environment associated with an exponential distribution with depth. In addition, detector gain shifts may lead to a slight movement of the ^{137}Cs photopeak into the ^{134}Cs window, thus adding to the ^{134}Cs window contribution. These small influences on ^{134}Cs window counts may lead to slight over-stripping of ^{134}Cs out of the spectrum. Evidence of this was observed in the data and thus two attempts at stripping with the original pure ^{134}Cs ratio and a modified ^{134}Cs stripping ratio were made. The modified stripping ratio was determined by verifying from the net ^{137}Cs spectra that the valley and plateau values to the right of the ^{137}Cs photopeak showed no signs of under or over-stripping.

The channel ranges used to calculate the mean valley and mean plateau value to the right of the photopeak were modified from those determined in section 7.5.4. to reduce the interference from ^{134}Cs . The mean valley value was determined from channels 86 to 95 and the mean plateau value to the right of the photopeak was determined from channels 127 to 131 (figure 7.32). However, the advantage of developing this method in salt marsh environments is due to the very small contribution that ^{134}Cs makes to the spectrum in comparison to ^{137}Cs .

The errors on the mean valley height value and mean plateau value to the right of ^{137}Cs photopeak were calculated with errors ranging from 3 % to 10 %. A relationship between the areas of known mean mass depth and spectral peak to valley ratio is determined, from which the mean mass depth for the other Caerlaverock sampling sites could be calculated.

From such spectral observations, a calibration correction value was determined and integrated depth inventories estimated. The values were then compared with the known inventories of the Caerlaverock calibration site to verify the method.

7.7.3 Results and Discussion

Figure 7.31 shows a typical spectrum collected at the centre of the calibration site at Caerlaverock and also shows the same spectrum after stripping out the pure ^{232}Th , ^{238}U , ^{40}K and ^{134}Cs contributions. Given that the concrete calibration pads do not represent infinite sources, the scattered portion within the net spectra is likely to contain a systematic error due to the difference in the scattering behaviour of the real and artificial (concrete) environments.

This spectrum is shown in more detail in figure 7.32. The selection of the valley region and the minimum plateau to the right of the ^{137}Cs photopeak is also shown. The influence of the ^{134}Cs spectral deconvolution is also illustrated. The pure ^{134}Cs spectrum was stripped away and over stripping was observed creating depressions in the spectrum. Figure 7.32 also demonstrates that the modified deconvolution of ^{134}Cs has led to less variation in the valley and minimum plateau area to the right of the photopeak.

Table 7.2 gives the spectral information extracted from each spectrum with an associated β measured from soil core data (section 7.3). Two sets of results are shown demonstrating the relatively small amount of influence the change in the ^{134}Cs deconvolution has on the chosen regions to determine the mean valley and mean minimum value to the right of the ^{137}Cs photopeak. In addition the systematic

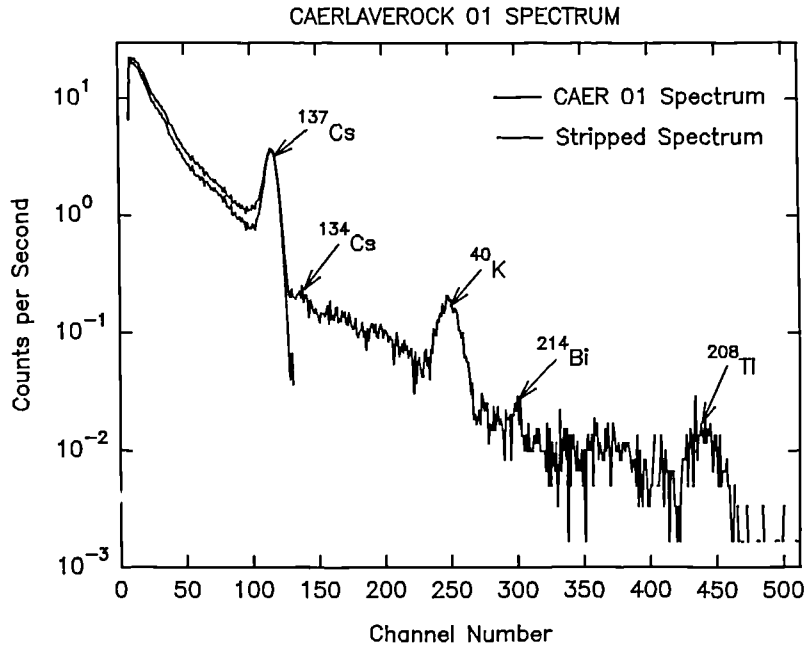


Figure 7.31 The whole and stripped spectrum collected at the centre of the Caerlaverock Calibration site.

contribution to the spectrum from the under-stripping of the scattered portion of the spectrum makes little difference to the underlying relationship between β and photopeak/valley ratio. Figures 7.33 and 7.34 demonstrate the relationships between the peak to valley step ratio and the mean mass depth (β). The modified ^{134}Cs deconvolution provides the better data fit as demonstrated in figure 7.34, although they both provide similar relationships as shown in equation 7.11 for the pure ^{134}Cs stripping spectrum and equation 7.12 for the 0.41x the ^{134}Cs spectrum.

$$\text{Log}\beta = 2.394 - 0.03456 \cdot \frac{P}{S} \quad (7.11)$$

$$\text{Log}\beta = 2.3889 - 0.03451 \cdot \frac{P}{S} \quad (7.12)$$

The error bars in figures 7.33 and 7.34 are 1σ standard deviations on each value. The error about the line of best fit is indicated by the 95 % confidence interval. Thus typical estimates of the mean mass depth derived from either graph for the Caerlaverock site will be determined predominantly by the errors on the spectral information.

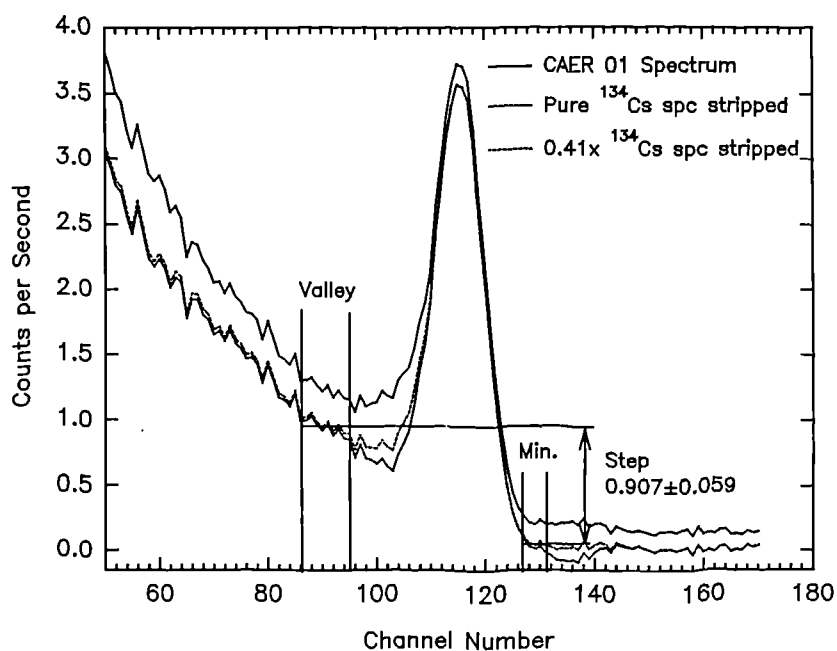


Figure 7.32 The unstripped and stripped ^{137}Cs photopeaks with the regions of interest used to determine the valley-step values. The pure ^{134}Cs deconvolution has led to slight over-stripping.

Typically errors will be between 10 and 15 % (1σ). Figures 7.33 and 7.34 show that the Kirkconnel spectral characteristics agree, within errors, with the Caerlaverock spectra. Assuming that the mean mass depth determined is representative of the spectrum collected, the difference in the detector response characteristics must be accounted for by the difference in the shape of the ^{137}Cs activity distribution profile. Applying the relationships shown in figures 7.33 and 7.34 and described by equations 7.11 and 7.12 enables the mean mass depth (β) of the other sampling sites at Caerlaverock to be determined (assuming similar depth distribution profiles). The final results, given in table 7.3, were determined from equation 7.12 (figure 7.34).

Table 7.3 provides a set of results very similar to those given in table 7.1. Clearly the mean mass depth increases into the higher energy intertidal areas of the Solway coastline. The exception to the rule is provided by position 45 (10.10 g cm^{-2}) where the spectrum was collected over intertidal mud and sediments. Although both sets of results are dependent upon the assumption that the change in depth distribution characteristics is similar across the whole site, table 7.1 has the added disadvantage of being dependent upon representative soil core inventory estimations. Here, however,

Table 7.2 Spectral components used to determine a relationship with mean mass depth of source burial. Two examples of ^{134}Cs deconvolution are illustrated.

Mn Mss	Depth Net Peak	Mean Valley	Mean Min	Valley Step	Peak/ Step
	g cm ⁻² Area				
using pure ^{134}Cs stripping					
7.2	43.2±1.8	0.999±0.097	0.038±0.026	0.960±0.032	44.9±5.2
10.78	34.0±1.3	0.909±0.094	0.011±0.025	0.898±0.094	37.8±4.4
11.24	35.4±1.4	0.936±0.060	0.030±0.036	0.906±0.070	39.0±3.6
13.23	35.8±2.1	0.962±0.111	0.002±0.032	0.960±0.032	37.3±4.9
20.70	20.1±1.2	0.662±0.078	0.024±0.034	0.638±0.078	31.5±4.7
26.5	10.5±0.61	0.363±0.066	-0.01±0.016	0.372±0.038	28.2±5.4
using 0.41 x ^{134}Cs stripping					
7.2	43.0±1.8	1.027±0.092	0.064±0.034	0.963±0.098	44.6±5.1
10.78	33.8±1.3	0.973±0.086	0.036±0.022	0.899±0.089	37.6±4.1
11.24	35.1±1.4	0.968±0.052	0.026±0.060	0.908±0.059	38.7±3.2
13.23	35.6±2.1	0.992±0.104	0.031±0.022	0.961±0.106	37.0±4.5
20.70	19.9±1.2	0.680±0.067	0.041±0.028	0.639±0.073	31.2±3.9
26.5	10.4±0.6	0.372±0.064	0.000±0.015	0.372±0.066	28.0±5.2

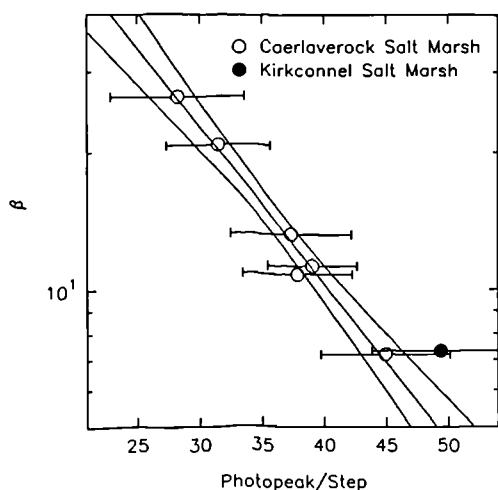


Figure 7.33 The Valley-step ratio vs Mean Mass Depth (β) determined with pure ^{134}Cs deconvolution.

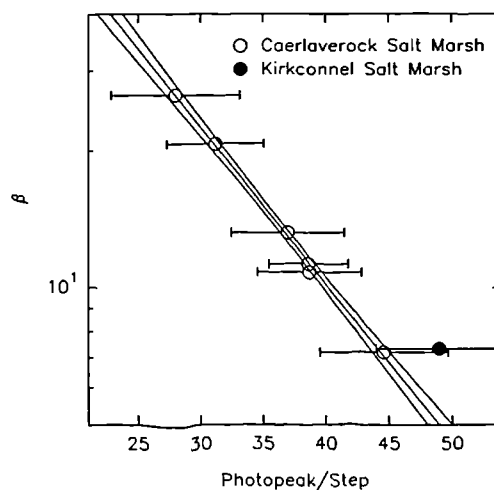


Figure 7.34 The Valley-step ratio vs Mean Mass Depth (β) determined with the modified ^{134}Cs deconvolution.

the results are based initially on a few comparisons with soil profiles, whilst the rest of the results are derived from spectral information only.

Having determined β from spectral information, it should be possible to derive a spectrally derived calibration correction for changes in source burial for particular

Table 7.3 The Change in Mean Mass Depth (g cm⁻²) derived from spectral data, across the Caerlaverock Calibration Site. 1 σ errors on individual values are between 10 and 15 %.

Transect No.	Hexagonal Shell No : Spacing m					
	0:0	1:2	2:8	3:32	4:128	5:256
1	11.34	12.69	12.39	9.89	7.05	4.65
2		12.84	11.26	9.92	10.60	8.29
3		11.57	12.03	11.32	20.50	20.18
4		14.64	13.56	16.52	26.47	10.10
5		12.47	12.51	12.08	21.87	16.14
6		9.89	14.42	10.30	5.32	5.01
Mean	11.34	12.35	12.70	11.67	15.30	10.73
1 σ	0.93	1.43	1.03	2.31	8.01	5.70
St.Err.		0.58	0.42	0.94	3.27	2.33

environmental contexts.

7.7.4 ¹³⁷Cs Calibration Correction for Changes in Mean Mass Depth (β)

Figure 7.35 demonstrates the change in detector response with changes in the mean mass depth associated with salt marsh sub-surface maxima. This considerable change in detector response will lead to obvious difficulties in detector response calibration as discussed in section 7.4. However, as discussed in section 7.7.3, investigations of the peak/valley-step ratio allow the estimations of the mean mass depth (β) and thus an appropriate calibration correction coefficient may be determined. The change in the calibration coefficient (N/A_x) with mean mass depth is illustrated in figure 7.36 (with 95% confidence intervals).

The determination of the calibration coefficient (N/A_x) is given by equation 7.13:

$$\begin{aligned} \text{Log}\left(\frac{N}{A_x}\right) &= \text{Log}\left(\frac{N}{A_x}\right)_0 - m\beta \\ &= 0.1396 - 0.0337 \cdot \beta \end{aligned} \quad (7.13)$$

Equation 7.13 in conjunction with the mean mass depth (β) values illustrated in table

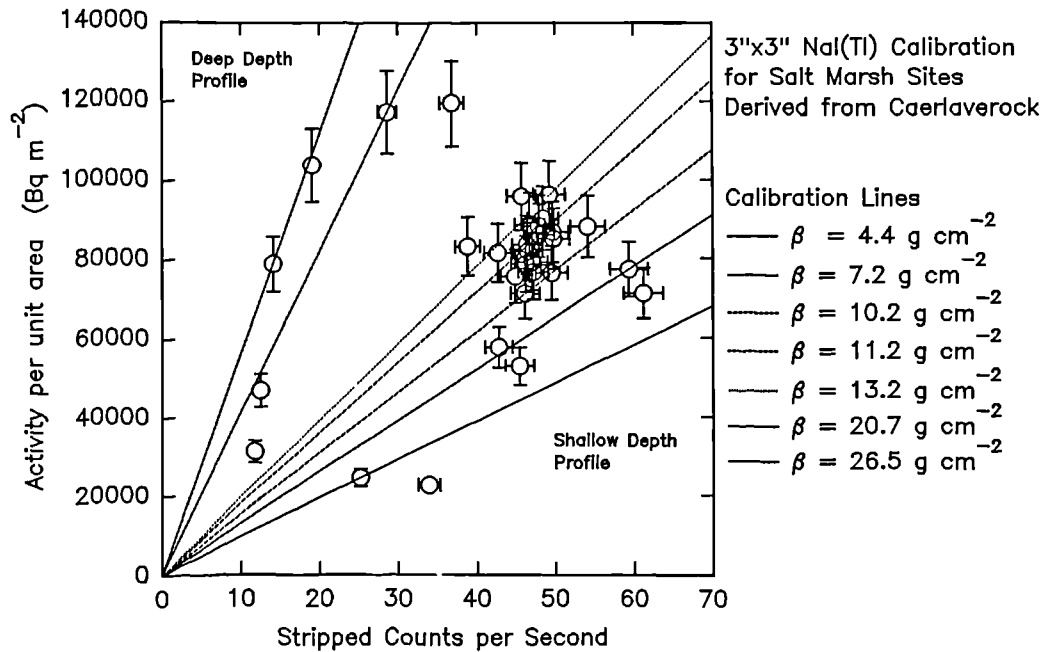


Figure 7.35 The change in detector response across the Caerlaverock salt marsh calibration site.

7.1 and 7.3 was used to determine the mean mass depth corrected activities across the Caerlaverock calibration site.

The comparison between the uncorrected in-situ derived inventory estimates and soil core derived estimates (0-30 cm), is shown in figure 7.37. The calibration was based on inventory estimates at the centre of the calibration site. As with figure 7.35, the cluster of points about the 1:1 line reflects the number of measurements made around the hexagon which is centrally weighted.

However, it is the magnitude of the scatter which is important, whilst the cluster of points will reflect the reproducibility of the technique. Figure 7.37, demonstrates the traditional handicap of the use of in-situ gamma spectrometry for inventory estimation in these salt marsh environments where source burial change is considerable. This results in a very poor agreement between

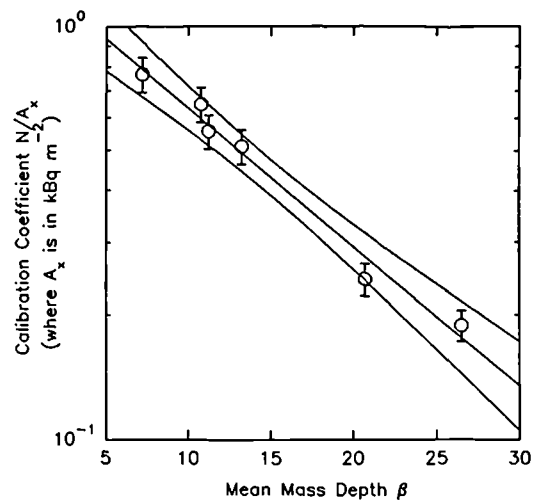


Figure 7.36 The change in the calibration coefficient with β (g cm^{-2}) for the Caerlaverock Salt Marsh.

the two techniques.

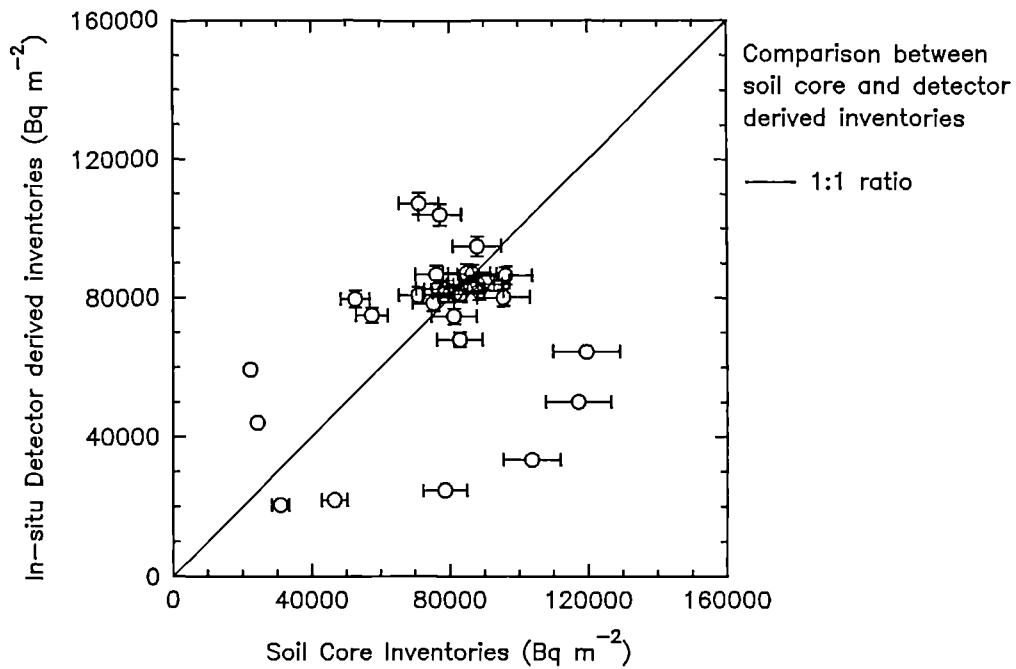


Figure 7.37 The comparison between in-situ detector uncorrected calibrations and soil core derived ^{137}Cs activity estimations (Bq m^{-2}) across the Caerlaverock Calibration site.

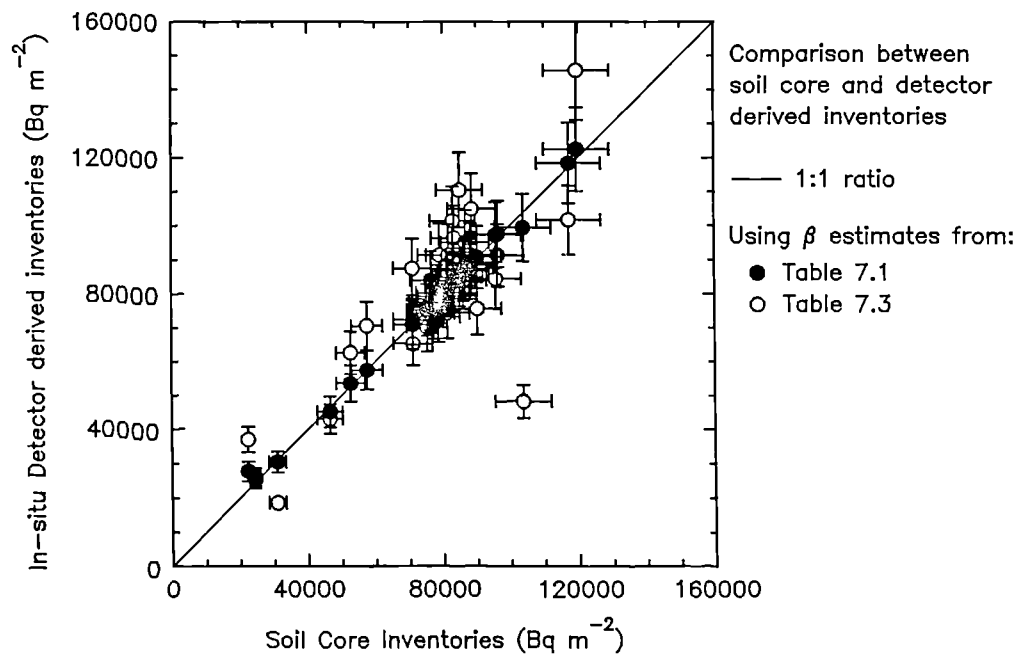


Figure 7.38 The comparison between in-situ detector β corrected calibrations soil core derived ^{137}Cs activity estimations (Bq m^{-2}) across the Caerlaverock Calibration site.

In contrast figure 7.38 demonstrates the improvement in the comparison between in-situ and soil core derived estimates once the spectral derived calibration correction has been undertaken. The estimates of β in table 7.1 are based on photopeak to soil core activity ratios and hence a good correlation between the two estimates is expected because any error on β brought about by sampling error is systematically ignored. Of particular importance are the estimates of β derived from spectral information (table 7.3). Error contributions to this second set of estimates of β must include the contributions from stripping, counting statistics in the peak/valley-step ratio determination as well as, and in particular, sampling error on the soil core derived estimates. This considered, figure 7.38 demonstrates good agreement between the spectrally corrected NaI activity estimates and the soil core derived estimates.

There are, however, complicating factors which will limit this application. For example, position 45 was measured and sampled in the intertidal sands outside the salt marsh, and is likely to have a different characteristic source profile. This has resulted in a lower β estimate and thus an underestimation of ^{137}Cs activity, shown by the single outlier in figure 7.38. Similar problems associated with sampling at the very edge of the salt marsh may be overcome by collimating the detector, thereby restricting the field of view. Similarly, areas of standing water where prevalent within the field of view of the detector, result in altered spectral information ie, changing the photopeak/valley-step ratio from that otherwise expected. Changes in the shape of the depth distribution brought about by changes in depositional and erosional conditions are also likely to lead to changes in the photopeak/valley-step ratio. The degree of influence will depend upon the magnitude of the change and its spatial extent within the context of the field of view. However, it is likely, given the consistent agreement between the Caerlaverock results, that there is some tolerance in this technique to these variables and in particular some change in source burial shape.

This experiment provides a significant development in the application of in-situ gamma spectroscopy to salt marsh environments, not only to predict the mean mass depth (β) but to derive a calibration correction from spectral derived characteristics for such environments where the change in mean mass depth may be systematic. Any minor

unsystematic change in the salt marsh environment has not brought about a significant error in the final estimate. Figure 7.38 demonstrates that ^{137}Cs inventory estimation from spectral information can be derived with between 10 and 20 % precision, depending on the environmental conditions. Application of this new technique to salt marsh environments will greatly facilitate the speed with which activity estimation can be made across such environments, with additional information of source burial across the salt marsh.

7.8 SUMMARY AND DISCUSSION

This chapter has demonstrated the importance of accounting for the depth distribution profile and its effects on in-situ detector response characteristics. The soil sampling technique is very important in accurately describing the shape of the distribution profile. The adapted 105 mm diameter x 450 mm length corer has proved ideal for this purpose and demonstrated the inadequacies of the traditionally used commercially available equipment such as the 38 mm diameter x 150 mm length Leonard Farnell corer.

When comparing depth distribution profiles between contrasting sites for in-situ gamma spectroscopy, it is important to work in units of mass depth (g cm^{-2}) as this enables soil density and thus also water content to be taken into consideration. The mean distribution of activity within the soil profile is described in terms of the mean mass depth β . The amount of temporal and seasonal variation in water content is dependent upon the moisture holding capacity of the soil, subsurface movement and evaporation rates. For example, a peaty soil is likely to have very much larger variations in moisture content than a loam, clay or sediment. Consequently, a greater temporal variation in detector response is likely to occur over peaty terrain than denser clay rich soils and sediments which have a smaller pore space capacity.

The photopeak/valley-step ratio provided a useful and robust spectral derived function used to measure mean mass depth β . This had been verified initially through laboratory based experimental modelling. The flexibility of the stripping coefficients for full spectral stripping was also verified through experimental work for application to salt

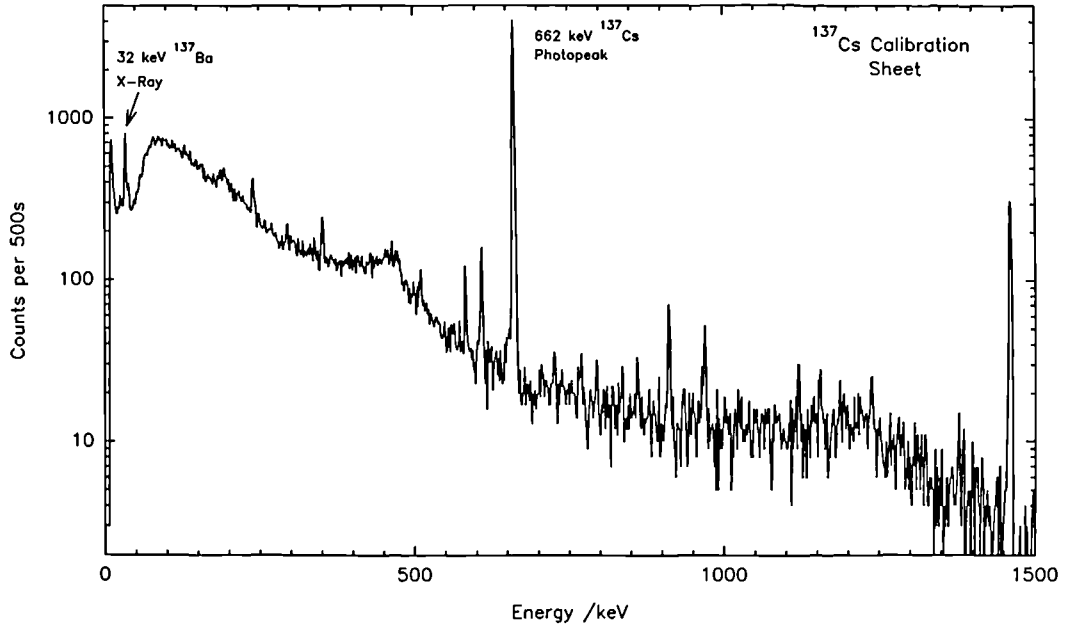


Figure 7.39 The GMX HPGe detector spectrum of ^{137}Cs calibration sheet representing a surface source. The ^{137}Cs Peak/Valley-step ratio ≈ 704 .

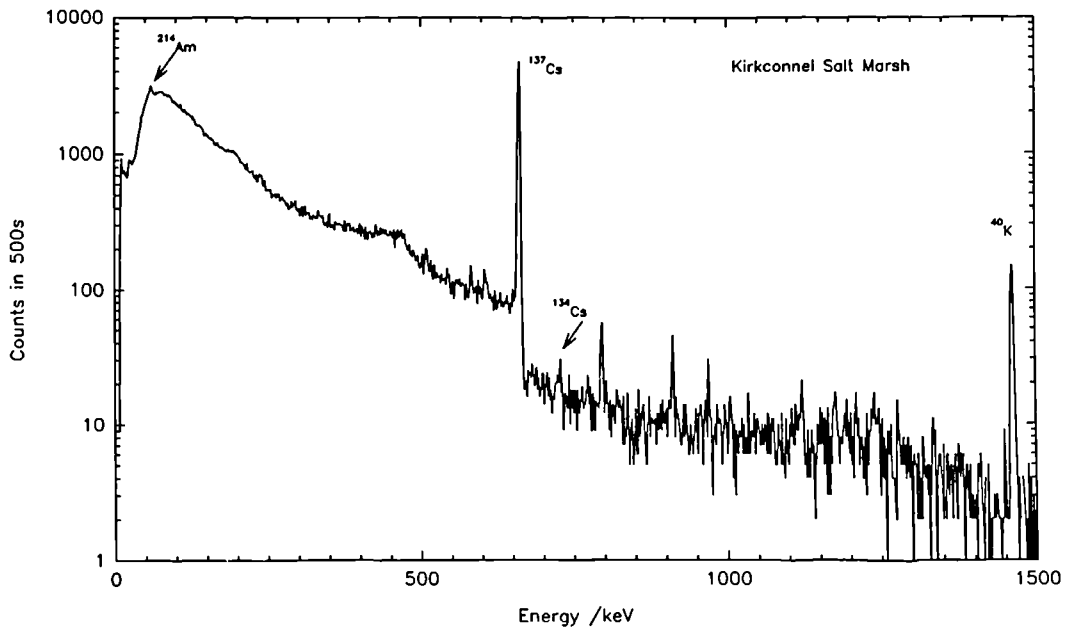


Figure 7.40 The GMX spectrum collected on the Kirkconnel salt marsh. The ^{137}Cs Peak/Valley-step ratio ≈ 103 and represents a mean mass depth of 7.33gcm^{-2} .

marsh environments. These experiments demonstrated the problems of source burial, either through increased air path length and/or through peat and/or water overburden. This clearly showed how the ^{40}K stripping ratios changed for ^{137}Cs and ^{134}Cs with source

burial. This, coupled with changes in source geometry, is likely to explain the ^{134}Cs anomaly observed at the Raithburn Valley with in-situ and aerial survey measurements.

The salt marsh environment provided a useful area to determine the application of NaI(Tl) detectors to this problem because: a) there is a rapid change in sub-surface maxima across the site with respect to the energy of the intertidal environment, b) the contribution of ^{134}Cs to the spectrum is small compared to ^{137}Cs , thus minimising the problems associated with spectral deconvolution of ^{134}Cs , and c) as demonstrated in chapter 6, the soil sampling errors are considerably smaller, making soil core comparison with in-situ spectrometric measurement easier. The results proved highly successful and the derived mean mass depth to valley-step relationship was used to determine the mean mass depth from the other Caerlaverock sampling sites. These measurements were then applied to determine calibration correction coefficients and thus activity estimates were derived successfully across the salt marsh. These values were highly compatible with soil sample derived estimates.

This experiment has provided the first successful application of spectral derived calibration corrections for in-situ activity estimation within an environment of changing β . However, application of this technique to terrestrial environments may be complicated by enhanced concentrations of ^{134}Cs with respect to ^{137}Cs . This will require careful deconvolution techniques.

The problem of spectral deconvolution is solved however by using high resolution HPGe detectors such as n-type GMX or LOAX detectors. Figure 7.39 and 7.40 demonstrate two spectra collected by an n-type 50 % GMX HPGe detector from the ^{137}Cs sheet representing a surface source and a buried profile at Kirkconnel respectively. The lack of spectral interferences allows the Compton edge, valley-step and photopeak areas to be rapidly observed and calculated. No ambiguities from ^{134}Cs interferences exist and a relationship with terrestrial "exponential like" profiles may be readily measured and determined. In addition, application of the photopeak/valley ratio may provide a useful and rapid means of measuring changes in soil water content for a given site.

8. DISCUSSION AND CONCLUSIONS

8.1 SOME OF THE ENVIRONMENTAL INFLUENCES ON THE MEASUREMENT OF RADIONUCLIDE INVENTORIES

One of the challenges which faces environmental and earth scientists is the collection of spatially representative samples and the determination of the spatial distribution from a series of spatially isolated measurements. This problem is partly overcome by using in-situ and remote sensing measurement techniques which are less spatially restricted. However, quantification and interpretation of these remotely sensed measurements are, at best, often dependent upon estimates determined from other analytical techniques, usually derived via soil sampling. Absolute quantification of these advanced remote sensing techniques can be achieved through traceable ground sampling, the results from which can in turn be put into a spatial context through comparison with remote sensing data. There is, therefore, a mutual dependence between ground based monitoring and remote sensing techniques. This work has examined these challenges in the context of the measurement of both naturally occurring radionuclides (^{40}K , ^{214}Bi , ^{208}Tl) and anthropogenic radionuclides (^{137}Cs and ^{134}Cs). Through the direct comparison of the results from the three techniques of soil sampling, in-situ and aerial gamma ray spectrometry, the environmental factors, including spatial and vertical variability, which influence the measurements by and comparison between these analytical techniques were identified and quantified.

Each measurement technique has a number of advantages and disadvantages. For example, whilst soil sampling enables radionuclide activities within samples to be measured to high levels of precision and the chemical speciation and distribution within the profile to be studied, its spatial representability is in doubt unless further time consuming and therefore costly samples are taken with a view to estimating sampling error and spatial dependence. In-situ gamma spectroscopy has the advantage of making spatially averaged measurements which account for small scale variability and allow for rapid and cheap estimates of soil activity concentrations. However, detailed knowledge of the distribution of activity within the soil profile along with chemical speciation is

lost, and this in turn may influence the validity of the calibration used with in-situ and airborne detectors. In addition, field work accessibility, mobility and time constraints may inhibit the spatial mapping capability of in-situ techniques. Aerial survey shares the immediate advantages and disadvantages of in-situ gamma spectroscopy, but has the very great benefit of rapid accessibility to all environments and can produce rapid spatial representations of activity distribution on scales dependent upon flying altitude, integration time and flight line spacing. All three techniques provide complementary information in the study of environmental radioactivity. Whilst offsetting the problems of sampling error and spatial variability, aerial survey results can direct the more time consuming field based soil sampling to areas of particular interest, and, in doing so, help to verify the sensitivity estimates of in-situ and aerial survey measurements.

This thesis has examined and developed methods to quantify some of the main influences which control the precision of activity estimation through soil sampling with laboratory based gamma spectrometry, in-situ gamma spectrometry and airborne gamma spectrometry. In particular, the methodologies developed have enabled effective comparison between these techniques to be made, enhancing their compatibility and effective use.

8.2 THE MAIN IMPLICATIONS AND CONTRIBUTIONS OF THIS THESIS

8.2.1 Radionuclide Distribution and Measurement

Having summarised the issues which confront the scientist making environmental radioactivity estimates, the introductory chapters reviewed the factors which control the distribution of radionuclides in the environment and the techniques and methods used to measure environmental radioactivity. Chapter 3 described the principal methods and tools used during this work, the calculation of the fields of view of in-situ and aerial survey detectors, and demonstrated the dependence of the field of view on photon energy, platform height and source burial. In addition, chapter 3 demonstrated that the minimum detection limits (MDL) are controlled by the nature and levels of background radioactivity.

As might be expected from the discussion in these introductory chapters, the distribution of radioactivity in the environment is highly heterogeneous which is likely to influence the measurement of that distribution. However, little work had previously been carried out on the quantification of spatial variability of radionuclides on both a micro and macro scale. Hence, the influence of spatial variability on radionuclide estimation and its influence on comparisons of the measurement techniques was not fully understood. To establish the importance of the controls of spatial variability and other environmental influences on the measurement of the distribution of radioactivity, an experiment was designed to estimate the distribution of radioactivity across a tight geometry valley with the three monitoring techniques.

8.2.2 Identification of Environmental Influences on Radioactivity Estimation

It was through the comparison of activity estimates derived from the three techniques of soil sampling, in-situ and aerial gamma ray spectroscopy used to describe the activity across a upland tight geometry valley (Raithburn Valley), that some of the environmental factors acting on these estimates were identified. Although the results from the three techniques showed a similar spatial distribution across the valley, the final estimates were significantly influenced by differences in the sampling area of each technique and by the underlying spatial distribution. This made direct comparison between each technique difficult. For example, ^{137}Cs estimates from soil samples ranged from 2.3 kBq m^{-2} to 53 kBq m^{-2} , whilst the aerial survey estimates ranged from 4 kBq m^{-2} to 12 kBq m^{-2} . The distribution of the radionuclides within the valley bottom and their spatial vertical and lateral variability, controlled by their long term chemical and physical behaviour, is likely to have had an impact on the activity estimation derived from each measurement technique and the comparisons made between them. This was sufficient to inhibit the determination of the influence of the topographic shape on the radiation field and thus on in-situ and aerial survey detector response.

The source burial effects observed across the valley, particularly in ^{40}K , led to underestimation through soil sampling whilst overestimating activity through in-situ and airborne techniques. Later experimental modelling verified that ^{40}K burial influences

the residual counts observed in the ^{134}Cs and ^{137}Cs windows through increases in photon scattering which are greater than those estimated for stripping coefficients. As discussed in section 8.2.8, this is likely to significantly contribute to the ^{134}Cs window particularly when activity levels are low and close to the MDLs. In such circumstances, particularly where the MDL is likely to change with each measurement across site, no ^{134}Cs activity estimate or distribution can be made. The change in topography from a flat plane to a valley shape is likely to have had some additional influence on the scattering characteristics of the radiation field.

The conclusions from these results have implications on radiological assessment. Confidence in the representative nature of simple soil core derived estimates of the distribution of radionuclides even over small areas was in doubt due to sample representability and spatial variability. In-situ techniques clearly measure the photon fluence which has direct radiological implications particularly in terms of gamma dose and is directly related to the amount of activity in the ground. The same activity with different source characteristics (source distribution or soil type) will lead to a different photon fluence although the gamma dose implications from the new photon fluence are still valid. However, conversion of the photon fluence rate ($\gamma\text{s}^{-1}\text{ m}^{-2}$) in terms of activity per unit area (Bq m^{-2}) or activity per unit mass (Bq kg^{-1}) is restricted by variations in soil type and source depth characteristics as well as minimum detection limits and spectral processing parameters. Thus effective comparison between these techniques is likely to be controlled by one or more of these variables.

8.2.3 Quantification of the Self Attenuation Characteristics of Soils

The observed density and compositional variation of soils across the Raithburn Valley prompted an investigation into their self attenuation characteristics. Wet soil densities ranged from about 400 kg m^{-3} to 2000 kg m^{-3} and from about 300 kg m^{-3} to 1600 kg m^{-3} for dry ground soils. This variation potentially provided a considerable influence on in-situ and laboratory based gamma spectroscopy. A series of laboratory based experiments and calculations was devised to determine the importance of the influence of density and soil composition on the self attenuation characteristics of a wide range

of British Soil samples and Geostandard Reference Soils. This provided the first comprehensive measurement of μ and μ_m for a range of British and International soils.

Experimental observations showed that density dominated the self attenuation characteristics of soils at energies of 662 keV (^{137}Cs) and 1330 keV (^{60}Co). The influence in soil composition was observed with a coefficient of variation (CV) in μ_m of only 8 % for the range of soils. At 59.6 keV (^{241}Am) the influence of μ_m was more pronounced with a CV of about 21 % illustrating a greater dependency upon the composition of the soil and therefore its Z_{eff} . These observations and the change in μ_m with energy were verified by the calculation of μ_m with energy for a range of 27 possible soil compositions based upon 36 of the more abundant and potentially more important elements for photon interaction in the soil. The CV of μ_m for energies above 200 keV was observed to be about 5 % which is equivalent to the error quoted by Storm and Israel (1970) from which the elemental photon cross sections were determined. However, when organic content and possible water content were included, this CV increased to about 10 %, which is equivalent to the experimental results. At energies below 200 keV, the observed CV of 15 % at 60 keV was considerably increased if organic content was taken into account. It was concluded that soil compositions used by Beck *et al* (1972) and Mudahar and Sahato (1988 a,b) and subsequently by others in their calculations are useful only for energies above 200 keV.

These results have implications for:

- a) Environmental gamma ray spectrometry and the representative sampling depth required for effective comparison with in-situ gamma spectrometry. The consequences of stratification of sources and variations in soil self attenuation will also have considerable influences on photon fluence from the soil surface.
- b) Laboratory based gamma spectroscopy and the effect of change in sample composition and density on the absolute efficiency calibrations.

These implications are discussed in sections 8.2.4 and 8.2.5.

8.2.4 Effective Soil Sampling Depth

For energies above 200 keV, μ_m is more dependent upon photon energy than sample composition. Thus effective sampling depth, defined in chapter 5 depends upon photon energy and soil density. For ^{137}Cs , an average half depth of about 11 cm (possible range of 22 cm to 6 cm) was determined, suggesting that the standard 30 cm soil core was reasonably representative, particularly as most of the ^{137}Cs inventory tends to be concentrated in the upper 15 cm of the soil column. At most, 12% of the photon fluence originating from a narrow activity layer buried below 30 cm, perhaps in salt marsh environments, would reach the surface. This has implications not only for relating photon fluence with in-situ detectors, but also for making radiological dose assessments. For example, in their radiological assessment of the Solway intertidal merse sediments, McKay *et al* (1991) sampled to about 15 cm depth which is likely to lead to an underestimation of the radiological impact, given the typical source burial characteristics. Samples should be cored to depths of about 30 cm (depending on sediment density) when determining ^{137}Cs contributions to dose.

Similarly, at the higher energies associated with the natural radionuclides, eg 1500 keV, the half depth is of the order of about 15 cm (typical range of 29 cm to 8 cm). This suggests that a representative sample should originate from a sampling depth of about 45 cm. This is particularly important when trying to correlate inventories quantified in terms of activity per unit area (Bq m^{-2}). However, if calibrated in terms of activity per unit mass ($\text{Bq}_{\text{wet}}\text{kg}^{-1}$) and assuming a uniform distribution with depth, then any sampling depth will provide an activity concentration estimate. If source burial occurs as demonstrated in the Raithburn Valley, ie. typically up to 100 % of the activity occurred below 30 cm, then as much as 35 % of the photon fluence may penetrate from this depth (assuming soil density of about 0.6 g cm^{-3}). This results in underestimations of the underlying geological activity concentrations whilst overestimating the activity concentrations of the overlying soil/peat horizons, as experienced in the Raithburn Valley.

At energies below 200 keV, such as for ^{241}Am , the problem of effective sampling depth

in addition to density, is compounded by variations in soil composition. However, experimental observations of μ_m from a range of Caerlaverock samples showed that, given a dominant sediment composition, changes in μ_m across the site are controlled by the proportions of organic matter to sediment content. This will have a direct influence on soil density and thus may help simplify and aid the application and interpretation of in-situ and aerial survey gamma spectrometry to the mapping of ^{241}Am in salt marsh environments.

8.2.5 Laboratory Based Gamma Spectrometry

The calculations and experimental observations indicated that the efficiency calibrations of laboratory based semiconductor detectors are susceptible to change with sample density and composition, particularly for the larger 150 cm³ geometry containers used. A set of hybrid soils, providing a density range from 0.5 to 1.5 g cm⁻³, were spiked with known amounts of mixed gamma solutions. Significant density corrections were determined for the radionuclides of interest, with differences in efficiency calibration ranging from 64 % for ^{241}Am (59.6 keV), to 17 % for ^{137}Cs (662 keV) and 10% for ^{214}Bi (@ 1765 keV) for the 150 cm³ sample container on a coaxial Ge(Li) and HPGe detector. The magnitude of the potential density correction was observed to decrease with increased detector crystal size. With a 50% relative efficiency GMX HPGe crystal the correction factors were reduced to 45 % for ^{241}Am and 11 % for ^{137}Cs . Similarly, a reduction in sample size also to a 75 cm³ container reduced the correction factor from 60 % to 34 % for ^{241}Am on the Ge(Li) detector. Further reduction in container size to 30 cm³ (petri dish) with the larger detector crystal geometry (50% GMX detector) resulted in negligible correction factors for both ^{241}Am and ^{137}Cs . Similar, but more extensive geometrical observations were described through analytical solutions with experimental observations by Galloway (1991b, 1993).

Experimental measurements of μ and μ_m from the hybrid calibration soil set and samples collected from Caerlaverock salt marsh were very similar, indicating that the laboratory based self absorption calibration correction determined for ^{241}Am is valid for the Caerlaverock site. However, comparisons with IAEA reference materials suggested

that simple density corrections derived from the hybrid soils for low energy photons (<200 keV) would not be valid for a wider range of soils and sediments. Thus standard self absorption corrections, particularly for the larger sample containers, were better based on estimates of μ . This highlights the difficulties in determining certified values for low energy photon emitting radionuclides for ^{241}Am , through inter-laboratory comparison with gamma spectrometric techniques. These difficulties are compounded when each laboratory uses different calibration procedures and soil compositions, with no account taken for the differences in self absorption. This also has implications for ^{210}Pb dating, Anderson *et al* (1992) noted variations in ^{210}Pb transmission through 20 g samples vary as much as 15 %, as a result of changes in Z_{eff} . Hence, for accurate ^{210}Pb dating, self absorption corrections are required.

Analysis of these results demonstrated the need for sample self absorption correction, particularly if large container geometries are being used. In addition, efficiency calibrations based on single standard density material, which remain common practice, may lead to significant under or over estimations of sample activity concentration, not only for low energy photon emitters but also for the higher energies, such as ^{137}Cs . Thus precision estimates on activity concentration determination quoted in the literature are frequently misleading, particularly those quoted to single percent precision levels with no apparent appreciation of the error attributed to efficiency calibration. Precision estimates must include these contributions, giving errors of about 3 or 4 % for ^{137}Cs .

The calibrations are traceable to IAEA and NBS standards.

8.2.6 Sampling and Sub-sampling Errors

Having analysed a sample, the representability, both from the whole sample and of the whole sample from the environment, was quantified. The grinding and homogenisation procedure adopted and developed during the course of this research provided laboratory sub-sampling errors which were comparable to the analytical precision already determined. Some improvement in sub-sampling error was observed with increased container size as suggested from geochemical sampling theory (Ingamells *et al* 1974

a,b). However, the exception to these observations was provided by ^{214}Bi . Here the scatter of a time series of activity estimates indicated a problem with container sealing, inhibiting equilibration of ^{214}Bi with its parent ^{222}Rn . The time required for the sample to reach equilibration is dependent upon the ^{222}Rn generation and leakage.

Sampling error was quantified by examining the influence of micro (1 to 2 m) scale spatial variability upon activity estimation, as well as the change in spatial variability with increased sample spacing. On the micro scale, sampling variations were observed to be about 30 % for ^{137}Cs using the 38 mm diameter Leonard and Farnell corer in Chernobyl contaminated soil. Some decrease was observed in this variation by increasing sampling size to the 105 mm diameter corer but not on the magnitude expected by geochemical sampling theory (Ingamells *et al* 1972 and Ingamells 1974 a,b). This is likely to be due to the non-normal distribution of the activity caused by some spatial component in its distribution brought about by the depositional mechanisms as well as the soil's own natural variability in clay and organic content. However, in well mixed sedimentary deposits in salt marsh environments, a decrease in the sampling error was observed from 10 % to 5 % for ^{137}Cs from the 38 mm to the 105 mm corer respectively.

8.2.7 Spatial Variability and Statistically Representative Sampling Plans

Spatial variability occurs on both the macro regional scale and the micro scale. The airborne radiometric remote sensing technique spatially averages the small scale variability within each field of view allowing the regional variability to be mapped. Having established the influence of sampling error, the need to spatially relate spatially isolated measurements (e.g. soil samples) with spatial extensive measurement (e.g. aerial survey measurements) is compounded by the influence of spatial variability.

The initial solution of matching ground based data with aerial survey data was derived by producing a sampling pattern which was constructed to spatially match the weighting of an airborne detector at 100 m altitude. The sampling pattern was designed so that the samples would not be unduly influenced by any potential spatial or linear feature

running across the site and thus compromising the representative nature of the samples. The sample inventories were then averaged to determine the mean activity concentration and the *CV* used as an estimate of sampling error and site variability. Typical values of between 20 and 30 % were observed. Given the inherent problem of sampling error, spatial distribution was also only observed on a qualitative level from the data collected for these simple centre weighted calibration sites.

The simple centre weighted calibration sites, although useful for calibration of fixed height detectors and providing an estimate of spatial variability within the field of view of a detector at 100 m height, were not capable of determining spatial variability estimates for a range of detector altitudes. The expanding hexagonal sampling plan with six samples collected at the corner of each shell, expanding out on a x2 or x4 scale, enabled spatial variability with sample spacing to be observed from a micro 2 m to a macro 256 m scale. The contributions from each shell were weighted appropriately to determine the activity observed by a detector at a range of altitudes from 1 m to about 200 m. This also enabled the determination of spatially corrected height correction coefficients.

Spatially weighted inventory estimates at aerial survey altitudes (100 m) from both salt marsh and terrestrial sites typically had 1σ errors again of between 20 and 30 %. Taking the number of samples used in each shell into account, a standard error of about 10 % was calculated for calibration purposes. On salt marsh sites spatial variability fell as the effective field of view of the detector was reduced and better levels of calibration precision were determined due to smaller sample to sample activity variation. This was not the case for terrestrial deposits of Chernobyl fallout at Longbridgemuir where variability was observed to be similar on the micro sampling scales (2m scale) as upon the macro sampling scale (128⁺ m). Here a *CV* of between 20 and 30 % was again observed at all sampling scales for ¹³⁷Cs and ¹³⁴Cs. It is interesting to note that this *CV* of about 30% has been observed on all sampling scales (<256 m) and on all sites associated with weapons testing and Chernobyl fall out. Although this suggests that the expanding hexagon requires an unnecessary amount of sampling effort in terrestrial environments, its application does serve to verify the degree of spatial change in these

environments so that detector height correction coefficients can be verified and corrected for as appropriate. The application of the expanding hexagon has successfully quantified variability with sample spacing and characterised spatial variability for different depositional contexts.

8.2.8 Source Burial and Photon Fluence

Quantification of spatial variability and the confidence with which comparisons can be made between soil sampling patterns and in-situ or aerial survey techniques have enabled the influence of source burial on detector response to be investigated. Following crude estimates of source burial determined from the 38 mm corer, the adapted 105 mm golf hole corer enabled detailed source depth distributions to be determined from single intact cores with minimal soil column smearing to depths of up to 45 cm.

Photon fluence from a source distributed in soil is a function not only of source depth (cm), but also soil density (g cm^{-3}) for energies above 200 keV whilst the influence of soil composition for energies below 200 keV is a further complicating factor. Thus for photon energies above 200 keV, depth distribution was described in terms of *mass depth* (g cm^{-2}). The source depth characteristics were quantified as the *mean mass depth* or *mass relaxation per unit area* (β). β can be calculated from an assumed negative exponential source distribution, where applicable, or from the integration of the mass depth with activity concentration (Bq kg^{-1}). The influence of water content on β was discussed with some observations implying that the effect was more significant in organic soils than in clay rich soils principally due to the smaller pore space capacity of clay rich soils.

Following the observations of Zombori *et al* (1992) with a HPGe detector of the change in forward scattering with the burial of a point source under water, a series of experimental models was constructed with an extended layer ^{137}Cs sheet source, absorbers (1 cm thickness perspex sheets) and concrete calibration pads, to investigate photon scattering characteristics. In particular, source burial characteristics were

simulated for ^{137}Cs with the NaI(Tl) detector and a relationship between the full energy photopeak/valley ratio (a function of forward scattering), and extended layer source burial was determined. The experiments were also able to demonstrate the sensitivity of β determination and its dependency not only upon source depth but also, importantly, upon source profile shape. This demonstrated the problem of using a single quantitative value such as β to describe source burial. However, given an environment where source burial can be observed to change systematically, it was thought to be possible to derive a calibration correction coefficient from pure spectral data. To achieve this, full spectral stripping was needed and thus verification of the stripping coefficients was required.

The concrete calibration pads and perspex sheets were used to model the change in the stripping coefficients with source burial, representing either geological cover with low activity peat and/or water. In addition Appendix J discusses the influence of air path length on stripping ratios. Similar characteristics were observed in the change in stripping coefficients for both in-situ and aerial survey detector geometries. The most marked influence on the stripping coefficients for ^{137}Cs and ^{134}Cs was observed to be from burial of ^{40}K . This confirms the observations made within the Raithburn Valley and suggests that ^{134}Cs determination, because of its low concentrations which were close to and below the minimum limits of detection, is particularly sensitive to changes in ^{40}K burial. Thus the suitability of a set of ^{40}K stripping coefficients may be corrupted by source burial effects and other changes in the scattering environment resulting in stripping residuals developing in the ^{134}Cs window. The very low count rates of ^{134}Cs result in the residual contribution being highly significant, perhaps contributing as much as 100 % of the counts in the ^{134}Cs window when activities are at or below the minimum detection limits, whilst contributing less than 7 % to the ^{137}Cs window with the Raithburn valley data set. Similar contributions are likely with the 16 litre NaI aerial survey detector. U and Th stripping coefficients change less markedly with burial and this was attributed to the attenuation of the lower energy full energy photopeaks being compensated by the increased scattering from higher energy photons.

The small sampling errors observed at the Caerlaverock calibration site, combined with

large changes in ^{137}Cs source mass depth characteristics, provided a good site with which to determine the potential of deriving β from spectral characteristics with a NaI(Tl) detector. Relatively uniform distributions of natural radionuclide concentrations with depth enabled full spectral stripping with spectra derived from the concrete calibration pads to be carried out on the spectra collected with the 3"x3" NaI(Tl) detector. These were then interrogated to determine the photopeak/valley ratio. Although the scattering properties of the concrete pads are unlikely to be identical to those observed in the salt marsh environment, any difference is likely to be systematic and thus not obscure any relationship between β and photopeak/valley ratio. A good correlation was determined from the sites of known β with photopeak/valley ratios, with a similar relationship to that observed in the laboratory. From this data, the mean mass depth of the rest of the Caerlaverock site was determined purely from spectral information. The results clearly demonstrated that β increased towards the near shore intertidal environment, as expected. Of major significance, however, was the development of the spectrally derived calibration correction. Application of this calibration correction to the remaining spectra collected at Caerlaverock provided the first example of an applied spectrally derived calibration correction. The estimates were compared with soil core derived inventories which provided positive evidence that the calibration correction worked across Caerlaverock salt marsh.

8.3 SUMMARY

Through the direct comparison of activity estimation through soil sampling and laboratory based analysis, in-situ and aerial gamma spectrometry, some of the major controls on environmental radioactivity estimation have been identified and quantified. As a result of this work, methodological recommendations have been made for the measurement and reporting of environmental radioactivity estimates in addition to making effective comparison between the measurement techniques of soil sampling with laboratory based analysis, in-situ and aerial gamma spectrometry. A spectrally derived calibration correction coefficient was developed to compensate for systematic changes in source burial and was successfully applied. Having investigated the influence of both spatial vertical and lateral variability on activity estimation, section 8.4 discusses further

areas of research including the influence of temporal and dynamic variability on environmental radioactivity estimation.

8.4 AREAS FOR FURTHER RESEARCH

Laboratory based work which may require further attention is the low energy self absorption correction for laboratory based HPGe detectors for the detection of ^{210}Pb (46.52 keV), ^{234}Th (63.28 keV) and ^{241}Am (59.6 keV), particularly for large container geometries commonly used by many environmental research laboratories. The measurement of the forward scattering from these primary photo peaks may afford a simple and effective method of determining the appropriate efficiency calibration for the soil type. This may, however, be made difficult by the position of the back-scatter peak, for example for a 60 keV photopeak the back-scatter peak is at about 48 keV. At higher energies, the ^{137}Cs forward scattering was observed to be considerable, and a relationship between the photopeak/valley step ratio and density may be useful for the direct determination of sample density and thus for an appropriate absolute efficiency calibration determination. This would provide a significant development in the rapid characterisation of such soil samples.

The incorporation of HPGe detectors into in-situ and aerial survey gamma ray spectroscopy would provide a significant development in the determination of β without the problems of spectral stripping for ^{137}Cs , thus potentially providing real time estimates of β . Observations within the laboratory and field have demonstrated the degree of forward scattering observable from different buried source profiles in the environment. Although lower efficiency detectors require longer counting times, a problem for aerial survey purposes, this may be overcome by summing the responses from arrays of HPGe detectors, even though this is likely to lead to some loss in spectral resolution. In addition, the problems of stripping for radionuclides of low concentrations from NaI(Tl) spectra, may be overcome by simultaneous use of HPGe detectors. This may require longer counting times for the HPGe detectors, and although spatial resolution is lost in terms of both activity estimates and β , further spectral detail will be provided which may aid the interrogation and stripping of the

large volume NaI(Tl) detectors and thus potentially resolve the consequences of changes in the scattering characteristics of the radiation field.

Flight trials undertaken in early 1993 have shown that preliminary estimates of β from spectral information would be useful. Potential errors in platform height of the order of 10 m would result in errors in the determination of β in the soil profile of the order of 1 g cm⁻² or less. Thus as detector response is less influenced by small changes in detector height, this would enable significant advantages in calibration correction to be realised. In addition, comparisons of aerial survey NaI(Tl) spectra over salt marsh sites with inland terrestrial sites show marked changes in the forward scattering components of the spectrum. Thus it may be possible for crude calibration corrections to be determined from unstripped aerial survey spectral data.

However, further investigation into source burial shape would also be required, as detector response has been demonstrated in the laboratory to be dependent upon source burial shape as well as mean mass depth. Thus source burial may be better described by two or more shape or statistical parameters which might include β . Further description of the source burial profile may be characterised from spectral properties due to the predominance of different scattering characteristics. The transferability of this technique of β determination between different salt marsh environments would also require verification, although given its flexibility across a large site it is likely to provide a useful tool. Application of this technique would provide a rapid means to investigate and spatially map the source depth distribution across salt marsh environments, establishing the long term dynamics and the sedimentary accretionary characteristics of these merses as well as determining the long term behaviour of the radionuclides and changes in gamma and beta dose rates.

Application of this technique to inland terrestrial sites would require further extensive characterisation of spectral shape and source burial shape. However, mans influence on the distribution of anthropogenic radionuclides through ploughing of soil also needs to be investigated. The influence of ploughing on the vertical and lateral spatial variability also has significant influence on radionuclide activity estimation through

remote sensing.

Although much work has been undertaken on the influence and measurement of snow and snow-water equivalent from in-situ and aerial survey techniques (e.g. Saito 1991 and Grasty *et al* 1979), little work has been undertaken on the influence of temporal variations in soil moisture content with soil type. This would be of use to determine the potential changes in β with soil type and thus the climatic and temporal dependence of the in-situ and aerial survey calibration. Clearly organic rich bodies such as monolithic peat would be capable of considerable changes in soil water content on a seasonal basis and in response to precipitation events, particularly within the important surface layers. This would therefore influence β significantly along with the observed change in photon fluence observed in the detector response as shown at Longbridgemuir. In contrast, higher density clay rich soils are likely to have a smaller seasonal change in soil moisture content and subsequently smaller changes in β as indicated by observations at SURRC. The measurement of forward scattering with soil moisture content may provide an effective way of estimating soil moisture content and movements within the soil/sediment water table.

Radon is an environmental factor which influences the determination of ^{214}Bi and thus ^{238}U levels. Ambient radon levels can be monitored before, during and after surveys by hovering above large areas of water. However, radon levels have climatical, geological, pedological and topographical associations and thus should not be subtracted using temporally and geographically isolated data. Correct ways of coping with ^{222}Rn must include the incorporation of on board radon monitoring equipment. This has been demonstrated (e.g. IAEA 1991) by the incorporation of "upward" looking detectors. These detectors are shielded from below by the "downward" looking detectors and thus principally measure the activity associated with the air and cosmic ray interference. This therefore also includes the ^{214}Bi derived from radon. However, even this method has to assume that there is the same amount of radon above the detector as there is below. If this is the case, then subtraction of the ^{214}Bi channel of the upward looking detectors from the downward looking detectors would provide the net ^{214}Bi associated with the underlying soil and geology. However, this is a loose assumption, as for

example, in valleys atmospheric inversion is a common occurrence which may result in more radon above the aircraft than below. Under normal conditions, ^{222}Rn levels may be expected to decrease with altitude. This problem, however, remains for in-situ gamma spectroscopy. One possible solution with HPGe detector use could be to monitor ^{226}Ra , a precursor of ^{222}Rn , although it has a low photon yield requiring longer counting times and there is also possible interference from ^{235}U .

Following the Raithburn valley experiment, quantification of the observations thus far made has required experimental work to be restricted to effectively flat planar surfaces. The potential influence of the topography upon the radiation field and thus upon the detector response can be calculated. Small undulations within the radiation field have been suggested, by Kogan *et al* (1971), to compensate for each other within the field of view of the detector. However, as the solid angle Θ increases due to topographical changes about the detector, then the response of the detector increases. This has been described by Allyson (1994), Schwarz *et al* (1992) and Kogan *et al* (1971). However, these effects have not been identified and quantified as yet through experimental work.

The effect of biomass within forest systems and particularly the attenuation effects of the tree canopy provide an additional environmental factor to consider. There are likely to be at least two possible factors applying, i) the effect of the attenuation by the biomass on the underlying radioactivity, which is thought to be as much as 15 % (IAEA 1976), and ii) the effect of bringing the source closer to the aircraft through deposition of radionuclides on leaves and uptake of radionuclides through the root system. Dose effects from ^{137}Cs have been observed to be up to 1.4 times as much within forest systems (Miller *et al* 1990) with in-situ spectrometric measurements. This was thought to be due to radionuclides being concentrated higher up in the low density soil profile within the forest litter. This is particularly important in areas of fresh deposition.

8.5 FINAL CONCLUSIONS

Comparison between activity estimates derived from soil sampling with laboratory based gamma ray spectrometry, in-situ gamma ray spectrometry and airborne gamma ray spectrometry, has enabled the influence of spatial horizontal, vertical and compositional characteristics of soils and radionuclide distributions on activity estimation to be assessed. The methodologies developed during this work serve to aid the calibration of environmental gamma ray spectrometry and, in particular, the verification and interpretation of in-situ and aerial survey techniques. Each technique has its advantages and disadvantages, including the rate at which activity estimates can be made.

This thesis has shown that the sampling area and volume, including that associated with fields of view, coupled with the underlying change in activity distribution has a significant influence on the estimation of activity levels and its spatial distribution. In the pursuit of quality environmental activity estimates and effective comparisons between the three techniques used, the following recommendations in particular have been made:

- 1) The self absorption characteristics of soils should be accounted for in both: a) the systematic correction for self absorption in laboratory based gamma spectrometry; and b) the estimation of the effective soil sampling depth required for comparison with in-situ gamma spectrometry.
- 2) Sub-sampling errors should be minimised by sample homogenisation and the use of large sample containers.
- 3) Field sampling errors should be accounted for to determine the precision of activity estimation. Field sampling errors are dependent upon sampling size, depositional mode and the underlying environmental characteristics.
- 4) Spatial variability must be accounted for in relating spatially isolated with spatially extensive estimates. Sampling plans are recommended to quantify spatial variability on different sampling scales enabling effective comparison between soil sample estimates, in-situ and airborne gamma spectrometry.
- 5) The vertical activity distribution and soil density have a significant influence on

photon fluence. Careful comparison of activity profiles must take into consideration soil/sediment density (as measured in the field). Quantification of source burial in terms of β (g cm^{-2}) provides a simple approach for profile comparison between sites.

6) Systematic changes in source burial can be accounted for directly from spectral information, thus enabling the estimation of β and a calibration correction. Methodologies for this approach have been developed, overcoming the principal limitations of in-situ gamma spectrometry in salt marsh environments.

7) Future research is particularly recommended in the characterisation of source burial shape from in-situ HPGe detectors, and its development for remote sensing applications.

The future of environmental gamma ray spectrometry is likely to lie with the development of improved efficiency and reduced cost of HPGe detectors, particularly as these avoid the disadvantages of spectral stripping for the primary photopeaks of interest, and allow for a far greater range of radionuclides to be detected. In addition, the interrogation of full spectra will lead to the characterisation of environmental factors such as systematic change in source burial and to in-situ calibration corrections.

Many of the problems encountered in this field of research are common to other areas of the environmental and geosciences, including sampling for trace element analysis, and the determination of spatial and vertical distributions. Having attempted to quantify small scale variability, ground samples are often best put into a spatial area and regional context through either airborne or satellite based remote sensing systems with image analysis. Ultimately, the cost effectiveness of many remote sensing techniques makes them ideal for putting ground based data into a spatial and temporal context, minimizing the time and expense devoted to the often more costly ground based sampling to that required for calibration and directing further detailed investigations to areas of need.

REFERENCES

- Adams, F. and Dams, K. (1975). *Applied Gamma Ray Spectroscopy*. 2nd Ed. Pergamon Press.
- Alexander, Peter, and Kosanke, Ken. (1978). The Quality of Airborne Radiometric Data. *Nevada Section - American Nucl. Soc. Aerial Techn. for Env. Monitoring. Topical Symp. Proc.*
- Allen, J.R.L. and Rae, J.E. (1986). Time sequence of metal pollution, Severn Estuary, southwestern U.K. *Marine Pollution Bulletin*. **17**, 427-431.
- Allen, J.R.L. (1991). Salt Marsh accretion and sea level movement in the inner Severn Estuary, south west Britain; the archaeological and historical contribution. *Journal of the Geological Soc. London*. **148**: 485-494.
- Allen, R.L. (1994). Distribution Geochemistry and Geochronology of Sellafield Waste in Contaminated Solway Firth Floodplain Deposits 1993. *Glasgow University PhD Thesis*.
- Allyson, J.D. (1994). Environmental Gamma Ray Spectrometry: Simulations of Absolute Calibration of In-situ and Airborne Spectrometry for Natural and Anthropogenic Sources. *Glasgow University PhD Thesis*.
- Anderson, R., Cook, G.T., MacKenzie, A.B., Thomson, J., and Harkness, D.D. (1992). *Gamma Spectrometry Determination of ²¹⁰Pb in North Atlantic Sediment Cores*. Paper Presentation to the Coordinating Group for Environmental Radioactivity. Sept. 1992. University of Bangor, N. Wales.
- Anspaugh, L.R., Phelps, P.L. and Huckabay, G.W. (1972). *IV Methods for the in-situ Measurement of Radionuclides in Soil*. Pico-Medical Division, Lawrence Livermore Lab. University of California, Livermore, California, 94550.
- Arnolds, O., Cutshall, N.H., Nielson, G. (1989). Caesium-137 in Montana Soils. *Health Physics*. **57**(6), Dec: 955-958.
- ASTM (1983) *Standard Method for Soil Sample Preparation for the Determination of Radionuclides*. American Standards, version 83. C999-83.
- ASTM (1990) *Standard Practice for Sampling Surface Soil for Radionuclides*. American Standards, version 90. C998-90.
- Bachauer, H., Bunzl, K. and Schimmack, W. (1982). The migration of ¹³⁷Cs and ⁹⁰Sr in multilayered soils; Results from Batch, Column and Fallout investigations. *Nucl. Technology*. **59**. Nov: 291-301.

- Bachauber, H., Bunzl, K. and Schimmack, W. (1986). Spatial Variability of the Distribution Coefficients of ^{137}Cs , ^{65}Zn , ^{57}Co , ^{109}Cd , ^{141}Ce , ^{103}Ru , $^{95\text{m}}\text{Ta}$ and ^{131}I in a Cultivated Soil. *Nuclear Technology* **72** (March): 359-371.
- Barnes, M.G. (1978). *Statistical Design and Analysis in the Cleanup of Environmental Radionuclide Contamination*. Water Resources Centre. Desert Research Institute, University Of Nevada System, Reno, Nevada. DRI Publication No. 45012. NVO 1253-12. 53pp
- Barnes M.G., Giacomini, J.J., Belman, R.T., Elliot B. (1980). *NTS Radiological Assessment Project: Results from the Frenchman Lake Region of Area 5*. Water Resources Center. Desert Research Institute, University of Nevada System, Reno, Nevada. DOE/DP/01253-17. 105pp.
- Baxter, M.S., Cook, G.J., McDonald, P. (1989). *An Assessment of Artificial Radionuclide Transfer from Sellafield to S.W. Scotland*. DOE/Rw/89/127.
- Beardsley, T. (1986). U.S. analysis incomplete. *Nature*. **321**: 187.
- Beattie, J.R. (1981). The Assessment of environmental consequences of nuclear reactor accidents. In: *Environmental Impact of Nuclear Power*. British Nuclear Energy Society
- Beck, H.L.; DeCampo, J. and Gogolak, C. (1972). *In-Situ Ge(Li) and NaI(Tl) Gamma-Ray Spectrometry*. HASL-258. United States Atomic Energy Commission - Health and Safety (TID-4500). 75pp.
- Beck, H.L. (1978). The Physical Properties of Environmental Properties of Environmental Radiation Fields and Their Utility for Interpreting Aerial Measurements. Nevada Section - American Nucl. Soc. *Aerial Techniques for Env. Monitoring, Topical Symp. Proc.*
- Billington, Douglas S. (1959). Ionizing Radiation and Metals. *Sci. Am.* Sept, 201-204.
- BNF, (1990). *Annual Report on Radioactive Discharges and Monitoring of the Environment, 1989*. British Nuclear Fuels plc, Health and Safety Directorate, Risley, Warrington, Cheshire, UK.
- BNF, (1991). *Annual Report on Radioactive Discharges and Monitoring of the Environment, 1990*. British Nuclear Fuels plc, Health and Safety Directorate, Risley, Warrington, 1989. Cheshire, UK.
- Bolt, G.H., Bruggenwert, M.G.M. (1976). *Soil Chemistry. A. Basic Elements*. 281pp, Elsevier Scientific Publishing Company.
- Bondiatti, E.A. (1981). *Mobile Species of Pu, Np, Cm, Am and Tc in the Environment*. Conf-810772-3. Oak Ridge National Laboratory. IAEA-SM-257/42.

- Bonnett, P.J.P. and Cambray R.S. (1989). The Chronology of Deposition of Radionuclides as recorded in the sediments of Ponsoby Twn, Cumbria. *Vth Int. Symp. in Palaeoclimatology, Ambleside, Cumbria*. Sept.
- Bonnett, P.J.P. (1990). A review of the Erosional Behaviour of Radionuclides in Selected Drainage Basins. Unpublished - Dept of Geog, Liverpool.
- Brady, N.C. (1984). Ninth Edition. *The Nature and Properties of Soil*. MacMillan USA. 750pp.
- Brisbin, L.I., Robert, J.R., Beyers J. *etal.* (1974). Patterns of radiocaesium in the sediments of a stream channel contaminated by production of reactor effluent. *Health Physics*, **27** (July): 19-27.
- Bristow, G. (1978). The application of airborne gamma-ray spectrometry in the search for radioactive debris from the Russian satellite Cosmos 954. *Current Research, part B, Geological Survey of Canada*. **1B**: 151-162.
- Browne, E. and Firestone, R.B. (1986). *Table of Isotopes*. John Wiley and Sons.
- Burcham, W.E. (1973). *Nuclear Physics. An Introduction*. 2nd Ed. Longman. 686pp.
- Burns, S.F., Thompson, D.H., Beck, J.N. and Meriwether John R. (1991). Thorium, Uranium and Caesium-137 in Louisiana Soils Migration Trends in a Soil Calena near Dubach, Louisiana, USA. *Radiochemica Acta*, **52/53**: 241-247.
- Bunzl, K. and Kracke, W. (1988). Cumulative Deposition of ^{137}Cs , ^{238}Pu and $^{239+240}\text{Pu}$ and ^{241}Am from Global fallout in Soils from forest, grassland and arable land in Bavaria (FRG). *J. Environ. Radioactivity*. **8**: 1-14.
- Burgess, T.M. and Webster, R. (1980). Optimal Interpolation and Isarithmic mapping of Soil Properties. I. Semivariogram and Punctual Kriging. *Journal of Soil Sci.* **31**: 316-331.
- Burns, S.F., Thompson, R.H., Beck, J.N. (1991). Thorium, Uranium and ^{137}Cs in Louisiana Soils. Migration Trends in a Soil Catena near Dubach Louisiana, USA. *Radiochemica Acta*. **52/53**: 241-247.
- Cambray, R.S., Cawse, P.A., Garland, J.A., Gibson, J.A.B., Johnson, P., Lewis, G.N.J., Newton, D., Salmon, L. and Wade, B.O. (1987). Observations on Radioactivity from Chernobyl Accident. *Nucl. Energy*. **26**: 77-101.
- Cameron, D.R., Nyborg, M., Toogoodm J.A. and Lavery, D.H. (1971). Accuracy of field sampling for soil tests. *Can. J. Soil. Sci.* **51**: 165-175.
- Cambell, J.B. (1979). Spatial Variability of Soils. *Annals of the Association of American Geographers*. **69**(4): 544-556.

- Cambell, J.B. (1978). Division of S-5 - soil genesis. Morphology and classification. *Soil Sc. Soc. Am. J.* **42**: 460-464.
- Carlson, S. (1978). A model for the movement and loss of ^{137}Cs in a small watershed. *Health Physics.* **34**: 33-37.
- Cawse, P.A. (1980). Studies of Environmental Radioactivity in Cumbria. Part 4. ^{137}Cs and plutonium in soils of Cumbria and Isle of Man. *AERE Harwell Report R9851*. HMSO London.
- Cawse, P.A. (1983). The accumulation of ^{137}Cs and $^{239+240}\text{Pu}$ in soils of Great Britain and transfer to vegetation. *In Ecological aspects of Radionuclide Release*; Eds. Crougthy, P.J., Bell, J.N.B. and Roberts, T.M. Blackwell Scientific Publications.
- Cawse, P.A. and Horrill, A.D. (1986). A survey of ^{137}Cs and Plutonium in British Soils in 1977. *AERE Harwell Report. R10155*. HMSO London.
- Chamberlain, A.C., Garner R.J., Williams D. (1961). Environmental Monitoring after accidental deposition of Radioactivity. *Reactor Science and Technology.* **14**: 155-167.
- Clark, M.J. and Smith, F.B. (1986). Radionuclide Deposition from the Chernobyl Cloud. *NRPB M139* and *Nature* **322**.
- Clark, M.J. and Smith, F.B. (1988a). Wet and Dry deposition of Chernobyl Releases. *Nature.* **322**: 245-249
- Clark, M.J. and Smith, F.B. (1988b). Radiological Aspects of Chernobyl in W.Europe. *NRPB M139* and *Radiological. Prot. Bull.* **75**.
- Clark, M.J. (1986a). Fallout from Chernobyl. *NRPB M139.* & *J. Soc. Radial. Prot.*
- Clark, R.H. (1986b). Chernobyl and the International Agencies. *NRPB M139* and *Radiological. Prot. Bull.* **75**.
- Coleman, N.T. and Le Roux, F.H. (1965). Ion-exchange displacement of Cs from soil Vermiculite. *Soil Sci.* **99**(4).
- Comans, R.N.J., Huller, M. and Depreter, P. (1991). Sorption of Cs on illite; Non-equilibrium behaviour and reversibility. *Geochemica et Cos. Acta.* **5**(2).
- Conradson, K., Nielson, A.A. and Windfeld, K. (1992). Analysis of geochemical data sampled on a regional scale. In Walden, A.T. and Guttorp, P. (1992). *Statistics in the Environmental and Earth Sciences.* Edward Arnold. 306 pp.
- Cook, G.T., Baxter, M.S., Duncan, H.J., Toole, J. and Malcolmson, R. (1984). Geochemical association of plutonium in the Caithness environment. *Nucl. Inst. and Methods in Physics Research.* **223**: 517-522.

- Coppola, M. and Reiniger, P. (1974). Influence of the chemical composition on the gamma-ray attenuation by soils. *Soil Sci.* **117**(6): 331-335
- Coughtrey, P.J. (1988). Models for radionuclide transport in soils. *Soil Use and Management.* **4**(3): 84-90.
- Coughtrey, P.J., Jackson, D.J., Jones, C.H. and Thorne, M.C. (1984). *Radionuclide Distribution and Transport in Terrestrial and Aquatic Ecosystems. A critical review of Data.* Vol. 5. A.A Balkema. 359pp.
- Cox, K.G., Bell, J.D. and Pankhurst, R.J. (1984). *The Interpretation of Igneous Rocks.* George Allan and Unwin Publ. 450 pp.
- Cremers. A., Elsen, A., DePeter, P. and Maes, A. (1988). Quantitative analysis of radiocaesium retention in soils. *Nature.* **335**: 247-249.
- Cressie, N. (1989). Geostatistics. *The American Statistician.* **43**(4): 197-202.
- Currie, L.A. (1968). Limits of Qualitative Detection and Quantitative Determination. *Anal. Chem.* **40**: 586-593.
- Cutshall, N.H. and Larsen, I.I. (1986). Calibration of a Portable intrinsic Ge γ -ray Detector using point sources and testing for field applications. *Health Physics.* **51**(1): 53-59.
- Darnley, A.G. (1984). Natural Background Radiation in Canada. *Geological Survey of Canada, Bulletin* **360**:39.
- Dickson, H.W., Kerr, G.D., Perdue, P.T. and Abdullah, S.A. (1976). Environmental γ -ray measurements using in-situ and core sampling techniques. *Health Physics.* (Feb) 1221-1227.
- Dickson, B.H., Bailey, R.C. and Grasty, R.L. (1981). Utilizing experimentally derived multichannel and airborne gamma ray spectra for the analysis of airborne data. *Proc, Sympos. of Uranium Expl.* Methods dev. of the NEA/IAEA R&D prog. Paris: 653-669.
- Dominik, J., Burns, D. and Vernet, J.P. (1987). Transport of environmental radionuclides in an alpine watershed. *Earth and Planet. Sci. Letters.* **84**: 165-180.
- Drichko, V.F., Krisyuk, B.E., Travniko, I.G., Lisachenko, E.P. and Bubenskaya, M.A. (1977). Frequency distribution of radium-226, thorium-228, and potassium-40 concentrations in various soils. *Soviet Soil Science.* **9**(5): 593-598.
- Drichko, V.F. and Lisachenko, E.P. (1984). Background concentrations of ^{226}Ra , ^{228}Th and ^{40}K in cultivated soils and agricultural plants. *Soviet J. Ecology.* **15**(2):81-85.

- During, C. and Mountier, S. (1967). Sources of error in Advisory Soil Tests, III Spatial Variance. *N.Z. J. Agric. Res.* **10**: 134-8.
- Durrance, E.M. (1986). *Radioactivity in Geology, principles and applications*. 441pp. Ellis and Horwood Ltd.
- Duval, J.S., Cook, B., and Adams, J.A.S. (1971). Circles of Investigation of an Airborne Gamma Ray Spectrometer. *Journal of Geophysical Research.* **76**(35).
- Eakins, J.D., Pattendes, N.J. and Cambray, R.S. (1981). Studies of Environmental Radioactivity in Cumbria Part 2: Radionuclide Deposits in Soil in Coastal Regions of Cumbria. *UKAEA Harwell, AERE R9873*.
- Eichholz, G.G. (1977). *Environmental aspects of Nuclear power*. 683pp. Am. Abbor. Science Publ. Inc
- Eisenbud, M. (1973). *Environmental Radioactivity*, 2nd Ed. Academic Press, New York. Quoted from Whicker and Schultz. (1982).
- El-Fawaris, A.H. and Knaus, R.M. (1984). ^{137}Cs Movement in a southern coastal plain ecosystem. *Health Physics.* **46**(4): 883-890.
- Evans, D.W., Alberts, J.J., Clark, I.I.I. and Roy, A. (1983). Reversible ion-exchange fixation of ^{137}Cs leading to mobilization from reservoir sediments. *Geochemica et Cosmochem. Acta.* **47**: 1041-1049.
- Fahad, A.A. Ali, A.W. and Shihab, R.M. (1989). Mobilization and fractionation of ^{137}Cs in Calcareous Soils. *Journal of Radioanalytical and Nuclear Chemistry.* **130**(1): 195-201.
- Faniran, A and Areola, O. (1978). *Essentials of Soil Study*. Heinemann, London. 278pp.
- FitzPatrick, E.A. (1983). *Soils. Their Formation, Classification and Distribution*. Longman Publ. 353pp.
- Fowler, Eric B., Gilbert, Richard O. and Essington, Edward H. (1974). *Sampling of Soils for Radioactivity: Philosophy, Experience and Results*. In: Atmosphere - Surface Exchange of Particles and Gaseous Pollutants. ERDA Symposium Series 38, : 706-727.
- Francis, C.W. and Brinkley, F.S. (1976). Preferential Adsorption of ^{137}Cs to Micaceous Minerals in Contaminated Freshwater Sediment. *Nature.* **260**: 511-513.
- Frankland, Juliet C., Ovington, J.O. and Macrae, M. (1962). Spatial and Seasonal Variation in Soil, Litter and Ground Vegetation in some Lake District Woodlands.

Frederickson, A.G. (1958). Some mechanical mechanisms for the fixation of U. in certain sediments. *Science*. **108**: 184-185.

Fry, F.A. (1987). The Chernobyl reactor accident: the impact on the United Kingdom. *The British Journal of Radiology*. **60**(719): 1147-1158.

Fry, F.A. and Milton, M.I. (1986). Thyroid contents of ¹³¹I in UK Residents after Chernobyl. *NRPB M139*.

Galloway, R.B. (1991a). Correction for sample self absorption in activity determination by γ spectrometer. *Nuclear Instruments and Methods in Physics Research*. **A300**: 367-373.

Galloway, R.B. (1991b). A simple method of correcting for variation of sample thickness in the determination of the activity of environmental samples by gamma spectrometry. *Meas. Sci. Technol.* **2**: 941-945.

Galloway, R.B. (1993). Correction for sample thickness in Activity Determination by Gamma-Ray Spectrometry. *Radioactivity and Radiochemistry*. **4**(3): 33-41.

Garland, J.A., McKay, W.A., Cambray, R.S., Burton, P.J. (1988). *Man Made Radionuclides in the Environment of Dumfries and Galloway*. Harwell Report, DOE Report No. DOE/RW/89.015: HL89/1105.

Garland, J.A., McKay, W.A., Cambray, R.S., Burton, P.J. (1989). Man Made Radionuclides in the Environment of Dumfries and Galloway. *Nucl. Energy*. **28**(6): 369-392.

Gilbert, R.O., Eberhardt, L.L., Fowler, E.B. and Essington, E.H. (1974). *Statistical Design Aspects of Sampling Soil for Plutonium*. In: Atmosphere - Surface Exchange of Particles and Gaseous Pollutants. ERDA Symposium Series 38,: 689-705.

Gilbert, R.O. and Simpson, J.C. (1985). Kriging for Estimating Spatial Pattern of Contaminants: Potential and Problems. *Environ. Monitoring and Assess.* **5**: 113-135.

Gillham, R.W., Cherry, J.A. and Linday, L.E. (1980). Caesium Distribution Coefficients in Unconsolidated Geological Materials. *Health Physics*. **39**(Oct): 637-649.

Govindaraju, K. (1989). *Geostandards News Letter; Special Issue of the Geostandards News Letter*. July, 1989. Publ: the International Working Group, "Analytical Standards of Minerals, Ores and Rocks". ISSN: 0150 - 5505.

Grasty, R.L. and Darnley, A.G. (1971). The Calibration of Gamma-Ray Spectrometers for Ground and Airborne Use. *Geological Survey of Canada*. **71**(17): 1-27.

Grasty, R.L. (1976). A Calibration Procedure for an Airborne Gamma-Ray Spectrometer. *Geological Survey of Canada*. **76**(16): 1-9.

- Grasty, R.L., Richardsan, K.A. and Knight, G.B. (1978). Airborne Detection of small Radioactive sources. Nevada Section - American Nucl. Soc. Aerial Techniques for Env. Monit. *Topical Symp. Proc.*
- Grasty, R.L., Kosanke K.L. and Foolesm, R.S. (1979). Fields of View of Airborne Gamma Ray Detectors. *Geophysics*. **44**(8): 1447-1457.
- Grasty, R.L. (1980). *The search for Cosmos 954*, in the "Search Theory and Application". Ed. Hevlev and Stone, Plenum Publishing Corporation, New York.
- Grasty, R.L. (1981). Skyshine and the Calibration of Ground Gamma-ray Spectrometry. *Geological Society of Canada*. Current Research part A, 80-1-A.
- Grasty, R.L., Glynn, J.E. and Grant, J.A. (1985). The Analysis of Multichannel Airborne Gamma Ray Spectra. *Geophysics*. **50**(12): 2611-2620.
- Gy, P. (1967). *Sampling of Materials in Bulk - Theory and Practice, Vol. 1*. Society de l'Industrie Minerale, St Etienne, France.
- Hamilton, E.I. and Clifton, R.J. (1987). The origin composition and distribution of "hot particles" derived from nuclear industry and dispersion in the Environment. *DOE. Rep. No. DOE/RW/88001*.
- Hanson, R.O. and Stout, Perry, R. (1968). Isotopic Distribution of Uranium and Thorium in Soils. *Soil Science*. **105**(1).
- Harmson, K. and de Haan, F.A.M. (1980). Occurrence and behaviour of uranium and thorium in soil and water. *Neth. J. agric. Sci.* **28**: 40-62.
- Harris, A. (1915). On a Criterion of Substratum Homogeneity (or Heterogeneity) in Field Experiments. *The American Naturalist*. **49**: 453. Quoted from Cambell, James B. (1979).
- Helfer, Irene K. and Miller, Kevin M. (1988). Calibration factors for the Ge Detectors used for Field Spectrometry. *Health Physics*. **55**(1): 15-29.
- Hine, J.H. (1952). The effective atomic numbers of materials for various γ -ray interactions. *Phys. Rev.* **85**: 725. Quoted from Mudahar and Sahota (1988b).
- Horrill, A.D., Lowe, V.P.W. and Howson, G. (1988). Chernobyl Fallout in Great Britain. *ITE Project. T07006*.
- Horrill, A.D. and Lindley, D.K. (1989). A monitoring method for assessing the distribution of environmental contamination based on land classification. *Int. Symp. on Env. Contamination following a major nuclear accident*. IAEA Vienna. IAEA-SM-306/43

- Hubbell, J.H. (1982). Photon Mass Attenuation and Energy absorption Coefficients from 1 keV and 20 keV. *Int. J. appl. Radiation Isot.* **33**: 1269-1290.
- Huijbregts, C.J. (1975). Regionalised Variables and Quantitative Analysis of Spatial Data. Chapter in: *Display and Analysis of Spatial Data*, Ed. Davis and McCullagh. p38-53.
- Hunt, S.E. (1980). *Fission, Fusion and The Energy Crisis*. 2nd Edition. 166pp. Pergamon Press.
- Hursthouse, A.S., Baxter, M.S., Livens F., and Dine, H.J. (1991). Transfer of Sellafield derived ^{237}Np , to and within the Terrestrial Environment. *J. Env. Radioactivity*. **14**: 147-174.
- IAEA. (1976). *Radiometric Reporting Methods and Calibration in Uranium Exploration*. Tech. Report Series. **174**. IAEA Vienna.
- IAEA. (1979). *Gamma-Ray Surveys in Uranium Exploration*. Tech. Report. Series. **186**. IAEA Vienna.
- IAEA. (1990). *The use of gamma ray data to define the natural radiation environment*. Technical Report Series. Tec. Doc. **566**, IAEA Vienna.
- IAEA. (1991). *Airborne Gamma Ray Spectrometer Surveying*. IAEA, Technical Report Series **323**. IAEA Vienna, ISBN 92-0-125 291-9.
- ICRU (1993). *In-Situ Gamma-ray Spectrometry in the Environment*. Draft of the ICRU Report Committee. March 1993.
- Ingamells, C.O., Engelis, J.C., and Switzer, P. (1972). Effect of laboratory sampling error in geochemistry and geochronology. *24th IGC*. **10**: 405-415.
- Ingamells, C.O. (1974a). Control of Geochemical Error through sampling and subsampling diagrams. *Geochemica et Cosmoch. Acta*. **38**: 1225-1237.
- Ingamells, C.O. (1974b). New Approaches to Geochemical Analysis and Sampling. *Talanta*. **21**: 141-155.
- Irlweck, K. (1991). Distribution of $^{137(134)}\text{Cs}$ in Lake Sediments from Mondsee (Austria) before Chernobyl Accident. *Radiochemica Acta*. **52/53**: 233-236.
- Ivanovich and Harmon. (1982). *Uranium Series Disequilibrium*. Clarendon Press. 571pp.
- Jacob, P., Paretzke, H. and Herwig G. (1986). Gamma-Ray Exposure from Contaminated Soil. *Nuclear Science and Engineering*. **93**: 248-261.

Jacob, P., Meckbach, R., Paretzke, and Herwig G. (1993). Dose Rates in Air Caesium Deposition on Grassland. *Health Physics* in press

Joshi, S.R., Murdoch, A. (1988). Direct Determination of Geochronological Useful Radionuclides in Sediments by Low-Energy Photon Analysis. *Nuclear Instruments and Methods in Physics Research*. **A263**: 529-536.

Kaye, G.W.C. and Labey, T.H. (1991). *Tables of Physical and Chemical Constants*. Longman. 386pp.

Kaye, J.H., Brauer, F.P., Fager, J.E. and Reich Jr., H.G. (1973). Background Reduction of Ge(Li) Detectors. *Nuclear Instruments and Methods*. **113**(5).

Kazuko, M. and Takashi, O. (1982). Contents of Natural Radioactive Nuclides in Soil in Relation to Their Surface Area. *Journal of Geophysical Research*. **87**(b13): 10,857-10,860.

Knoll, G.F. (1979). *Radiation Detection and Measurement*. John Wiley and Sons. 816pp.

Knoll, G.F. (1989). 2nd Edition. *Radiation Detection and Measurement*. John Wiley and Sons. 754pp.

Koide, M. and Goldberg, E.D. (1981). $^{241}\text{Pu}/^{239+240}\text{Pu}$ in polar glaciers. *Earth and Planetary Science letters*. **54**: 239-247.

Kogan, R.M., Nazarov, I.M. and Fridman, Sh. D. (1971). *Gamma Spectrometry of the Natural Environment and Formations. Theory and Method Applications to Geology and Geophysics*. Printed in Jerusalem by Keter Press. 338pp. Available from the U.S. Dept. of Commerce - translated from Russian. National Technical Information Service, Springfield, Va. 22151. Also published in 1991, in Russian only.

Królas, K. Kubala, M. and Scheizor, T. (1987). Ground deposition of long-lived gamma emitters in Poland from the Chernobyl Accident. *Acta Physica Polonica*. **B18**(1): 1179-1186.

Lederer, C.M., Shirley, V.S. (Editors) (1978). *Table of Isotopes*. Part V, 7th Ad. Lawrence Berkeley Laboratory. University of California, Berkeley. John Wiley and Sons.

Livens, F.R. and Baxter, M.S. (1988 a). Particle Size and Radionuclide Levels in some west Cumbrian Soils. *The Science of the Total Environment*. **70**: 1-17.

Livens, F.R. and Baxter, M.S. (1988 b). Chemical association of Artificial Radionuclides in Cumbrian Soils. *J. Env. Radioactivity*. **7**.

Livingston, H.D. and Bowen, V.T. (1976). *Americium in the Marine Environment, relationships to plutonium*. In: Miller, M.W. and Stannard J.N. (Eds.) *Environmental Toxicity of Aquatic Radionuclides: Models and Mechanisms*. 107-130. Ann. Arbor. Sci. Quoted from Coughtrey *et al* (1984)

Løvborg, Leif; Wollenberg, Harold; Sørensen, Paul; and Hansen, John. (1971). Field Determination of Uranium and Thorium by Gamma Ray Spectrometer, Exemplified by Measurement in the Ilimaussaq, Alkalie Intrusion, S Greenland. *Economic Geology*. 88(3).

Løvborg, L. and Kirkegaard, P. (1974). Response of 3"x3" NaI(Tl) detectors to Terrestrial Gamma Radiation. *Nuclear Instruments and Methods*. 121: 239-251.

Løvborg, L., Gratsy, R.L., Kirkegaard, P. (1978a). A guide to the Calibration constants for aerial gamma ray surveys in geoexploration. *Topical Symp. Proc. Nevada Section -America Nucl. Soc. Aerial techniques for Envi. Monit.*

Løvborg, Leif, Bitter-Jensen, Lars and Kirkegaard, Peter. (1978b). Experiences with Concrete Calibration Sources for Radiometric Field Instruments. *Geophysics*. 43(3): 543-549.

Løvborg, L., Christiansen, E.M., Bitter-Jensen, L. and Kirkegaard, P. (1981). *Pad Facilities for the Calibration of Gamma Ray Measurements on Rocks*. Risø Nat. Lab. D.K. Roskilde, Denmark. October, 1981.

Løvborg, L. (1982). Error analysis of Calibration and Field Trials with Spectrometers and Counters. *Symp. of Uranium Exploration Methods*. OECD Nuclear Energy Agency in Collaboration with Int. Atomic Energy Agency.

Løvborg, L. (1983). *Total Count Calibration Blocks for the Use in Uranium Exploration*. Risø Nat. Lab. D.K. Roskilde, Denmark. DK 4000. Risø R-490.

Løvborg, L. and Mose, E. (1987). Counting statistics in radioelemental assaying with a portable spectrometer. *Geophysics*, 52(4): 555-563.

MacKenzie, A.B. and Scott, R.D. (1982). Radiocaesium and Plutonium in Intertidal Sediments from Southern Scotland. *Nature*. 299: 613-616.

MacKenzie, A.B., Scott, R.D. and Williams, T.M. (1987). Mechanisms for Northwards Dispersal of Sellafield Waste. *Nature*. 329: 42-45.

McBratney, A.B. and Webster, R. (1986). Choosing functions for semivariograms of soil properties and fitting them to sampling estimates. *Journal of Soil Science*. 37: 617-639.

McDonald, P., Cook, G.T., Baxter, M.S. and Thompson, J.C. (1990). Radionuclide Transfer from Sellafield to South West Scotland. *J. Env. Radioactivity*: 12: 285-298.

- McDonald, P., Cook, G.T. and Baxter, M.S. (1992a). Natural and Anthropogenic Radioactivity in Coastal Regions of the UK. *Radiation Protection Dosimetry*. **45(1/4)**: 707-710.
- McDonald, P., Cook, G.T., Baxter, M.S., Thompson, J.C. (1992b). The terrestrial distribution of artificial radioactivity in South West Scotland. *The Science of the Total Environment*. **111**: 59-82.
- McHugh, J.O. and Hetherington, J.A. (1987). Airborne Radioactivity in the Scottish Solway Coast. *J. Env. Radioactivity*. **5**: 333-342.
- McKay, W.A. and Baxter, M.S. (1985). The Partitioning of Sellafield derived Radiocaesium in Scottish Coastal Sediments. *J. Env. Radioactivity*. **2**: 93-114.
- McKay, W.A. and Pattenden, N.J. (1990). The transfer of Radionuclides from sea to land via the Air. A review. *J. Environmental Radioactivity*. **12**: 49-77.
- McKay, W.A., Bonnett, P.J.P, Barr, H.M., Howorth, J.M. (1991). *Artificial Radioactivity in Tide Washed Pastures in S.W. Scotland*. DOE Report No: DOE/HMIP/RR/91/056.
- Megumi, K., Oka, T., Yaskawa, K. and Sakanque, M. (1982). Contents of Natural Radioactive Nuclides in Soil in Relation to their Surface Area, *The Journ. of Geophysical Research*. **87(B13)**: 10857-10860.
- Meijer, R.J. de., Aldenkamp., F.J., Brummellium, M.J.A., Jansen, J.F.W. and Put, L.W. (1990). Radionuclide Concentration in the Northern Part of the Netherlands after the Chernobyl Reactor Accident. *Health Physics*. **58(4)**: 441-452.
- Mellander, H. (1989). Airborne gamma spectrometric measurements of the fallout over Sweden after the nuclear reactor accident at Chernobyl USSR. *IAEA/NENF/NM-89-1*
- Michio, A., Hirose, K. and Sugimura, Y. (1991). The Temporal Variation of Stratospheric Fallout Derived from the Chernobyl Accident. *J. Env. Radioactivity*. 103-115.
- Miller, J.M. and Taylor, K. (1966). Uranium Mineralization near Dalbeatie Kirkudbrightshire. *Bull. of Geol. Soc. of Great Britain*. **25**: 1-18.
- Miller, G.R., Horrill, A.D., Thompson, A.J. and Howson, G. (1989). *Radioactivity in Scottish Soils and Grassy Vegetation*. ITE Project TO7006el.
- Miller, K.M., Kuiper, J.L., Helfer, I.K. (1990). ¹³⁷Cs Fallout Depth Distributions in Forest Soils Versus Field Sites. Implication for external gamma dose rates. *J. of Env. Radioactivity*. **12**: 23-47.

- Miyahara, K., Ashida, T., Kohara, Y., Yusa, Y. and Sasaki, N. (1990). *Effect of Bulk Density on Diffusion of Caesium in Compacted Sodium Bentonite*. *Radiochemica Acta*. **52/53**: 293-297.
- Mudahar, G.S. and Sahota, H.S. (1986). A New Method for Simultaneous Measurement of Soil Bulk Density and Water Content. *Appl. Radiation Isot.* **37(7)**: 563-565.
- Mudahar, G.S. and Sahota, H.S. (1988 a). Soil: A radiation Shielding Material. *Appl. Radiation Isot.* **39(1)**: 21-24.
- Mudahar, G.S. and Sahota, H.S. (1988 b). Effective Atomic Number Studies in Different Soils. For Total Photon Interaction in the Energy Region 10-5000 keV. *Appl. Radiation Isot.* **39(12)**: 1251-1254.
- Myres, W.A. and Lindner, M. (1973). *J. Inorg. Nucl. Chem.* **33**: 3233. Quoted from Ivanovich and Harmon, 1982.
- NEA. (1987). *The radiological impact of the Chernobyl Accident; in OECD countries*. 185pp. Nuclear Energy Agency - Organisation for Economic Co-operation and Development.
- Ohnuki, Toshikik and Tanaka, Tadao. (1989). Migration of Radionuclides controlled by several different migration mechanism through a sandy soil layer. *Health Physics*. **56(1)**: 47-53.
- Oughton, D.H. (1992). *Hot Particle Sampling*. Presentation to the Coordinating Group for Environmental Radioactivity. Sept. 1992. University of Bangor, N. Wales.
- Osburn, W.S. (1965). Primordial Radionuclides, their distribution movement and possible effect within terrestrial ecosystems. *Health Physics*. Vol **11**:1275-1295.
- Palten, B.C. and Witkamp, M. (1967). Systems analysis of ¹³⁴Cs kinetics in terrestrial Microcosms. *Ecology*. **48(5)**: 813-824.
- Papastefanou, C., Monolopoutin, M. and Charalanbous, S. (1988). Caesium-137 in soils from Chernobyl fallout. *Health Physics*. **55(6)**: 985-987.
- Parkinson, J.A. and Horrill, A.D. (1984). An Assessment of Variation due to Laboratory and field conditions in the measurement of radionuclides. *Nucl. Inst. and Methods in Physics Research*. **223**: 598-601.
- Pennock, D.J. and De Jong, E. (1987). The influence of slope curvature on soil erosion and deposition in hummock terrain. *Soil Sci.* **144(3)**: 209-217.
- Pierson, D.H., Cambray, R.S., Cawse, P.A., Eakins, J.D. and Pattenden, N.J. (1982). Environmental Radioactivity in Cumbria. *Nature*. **300**: 27.

- Potts, M.J. (1978). Accuracy and Precision in Airborne Radiometric Measurement. *Nevada Section - American Nucl. Soc. Aerial Techniques for Environmental Monitoring*. Topical Symp. Proc. 79/4327.
- Ritchie, J.C. Clebsch, E.E.C., Rudolph, W.K. (1970). Distribution of fallout and natural Gamma Radionuclides in litter, humus and surface mineral soil layers under natural vegetation in the Great Smoky mountains, N. Carolina - Tennessee. *Health Physics*. **18**: 479-489.
- Ritchie, J.C. and McHenry, J.R. (1977). The Distribution of ^{137}Cs in some watersheds in the Eastern United States. *Health Physics*. **32**: 101-105.
- Ritchie, J.C. and McHenry, J.R. (1990). Application of Radioactive Fallout ^{137}Cs for Measuring Soil Erosion and Sediment Accumulation Rates and Patterns: A Review. *J. of Environmental Quality*. **19**(2).
- Roca, V., Napolitano, M., Sparanza, P.R., and Gialanelka, G. (1989). Analysis of Radioactivity levels in Soils and Crops from the Campania Region (S. Italy) after the Chernobyl Accident. *J. Env. Radioactivity*. **9**: 117-129.
- Rogowski, A.S. and Tamura, Tauneo. (1970). Erosional Behaviour of ^{137}Cs . *Health Physics*. **18**: 467-477.
- Rogowski, A.S. (1972). Watershed Physics. Soil Variability Criteria. *Soil Sci*. **8**(4).
- Rouston, R.C., Jansen, G. and Robinson A.V. (1977). ^{241}Am , ^{237}Np and ^{99}Tc sorption of two United States subsoils from differing weathering intensity areas. *Health Physics*. **33**: 311-317.
- Russo, D. (1984). Design of an optimal sampling network for estimating the semivariogram. *Soil Science Society of America J*. **48**: 708-716.
- Rybacek, K., Jacob, P. and Macklach, R. (1991). In-situ Determination of Deposition Radionuclide Activities: Improvement of the Method by Deriving Depth Distributions from the measured Photon Spectra. *Health Physics -Submitted Sept. 1991*
- Saito, K. and Moriuchi, S. (1985). Development of a Monte Carlo Code for the Calculation of Gamma-Ray Transport in the Natural Environment. *Radiation Protection Dosimetry*. **12**(1): 21-28.
- Saito, K. (1991). Doses due to Terrestrial gamma rays as the snow cover. *Radiation Protection Dosimetry*. **35**(1): 31-39.
- Saksena, R.S., Chandra, S. and Singh, B.P. (1974). A gamma transmission method for the determination of moisture content in soils. *Journal of Hydrology*. **23**: 341-352.

- Sanchez, A.L., Schell, W.R. and Thomas, E.D. (1988). Interactions of ^{57}Co , ^{85}Sr and ^{137}Cs with Peat under precipitation conditions. *Health Physics*. **54**(3): 317-322.
- Sanchez, A.L., Schell, W.R. and Sibley, T.H. (1981). *Distribution Coefficients for Radionuclides in aquatic environments*. NUREG/CR-1852, Vol 5. College of Fisheries, University of Washington. Quoted from Coughtry *et al* (1984).
- Sanderson, D.C.W. and Scott, E.M. (1989). An Aerial Radiometric Survey in West Cumbria in 1988. *MAFF Food Science Report*. N611.
- Sanderson, D.C.W., Allyson, J.D., Martin, E., Tyler, A.N. and Scott, E.M. 1990. An Airborne Gamma Ray Survey of Three Ayrshire Districts. *SURRC Report*.
- Sanderson, D.C.W., Allyson, J.D. and Tyler, A.N. (1992). Chapelcross Aerial Survey. *SURRC Report for BNFplc*.
- Sanderson, D.C.W., Allyson, J.D. and Tyler, A.N. (1993 a). Aerial Radiometric Survey of South West Scotland. *SURRC preliminary report for Scottish Office*.
- Sanderson, D.C.W., Allyson, J.D., Tyler, A.N. and Murphey, S. (1993 b). Springfields Aerial Survey. *SURRC Report for BNFplc*.
- Sanderson, D.C.W., Allyson, J.D., Tyler, A.N., Ni Riain, S. and Murphy, S. (1994). An Airborne Gamma Ray Survey of Parts of SW Scotland in February 1993. Final Report. *SURRC report for Scottish Office*.
- Sawney, B.L. (1972). Selective sorption and fixation of cations by clay minerals: A Review. *Clays and Clay Minerals*. **20**: 93-100.
- Schimmack, W., Bunzl, K. and Bachhuber, H. (1987). Variability of the sorption of Cs, Zn, Sr, Co, Cd, Ce, Ru, Tc and I at trace concentrations by a forest soil along a transect. *Environment International*. **13**: 427-436.
- Schultz, R.K., Overstreet, R. and Barshad, I. (1960). On the Soil Chemistry of ^{137}Cs . *Soil Sci*. **89**: 16-27.
- Schultz, R.K. (1965). Soil Chemistry of Radionuclides. *Health Physics*. **11**: 1317-1324.
- Schwarz, G.F., Klingele, E.E. and Rybach, L. (1992). How to handle rugged topography in airborne gamma-ray spectrometry surveys. *First Break* **10**(1): 11-17.
- Scott, R.D., MacKenzie, A.B., Shaban, Y.A.B., Hooker, P.J. and Houston, C.M. (1991). Uranium Transport and Retardation at the Needles Eye Natural Analogue Site, SW Scotland. *Radiochemica Acta*. **52/53**: 357-365.
- Shafroth, Stephen M. (1967). *Scintillation Spectroscopy and Gamma Radiation*. Vol.1. Gordon and Breach Science Publ. 446pp.

- Silant'ev, A.N. and Shkuratova, I.G. (1988). Changes in ^{137}Cs migration parameters in soil. *Sov. At. Energy (USA)*. **65(2)**: 687-691.
- Smith, F.B. and Clark, M.J. (1986). Radionuclide Deposition from the Chernobyl Cloud. *NRPB M139 and Nature*, **322**: 690-691.
- Smith, F.B. and Clark, M.J. (1989). The transport and deposition of airborne debris from Chernobyl nuclear power plant accident with special emphasis on the consequences to the U.K. (*Meteorological Office paper No. 42*). HMSO London. 56pp.
- Sowa, W., Martini, E., Gehrike, K., Marshner, P., Naziry, M.J. (1989). Uncertainty of in-situ gamma spectrometry for environmental monitoring. *Radiation Protection Dosimetry*. **27(2)**: 93-101.
- Storm, E. and Israel, H.I. (1970). Photon Cross Sections from 1 keV to 100 MeV for elements $Z = 1$ to $Z = 100$. *Nucl. Data Tables*. **A7**: 565-681
- Stroosnijder, L., and De Swart, J.G. (1974). Column Scanning with Simultaneous use of ^{241}Am and ^{137}Cs Gamma Radiation. *Soil Science*. **118(2)**: 61-69.
- SURRC (1992). The Calculation of the Mass Attenuation Coefficients of Soils. *Internal Report*.
- Sutherland, R.A. and De Jong, E. (1990). Statistical Analysis of gamma emitting radionuclides concentrations for three fields in Southern Saskatchewan, Canada. *Health Physics*. **58(4)**: 417-428.
- Sully, M.J., Flocchini, R.G. and Nielson, D.R. (1987). Linear Distribution of Naturally Occurring Radionuclides in Mollic Xerofluvent. *Soil Sci. Soc. Am. J.* **51**: 276-281.
- Talibudeen, O. (1964). Natural Radioactivity in Soils. *Soils and Fertilizers*. **27(5)**: 347-359.
- Torgessen, T. and Longmore, M.E. (1984). ^{137}Cs Diffusion in highly organic sediment of hidden lake, Fraser Island, Queensland. *Aust. J. Mar. Freshwater Res.* **35**: 537-548.
- Veen, A.W.L. and Mejer, R.J. (1989). Radionuclide levels at two sites in a water extraction area in the Netherlands after Chernobyl. *Water Air and Pollution*. **44**: 83-92.
- Visman J. (1969). A General Sampling Theory. *Mater. Res. Stand.* **9(11)**: 8-13.
- Visman J. (1972). The amount of material needed for a trace element analysis. *Ark. Mineral. Geol.* **3(6)**, 131-139.

- UNSCEAR. (1982). *Ionising Radiation: Sources and Biological Effects*. United Nations Scientific Committee on the Effects of Atomic Radiation, 1982 Report to the General Assembly, U.N. New York.
- Wallenberg, Harold A., Paterson, Wade H., Smith, Alan R. and Stephens, Lloyd D. (1969). Natural and Fallout Radioactivity in the San Francisco Bay Area. *Health Physics* 17: 313-321.
- Wallenberg, H.A. and Smith, A.R. (1990). A Geochemical Assessment of Terrestrial Gamma-Ray Absorbed Dose Rates. *Health Physics*. 58(2): 183-189.
- Wallenberg, H.A., Revzan, K.L. and Smith, A.R. (1994) Application of Airborne Gamma Spectrometric Survey Data to Estimating Terrestrial Gamma-Ray Dose Rates: An Example in California. *Health Physics* 66(1): 10-16.
- Webster, R. (1975). Soil Transect Correlograms of North Oxfordshire and their interpretation. *Journal of Soil Science*. 26(2): 177-193.
- Webster, R. and Burgess, T.M. (1980). Optimal Interpolation and Isarithmic Mapping of Soil Properties. III Changing Drift and Universal Kriging. *Journal of Soil Science*. 3(1): 505-524.
- Whicker, F.W. and Schultz, V. (1982). *Radioecology: Nuclear Energy and the Environment, Vol. 1*. CRC Press Inc.
- Wilding, L.P. and Drees, L.R. (1983). Spatial Variability and Pedology. *In Paedogenesis and Soil Taxonomy. 1. Concepts and Interactions*. (Eds. Wilding, L.P., Smeck, N.E., Hall, L.P.) pp 53-116. Elsevier Science Publishing Co. Inc.
- Williams, D., Cambray, R.S., Maskell, S.C., (1957). An airborne radiometric survey of the Windscale area, October 19-22nd. *AERE Report R-2890*.
- Winkelmann, I., Endrulat, H.J., Fouasnon, S., Gesewsky. P., Haubelt, R., Klopfer, P., Köhler, H., Kohl, R., Kicheida, D., Leising, C., Müller, M.K., Neumann, P., Schmidt, H., Vogl, K., Weimer, S., Wildermuth, H., Winkler, S., Wirth, E., Wolf, S. (1987). *Radioactivity measurements in Fedrela Republic Germany after Chernobyl accide:u*. Neuherberg, Bundesgesundheitsamt, ISH-Heft, 116. From Jacob and Likthariov (1993)
- Zirschky, John. (1985). Geostatistics for environmental Monitoring and Survey Design. *Environmental Int*. 11: 515-524.
- Zombori, P., Andrasi, A., Nemeth, I. (1992). A New Method of determining Radionuclide Distribution in Soil by In-Situ Gamma-Spectrometry. Budapest; Hungarian Academy of Sciences, Central Reserach Institute for Physics, Institute for Atomic Research; Report No. KFK-1992-20/K.

APPENDIX A: THE CALIBRATION OF AN IN-SITU 3"x3" NaI(Tl) DETECTOR

The calibration curves for ^{137}Cs and ^{134}Cs in terms of activity per unit area (Bq m^{-2}) are shown in figures A.1 and A.2. Calibration for ^{40}K , ^{214}Bi and ^{208}Tl in terms of activity per unit area (Bq m^{-2}) and per unit mass (Bq kg^{-1}) are shown in figures A.3 to A.8. The calibration coefficients are given in table A.1 and A.2.

Radiocaesium Calibration

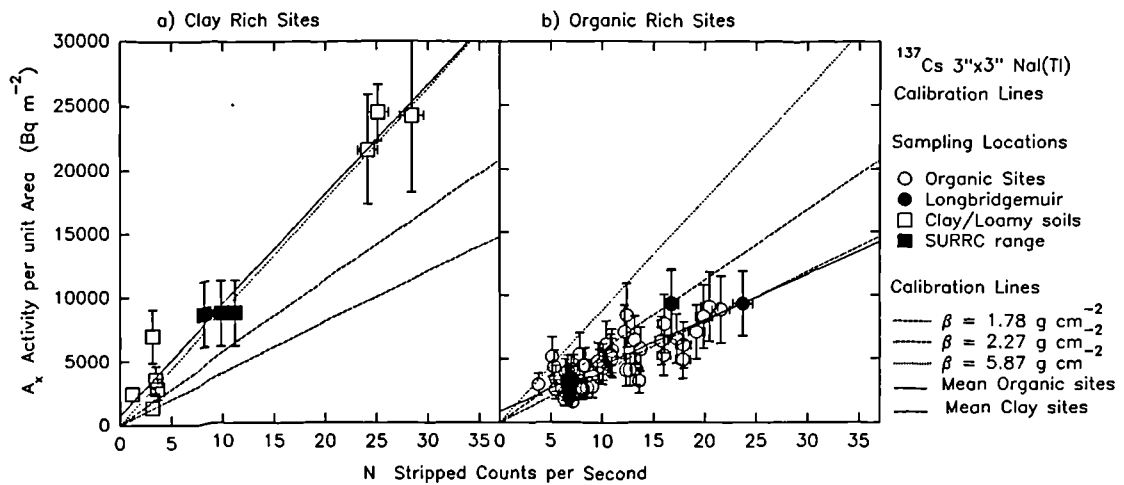


Figure A.1 ^{137}Cs calibration curves for: a) clay rich soils; and b) organic rich soils. Curves described in terms of *mean mass depth* (β) and soil type.

Figure A.1 shows the calibration curves for ^{137}Cs and is interpreted with points of known *mean mass depth* (β). There are two dominant calibration trends, one associated with organic rich sites and the second associated with higher density clay and loamy soils. The two trends have been isolated and used to determine two sets of calibration coefficients as given in both figure A.1 and table A.1. These calibration lines can be interpreted in terms of β as determined from the samples collected at the SURRC site and the Longbridgemuir site. The range in stripped count rate is significantly greater at the Longbridgemuir site than at SURRC, indicating that photon fluence rate is more sensitive to changes in water content in peaty sites.

The scatter of points for the peaty sites lie approximately between the two calibration

Table A.1 The ^{137}Cs and ^{134}Cs calibration coefficients with β for the 3"x3" NaI(Tl) detector. *Analytical solutions derived from photon fluence equations (Allyson 1994).

Element	β	Calibration Coefficients for A_x determination	Bq m^{-2} N/A_x	Analytical Solutions* N/A_x
^{137}Cs	Organic	$831 + 361 \cdot N$	0.00277	
	Clay	$318 + 967 \cdot N$	0.00103	
	0			0.00450
	## 1.78		0.00253	
	## 2.27		0.00179	
	5.0			0.00135
	# 5.87		0.00130	
	12			0.00080
^{134}Cs	Organic	$19.7 + 365 \cdot N$	0.00274	
	Clay	$-44.1 + 647 \cdot N$	0.00155	
	## 1.58		0.00250	
	## 2.01		0.00190	
	# 4.01		0.00140	
	## 4.45		0.00136	

Determined from a 38 mm corer at SURRC

Determined from the 105 mm corer at Longbridgemiur.

lines of 1.78 g cm^{-2} and 2.27 g cm^{-2} . Whilst much of this scatter must be attributed to sampling error, changes in β across these sampling sites must also contribute to this scatter. A similar set of results is observed for ^{134}Cs in figure A.2 and table A.1. It is interesting to note that at low stripped count rate N , there appears to be an excess in counts from the calibration line associated with the clay rich soils. This must be attributed to measurements being inferred from below the minimum detection limits, from which the residual count rate must be derived from ^{40}K under-stripping.

Table A.1 gives the calibration coefficients (N/A_x) derived from figures A.1 and A.2 for ^{137}Cs and ^{134}Cs . The ^{137}Cs results are also compared with analytical solutions derived from photon fluence equations (Allyson 1994). The results demonstrate that (N/A_x) decreases with increasing β , and the experimentally derived results are consistent with those determined from the analytical estimates of N/A_x .

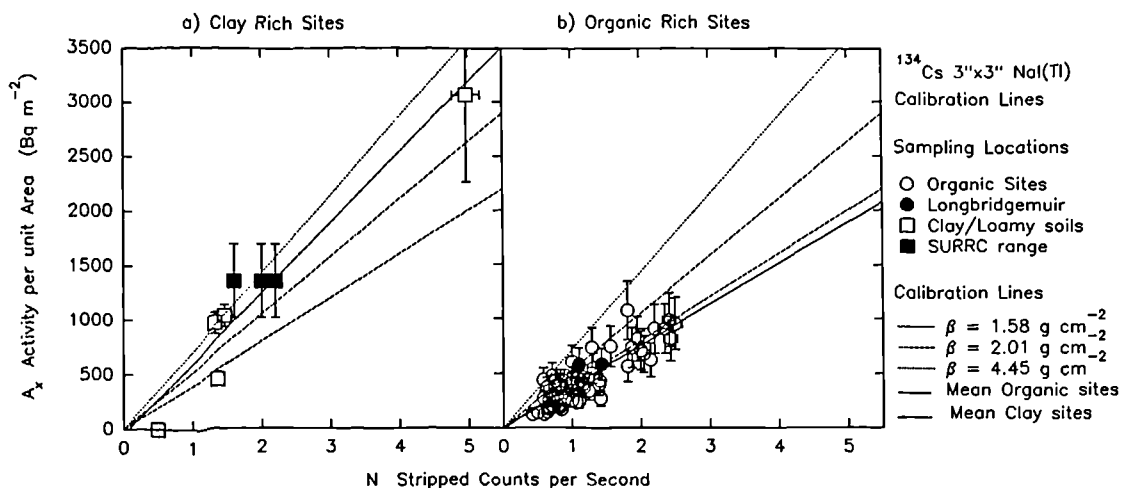


Figure A.2 ^{134}Cs calibration curves for: a) clay rich soils; and b) organic rich soils. Curves described in terms of *mean mass depth* (β) and soil type.

Primordial Radionuclide Calibration Results and Discussion

The discussion in chapter 7 included source distribution characteristics of the primordial radionuclides. The geochemical and physical properties of the primordial radionuclides are discussed in chapter 3 along with their characteristic environmental behaviour. In salt marsh environments, clay, loamy and mineral rich soils, the vertical distribution can be assumed to be constant with depth. However, in the more organically rich soils, typically lower in density, the concentration of primordial radionuclides associated with the underlying geology is found at the base of the soil profile. This has consequences for both sampling of and measurement of primordial radionuclide concentrations through environmental gamma ray spectrometry. As discussed in chapter 4 and 7, low activity peat overburden is likely to provide a buried source profile for the natural radionuclides. This is likely to lead to penetration of gamma photons from beneath the standard 30 cm soil core depth, resulting in overestimation of the soil profile activity and underestimation of the geological strata activity.

The Calibration for ^{40}K is shown in figures A.3 and A.4 for activity concentrations in terms of Bq m^{-2} and Bq kg^{-1} respectively. The calibration coefficients (N/A_x) are given

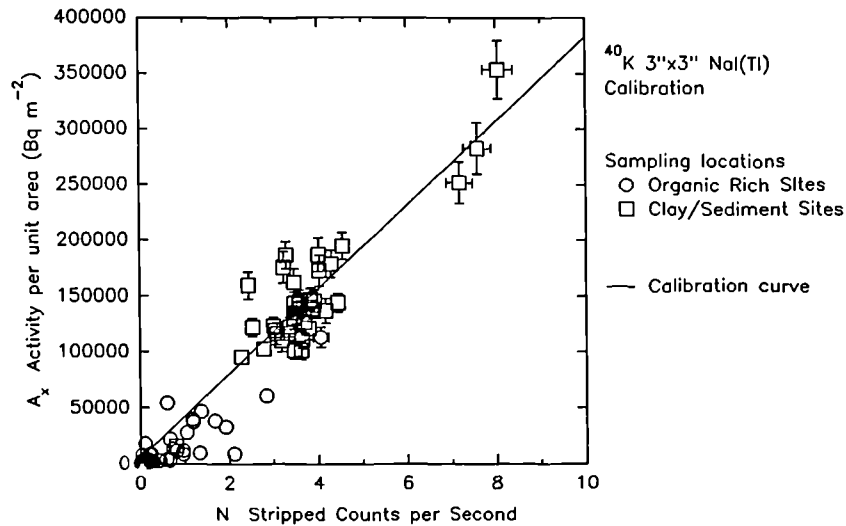


Figure A.3 ^{40}K Calibration in terms of activity per unit area (Bq m^{-2})

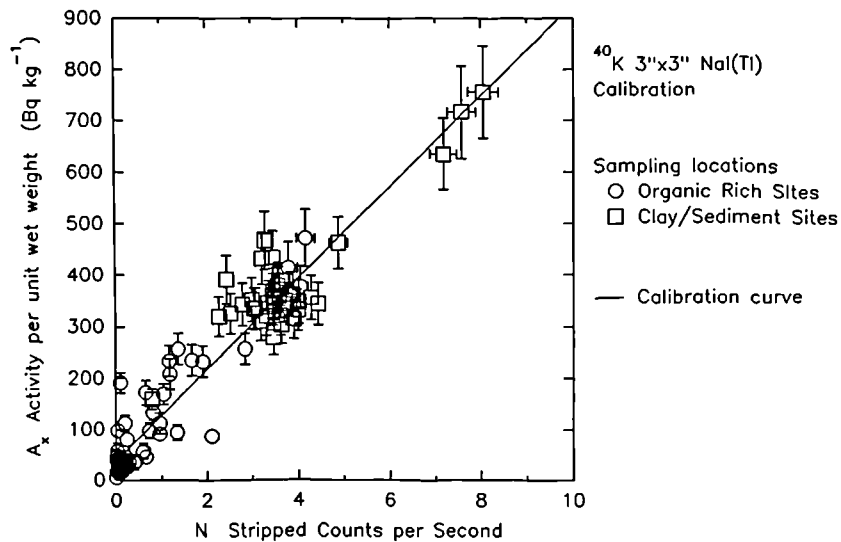


Figure A.4 ^{40}K calibration in terms of activity per unit weight (Bq kg^{-1})

in table A.2. Figure A.3 shows a scatter of points below the mean calibration line associated with the lower density peaty soils, whilst the higher density soils tended to concentrate on or above the calibration line. The calibration line shown is based upon the higher density soils as there is an underestimation of ^{40}K through the lower density (ρ) soil core derived activity, or overestimation through in-situ gamma spectrometry. The mean calibration coefficient (N/A_x) for these soils as given in table A.2 corresponds well with that derived from the analytical solutions of photon fluence equations for a mean soil density of 1.5 g cm^{-2} .

Table A.2 The calibration coefficients for ^{40}K , ^{214}Bi and ^{208}Tl in terms of Bq m^{-2} and Bq kg^{-1} . *High ρ sites represent clay, loamy and sediment sites.*

	Soils Used	Calibration Coefficients for A_x	N/A_x	*Analytic. Solution ρ g cm^{-3} N/A_x	
^{40}K Bq m^{-2}	high ρ	$4907 + 37800 \cdot N$	2.644×10^{-5}	1	4.0×10^{-5}
	All	$-4565 + 39000 \cdot N$	2.564×10^{-5}	1.5	2.667×10^{-5}
$\text{Bq}_{\text{wet}} \text{kg}^{-1}$	All	$38.4 + 88.8 \cdot N$	0.01126		0.012
^{214}Bi Bq m^{-2}	high ρ	$-955 + 15180 \cdot N$	6.586×10^{-5}	1	6.00×10^{-5}
				1.5	4.00×10^{-5}
$\text{Bq}_{\text{wet}} \text{kg}^{-1}$	high ρ	$-1.65 + 38.9 \cdot N$	0.02573		0.018
^{208}Tl Bq m^{-2}	All	$-424 + 4040 \cdot N$	2.4745×10^{-4}	1	3.0×10^{-4}
				1.5	2.0×10^{-4}
$\text{Bq}_{\text{wet}} \text{kg}^{-1}$	All	$0.178 + 8.71 \cdot N$	0.1148		0.09

The estimation of activity in terms of wet weight ($\text{Bq}_{\text{wet}} \text{kg}^{-1}$), automatically excludes the density factor and a more flexible calibration coefficient is derived. This is demonstrated in figure A.4 and in table A.2. The higher activity points fall into line along the calibration curve. The subsequent scatter about the calibration curve must be associated with sampling error and source burial. The calibration coefficient (N/A_x) in terms of $\text{Bq}_{\text{wet}} \text{kg}^{-1}$ corresponds well with that derived from photon fluence equations (Allyson 1994) in table A.2. Thus the calibration in terms activity per unit wet weight,

ie. that observed in the environment, provides a more reliable and flexible calibration.

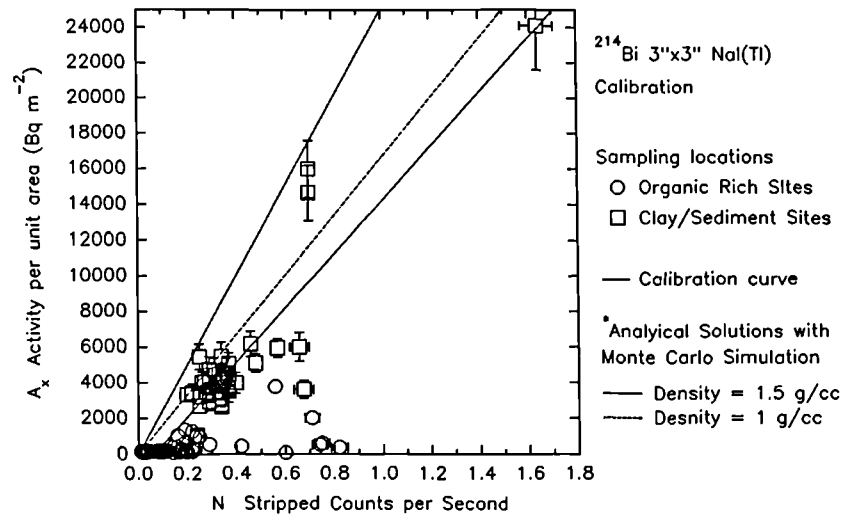


Figure A.5 ^{214}Bi Calibration in terms of activity per unit area (Bq m^{-2})

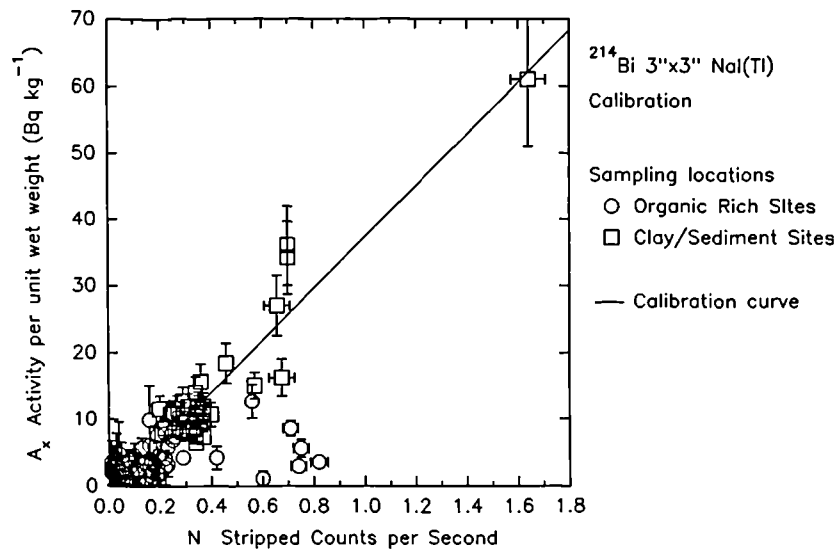


Figure A.6 ^{214}Bi Calibration in terms of activity per unit wet weight (Bq kg^{-1})

Figures A.5 and A.6 illustrate ^{214}Bi calibration curves in terms of activity per unit area (Bq m^{-2}) and per unit wet weight (Bq kg^{-1}) respectively. The scatter of points about the calibration regression is greater in figure A.5 for ^{214}Bi than was observed in figure A.3 for ^{40}K . There are two principle reasons for this:

1. Higher energy photons of ^{214}Bi (1760 keV) penetrating from greater depths in the soil profile. Given that the similar effect for ^{40}K was not so marked, it is

likely that the second reason will account for the majority of this scatter.

2. ^{222}Rn (radon), which forms an inert gas released through porous soil, with a half life of 3.83 days, causes a higher detector response. Its decay products become attached to air borne particles and include ^{214}Bi .

Once ^{214}Bi is airborne, the detection geometry is change considerably, completely surrounding the detector in a 4π geometry. Thus the detection efficiency is increased substantially and is particularly pronounced in the porous organic rich soils as was observed at Lakin Farm on Arran (chapter 6). Thus the high density soils only were used to determine the calibration coefficient (N/A_s) (figure A.5). When comparing the derived calibration coefficient with that derived from photon fluence equations, the airborne radon component appears to increase the calibration coefficient (detection efficiency) considerably from that otherwise expected (table A.2). This problem is seen more clearly when source density and distribution is taken into consideration in figure A.6, where the calibration is in terms of Bq wet kg^{-1} . Here, the airborne component is still obvious even for the higher density soil sites. This has again resulted in a calibration coefficient very different from that expected by calculation from photon fluence equations. The negative intercept in A.6 is likely to be controlled by the airborne radon component.

Another possible cause for this discrepancy is associated with laboratory analysis. There are two potential ways of underestimating the ^{214}Bi concentrations. The first may be brought about by changes in the background level of ^{222}Rn and thus ^{214}Bi in the detector counting room. However, the detectors were placed in a low background environment and repeat background measurements showed negligible change in the observed background. The second cause is the potential leak of ^{222}Rn from the soil sample and out of its container geometry. Although every effort is made to seal the container, leakage of ^{222}Rn cannot be excluded and thus true ^{214}Bi equilibration within the sample may not be reached. However, quality assurance checks with international standard reference materials and repeat bulk sample measurements have demonstrated that estimated ^{214}Bi activity is repeatedly achieved as illustrated in table 5.8 and figure 6.2, although the observed variance is greater than that observed with the other radionuclides.

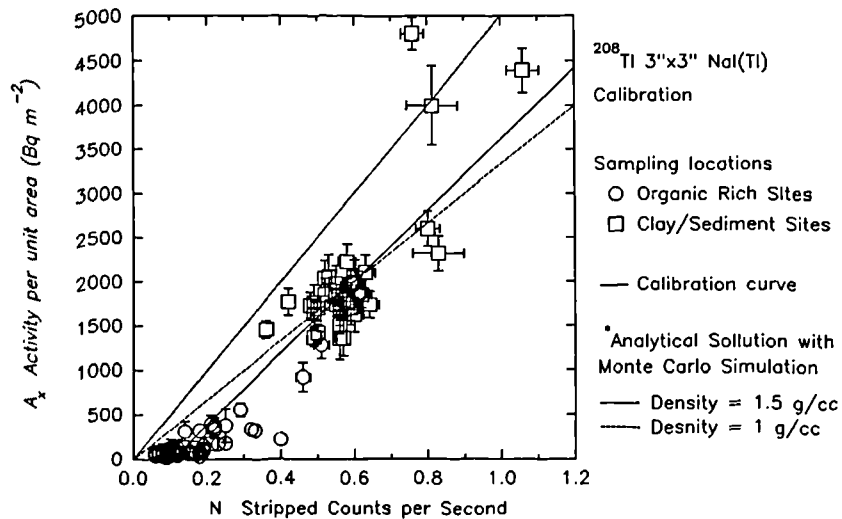


Figure A.7 ^{208}Tl calibration in terms of activity per unit area (Bq m^{-2})

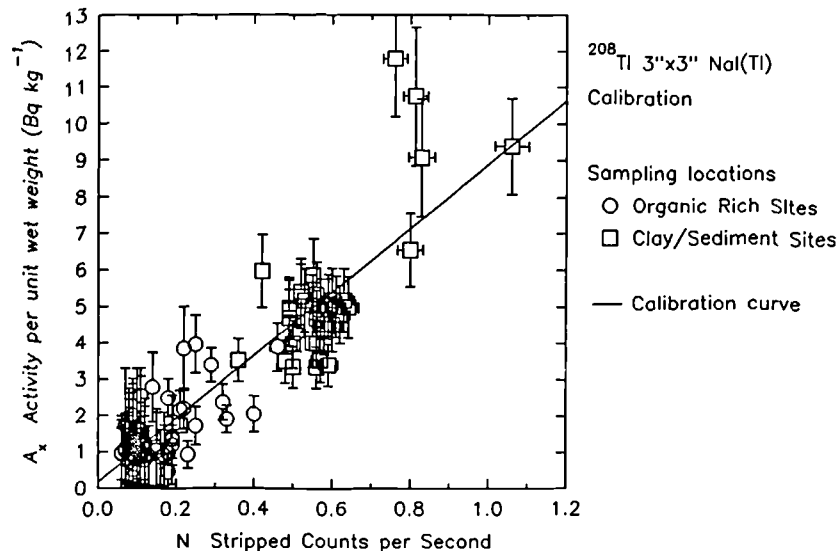


Figure A.8 ^{208}Tl calibration in terms of activity per unit wet weight (Bq kg^{-1})

^{208}Tl calibration is shown in figures A.7 and A.8 in terms of Bq m^{-2} and Bq kg^{-1} respectively with the respective calibration coefficients listed in table A.2. All the points are used to derive a calibration coefficient. However, there is evidence in figure A.7 of a density effect on the potential calibration coefficient which is demonstrated by the scatter of points associated with the higher activity sites. The domination of the organic soils in which the soil core derived activities underestimate the activity observed by the detector lead to a negative intercept activity and is expressed in terms of Bq m^{-2} . The overall calibration coefficient (N/A_x) is in good agreement with those derived by

calculation (Allyson 1993) as demonstrated in table A.2, with the calibration coefficient lying between those calculated for soils of density 1 g cm^{-3} and 1.5 g cm^{-3} .

As with ^{40}K , taking density into account and deriving a calibration coefficient in terms of activity per unit wet weight as illustrated in figure A.8 and table A.2, provides a better and more flexible calibration coefficient which corresponds well with that calculated. The organic rich soils now pull the intercept almost through zero, suggesting that the negative intercept in figure A.7 is controlled by a density effect. There are still a few high activity points which provide a scatter about the calibration curve. This scatter must be attributed to sampling error or source burial.

Conclusions

1) For ^{137}Cs and ^{134}Cs calibration, the coefficients are highly dependent upon source burial in terms of *mean mass depth* β (g cm^{-2}). Sampling error accounts for a considerable amount of the scatter about each calibration curve although variations in source burial characteristics, which may also be attributed to water content and overall soil density, must also contribute to this scatter. Two distinct trends in the calibration coefficients have been observed, although in reality there is likely to be a complete range in calibration curves associated with source burial in different soil types and age of deposits.

2) The calibration of the primordial radionuclides is observed to be very much more flexible in terms of activity per unit wet mass ($\text{Bq}_{\text{wet}}\text{kg}^{-1}$). Calibration in terms of Bq m^{-2} is controlled by soil density. Sampling in low density soils underlain by hard rock provides difficulty in obtaining representative samples. ^{222}Rn remains problematic in the calibration of in-situ detectors.

APPENDIX B: AERIAL SURVEY DETECTOR CALIBRATION

Table B.1 Calibration Factors (N/A_x) for ^{137}Cs and ^{134}Cs at 100 m altitude.
**Analytical solution to photon fluence equations (Allyson 1994).*

Sampling Site	Mean Mass Depth β g cm ⁻²	N at 100 m $\pm \sigma$	N/A_x cps/kBqm ⁻²
^{137}Cs			
<i>Terrestrial Sites</i>			
<i>Circular Calibration Sites</i>			
Myres Hill	---	68.3 \pm 2.6	9.59 \pm 0.60
Leana Hill	---	24.3 \pm 1.6	8.63 \pm 0.78
Lakin Farm	---	24.7 \pm 1.6	6.87 \pm 0.65
Raithburn	---	48.2 \pm 2.2	10.5 \pm 0.78
	Mean $\pm \sigma$		8.90 \pm 1.34
<i>Expanding Hexagonal Plan</i>			
Longbridgemuir	3.6	65.0 \pm 2.4	6.75 \pm 0.67
<i>* Analytical Solutions for ^{137}Cs</i>			
	2		8.0
	5		6.2
<i>Salt Marsh Sites</i>			
<i>Expanding Hexagonal Plan</i>			
Caerlaverock	\approx 13	202 \pm 4.5	2.71 \pm 0.40
Warton Bank	> 14	433 \pm 6.6	1.79 \pm 0.32
Wigtown Bay	\approx 13	458 \pm 6.8	2.88 \pm 0.42
^{134}Cs			
<i>Terrestrial Sites</i>			
<i>Circular Calibration Sites</i>			
Myres Hill	---	8.20 \pm 2.86	10.2 \pm 3.6
Raithburn	---	5.75 \pm 2.40	14.4 \pm 5.1

The calibration coefficients for ^{137}Cs are dependent upon source profile. The scatter of points from the Ayrshire sites (Myres Hill, Leana Hill, Lakin Farm and Raithburn,

sampled in 1990) are greater than the estimated *standard error of the mean* for each locality. This suggests that variations in source burial is likely to be controlling the underlying variation in N/A_x between each site. The calibration coefficients determined experimentally for these sites agree with those determined through analytical solutions (Allyson 1994) of a mean mass depth of about 2 g cm^{-2} . The Longbridgemuir site sampled three years later has a significantly lower calibration coefficient with a β of 3.6 g cm^{-2} , and similar to that observed at Lakin Farm. This is consistent with (N/A_x) determined through photon fluence equations.

The calibration coefficients for the salt marsh site are significantly lower than those determined for terrestrial sites. It is interesting to note that the calibrations determined for the Solway sites (Caerlaverock and Wigtown Bay) are in agreement both in terms of mean mass depth and (N/A_x) . The Warton Bank site, with a potentially higher mean β has a significantly lower (N/A_x) .

The calibrations for the natural radionuclides are given in table B.2. As a consequence of the observations made in appendix A, the calibrations are given in terms of Bq m^{-2} and Bq wet kg^{-1} . As table B.2 shows, there is a greater variation in the calibration coefficients for Bq m^{-2} than Bq kg^{-1} . As with Appendix A, this can be explained by the influence of soil density, as the comparison with analytical solutions (Allyson 1994) shows. The N/A_x values for Lakin Farm tend to be slightly higher than those for the salt marsh environments. This can be explained by source burial by low activity soils at the Lakin Farm site. There is, however, a considerable problem with ^{214}Bi calibration brought about by the atmospheric ^{222}Rn .

Table B.2 Calibration Factors (N/A_x) for ^{40}K , ^{214}Bi and ^{208}Tl at 100 m altitude.
**Analytical solutions (Allyson 1994).*

Sampling Site	Soil Density g cm^{-3}	N at 100 m	N/A_x kBq m^{-2}	N/A_x Bq kg^{-1}
^{40}K				
Lakin Farm	0.8	31.0 ± 1.76	0.875 ± 0.174	0.146 ± 0.029
Caerlaverock	1.5	42.3 ± 2.05	0.313 ± 0.017	0.126 ± 0.007
Wigtown	1.5	47.9 ± 2.18	0.289 ± 0.016	0.131 ± 0.007
<i>Analytical Solutions*</i>				
				0.19
	0.6		1.07	
	0.8		0.80	
	1.0		0.633	
	1.6		0.40	
^{214}Bi				
Lakin Farm	0.8	2.95 ± 0.54	3.80 ± 1.02	0.516 ± 0.253
Caerlaverock	1.5	5.88 ± 0.77	7.58 ± 3.00	1.03 ± 0.407
Wigtown	1.5	33.1 ± 1.80	0.284 ± 0.12	0.132 ± 0.056
<i>Analytical Solutions*</i>				
				0.32
	0.6		1.92	
	0.8		1.267	
	1.0		1.067	
	1.6		0.667	
^{208}Tl				
Lakin Farm	0.8	5.42 ± 0.23	14.68 ± 3.31	2.61 ± 0.59
Caerlaverock	1.5	6.32 ± 0.50	3.616 ± 0.346	1.37 ± 0.13
Wigtown	1.5	11.5 ± 1.07	3.705 ± 0.355	1.70 ± 0.16
<i>Analytical Solutions*</i>				
				2.1
	0.6		11.667	
	0.8		8.667	
	1.0		7.00	
	1.6		4.667	

Sample Name	Primary Unattenuated Photon Detected / cps		Background Counts / cps		Attenuated Primary Photon Signal		Background Subtraction from 1/cps		Linear Attenuation Coefficient			Mean Attenuation Coefficient					
	75.75	107.7	101.3	0	0	0	12.77										
CANBOURN 15-30	76.05	75.75	107.2	0	0	0	8.32	75.3	75.67	0.0822	0.123	0.0873	0.0793	0.282	1.44	0.0570	0.0563
LEZARD 0-15	76.05	75.75	107.2	0	0.08	0	12.94	78.3	78.72	0.0790	0.101	0.0719	0.0673	0.274	1.507	0.0525	0.0477
DORNIKE 0-15	76.05	75.75	107.2	0	0	0	13.78	75.13	77.45	0.0867	0.111	0.0739	0.0750	0.264	1.473	0.0388	0.0302
CAERB04 0-5	76.05	75.75	107.2	0.47	1.96	0	23.85	77.85	76.87	0.0878	0.0869	0.0756	0.0708	0.237	1.17	0.0770	
CAERB04 5-10	76.05	75.75	107.2	0.83	2.875	0	18.11	77.85	76.87	0.0878	0.0869	0.0756	0.0708	0.237	1.17	0.0770	0.0536
CAERB04 0-15	76.05	75.75	107.2	0	0.47	0	17.62	76.52	77.02	0.0878	0.109	0.0735	0.0791	0.235	1.384	0.0580	0.0531
CAERB04 0-15	76.05	75.75	107.2	0	0.33	0	13.32	72.37	71.4	0.0878	0.116	0.0865	0.0741	0.235	1.37	0.0568	0.0511
IAEA Soil 6	76.05	75.75	107.2	0	0.105	0	21.13	84.32	82.28	0.0878	0.0756	0.0616	0.0723	0.239	1.018	0.0608	0.0603
IAEA 306	76.05	75.75	107.2	0	0.2	0	26.17	89.6	90.2	0.0878	0.0551	0.0376	0.0700	0.294	0.788	0.0566	0.0477
BULK SAMPLE 0-12 cm	76.05	75.75	107.2	0	0.48	0	19.32	81.47	81.32	0.0878	0.0550	0.0639	0.0748	0.237	1.271	0.0563	0.0318

APPENDIX D The Absolute Efficiencies Determined from Peat and Elginhaul Soil for the Coaxial Ge(Li) & HPGe Detectors

Nuclide	Energy keV	Absolute Efficiency									
		Ge(Li) Peat	Error	HPGe Peat	Error	Ge(Li) E.Soil	Error	HPGe E.Soil	Error		
²⁴¹ Am	59.6	0.00498	0.000177	0.0435	0.00132	0.007609	0.000264	0.067221	0.000264	0.002092	
¹⁰⁹ Cd	88.03	0.02156	0.000704	0.04613	0.00149	0.030364	0.001	0.064039	0.001	0.002114	
⁵⁷ Co	122.06	0.03352	0.000589	0.0454	0.000789	0.04345	0.000814	0.059781	0.000814	0.0011	
¹³⁹ Ce	165.8	0.03512	0.000638	0.03887	0.000699	0.044682	0.000891	0.04917	0.000891	0.000953	
²⁰³ Ce	279.2	0.02404	0.000544	0.02544	0.000571	0.031407	0.000963	0.03357	0.000963	0.00068	
¹¹³ Sn	391.69	0.01935	0.000829	0.02055	0.000879	0.023183	0.001017	0.02479	0.001017	0.001074	
⁸⁵ Sr	514	0.01549	0.000325	0.01606	0.000336	0.017861	0.000412	0.019077	0.000412	0.000419	
¹³⁷ Cs	661.64	0.01278	0.000388	0.01359	0.000413	0.014783	0.00032	0.016062	0.00032	0.000348	
⁸⁸ Y	898	0.00946	0.000364	0.01021	0.000393	0.010737	0.00042	0.011851	0.00042	0.000056	
⁶⁰ Co	1173.2	0.007672	0.000061	0.008317	0.000066	0.008667	0.000087	0.00959	0.000087	0.000096	
⁶⁰ Co	1332.5	0.006864	0.000054	0.007508	0.000059	0.007766	0.000078	0.008602	0.000078	0.000086	
⁸⁸ Y	1836	0.005358	0.000147	0.005851	0.00016	0.005912	0.000031	0.006561	0.000031	0.000184	

APPENDIX F OBSERVATIONS ON THE TEMPORAL CHANGE IN DETECTOR RESPONSE WITH SOIL WATER CONTENT

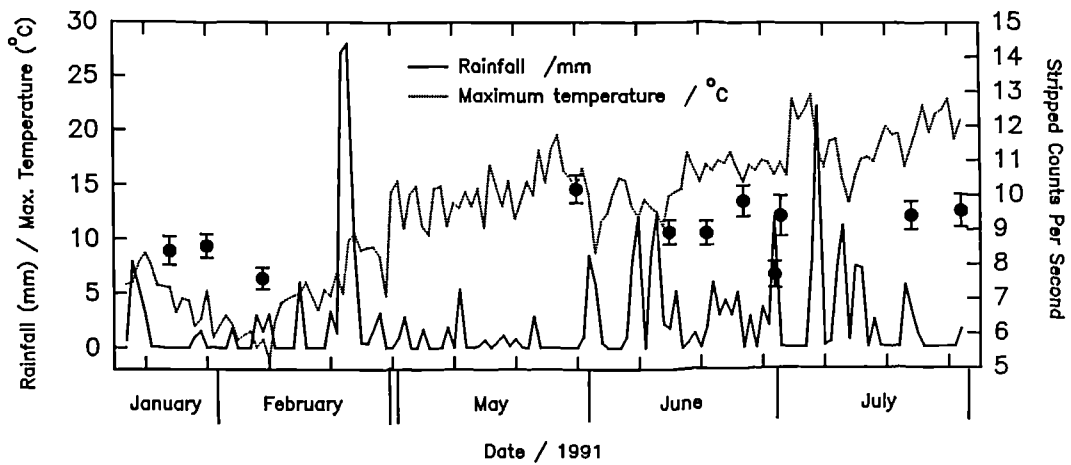


Figure F.1. The variation in detector response for ^{137}Cs at SURRC (loamy soil) with rainfall and temperature. Mean detector response is 9.1 ± 0.8 cps (9 %).

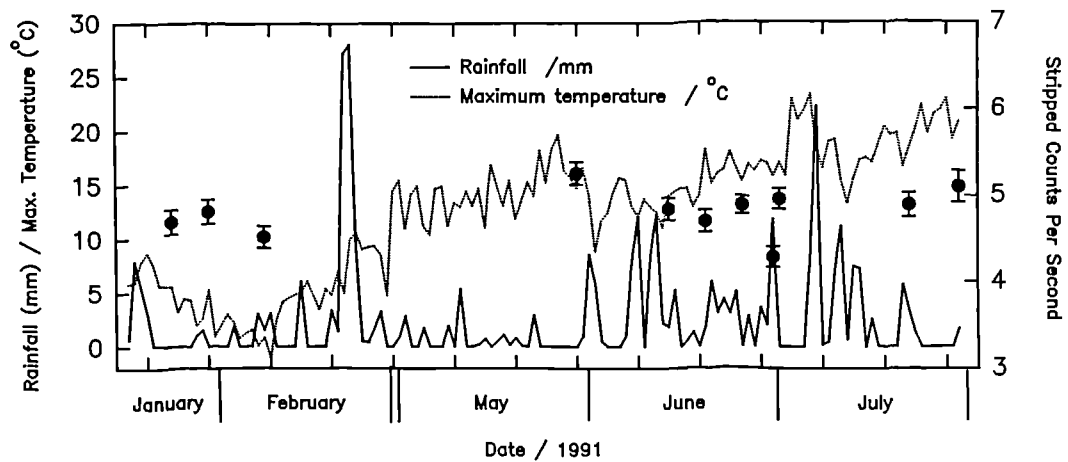


Figure F.2 The variation in detector response for ^{40}K at SURRC (loamy soil) with rainfall and temperature. Mean detector response = 4.8 ± 0.23 (5 %).

The mean observations of the months indicated in figures F.1 and F.2, are $9.1 \text{ cps} \pm 9\%$ (1σ) for ^{137}Cs and $4.8 \text{ cps} \pm 5\%$ (1σ) for ^{40}K . The error on any one reading was determined by up to 8 consecutive observations by replacing the detector in approximately the same position. Such repeat observations provided an error estimate of $\pm 5\%$ for ^{137}Cs and $\pm 3.5\%$ for ^{40}K . Thus the error over the year associated with

soil moisture changes is significant.

However, only extreme variations in climatic conditions provided the significant changes in detector response. On 8th February (1991) a measurement was made over 2-3 cm of snow cover resulting in a more significant reduction in count rate for ¹³⁷Cs (7.62 cps) than for ⁴⁰K (4.52 cps). On the 1st July a measurement made during heavy rainfall resulted in a drop in the detector response to 7.68 cps and 4.28 cps respectively. A repeat measurement on the following day revealed a return to normality, as a result of rapid evaporation of soil moisture in the warmer summer conditions.

APPENDIX G. INSTALLATION OF THE CONCRETE CALIBRATION PADS.

Four "portable" concrete calibration pads were purchased from the Canadian Geological Survey. The four blocks were constructed from low activity concrete, of which three had been doped and sealed with equilibrated ^{238}U , ^{232}Th and ^{40}K .

Table G.1. Summary statistics of Pre-installation background checks.

PAD 1	Ch.1	Ch.2	Ch.3	Ch.4	Ch.5	Ch.6
Mean Value:	16.37	8.48	10.01	1.71	1.05	60.71
Standard Deviation:	0.09	0.05	0.08	0.03	0.03	0.28
Standard Error:	0.03	0.02	0.03	0.01	0.01	0.10
PAD 2						
Mean Value:	16.09	8.29	9.69	1.74	1.00	59.41
Standard Deviation:	0.14	0.15	0.18	0.05	0.02	0.26
Standard Error:	0.05	0.05	0.06	0.02	0.01	0.09
PAD 3						
Mean Value:	16.19	8.28	9.78	1.70	1.02	59.64
Standard Deviation:	0.08	0.09	0.06	0.03	0.03	0.09
Standard Error:	0.03	0.03	0.02	0.01	0.01	0.03
PAD 4						
Mean Value:	16.28	8.40	9.81	1.72	1.03	60.22
Standard Deviation:	0.15	0.09	0.10	0.04	0.04	0.32
Standard Error:	0.05	0.03	0.04	0.01	0.01	0.11

A dry, uniformly low activity environment was found for the pads. Five calibration bays were constructed with 2 m x 0.5 m x 0.5 m low activity concrete plinths as shown in figure G.1. The activity within each bay was assessed for the regions of interest (described in section 2.5) with the portable 3" x 3" NaI(Tl) detector. Eight spectral measurements were made within each bay and a small variation of 6 % (1σ) for channel 1 (^{137}Cs window) was observed between the bays. Each plinth was then measured and appropriate plinths were exchanged to equalise the background within each bay. This was then verified by repeat measurements. The background block was then placed into each bay and eight further readings were made in each position, the results are given in table G.1.

Table G.2 The final readings from each calibration pad after installation

PAD 1: Background	Ch.1	Ch.2	Ch.3	Ch.4	Ch.5	Ch.6
Mean Value:	16.37	8.48	10.01	1.71	1.05	60.71
Standard Deviation:	0.09	0.05	0.08	0.03	0.03	0.28
Standard Error:	0.03	0.02	0.03	0.01	0.01	0.10
PAD 2: K						
Mean Value:	33.10	23.10	33.04	1.48	0.88	141.23
Standard Deviation:	0.16	0.15	0.41	0.07	0.03	0.76
Standard Error:	0.07	0.07	0.18	0.03	0.01	0.34
PAD 3: Th						
Mean Value:	93.07	25.88	25.62	14.79	18.50	328.72
Standard Deviation:	0.35	0.26	0.17	0.16	0.23	0.93
Standard Error:	0.14	0.11	0.07	0.06	0.09	0.38
PAD 4: U						
Mean Value:	98.54	44.31	29.76	18.57	2.02	295.06
Standard Deviation:	0.36	0.22	0.42	0.25	0.03	0.92
Standard Error:	0.15	0.09	0.17	0.10	0.01	0.38

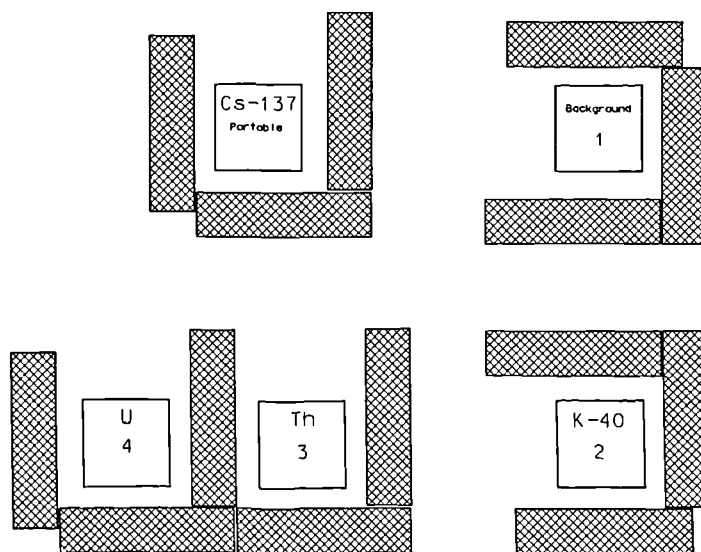


Figure G.1 The five concrete bays for the calibration pads including four concrete 1 m x 1 m calibration pads and 1 ¹³⁷Cs 1 m x 1 m sheet.

The uranium pad was then placed into each bay and raised so that the top of each pad was almost level with the top of the surrounding plinth. From each pad position, measurements were made in the other three positions to check for cross talk. Cross talk was found to be negligible even for a detector raised 20 cm above the surface of the

adjacent pads. The pads were then finally placed into their positions as shown in figure G.1. The readings collected in the final positions are given in table G.2.

The use of the plinths to separate the calibration pads is likely to make some contribution to the overall scattering associated with each position.

APPENDIX H. THE CONSTRUCTION OF AN EXTENDED LAYER ^{137}Cs CALIBRATION SHEET

The ^{137}Cs sheet was constructed from a 1 m x 1 m x 0.009 m plywood sheet. The sheet was divided into four 0.5 m x 0.5 m sheets and painted with a white water based emulsion. A known quantity (≈ 300 g) of the white paint was then taken and weighed accurately. A known quantity of ^{137}Cs with carrier solution was then pipetted into the paint. 45.3 kBq of ^{137}Cs was added and the paint was homogenised by tumbling for several hours.

A dry weighed paintbrush was then used to carefully paint one surface of each of the four sheets as uniformly as possible. Every attempt was made to paint uniformly across the surface of each sheet. The painting continued until all the paint was used. The paint brush and empty container were then weighed to account for unused paint, thus estimating the amount of paint and activity transferred to the plywood sheets. The sheets were then allowed to dry.

Having dried, the sheets were then painted with a tough red vinyl gloss paint to seal in the spiked emulsion paint. A coloured vinyl paint was chosen so that if the sheets should become damaged or scratched any exposure of the white spiked paint would immediately be seen. Following two coats of the red gloss paint, a coat of polyurethane boat varnish was used for final protection. The edges of the sheets were also protected by aluminium strips.

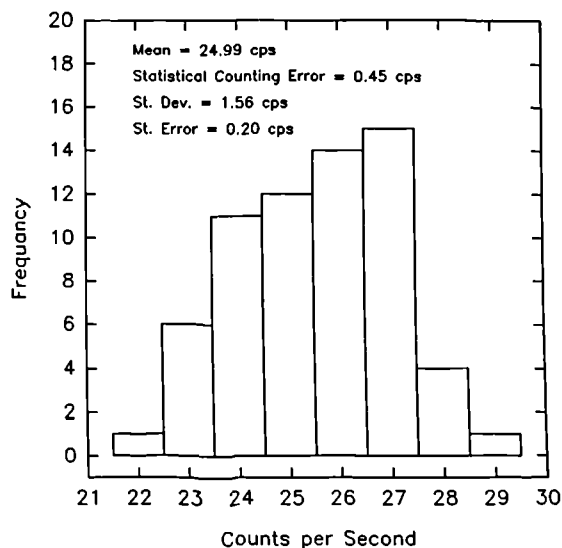


Figure H.1 Histogram illustrating the uniformity of ^{137}Cs activity concentration across the 1 m² pad

Prior to the construction of the final calibration sheet a test piece was made in exactly the same way. After each stage had dried, several wet swabs were made of the surface

of the sheet to determine the ease of ^{137}Cs removal. Removal of ^{137}Cs paint was possible until the gloss sealant was applied.

Uniformity of activity across the sheet was checked by collimating the 3" x 3" NaI(Tl) detector and recording regions of interest data for ^{137}Cs . 16 measurements were made with regular spacings across each board totalling 64 measurements. The results are shown in figure H.1.

The total ^{137}Cs activity applied was $40.67 \text{ kBq} \pm 4 \%$ for the 1 m square area (1st August, 1992). The weight of the board is 5000 g, the activity per gram is 8 Bq/g. This is well below the minimum activity of 100 Bq g^{-1} defined by the NRPB as radioactive material.

APPENDIX I. CHOICE OF ABSORBER MATERIALS

The mass attenuation coefficients of readily bought material could be calculated from their known compositions. Materials were chosen to mimic as closely as possible the mass attenuation coefficients (μ_m) of Beck's soil (Beck *et al* 1972), peat, water and air.

Plaster Board: pure gypsum. The purity of the gypsum varies according to geological origin, but in its purest form is $\text{Ca SO}_4 \cdot 2\text{H}_2\text{O}$

Purity is quickly determined by the whiteness of the gypsum. Calculation suggests that up to 20 % impurities can be tolerated without a significant change in μ_m . The Geostandard News Letter provides more complex chemical compositions for gypsum with varying degrees of purity. Typical gypsum composition is: S = 18.62 % Ca = 23.38 % O = 37.18 % H_2O = 20.94 %

Wood: Although varying in density, wood is composed of 50 % Cellulose and a little less than 50 % Lignin. As these are the predominant components, the chemical composition will be based on these. Cellulose - $\text{C}_6 \text{H}_{10} \text{O}_5$, Lignin - $\text{C}_{20} \text{H}_{20} \text{O}_5$

Mean composition is approximated by $\text{C}_{26} \text{H}_{30} \text{O}_{10}$, C = 62.14 % H = 6.02 % O = 31.84 % (N = 3% est)

Plastics:

Polythene - polyethylene: $(\text{C}_2 \text{H}_4)_n$ **Perspex** - Polymethylmethacrylate: $(\text{C}_4 \text{H}_6 \text{O}_2)_n$
C = 85.65 % H = 14.37 % C = 55.8 % H = 7.03 % O = 37.17 %

Polystyrene - $(\text{C}_8 \text{H}_8)_n$ **Polypropylene** - $(\text{C}_3 \text{H}_6)_n$
C = 92.3 % H = 7.7 % C = 85.62 % H = 14.38 %

The relationship between these absorber materials with Beck's soil composition, peat, air and water are shown in figures I.1 to I.4 respectively. The graphs show that above 150 keV, gypsum most closely reflects the mass attenuation coefficients represented by Beck's soil, followed by wood and perspex (figure I.1). Peat is most closely

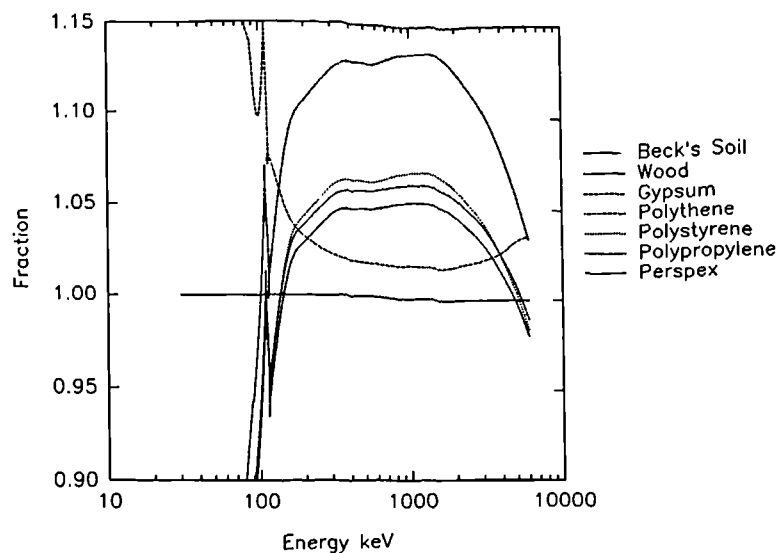


Figure I.1 Mass attenuation coefficients of absorber material relative to Beck's soil

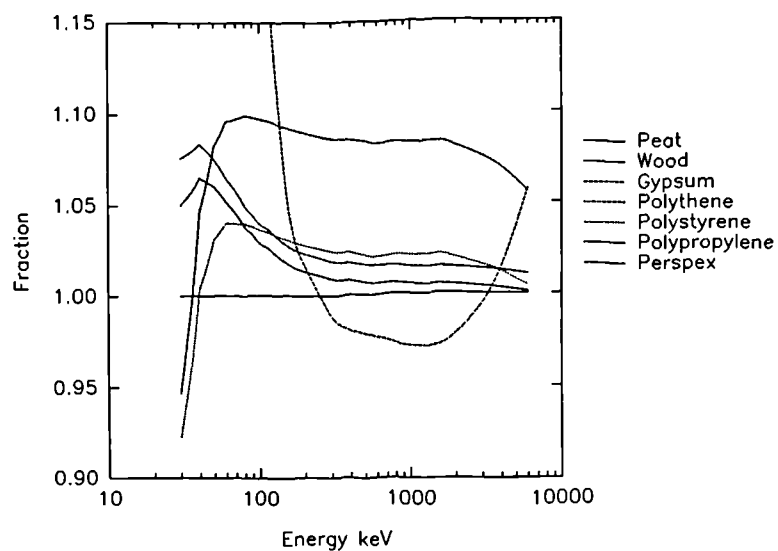


Figure I.2 Mass attenuation coefficients of absorber material relative to Peat

represented by wood and perspex (figure I.2). For air, gypsum displays considerable variation across the energy range. Wood and perspex most closely mimic air (figure I.3). Polypropylene most closely reflects the mass attenuation coefficient of water followed by polystyrene and perspex.

From these observations perspex was chosen as the attenuating media as it most closely reflects the mass attenuation coefficients of peat, water and air for energies above 150 keV. The error on these results is dominated by an approximate 5 % error from the original nuclear data tables. Although cheaper, wood was not chosen because

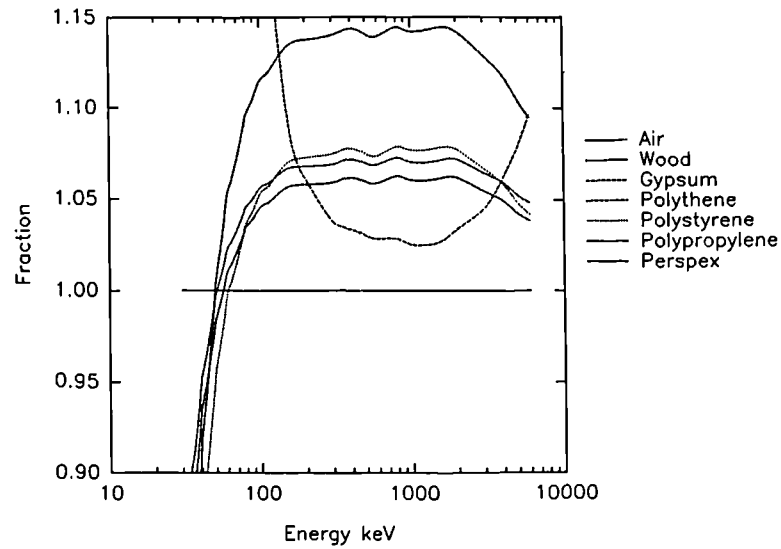


Figure I.3 Mass attenuation coefficients of absorber material relative to Air

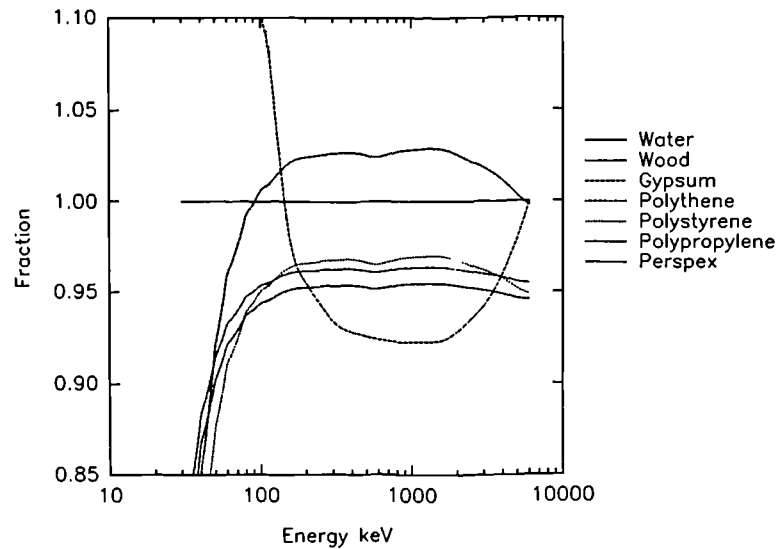


Figure I.4 Mass attenuation coefficients of absorber material relative to Water

chemically it was difficult to define the added contributions of glues and resins associated with plywood. For investigations below 150 keV, a hybrid of different attenuating media such as perspex and gypsum may be used to reflect environmental media.

Twenty 1 m x 1m x 0.01 m thick perspex sheets were constructed and used in the experiments discussed in chapter 7.

APPENDIX J. CHANGES IN STRIPPING COEFFICIENTS WITH INCREASE IN AIR PATH LENGTH

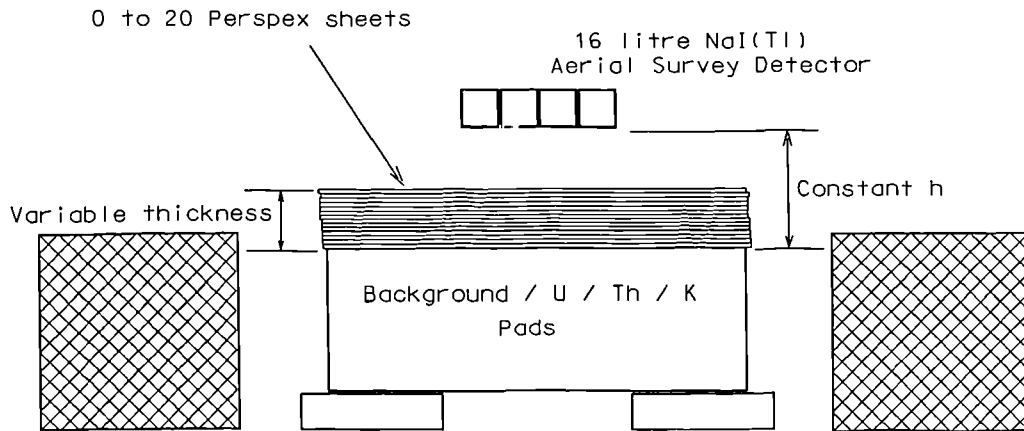


Figure J.1 The experimental set up to measure the change in stripping coefficient with detector height

The 16 litre NaI(Tl) aerial survey detector was used and supported at a permanent height of 30 cm as indicated in figure J.1. The experimental procedure followed that of experiment (i), although all 20 of the perspex sheets were added individually. Each sheet was calculated to represent approximately 9.6 m of atmosphere.

The height of the detector was kept constant to facilitate easier access and removal of the perspex sheets. Twenty sheets of perspex were placed upon each calibration pad and the minimum counting time was calculated from the appropriate window to obtain 1 % counting statistics. The ^{40}K window was chosen from the background pad. After each spectrum was recorded, one sheet was removed from the pad and another spectrum was collected.

The spectra were then converted to counts per second for each channel. For each active pad and sheets, the appropriate background spectrum was subtracted. The spectral contributions to each window from the source were calculated relative to the principal window used to measure the activity of the source, thus giving the stripping coefficients. The change in stripping coefficients with attenuating sheets, and hence the simulation of change in air path-length could be observed.

Results and Discussion of the change in stripping coefficients with absorber perspex sheets to simulate increase in air path length.

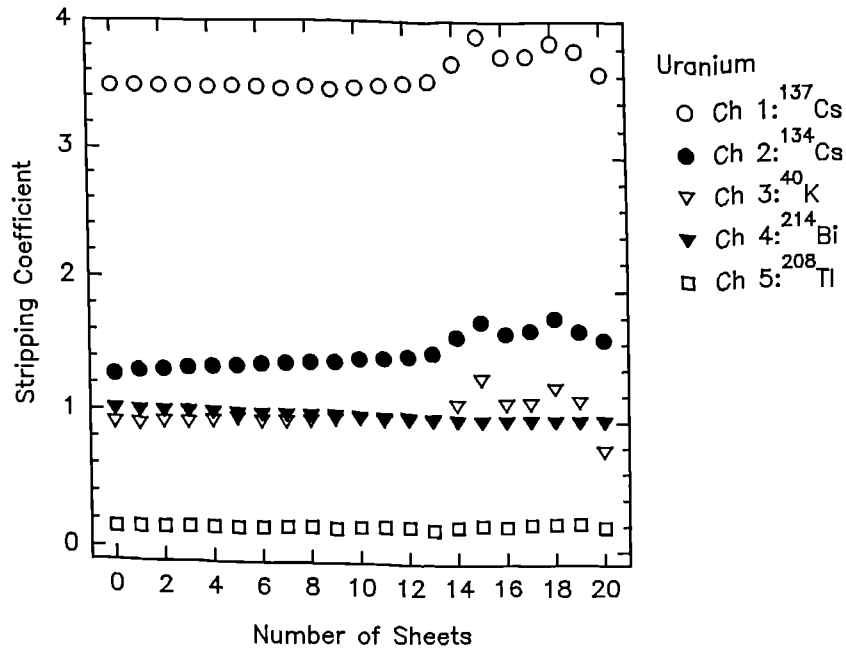


Figure J.2. The stripping coefficients associated with the ^{238}U decay series with perspex absorber sheets.

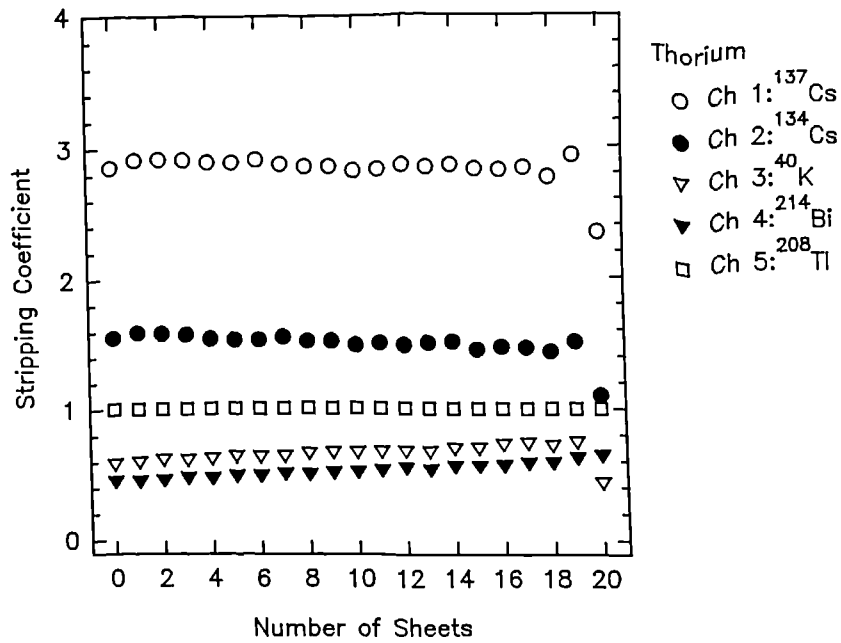


Figure J.3. The stripping coefficients associated with the ^{232}Th decay series with perspex absorber sheets.

Figures J.2 and J.4 show the change in stripping coefficients with the number of

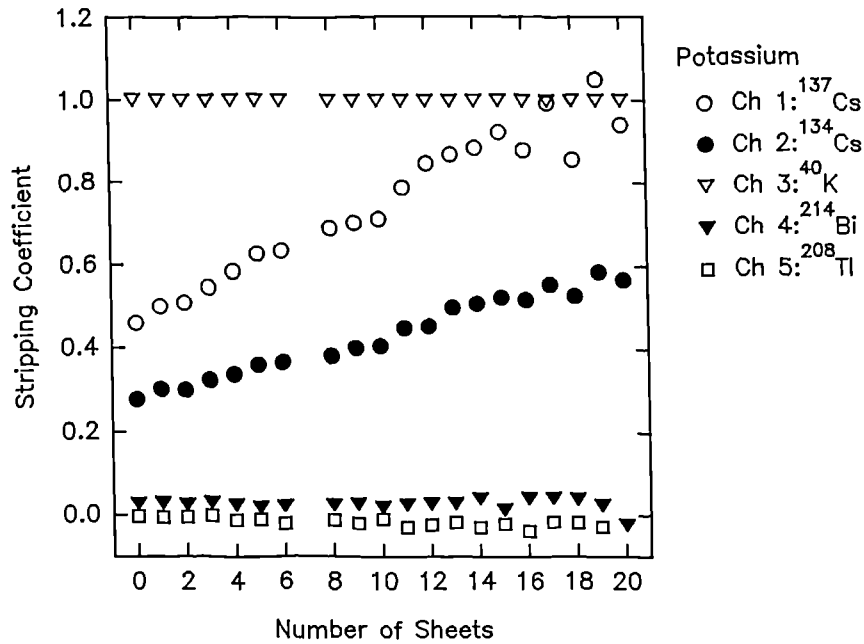


Figure J.4. The stripping coefficients associated with ^{40}K and perspex absorber sheets.

attenuating sheets for the U, Th and K pads respectively. There is no marked change in stripping coefficients with the number of perspex sheets for the U and Th pads (figures J.2 and J.3). As with the 3" x 3" NaI(Tl) detector, figure J.4 shows that the ^{40}K contribution to the ^{137}Cs and ^{134}Cs windows underwent a considerable change with the number of absorber sheets. Thus the contribution to the ^{137}Cs window from ^{40}K was vulnerable to changes in detector height. ^{40}K stripping coefficients determined at ground level are not applicable to aerial survey altitudes.

Given the dominant aerial survey altitude during the survey, the appropriate set of stripping coefficients can be chosen. For example, for a mean height of 80 m, the stripping coefficients are determined from 8 perspex sheets. This set of experiments is less affected by the fact that the source is a finite plane. As discussed in chapter 3, the solid angle subtended by the detectors at aerial survey altitudes is smaller than that observed at ground level, suggesting that these stripping coefficients would be more representative.